Experimental design as an optimization tool for inductively coupled mass spectrometry methods

Master's thesis
Wille Kilpeläinen
University of Helsinki
Chemistry and Molecular Sciences
June 30, 2020

HELSINGIN YLIOPISTO — HELSINGFORS UNIVERSITET — UNIVERSITY OF HELSINKI

Tiedekunta — Fakultet — Faculty	Koulutusohjelma — Utbildningsprogram — Degree
Faculty of science	Chemistry and molecular sciences

Tekijä — Författare — Author
Wille Kilpeläinen

Työn nimi — Arbetets titel — Title

Experimental design as an optimization tool for inductively coupled mass spectrometry methods

Oppiaine — Läroämne — Subject
Analytical chemistry

Työn laji — Arbetets art — Level	Aika — Datum — Month and year	Sivumäärä — Sidoantal — Number of pages
Master's thesis	16.7.2020	95

Tiivistelmä — Referat — Abstract

Inductively coupled mass spectrometry (ICP-MS) is a state-of-the-art technique for elemental analysis. The technique allows fast and simultaneous analysis of multiple elements with a wide dynamic range and low detection limits. However, multiple adjustable parameters and the complex nature ICP-MS instruments can make the development of new analysis methods a tedious process.

Design of experiments (DOE) or experimental design is a statistical approach for conducting multivariate experiments in a way that gives maximal amount of information from each experiment. By using DOE the number of experiments needed for analytical method optimization can be minimized and information about interrelations of different experimental variables can be obtained.

The aim of this thesis is to address the utilization of DOE for ICP-MS method developement as a more efficient mean to optimize analytical methods. The first part of this two part thesis gives an overview on the basics of ICP-MS and DOE. Then a literature review on applying experimental design for ICP-MS method optimization is given and the current state of the research is discussed.

In the second part, two new ICP-MS methods for simultaneous determination of 28 elements from six middle distillate fuels, diluted with xylene or kerosine, are presented. The method developement involved optimization of the integration times and optimization of test sample dilution ratios and viscosities using univariate techniques. In addition, experimental designs were succesfully utilized together with desirability approach in multivariate optimizations of the plasma conditions and sample matrix compositions to achieve the best possible analyte recoveries from various matrices.

Avainsanat — Nyckelord — Keywords
ICP-MS, experimental design, inductively coupled mass spectrometry, multivariate optimization, DOE

Säilytyspaikka — Förvaringsställe — Where deposited
Digital Repository of the University of Helsinki - HELDA/eThesis

Muita tietoja — övriga uppgifter — Additional information
The thesis was funded by Neste (Neste Oyj, Espoo, Finland) and the research was conducted at Neste's research facility in Porvoo Finland

Acknowledgements

I wish to express my gratitude to my supervisor, research scientist Sonja Sirviö, for her confidence in my independent work and for being available every time I needed advice. I would also like to show my special regards to Prof. Mikko Oivanen and to Dr. Katriina Lipponen who reviewed my masters thesis together with Sonja Sirviö. In addition I want to thank all my co-workers for their support and for sharing their knowledge with me.

The research was funded by Neste Oyj and the way the company provides special opportunities for students, shares expertise and contributes to open access science by funding master's theses is to be appreciated.

Contents

List of Abbreviations

CA	Cluster Analysis
CCD	Central Composite Design
CRC	Collision/Reaction Cell
CV-ICP-MS	Cold Vapour Inductively Coupled Mass Spectrometry
DOE	Design Of Experiments
DRC	Dynamic Reaction Cell
IEC-ICP-MS	Ion Exchange Chromatography - Inductively Coupled Mass Spectrometry
ICP-OES	Inductively Coupled Optical Emession Spectroscopy
ICP-MS	Inductively Coupled Mass Spectrometry
ICP-QMS	Inductively Coupled Quadrupole Mass Spectrometry
ISTD	Internal standard
LOD	Limit Of Detection
LOQ	Limit Of Quantification
m/Z	Mass to charge ratio
OVAT	One Variable At the Time
PCA	Principal Component Analysis
PLSR	Partial Least Squares Regression
RF	Radio Frequency
SBR	Signal to Background Ratio
SF-ICP-MS	Sector Field Inductively Coupled Mass Spectrometry
TOF-ICP-MS	Time Of Flight Inductively Coupled Mass Spectrometry

1 Introduction

Metals present in intermediate distillate products and fuels can poison catalytes used in fuel refinement prosesses and cause damage to modern engines. Many metals are also toxic to living organisms and burning fuels contaminated with these so-called heavy metals releases the enviromental toxins into the atmosphere along with the exhaust gasses. As the elemental composition can also affect the market value of chemicals, it is essential to monitor the concentration of elements present in feedstock materials, refinery intermediate products and in commercial fuels.

In addition, an increasing demand for renewable biofuels makes it necessary to find new feedstocks for their production. This leads to a growing diversity of novel raw materials and smaller feed batches, that all need to be analyzed prior processing. The increasing sample throughput and variability leads to a growing demand for more convenient and robust methods for elemental analysis of organic matrices. At the same time, ever more stricter specifications bring pressure to further push down the detection limits and to use state-of-the-art analytical techniques to achieve this goal. Using *Inductively coupled plasma mass spectrometry* (ICP-MS) is a promising option for elemental analysis of middle distillate products and comparable organic matrices.

1.1 Inductively coupled mass spectrometry

ICP-MS has gained popularity during the last decade over inductively coupled optical emission spectroscopy (ICP-OES) as the technique of choice for elemental analysis, as it allows fast and simultaneous analysis of multiple elements with wide dynamic range and lower detection limits compared to ICP-OES.[1] Therefore, the technique is today used in several different fields, including enviromental and life sciences[2], oil industry[3], in food analysis[4] and for clinical applications[1].

A typical ICP-MS instrument

A schematic drawing of a representative ICP-MS instrument[5,6] is shown in Figure 1. In a typical ICP-MS instrument a liquid test sample is introduced into the instrument along a hose and atomized in a *nebulizer*. The polydisperse aerosol formed in the nebulizer is then guided through a *spray chamber*, a compartment that acts as a highpass filter and only allows the smallest droplets to pass through.[6]

After the sample aerosol leaves the spray chamber, it is guided into a hot argon plasma. Energy provided to the plasma by an induction coil causes the solvent to evaporate, brakes down the molecules of the sample matrice and eventually ionizes the gaseous sample matrix. When analyzing organic matrices, a stream of oxygen is added to the plasma to oxidize the carbon of the matrix to prevent sooting. It is also a common practice to use a higher plasma RF power when organic matrices are analyzed.[7]

Ions formed in the plasma are then guided to a mass analyzer, used to separate the analyte ions. The most commonly used mass analyzers used with ICP-MS include *quadrupole mass analyzers*(QMS) *time of flight analyzers*[8] (TOF)[9] and *double focusing magnetic sector*

mass analyzers (SFMS)[10,11]. After passing throughthe mass analyzer the ions are detected at a detector, most commonly by using a *discrete dynode electron multiplier*.[12]

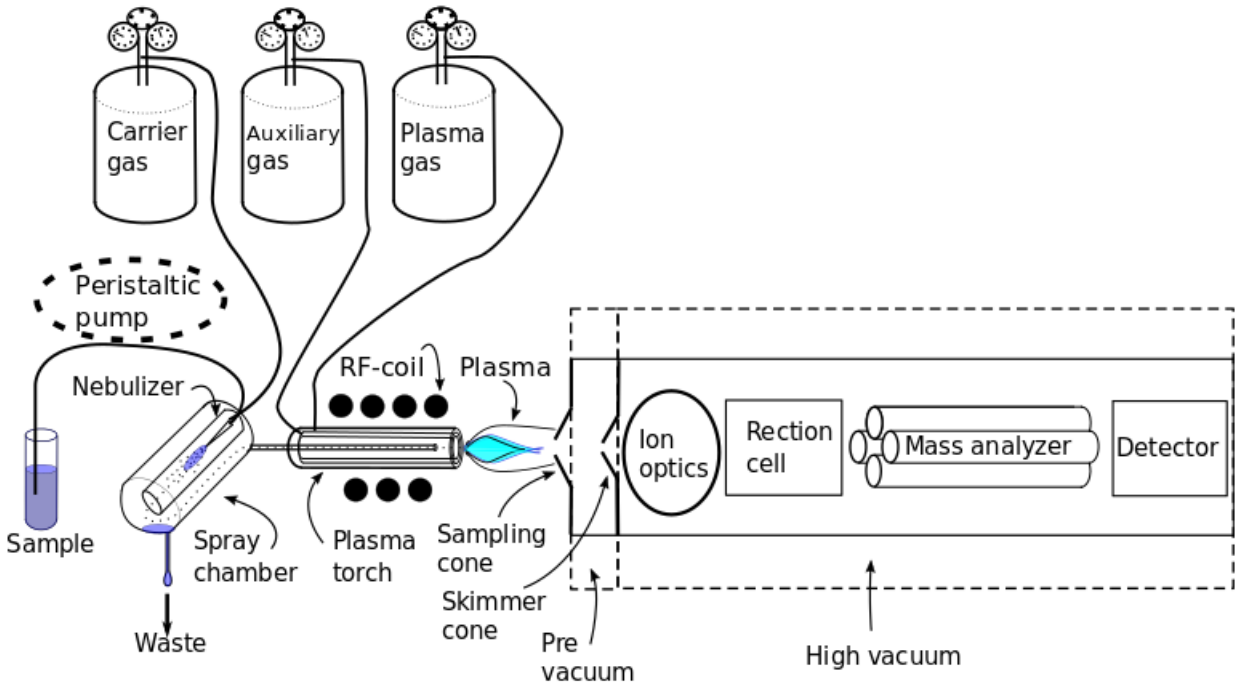

Figure 1 A schematic diagram of an ICP-MS instrument.

Spectral interferences

Spectral interferences are ionic species having the same m/Z ratio with analyte ions. Elements causing spectral interferences can originate from solvent, matrix, plasma gases, or from the surrounding air. Common interferences include *polyatomic interferences*, for example argides, such as $^{40}Ar^{16}O^{+}$, oxides such as $^{35}Cl^{16}O^{+}$, hydroxides like $^{48}Ca^{16}O^{1}H^{+}$ or hydrides like $^{40}Ar^{1}H^{+}$. In addition *isobaric interferences*, i.e. interfering monoatomic ions, and double charged ions can also cause signals overlapping with an analyte.[13] A comprehensive list of spectral interferences have been put together by T. May and W. Wiedmeyer.[14]

The formation of polyatomic interferences can be reduced by using the so called *cold* or *cool plasma conditions*,[13,15,16] On the other hand, it might sometimes be useful to increase the plasma temperature to suppress the formation of interfering metal oxides in the plasma.[13,15] For isobaric interferences and sometimes also for polyatomic interferences, correction equations can be used to compensate for measurement errors caused by an interference.[13]

An often used strategy to remove polyatomic or isobaric interferences from the ion beam is to guide the beam through a compartment called *collision/reaction cell* (CRC) located before the mass analyzer.[17] A CRC can be used to filter out polyatomic interferences based

on their larger size compared to analyte ions. In this application, the cell is pressurized with a chemically inert collision gas, such as He, Ar, N_2 or Xe and an electric potential is set between the CRC and the mass analyzer.[18] The collisions between the ions and the particles of the collision gas reduce the kinetic energy of the ions and if the CRC parameters are properly adjusted, the interfering polyatomic ions are discriminated from the ion beam in a process called *kinetic energy discrimination*, as they do not have sufficient energy to enter the mass analyzer.

In addition to removing polyatomic interferences by using kinetic energy discrimination, collicion/reaction cells pressurized with reaction gases, such as H_2 or O_2, can be used to convert spectral interferences to non-interfering chemical species by chemical reactions. Other strategies for interference reduction include: using a dynamic reaction cell (DRC), a compartment that can act as a mass filter in addition to acting as reaction cell[17,19], and using ICP-MS/MS[20] or high resolution SFMS[10,11] instruments for resolving the interferences.

Matrix intrerferences

In addition to spectral interferences, the sample matrix can cause *matrix interferences*, where the sample matrix causes a suppression of analyte signals. In the so-called *sample transport effects* the composition of the sample matrix disrupts the sample introduction by influencing droplet formation and droplet selection, or by changing the sample flow rate to the nebulizer, especially, when analyzing organic matrices by using free aspiration for sample introduction.[13] In *ionization interferences*, the matrix components change the ionization equilibria of the analytes.[21,22] The *Space-charge-induced matrix interferences* are believed to arise from poor transmission of lighter ions through ion optics as a high amount of heavier ions in the ion beam has a tendency to defocus the ion beam by pushing low-mass analytes out of the beam.[13,23]

Introduction of organic matrices into an ICP-MS instrument

Usually aquaeous samples are introduced into an ICP-MS instrument and a laborous sample preparation step such as wet digestion or dry ashing with a subsequent dilution in mineral acid is usually needed to introduce the analytes into the aquaeous matrix.[4,24] Alternatively, organic matrices can be directly introduced into an ICP-MS instrument.[25] By the direct introduction of organic matrices the time spend on sample preparation is vastly reduced and dozens of elements can be determined simultaneously in just a few minutes in a concentration range extending several orders of magnitude from sub ppb to ppm levels. This makes the technique highly suitable for use in high throughput laboratories.

Various solvents including aromatic hydrocarbons and alcohols have been be used as solvents[25] and some matrices, such as diesels[26] can even be fed into the plasma without any dilution or any other sample preparation. However, a less robust plasma is obtained when using organic solvents and the direct introduction of organic solvents often comes with the cost of increased detection limits.[27] Volatile solvents have a tendency to cause more disruption of the plasma.[28] For this reason, kerosine and xylene are often the preferred solvents for hydrocarbon matrices. Other drawbacks of the direct introduction of organic matrices

include interferences caused by the matrix[27], precipitation of matrix components that can clog the nebulizer, carbon deposit accumulating on the instruments surfaces and sample deterioration[29] caused by precipitation of analytes.

1.2 ASTM D8110 standard

Regardless of the benefits of the direct introduction of organic matrices, no standard test methods concerning ICP-MS elemental analysis by direct introduction of organic matrices had been in use until ASTM international published the ASTM-D8110 standard in 2017[30] The standard describes a methodology for simultaneous determination of seven elements (Al, Ca. Cu, Fe, Pb, Mg and K) from light to middle fraction petroleum distillates diluted with an organic solvent of choice. Internal standard method is used for calibration.

A previously existing method had been in use at Neste for ICP-MS analysis of varying organic matrices, including middle distillate fuel products, renewable feedstocks and various synthesis products from test reactors. The release of the ASTM D8110 standard made it topical to update and validate the in-house ICP-MS method and to ensure its compatibility with the new ASTM D8110 standard.

1.3 Experimental design

Dozens of adjustable parameters of an ICP-MS instrument and several measurable responses on multiple analytes can become a challenge, when it comes to developing and optimizing new methods. In addition, a very robust method is needed if a large variety of different sample matrices are to be analyzed in the same analysis runs. Nevertheless, the most common approach for optimization of instrumental conditions is to adjust each parameter one at the time, which is a tedious and time consuming process and might not give the best possible results. To overcome the shortcomings of these so-called *univariate studies*, *multivariate techniques* can be used instead. One such approach is to use *experimental design* or *Design of experiments* (DOE) together with regression analysis for simultaneous optimization of multiple instrument parameters.

Experimental design is a statistical approach for designing multivariate experiments in a way that allows to gather maximal amount of information from each experiment. By doing so, DOE minimizes the number of experiments needed to be performed in addition to giving more information about the behavior of the studied system, including interactions between variables. This goal is achieved by conducting experiments in a predetermined way, so that for each experiment, multiple variable values are changed simultaneously. Optimization studies using DOE are often conducted in two phases:

1. In a preliminary **screening study** the factors that have the most influence on the measured response are identified and selected for further optimization. Non-influential factors are then set to fixed values and omitted from subsequent studies to reduce the number of experiments needed. The experimental designs used in the screening phase usually have two *levels* and a *linear model* or a *second order interaction model* is used in the regression analysis. Usually additional experiments at the center of

the *experimental domain* are included in the *design matrix* and *analysis of variance* (ANOVA) is used to estimate the significance of the studied effects. Some of the most often used experimental designs for screening include: *two level full factorial design*[31], *two level fractional factorial designs*[32] and *Plackett-Burman design*[33,34].

2. In a following **optimization** stage, *response surface methology* (RSM) is used to find the optimal conditions. In RSM an appropriate experimental design with multiple levels is selected and regression analysis is used to calculate the coefficients of the used polynomial model, most often a *quadratic model* with interaction terms. After solving the coefficients of the used model, the response of the system can be mathematically modelled and the optimal values for the responses can be calculated. The most commonly used experimental designs for optimization include: *three level full factorial design*[35], *central composite design* (CCD)[36], *Box-Behnken design*[37,38] and *Doehlert design*[39,40]

Experimental designs in analytical chemistry

Although DOE and other statistical techniques can offer benefits over univariate studies when it comes to method developement, optimization and validation, these methods have seen relative little use in analytical chemistry. Nonetheless, the whole field of *chemometrics* have arised from applying methods originating from statistics and computer science to accelerate the study of chemistry. Indeed, during the last two decades several reviews have been published on how to utilize DOE in chemical sciences[32] and in analytical chemistry,[39,41] including optimization of chromatrographic systems[42,43], spectroanalytical[44,45] and electroanalytical techniques[45], ICP-OES[40], mass spectrometry[46] and food analysis[47]. Also, a book have been published on using chemometric techniques in atomic spectroscopy[48]. However, no reviews have been focused exclusively on using DOE for optimization of ICP-MS methods and the research on the subject is somewhat scarce.

1.4 The aim of the present work

The aim of the present work was to update and validate the existing in-house ICP-MS method and to investigate the possibilities of utilizing experimental designs in the ICP-MS method developement. The results of this investigation are presented in the current thesis consisting of two parts:

1. In the first part, the current state of research on applying these principles for ICP-MS method developement is reviewed and the findings are discussed.

2. The second part presents the developement and validation of two ICP-MS methods consistent with the ASTM D8100 standard. The methods can be used for simultaneous quantification of 28 elements* from various middle distillate fuels, comparable biofuels and gasoline, after simple dilution with xylene or kerosine. The developement of the first method using xylene as the solvent, included optimization of integration times in addition to optimization of sample and calibration standard matrix compositions by adjusting dilution ratios and viscosities to minimize sample transport effects.

   The development of the second method included optimizations of test sample compositions and plasma conditions (carrier gas flow rate, sampling depth) by using experimental designs and response surface methodology. In these studies desirability approach was used for multiresponse optimization to find the best overall analyte recoveries.

   Extensive validation was performed for both methods and for multiple sample matrices. The accuracy and precision of the methods were determined by analyzing spiked fuel samples. The limit of detection (LOD) and the blank equivalent concentration were evaluated for each analyte.

* Analytes included: Al, B, Na, Mg, Al, Si, P, K, Ca, Ti, V, Cr, Mn, Fe, Co, Ni, Cu, Zn, As, Sr, Mo, Pd, Cd, Sn, Ba, W, Pt and Pb.

Applying multivariate techniques on ICP-MS method development: A literature review

ICP-MS have existed as an analytical technique since the commercialization of the first ICP-MS instrument in 1983.[5] At the same time the development of computers made it possible to solve the tedious calculations required for using the DOE methods, therefore starting the modern era of experimental design.[49] However, relatively few research articles using experimental design for ICP-MS optimization have been published so far. The research using DOE is largely focused on other things and only use DOE as a means for optimization, rather as the subject of the study itself. Therefore, it is often the case that no detailed descriptions on the experimental designs and interactions between the variables are published and the literature on using experimental designs for optimization of ICP-MS methods is scarce.

This chapter gives a review on the research that have used experimental designs for development of ICP-MS methodology. Although DOE have been used for multivariate optimizations of hyphenated ICP-MS techniques[50], for optimizations focusing on specialized sampling accessories[51–54] and for method optimizations focused on sample preparation[55,56], this research is considered to be outside of the scope of the current work as the thesis is focused on optimizing the instrumental parameters of ICP-MS instruments.

While only a few studies have been using DOE for mapping the interactions between different parameters of ICP-MS instruments, some trends can be seen in the results. In some cases it is also possible to draw connections between observed interactions and the physics of ICP-MS analysis. The reviewed research is loosely divided in four sections based on the compartment of the instrument that was optimized and the physical phenomena behind the desired outcomes. These compartments include: the plasma, collision/reaction cell and the acquisition parameters of mass analyzer. After a summary of the research on each compartment and on studies in which multiple compartments have been optimized simultaneously, the findings of the research is discussed.

2 Research applying experimental design for optimization of plasma conditions

One of the most important charasteristics of ICP-MS analysis is the quality of the inductively coupled plasma. The temperature of the plasma has a direct impact on the ionization degree of analytes and on the formation of spectral interferences. In addition, the gasflows of the plasma torch impact the dimensions of the plasma and the residence time of particles in the different zones of the plasma. Therefore, these parameters define the abundance and spatial distribution of varying species in the plasma. The spatial location from which the analytes are sampled, is in turn defined by the sampling depth of the instrument. Moreover, the composition of sample matrix can have a pronounced effect on the temperature of the plasma in addition to inducing other matrix effects and sample transport effects that, can affect the solvent load of the plasma and the composition of the sample aerosol.

Because of the complex interrelations between the plasma parameters and the physical characteristics of the plasma, interactions between the parameters can be expected in optimization. Indeed, such interactions have been found in multivariate optimizations of plasma conditions for reduced or increased polyatomic ion formation and for improved signal intesities.

2.1 Application of experimental design and RSM for optimization of cool plasma conditions

A designed experiment have been succesfully used by Bianchi et al. to achieve cool plasma conditions for simultaneous determination of ^{7}Li, ^{27}Al and ^{56}Fe from beverages with ICP-MS.[57] The effect of sampling depth, plasma power, ion lens 2 voltage and coolant flow were examined and the highest global analyte sensitivity (measured as the count rate of the analytes) was found by using desirability approach and RSM.

The study used a two level full factorial (2^4) design to evaluate the interactions between the factors and possible quadratic effects. An overview of the optimization can be seen in Table 1. The experimental domain was selected based on acceptable instrumental stability of $\leq 2\%$. The experiments were performed by analyzing standard solutions with 1 μg/l of each analyte and all the measurements were replicated six times except the central experiment from which ten replicates were measured.

As all of the factors showed significant quadratic effects, the factorial design was expanded by adding star points to create a CCD design that allows modelling of the quadratic effects. The best regression models (quadratic models with second and third order interactions) for the optimization were found by using a step-wise variable selection algorithm. After model fitting, a desirability function was computed for each response and an overall desirability function D was obtained as a geometric mean of the individual desirability functions and optimal parameter values were found at the maximum of this function.

The maximum desirabilities for all analytes were found at the same location. The most important effect on the responses of every analyte was the main effect of the plasma power that had a positive correlation with the analyte responses, so that the strongest analyte

signals were achieved by using the highest plasma power. The optimal sampling depth was 855 units, which corresponds to the smallest distance between the plasma and the sampling cone. plasma power of 670 W The optimal coolant flow was 13 l/min. As with the plasma power and the sampling depth, this value corresponds to the hottest plasma conditions within the experimental domain. The optimal lens 2 potential (0.3 V) was found at the middle of the studied range. nteractions were found, mostly between the plasma power, sampling depth and the coolant flow.

After the optimization, the method was succesfully validated and the applicability of the methods was proved by succesful determination of the analytes from commercial beverages. Based on the results of the study, the optimized cool plasma conditions had significantly reduced background signal at all of the measured m/Z ratios compared to normal "hot" plasma conditions. The authors conclude that using chemometric techniques for the optimization was a succesful strategy as the OVAT approach would have failed to find the optimal conditions.

Table 1 An overview of an optimization of cool plasma conditions for simultaneous determination of Al, Fe and Li.[57]

Analytes	Variables*	Responses	Design
^{7}Li ^{27}Al ^{56}Fe	x_1=Sampling depth (588-879 units) x_2=Plasma power (570-670 W) x_3=Lens 2 potential (-1.5 to -0.5 V) x_4=Coolant flow (13-18 l/min)	Global desirability of Li, Al and Fe signal intensities	A 2^4 full factorial design extended after screening to form a CCD

* Variable levels are given for the factorial design used in the screening phase

2.2 Multivariate optimization of sample uptake, carrier gas flow rate additional gas flow rate and plasma power for optimal Hg sensitivity of an cold vapor - ICP MS method

Experimental designs have been used by Pyhtilä et al.[58] in a two step optimization of plasma parameters of a method for analyzing mercury from peatland forest ditch water samples by using cold vapor ICP-MS (CV-ICP-MS). The method was optimized for the best Hg response measured from aquaeous Hg standards (10 ng/l).

In a preliminary screening study, sample uptake rate, carrier gas flow rate, additional gas flow rate and plasma power were studied by using a two level full factorial (2^4) design. An overview of the optimization is given in Table 2 The most influential factors were found

to be the RF power, carrier gas flow rate and additional gas flow rate. An interaction was found between the gas flows, and combined gas flow with equal flow rates for both gasses was used as a factor in a following optimization step along with the plasma power. The sample uptake rate was fixed and omitted from further optimization.

After the screening study, the combined gas flow rate and the plasma power were optimized using a CCD design and RSM. The results showed an apparent interaction between the gas flow rate and the RF power. Optimal conditions of found with a combined gas flow rate of 0.86 l/min and with plasma power of 1250 W. Sample composition was furher optimized by using OVAT approach and the method was found to be suitable for quantifying mercury from natural water samples after validation.

Table 2 An overview of optimization of Hg response measured with CV-ICP-MS[58]

Analytes	Variables	Responses	Design
^{200}Hg & ^{202}Hg	x_1=Plasma power (1100-1300 W) x_2=Carrier gas + additional gas flow (1:1 ratio, 0.82-0.9 l/min total)	Hg response	CCD

2.3 Multivariate optimization of plasma conditions for simultaneous measurement of S and P as respective oxides

Ciavardelli et al.[59] have utilized experimental designs in a multivariate optimization of plasma conditions for simultaneous determination of phosphorus and sulphur as respective oxide ions ($^{31}P^{16}O^+$ and $^{32}S^{16}O^+$) from protein samples without using a collicion/reaction cell. Four factors (sampling depth, sample uptake rate, extraction lens 1 voltage and plasma power) of an ICP-QMS instument were optimized to obtain maximum blank subtracted $^{31}P^{16}O^+$ and $^{32}S^{16}O^+$ signal intensities from aquaeous standard solutions.

A two level (2^4) full factorial design was used to screen for significant factors. Each experiment of the design was performed as a triplicate and six experiments were performed at the center of the design. The experimental domain was set based on the instruments limitations and on a maximum acceptable signal stability of ($< 5\%$). Standard least squares regression was used to fit a first order model to the data and ANOVA was used to evaluate the main effects and interactions of the factors. After quadratic effects were discovered, the experimental design was extended with star points to obtain a central composite design to allow the modeling with quadratic models (See Table 3 for experimental space). Desirability approach was then used to find the best overall desirability for the phosphorus and sulphur oxide ion signals.

Both measured responses resulted in very similar response surfaces and the optimized conditions were found to be optimal for the analysis of both $^{31}P^{16}O^+$ and $^{32}S^{16}O^+$, while the highest oxide formation was found by using small plasma power (959 W) and the lowest sampling depth (4.5 mm), as expected. The sample uptake rate was found to have

a major impact on the oxide formation while the highest oxide ion intensities were found using the highest sample uptake rate (0.88 ml/min). This is thought to happen because of the increased mass transport rate of the analytes and solvent (water) delivering the oxygen atom for the analyte ions. In addition the plasma temperature is decreased due the increased solvent loading, therefore favoring the oxide formation.

Significant interactions were found between sampling depth and the sample uptake rate and between sampling depth and the plasma power. Although the extraction lens potential had a significant effect on the responses, with optimal value of 135.2 V, this factor showed no interactions with other variables.

To verify the reliability of the model, the predicted responses at the optimum were compared to experimental responses. The optimized method was furher investigated and proved to be suitable for quantifying phosphorus and sulphur from protein samples as corresponding oxide ions and for calculating the degree of phosphorylation of proteins.

Table 3 An overview of the optimization of the plasma conditions for maximum $^{31}P^{16}O^{+}$ and $^{32}S^{16}O^{+}$ signal intensities by Ciavardelli et al.[59]

Analytes	Variables	Responses	Design
P ($^{31}P^{16}O^{+}$), S ($^{32}S^{16}O^{+}$)	x_1=Sampling depth (4.5-7.5 mm) x_2=Sample uptake (0.32-0.88 ml/min) x_3=Extraction lens 1 voltage (-135.2 to -164.8 V) x_4=Plasma power (930-1370W)	y_1=$^{31}P^{16}O^{+}$ signal intensity y_2=$^{32}S^{16}O^{+}$ signal intensity	CCD

2.4 Optimization of a direct injection high efficiency nebulizer - inductively coupled mass spectrometry method by using experimental design with priciple component analysis and cluster analysis

Experimental design have been used by Kahen et. al[60] together with principal component analysis (PCA) and cluster analysis (CA) to find optimal conditions for direct injection high efficiency nebulizer (DIHEN) - inductively coupled mass spectrometry (DIHEN-ICP-MS) method for simultaneous determination of seven elements (Ag, As, Ba, Cd, Hg, Ni, Pb & V) from organic matrices. The study used a Box-Behnken design to study the effects of three factors (DIHEN position, nebulizer gas flow and intermediate gas flow) on signal intensities and signal RSD% of the analytes, on BaO^{+}/Ba^{+} signal ratio and RSD%, and on Ba^{++}/Ba^{+} signal ratio and RSD%. The experiments were performed by measuring the responses from multielement standards diluted in xylene (200 ng/g) and three replicate measurements were obtained at the center of the design. An overview of the optimization is given in Table 4.

Two components (PC1, PC2) were extracted from the data using PCA. A significant correlation to PC1 was found for analyte signals and for Ba^{++}/Ba^{+} ratio. This indicates a similarity between the responses measured under different operating conditions. In contrast the BaO^{+}/Ba^{+} ratio was found to form a separate group with correlation to PC2, demonstrating a different behavior compared to the other responses.

To optimize the method, individual response functions $\hat{y}_i$ were calculated for every response. Two overall response functions $\hat{R}(\hat{y}_1, \hat{y}_2 \ldots, \hat{y}_i)$, one for signal intensity and another for signal RSD%, were then calculated for both groups of analytes/responses as a weighed geometric means of the individual response functions. This way four overall response functions were obtained: one for analyte signal intensities and for Ba^{+}/Ba^{++} ratio, another for analyte signal RSD% and for Ba^{+}/Ba^{++} ratio RSD%, third for BaO^{+}/Ba^{+} ratio and fourth for BaO^{+}/Ba^{+} ratio RSD%.

The best R values were obtained by using a short distance between the DIHEN tip and the plasma together, with a low Carrier gas flow rate. The DIHEN tip position was found to be the most influential variable on the overall analyte sensitivity, while the sensitivity was the highest with tip position of 3-4 mm, carrier gas flow rate of 0.10-0.12 l/min and intermediate gas flow of 1.5-1.7 l/min. These values were selected to be the best operation conditions. The best precision was obtained with slightly smaller nebulizer gas flow of 0.12-0.14 l/min.

The maximum BaO^{+}/Ba^{+} response was obtained with higher DIHEN tip position (5-7 mm) with intermediate gas flow rate of 1.7 to 1.9 ml/min and carrier gas flow rate of 0.12-0.13 l/min.

After the optimization, the precision, accuracy and detection limits of the method were investigated and the method was found to be precise and accurate method for trace metal analysis.

Table 4 An overview of the optimization of a new DIHEN-ICP-MS method performed by Kahen et al.[60]

Analytes	**Variables**	**Responses**	**Design**
V, Ni, Ba^{++}, As, Ag, Cd, Ba, BaO, Hg, Pb	x_1: DIHEN tip position (3-8 mm) x_2: Carrier gas flow (0.10-0.15 l/min) x_3: Auxiliary gas flow (1.5-2.1 l/min)	Analyte signal intensities BaO^{+}/Ba^{++} signal ratio Ba^{++}/Ba^{+} signal ratio Analyte signal RSD% BaO^{+}/Ba^{++} signal RSD% Ba^{++}/Ba^{+} signal RSD%	Box-Behnken

2.5 Utilizing experimental design to investigate the effects of nitric acid concentration and sample inlet flow rate on relative signal intensities

Tangen and Lund have examined[61] the effects of nitric acid concentration and sample inlet flow rate on the signal intensity of thirteen elements measured from aquaeous standards with an ICP-MS instrument equipped with a microconcentric nebulizer. As internal standard (^{103}Rh) was used in the study, the results give information on how the experimental conditions effect the plasma conditions, as using an ISTD compensates for sample import effects. The two factor study with 11 experiments used a central composite design with three center points. See Table 5 for an overview of the study.

Standards (10 or 100 μg/l) prepared with varying nitric acid concentration (0.14-2.8 mol/l), standards prepared in distilled water and blank samples for each matrix were measured by using varying uptake rate (34.5-172.5 μl/min). Blank subtracted analyte signals from the standard solutions were normalized with respect to ISTD signals after which the processed signals from the water matrix were substracted from the normalized signals of the acid matrix. The calculations were perfomed for each experiment and the results of the substraction were used as responses for each experiment. After the measurements, partial least squares regression (PLSR) was used for response surface modelling with a model accounting for the main effects, quadratic terms and second order interaction between the factors.

The data analysis revealed that although both factors, the nitric acid concentration and the sample inlet rate, had significant effects on the measured responses of most analytes, the results showed no significant interaction between the nitric acid concentration and the sample introduction rate, so the term was omitted from the RSM model. All the other effects were significant for the responses of one or more studied analytes. The effect of liquid flow rate was found to be less important compared to the effect of nitric acid concentration, as the flow rate only had significant effect on Ag.

The PLSR showed correlations between the studied analytes and the analytes were found to form three groups. For the first group (Cr, Pb, Tl, U and V) of analytes the signal was found to increase relative to Rh with increasing acid concentration, for the second group of elements (Ag, Cd, Se, Te and Zn) the signal intensity was found to decrease relative to Rh and for the last group (Mo) the relation was unchanged. This behavior was correlated with the first ionization potential of the elements, while the elements in the first group had lower ionization potential compared to Rh and the elements of second group had lower ionization potentials compared to Rh.

According to the authors, the results might be a result of cooling of the plasma, as cooling caused by increased acid concentration reduces the ionization efficiency of the elements so that the effect is more pronounced on elements having higher first ionization potential. As the relative signal intensities of Mo and Rh remained unchanged with varying acid concentration, Rh could be used as an ISTD for Mo to compensate for the acid effect. The authors suggest that similarily for other elements studied, internal standards could be selected from the same group of elements having the same distinct behaviour in

the study. It is concluded that although predicting the behavior of internal standards and analytes is difficult on strictly theoretical basis, multivariate mapping methods could provide an useful tool for selection of suitable internal standards.

Table 5 Overview of the study by Tangen and Lund[61]

Analytes	Variables	Response	Design
Ag, As, Cd, Cr, Mo, Pb, Rh, Se, Te, Ti, U, V & Zn	x_1=HNO_3 conc. (0.14-2.8ml/min) x_2=Sample uptake (34.5-172.5 μl/min)	Signal intensity relative to ISTD (Rh)	CCD

2.6 Using experimental design to optimize mixed Ar-N_2 plasma for increased robustness

Agatemor and Beauchemin have investigated[23] the benefits of using mixed Ar-N_2 plasma for reduction of matrix interferences on 17 analytes. The study used factorial designs in a two step optimization to achieve robust plasma conditions. First nebulizer gas flow (Ar) and sampling depth were optimized with fixed sheath gas (N_2 added to the auxiliary gas flow (Ar)) and fixed additional nitrogen gas flow added to the plasma gas (Ar). The fixed N_2 flows were optimized in a subsequent step, while keeping the nebulizer flow and the sampling depth fixed.

The optimization of the nebulizer gas flow and the sampling depth was performed by measuring two multielement standard solutions (10 μg/l), one containing 0.1 M of NaCl and another Na-free solution, prepared in 2% HNO_3. The ratio of the blank substracted signal intensity from the Na-matrix to the blank substracted signal from Na-free matrix was used as the response. The full factorial design used in the study had four levels for sampling depth and six levels for nebulizer gas flow. See Table 6 for an overview and for the experimental space.

Contour plots of the relative signal intensities measured from the two matrices were plotted and all the elements were found to have similar responses. However, the authors do not mention the model used as the response function. Small nebulizer gas flows were found to produce the most robust plasma, a finding consistent with previous experiments. The sampling depth on the other hand was found to have little effect on the relative signal intensities. Factor values were selected to give good average responses for the analytes and the optimal values of nebulizer gas (0.80 l/min) and sampling depth (5.0 mm) were fixed for the following optimization step.

A second optimization study (Table 7) with fixed nebulizer gas flow and sampling depth was conducted to optimize the N_2 flow rates of the plasma and sheath gasses. The optimization used a full factorial design with six levels for the sheath gas flow and 5 levels for the plasma gas flow. The experiments were conducted the same way as in the first stage

of the optimization and the relative signal intensity from different matrices (with Na and without Na) was used as the response.

The results of the second optimization stage showed that the both N_2 gas flows were found to reduce the matrix effects, while the best signal ratio for most analytes was achieved with intermediate rate for plasma gas N_2 flow (0.02 l/min) and sheath gas flow (0.09 l/min). The effect of adding N_2 to the plasma gas is said to be in agreement with previous research demonstrating reduced matrix effects by shaping the size and volume of the plasma in addition to increasing the temperature and electron density of the plasma.

The optimized method was characterized by evaluating the sample introduction efficiency, robustness, spatial ion distribution in the plasma, sensitivity and detection limits of the method. The features of the mixed gas plasma were then compared to those measured with of a robust Ar plasma. The mixed plasma was found to give improved detection limits and reduced matrix effects for some elements, while the Ar plasma was found to give superior results for other elements. The new method was used to determine U (2.6 μg/l) and Mo (9.6 $\pm$1 μg/l) from a certified sea water sample and the results were in an agreement with the certified values.

Table 6 Optimization of nebulizer gas flow rate and sampling depth for a robust N_2-Ar plasma.[23]

Analytes	**Variables**	**Response**	**Design**
Li, Be, Al, V, Co, Mo, Ru, Rh, Pd, Ce, Ir, Pt, Ti, Pb, Bi, Th, U	x_1=Nebulizer gas flow (0.7-1.2 l/min) x_2=Sampling depth (5-7 mm)	Signal ratios of the analytes measured from sample matrices with an without Na	Full factorial with 6 levels for x_1 and 4 levels for x_2

Table 7 Optimization of N_2 sheath gas flow rate and amount of additional N_2 mixed with plasma gas (Ar) for a robust N_2-Ar plasma.[23]

Analytes	**Variables**	**Response**	**Design**
Li, Be, Al, V, Co, Mo, Ru, Rh, Pd, Ce, Ir, Pt, Ti, Pb, Bi, Th, U	x_1=Sheath gas (N_2) (0.00-0.15 l/min) x_2= Additional N_2 in the plasma gas (0.00-0.04 l/min)	Signal ratios of analytes measured from sample matrices with an without Na	Full factorial with 6 levels for x_1 and 4 levels for x_2

2.7 Optimization of carrier gas and auxiliary gas flow rates to minimize oxides and doubly charged species

De Souza *et al.* have used[62] a central composite design for the optimization of plasma power, nebulizer gas flow (Ar) and auxiliary gas flow (Ar) to achieve maximum ISTD (In) sensitivity with minimum production of oxides and double charged species when measuring multiple analytes from oil matrices diluted in xylene. In addition to the varying flow of argon, a fixed supply of oxygen (0.1 l/min) was delivered to the nebulizer gas stream. Each experiment was performed as a duplicate and the following responses were measured from standard solutions diluted in xylene (50 μg/kg): In signal intensity, LaO^+ signal intensity and Ba^{++} signal intensity. The experimental space is not given in the research article.

Both, the Ba^{++} and the LaO^+ responses are mentioned to have minimum values with plasma power of 1300 W. Optimal conditions for the gas flows were found to be within a region bounded by carrier gas flow of 0.34 to 0.42 l/min and optional gas flow of 1 to 1.2 l/min. Both the maximum In^+ response and minimum LaO^+ response were achieved by using optimized conditions. However, these conditions did not result the best (minimum) response for Ba^{++}

A subsequent univariate studies were conducted to further define the optimal gas flows and to optimize DRC conditions. The optimized method was tested on lubricating oil samples and biodiesel samples with good results.

2.8 Multivariate optimization of plasma gas flows for optimal analyte sensitivities

Woller et al.[63] have used experimental design together with simplex optimization to optimize parameters of micro concentric nebulizer (Carrier gas flow, auxiliary gas flow and plasma gas flow) in the purpose of developing a a method for determining redox species of arsenic and selenium with hyphenated anion-exchange chromatography-ICP-MS. The optimization experiments were performed by measuring the signal intensity of the elements in a standard solution containing 10 ng/l of Mg, Rh, Pb, Ce and Ba. As all elements were found to have similar behaviour, the Rh signal was used as the response in the optimization.

In the first stage of the optimization the linear effects and variable interactions were studied with a 2^3 factorial design having an additional experiment at the center and with each experiment performed as triplicate. Based on the results, the linear model used with the design was insufficient to describe the response. To account the quadratic effects, star points were added to the design to form a central composite design (Table 8).

Analysis of the results showed that the carrier gas flow has the most influential effect on the response. The plasma gas flow also showed significant effects, although less pronounced compared to the carrier gas flow. In contrast, the auxiliary gas flow showed only a very small effects. A significant but small interaction was found between carrier gas flow and auxiliary gas flow. The quadratic effects had minor influence on the response. A good agreement between predicted and experimental values was found.

The optimal flow rates were determined, by using simplex algorithm, to be 0.9 l/min

for nebulizer gas flow, 14.5 l/min for plasma gas flow and 0.9 ml/min for auxiliary gas flow.

After optimizing the gas flows the formation of oxides and double charged species were evaluated in addition to signal stability and noise level. A subsequent optimization of chromatographic separation of As and Se species was performed and the analytical charasterictics of the method were examined and the method was found to have an excellent repeatability and accuracy in addition to sufficient LOD for As speciation analysis.

Table 8 Overview of a multivariate optimization of plasma gasses by Woller et al.[63]

Analytes	**Variables**	**Response**	**Design**
^{103}Rh, ^{24}Mg & ^{208}Pb	Carrier gas flow rate (0.68-0.968 l/min) Plasma gas flow rate (13.32-16.68 l/min) Nebulizzer gas flow rate (0.632 - 0.968 l/min)	Analyte signal intensities	CCD

3 Research using experimental design to optimize collision/reaction cell parameters

Experimental designs have been used for simultaneous optimizations of several CRC parameters, such as multiple electrical potentials inside an ICP-MS instrument and the flows of reaction/collision gasses used to discriminate spectral interferences in order to improve the signal to background ratio of analytes. As kinetic energy discrimination is often used to remove polyatomic interferences, the parameters affecting the kinetic energy distribition of ions or the potential energy barrier between CRC and mass analyzer, can be expected to have interactions when optimizing a CRC. Indeed, this is true for many instrument parameters.

3.1 Optimization of CRC parameters for optimal signal to background ratio

Kadar et al.[64] have used experimental designs in an optimization of hexapole reaction/collision cell conditions to reduce spectral interferences when analyzing multiple elements (V, Cr, Co, Ni, As and Se) from various foodstuffs with ICP-QMS. A central composite design was used to optimize He flow, H_2 flow, hexapole bias and quadrupole bias to obtain the best possible signal to background ratio (SBR) (Table 9).

The signal to background ratio of each analyte was obtained by dividing blank substracted analyte signals, measured from aqueous multi-element standards (10 μg/l), with analyte signals measured from a blank solution. A quadratic polynomial model was fitted and validated for the SBR response of each analyte. A weighted average of the SBR responses of different analytes was then calculated for each experiment and a quadratic polynomial model was fitted to the averaged SBR responses of the experiments to obtain the response function.

Statistical analysis using ANOVA showed that the quadratic model was adequate for predicting the SBR response within the experimental space. All the linear and quadratic effects of the factors were found to be significant, in addition to all the second degree interactions between the variables. It was found that the highest CRC gas flows produced the best SBR response. However, to maintain good sensitivity and to avoid any pressure regulation problems, smaller gas flows were selected to be used in the method. Better SBR was obtained with the total gas flow by using either one of the CRC gasses alone. Due to the fact that H_2 forms secondary inteferences in the CRC, He was chosen to be used as a collision gas (4.5 ml/l) with a small additional H_2 flow (0.5ml). The highest hexapole and quadrupole biases were found to produce the best spectral interference reduction and the best SBR. The optimized values for hexapole and quadrupole biases were -9.5 V and -13.2 V respectively. It should be noted that kinetic energy discrimination do not happen with these voltages as there is no potential barrier between the hexapole and quadrupole.

After the CRC optimization, the CRC parameters were fixed and the carrier gas flow was decreased in a subsequent optimization step to minimize non-spectral interferences. The method was then validated and found to be suitable for the determination of all sevent

analytes from digested food samples.

Table 9 Overview of an experimental design used for CRC optimization by Kadar et al.[64].

Analytes	Variables	Response	Design
As Co Cr Fe Ni Se V	x_1=He flow rate (0.5 - 5 ml/l) x_2=H_2 flow rate (0.5 - 5 ml/min) x_3=Hexapole bias (-9.3 to -1.3 V) x_4=Quadrupole bias (-20.0 to -9.0 V)	Weighed average of the signal to background ratios of the analytes	CCD

3.2 Optimization of collision/reaction cell parameters of a vapor generator - ICP-MS method to achieve optimal sensitivity for ^{32}S

Colon et al.[65] have used experimental designs in the development of a new method for quantifying total reduced sulphur in natural waters. To avoid oxygen based polyatomic interferences overlapping with ^{32}S, ^{33}S or ^{34}S signals, the method uses a vapour generator coupled to an ICP-QMS instrument (VG-ICP-MS) so that the sulphur present in samples is converted to gaseos hydrogen sulfide prior introduction into the plasma, therefore preventing the formation of interfering oxygen species by removing the aquaeous sample matrix. However, this approach by itself was not sufficient for reducing the signal background enough to allow the determination of sulphur, so collision/reaction cell was utilized to reduce the background.

To maximize the sensitivity of the method, multiple collision/reaction cell parameters were simultaneously optimized in a three phase multivariate optimization. The experiments were performed by measuring a blank solution and a sulfide standard solution μg/l in duplicates and the slope of the ^{32}S calibration curve was used as the response in all phases of the optimization.

In the first phase, a fractional factorial design was used to screen for significant instrument parameters (octopole bias, quadrupole bias, cell exit potential, He flow and H_2 flow). As the results showed that the H_2 flow (1-7 ml/min) and cell exit potential (-9 to -13 V) did not affect the instruments sensitivity with the studied factor levels, the parameters were set to fixed values for the rest of the optimization.

A following optimization stage using a 2^3 full factorial design with three replicates at the center was then used to study the interactions of the remaining factors: octopole bias, quadrupole bias and He flow rate (see Table 10 for experimental space). The evaluation of the results with ANOVA showed that with the studied factor levels, the octopole bias and He flow rate had statistically significant effects on the response, while the quadropole bias did not. The only significant interaction between the variables was the interaction between

the octopole bias and He flow rate. As the quadrupole bias did not affect the sensitivity, it was set to a fixed value for further studies.

As an interaction was found between the octopole bias and He flow rate, it was necessary to optimize these variables by using a multivariate technique. Therefore, a simplex optimization was utilized in the optimization and the maximum sensitivity was found by the simplex algorithm at vertex 23. The best sensitivity was obtained with octopole bias of -3.8 V and He flow rate of 0.7 ml/min. The optimized parameters were used in evaluation of the performance of the new method. The reliability of the method with optimized instrument parameters was confirmed by comparing the results to results obtained with a potentiometric reference method and the new method was succesfully applied to natural water samples.

Table 10 Overview of the second phase of the optimization of a new method for determination of S from natural waters performed by Colon et al.[65]

Analytes	Variables	Response	Design
^{32}S	x_1=Octopole bias (-12 to -3.4 V) x_3=Quadrupole bias (-10 to -6 V) x_3=Helium flow rate (0.5 to 8 ml/min)	^{32}S Calib. curve slope	2^3 full factorial

3.3 Multivariate CRC optimization of selenium-79 determination from spent nuclear fuel

Brennetot et al.[66] have conducted a two phase study utilizing experimental designs to optimize an ICP-MS method for determination of ^{79}Se from spent nuclear fuel. The study was designed to minimize an $^{39}Ar^{40}Ar_2^+$ interference on ^{79}Se by simultaneous optimization of multiple plasma and CRC parameters. The experiments were conducted by measuring aqueous Se standards (5 ppb) and blank samples. Two responses were used in the optimization: signal intensity at m/Z 80 corresponding to ^{80}Se signal measured from the Se solutions and signal intensity at m/Z 80 corresponding to $^{40}Ar_2^+$ background measured from the blank solutions.

A Plackett and Burman design consisting of 14 experiments including two central experiments, was used in a screening phase to assess the influence of 10 factors (extraction potential, focus, pole bias, hexapole bias, nebulizer gas flows, auxiliary gas flow, DA potential, D2 deflector potential, O_2 reaction gas flow and collision gas flow). The experiments of the screening design were repeated four times using a different collision gas (He, Ar, Ne or N_2) in combination with oxygen, and once using oxygen as the only CRC gas in a 9 factor design.

The analysis of the results with ANOVA showed that all the studied factors had significant effects on the responses, except the D2 deflector potential, that showed no significant effects on either of the studied responses. The factor was therefore fixed and omitted from further study. The relative importance of the significant effects was similar regardless of the studied reaction+collision gas mixture. Although the nebulizer gas and auxiliary gas flows showed significant effects on Se and $^{40}Ar_2^+$ signals, the factors were set to fixed values for the rest of the optimization to simplify the design and to avoid taking into account an expected interaction between the gas flows.

As many of the studied factors showed quadratic effects, a Doehlert design was used in a subsequent optimization step to account for these effects and to optimize the extraction potential, focus potential, pole bias, hexapole bias, DA voltage, O_2 flow rate and collision gas flow rate (see Table 11 for the factor values). As in the screening, independent optimizations were performed with oxygen as the only CRC gas and for O_2 combined with one of the collision gasses (He, Ar, Ne or N_2). A Doehlert design with more than two factors has 3, 5 or 7 levels depending on the variable, this makes it a non-rotable design. Therefore, the level values for the studied factors were selected so that the factors showing the most pronounced effects in the screening were set to have most levels to gain maximum amount of information from these factors.

ANOVA of the responses showed that the significant effects were the same found with the screening design and that the studied variables showed comparable effects with different collision/reaction gas mixtures. The significant effects were the same for the ^{80}Se response and for $^{40}Ar_2^+$ response with minor differences. The linear effects of the hexapole bias, pole bias, focus and extraction potential were found to be significant for both responses while the quadratic effects of hexapole bias and pole bias were only significant for the ^{80}Se response.

Two factors were found to have an opposing effect depending on the response. The hexapole bias had a positive effect on the $^{40}Ar_2^+$ response while a negative effect was observed for the ^{80}Se signal. On the other hand, the extraction potential had a negative effect on the $^{40}Ar_2^+$ signal and a positive effect on the ^{80}Se signal. The opposing effects of these parameters made them important factors to optimize for achieving the best signal to background ratio by increasing the extraction potential and decreasing the hexapole potential.

No notable interactions on Se sensitivity between studied factors were found. In contrast, when the background measured from blank samples was examined, the following interactions were observed: an interaction between the hexapole bias and the O_2 flow rate, between the pole bias and the focus and between the O_2 flow and the He flow. These interactions can be expected as all the factors affect on the kinetic energy of the ions and therefore the discrimination of the interferences. The response surfaces for $^{40}Ar_2^+$ signal and for the ^{80}Se signal had differing shapes. This made it possible to find a common area of interest in the experimental domain, giving the best possible Se signal intensity, with the least amount of interference.

Further analysis showed that the selection of the CRC gas had a pronounced effect on the responses. The responses with optimized CRC gas flows were compared and the highest

desirability accounting for both Se^+ sensitivity and for Ar_2^+ was achieved by using O_2 (0.61 l/min) - He (8 l/min) mixture. While a better sensitivity was achieved by using O_2 alone, the interference reduction was less sufficient.

After the optimization, method was tested on a real spent nuclear fuel sample.

Table 11 An overview of the optimization of CRC parameters for optimal signal to background ratio for ^{79}Se determination from spent nuclear fuel with ICP-MS[66]

Analytes	**Variables**	**Responses**	**Design**
Se	x_1=Hexapole bias (-1.5. to 1.5 V) x_2=Extraction potential (-730 to -514) x_3=Pole bias (-7.8 to -3.6 V) x_4=Focus voltage (3.6-8.4 V) x_5=DA potential (-54 to -20 V) x_6=O_2 flow rate (0.48 0.61 ml/min) x_7=He flow rate (4.5-6.5 ml/min)	y_1=^{80}Se sensitivity, y_2=$^{40}Ar_2^+$ background	Doehlert design

4 Optimization of acquisition parameters

Multiple acquisition parameters have been simultaneously optimized by using DOE. These parameters are used to define the behavior of the mass filter used to separate the analytes. If sustained signals are measured instead of rapid analyte pulses formed by LA-ICP-MS or hyphenated chromatographic techniques, these parameters, with the exception of measurement time, should not affect the precision of the measurements according to counting statistics. However, the ideal world where all the noise is random by nature does not exist, so there can be a need for optimization of the acquisition parameters.

4.1 Optimization of acquisition parameters for determination of lead isotope ratio

Quetel et al.[67] have used a 2^4 full factorial design to optimize acquisition parameters of an ICP-QMS instrument in order to find the best possible conditions for determination of lead isotopic ratios. The studied factors included the following quadrupole parameters: measurement dwell time, number of replicates per measurements and sweeps per replicate. As ^{204}Pb is less abundant compared to other stable isotopes of lead (^{206,207,208}Pb) a "time factor" was added as a fourth factor to increase the dwell time at m/Z 204. The dwell time of the measurements of ^{204}Pb was set to a be the product of the "time factor" and the dwell time of the other isotopes to obtain more counts from the weaker signal. See Table 12 for an overview of the factors and responses included in the study.

The experiments of the optimization study were performed by measuring the four isotopes of lead from an aquaeous isotopic lead standard (50 ng/ml) with varying acquisition parameters. Each experiment of the design was repeated five times, except the center experiment from which nine replicates were measured, and the average precision of the measurements was calculated together with mass bias. The precision of the measured isotope ratios was used as a response. Multiple linear regression was used for model fitting and ANOVA was used to estimate the influence of the factors.

The precision of the measured isotope ratios varied between from 0.08% and 1.96% between the experiments. The data analysis revealed that the time factor had the greatest effect on the precision of the studied isotope ratios. As the time factor alters the measurement time of ^{204}Pb, increased precision of the isotope ratios of including this isotope can be expected. Suprisingly, the same behavior was found also with precisions of ^{206}Pb/^{207}Pb and ^{208}Pb/^{206}Pb ratios as well. The authors suppose that the unexpected behavior is caused by changes in the duration of the measurement sweeps so that non-random noise is filtered out with particular measurement intervals. Based on this hypothesis, the frequency of the noise was estimated to be within a frequency range of 3.6 to 14.3 Hz.

The number of replicates and the number of sweeps per replicate were also found to have a significant effects on the precision. Only two interactions were found between the studied factors: an interaction between the time factor (determinig number of replicates for ^{206}Pb/^{204}Pb ratio), and between the time factor and dwell time for ^{207}Pb/^{204}Pb. The dwell time on it self had little effect on the precision.

The best precision for routine analysis (with measurement time less than 10 minutes) was found using high number of sweeps per replicate, a high number of replicates and a high time factor i.e. high dwell time for ^{204}Pb together with short dwell time for other analytes.

The effect of the mass counting mode i.e. the number of points measured at particular m/Z, was studied with further experiments and better precisions were obtained by measuring three points per peak compared to one point per peak. Finally the reproducibility and repeatibility of the method were estimated in measurements over several weeks and the precision of the method was found to be within (0.1-0.35%), while the best obtained precisions were found to be close to the precision predicted by counting statistics (0.05 - 0.7%).

Table 12 An overview of the acquisition parameter optimization performed by Quetel et al.[67] to maximise the precision of lead isotope determination

Analytes	**Variables**	**Responses**	**Design**
^{204}Pb, ^{206}Pb, ^{207}Pb, ^{208}Pb	x_1=Measurement dwell time (25-75 ms) x_2=Sweeps per replicate (10-40) x_3=Replicates per analysis (5-15) x_4="Time factor"* (5-13)	y_1=precision of ^{206}Pb/^{204}Pb ratio y_2=precision of ^{207}Pb/^{204}Pb ratio y_3=precision of ^{208}Pb/^{204}Pb ratio y_4=precision of ^{206}Pb/^{207}Pb ratio y_5=precision of ^{208}Pb/^{206}Pb ratio	2^4 full factorial

* The dwell time used for the ^{204}Pb measurement was set by the "time factor" to be $x_1 \times x_4$.

5 Simultaneous optimization of multiple instrument compartments

Studies have been conducted for simultaneous optimization of plasma parameters, CRC parameters and acquisition parameters. As plasma conditions can affect the kinetic energy of ions, there is a theoretical possibility for interactions between the plasma parameters and CRC parameters. In addition periodical fluctuations in analyte signal can cause issues if they interfere with the acquisition parameters. Based on these hypothetical interactions, the use of multivariate methods to simultaneously optimize different instrument parts could offer benefits over univariate optimization.

5.1 Simultaneous optimization of multiple plasma, CRC and aquisition parameters for optimal Gd sensitivity

Brennetot et al.[68] have optimized analytical conditions of a multiple collector ICP-MS (MC-ICP-MS) method for isotopic analysis of gadolinium measured from nuclear waste, by using experimental designs. The aim of the two step optimization was to provide the best possible gadolinium signal intensity and mass bias stability. The sector field instrument used, was equipped with a hexapole CRC. The signal intensities and signal RSD of six gadolinium isotopes were used as responses in both stages and all the experiments were performed by measuring aqueous Gd standard solution (200 ppb).

A preliminary screening study with a Blackett-Burman design was performed to evaluate the influence of ten factors, including seven instrument parameters (nebulizer, and plasma gas flow rates, plasma power, torch position, cone potential, CRC argon flow and hexapole RF power) and three acquisition parameters (Integration time, number of sweeps and number of blocks). The experimental design consisted of 14 experiments including two additional experiments at the center of the design.

Statistical analysis using ANOVA and regression analysis based on a first order model, revealed that the nebulizer gas flow, hexapole RF power and cone potential had the most significant impact on the Gd signal intensity on every measured isotope. The results also showed significant curvature, indicating an expected lack of fit of the first order model. No factors were found to influence the RSD of the signal.

As the nebulizer gas flow, hexapole RF power and the cone potential had the most prominent effect on the signal intensity, these factors were included in the following optimization step. Although showing only minor significance in the screening, the CRC argon flow rate and auxiliary gas flow were included in the optimization step. As the both factors affect the kinetic energy distribution of ions, it was assumed that they might have interactions not resolved by the first order model used with the Blackett-Burman design. The rest of studied factors were set to fixed values and omitted from the optimization step as insignificant.

The optimization step of the study used a CCD consisting of 44 experiments to optimize the remaining five factors (see Table 13 for the experimental space). Statistical analysis with ANOVA and regression analysis showed that the CRC gas flow rate, nebulizer gas flow,

cone potential and the hexapole RF power had significant effects on the response. The only significant interaction between the factors was found to be a first order interaction between nebulizer gas flow rate and auxiliary gas flow rate, therefore also a change in auxiliary gas flow affects the response.

The flow rate of 0.9 l/min was found to be optimal for both, the nebulizer gas and for the auxiliary gas. The interaction between the gas flows implies, that to get the best possible response, the total gas flow should remain unchanged if the gas flows have to be changed i.e. one of the gas flows should be decreased if the other one is increased.

Desirability approach was used to find optimum conditions to produce the best overall signal intensity for all gadolinium isotopes. The best response was achieved with CRC gas flow rate of 1.14 ml/min, nebulizer and auxiliary gas flows of 0.9 l/min cone potential of 700 V and hexapole RF power of 100 %.

The robustness of the optimized method was tested by measuring gadoline standards and an excellent agreement between the predicted response and an experimental response measured using the optimized parameters. The optimized method was used to determine the ^{158}Gd/^{238}U ratio in a spent nuclear fuel sample and the method was found to be very accurate.

Table 13 An overview of the second phase of the optimization of isotopic Gd analysis to maximize the Gd sensitivity[68]

Analytes	Variables	Response	Design
^{154}Gd, ^{155}Gd, ^{156}Gd, ^{157}Gd, ^{158}Gd, ^{160}Gd	x_1=CRC gas (Ar) flow rate (0.42-1.38 ml/min) x_2=Nebulizer gas flow rate (0.66-1.14 l/min) x_3=Cone potential (415-985 V) x_4=Hexapole RF potential (53-100 V) x_5=Auxiliary gas flow rate (0.66-1.14 l/min)	Overall signal intensities of the Gd isotopes calculated by desirability approach.	CCD

5.2 Multivariate optimization of multiple instrumental parameters to optimize the precision of an Pu analysis

Stürup et al.[69] have studied the influence of dwell time, number of sweeps per measurement and sample uptake rate to optimize the precision of an SF-ICP-MS instrument for determination of plutonium isotopes. The optimization was carried out by using a CCD with four center experiments. In each experiment an aquaeous plutonium sample (10 pg/ml of ^{239,240}Pu) was measured with varying instrument parameters and the RSD of the measurements was used as a response. The dwell times for ^{239}Pu and ^{242}Pu measurements

were set to equal. As ^{240}Pu was less abundant isotope in the samples the dwell time was set to be 4.5 times higher compared tothe dwell time for ^{240}Pu.

A quadratic model was fitted to the data and the following effects were found to be significant: the linear effects of each factor, the quadratic effect of the dwell time and the the interaction between number of sweeps and sample uptake rate. The sample uptake rate and the number of sweeps were found to be the most influential factors, while the dwell time had little effect on precision.

The optimum precision was found with high sample uptake rate (1.15 ml/min) and high number of sweeps (65) and dwell time (4ms), yet acceptable precision (RSD < 1.5) was found with broad range of parameter values. Although good conditions were found at the edge of the experimental design, the optimals conditions were selected well within the experimental domaint to obtain more precise prediction for the RSD. The optimized precision ^{240}Pu/^{239}Pu was found to be near theoretical precision limited by counting statistics and comparable previous methods.

The optimized method was used for determining plutonium isotopes from prepared soil samples and the accuracy of the isotope ratio measurement confirmed by comparison to α-spectrometry and spectral convolution.

Table 14 An overview of a multivariate optimization of the precision of an Pu analysis by St"urup et al.[69]

Analytes	**Variables**	**Response**	**Design**
^{239}Pu, ^{240}Pu & ^{242}Pu	x_1: Dwell time (1-5 ms for ^{239}Pu) x_2: Number of sweeps per measurement (48 - 82 per isotope) x_3: Sample uptake rate (0.3-1.5 ml/min)	Precision of ^{240}Pu/^{239}Pu signal ratio	CCD

6 Discussion

6.1 Multivariate optimization of plasma conditions by using experimental design

The most research on optimizing plasma conditions with DOE have focused on improving the sensitivity or SBR of the studied methods by increasing the ionization degree of analytes and by controlling the oxide formation in the plasma. The formation of single charged species often go hand in hand with the formation of oxides as both are controlled by the plasma temperature while increasing the temperature increases the ionization degree of the analytes, while the oxide formation is higher within the cooler regions of the plasma.

The opposite of these species behavior is clearly visible in the response surfaces plotted by De Souza et al.[62] showing the opposite behaviors of these responses with varying nebulizer gas flow and auxiliary gas flow, while the optimal gas flow rates produced both the highest In signal and the lowest LaO^+ signal. In contrast the measured Ba^{++} response was similar to the In response, so that the formation of double charged species could not be avoided while maintaining a good alalyte signal.

Similar trend is visible in the response surfaces plotted by Kahen et al.[60] showing BaO^+/Ba^+ response and a combined response for multiple analytes and for Ba^{++}/Ba^+ with varying DIHEN tip position, nebulizer gas flow and auxiliary gas. Based on the PCA analysis conducted by Kahen et al. signal intensities of multiple analytes had similar responses with each other and with Ba^{++}/Ba^+. While the BaO^+/Ba^+ response formed another group by itself.

In addition Ciavardelli et al.[59] and Agatemor et al.[23] found that the signal intensities of different analyte ions had very similar response surfaces. Therefore the simultaneous optimization of signal intensities of multiple analytes together with reduced oxide formation is a reasonable goal as the same conditions provide the best response for all the analytes.

However this might not be the case for responses other than sensitivity. Based on the work from Tangen and Lund[61], when signal intensities normalized to an ISTD (Rh) are used as responses, different analytes have very different responses on varying nitric acid concentration and sample inlet flow. This is thought to be a result of plasma cooling. Similar behavior is seen in the results of the expertimental part of this thesis, where large variation between recoveries of different analytes was observed with varying carrier gas flow and nebulizer flow rate and dilution ratio, when using ISTD for calibration. Tangen and Lund suggested, that using multivariate mapping methods to group elements based on their behavior could be used to find a suitable ISTD for each group of elements. Although, desirability approach can be used to find succesfully to find the best global desirability of plasma conditions as illustrated by Bianchi et al.[57], the result is always a compromize between different responses.

The fact that Tangen and Lund have demonstrated a possibility to use multivariate mapping methods to group elements based on their responses opens interesting possibilities to deal with situations, where multiple responses have very different response surfaces and are therefore in conflict with each other. Unsupervised learning methods could be used to find suitable internal standards for multiple analytes, so that the relative signal intensities

of the analytes and their corresponding ISTDs would remain unchanged in different plasma conditions. Multivariate optimization could then be used to optimize the sensitivity of the analytes, so that the relative signals would remain unchanged and the optimal sensitivity would be optimal for all the analytes.

As expected, multiple interactions have been found between different plasma parameters. These include interactions between plasma power, sampling depth and Coolant gas flow[57]. An interaction between nebulizer gas and additional gas, in addition to combined gas flow and plasma power.[58] Between the sampling depth and sample uptake rate, and an interaction between sampling depth and plasma power[59]. In addition, Brennetot et al.[68] found an interaction between nebulizer and auxiliary gas flows, which brought a situation where the both gasses had to changed/optimized simultaneously for optimal performance. As the detected interactions depend on the selection of the experimental space, the list should not be considered all-inclusive, as not all interactions might be present in each optimization and all possible interactions might not have been found as only a few studies have been used DOE for plasma optimization for ICP-MS.

Neverheless, interactions should be expected between the gas flows, sampling depth and sample introduction rate. To overcome the challenges caused by these interactions, multivariate techniques should be preferred when optimizing the plasma conditions. Previous reseach can help to map the possible interactions so that suitable experimental designs and regression models can be used for efficient optimization. As the sample introduction system and the inductively coupled plasma is very similar in ICP-OES and in ICP-MS, literature on multivariate optimization of ICP-OES methods can also give additional advice on how to desing experiments for ICP-MS plasma optimization.

6.2 Multivariate optimization of collision/reaction cell parameters by using experimental designs

As can be expected, interactions were found in the multivariate optimizations of varying CRC electrode potentials and gas flows in all three studies. Two of the optimization studies used kinetic energy discrimination to reduce interferences and interactions were encountered in both studies. Colon et. al[65] found an interaction between octopole bias and He flow rate when optimizing the sensitivity of ^{32}S response. Brennetot et al.[66] encountered multiple interactions while optimizing CRC conditions for improved SBR and reduced $^{40}Ar_2{}^+$ interference on ^{40}Se. Interactions between hexapole bias and O_2 flow rate, between pole bias and focus, and between O_2 and He flow rates were found to affect the $^{40}Ar_2{}^+$ signal. The noticed interactions might originate from effects on the kinetic energy distribution of ions and the discrimination voltage and their relative magnitude.

However, when Kadar et al.[64] optimized CRC parameters to achieve the best possible SBR for multiple analytes, they discovered significant interactions between all the studied factors (He flow, H_2 flow, hexapole bias and quadrupole bias), despite the fact that the optimized conditions did not allow kinetic energy discrimination. This suggests that the physics behind the interactions encountered in the CRC optimization studies is more complex, and cannot explained with simply with effects on the kinetic energy of the ions

relative to the potential energy wall used for discrimination.

6.3 Interactions between instrumental parameters of different instrument parts

Quetel et al.[67] found a suprising interaction between acquisition parameters when measuring Pb isotopes with ICP-QMS as the dwell time on ^{204}Pb was found to interact with the number of replicate measurements and with the dwell times of other isotopes, so that the dwell time on ^{204}Pb affected the precision when measuring other isotopes. The authors suggest that this might be caused by non random noise within frequency range of 3.6 to 14 Hz possibly caused by the peristaltic pump used for sample introduction. When Stüurup et al.[69] optimized the measurement dwell time and the number of sweeps per measurement of an SF-ICP-MS instrument together with the sample uptake rate for optimal precision of ^{140}Pu/^{139}Pu ratio, they found an iteraction between the number of sweeps and the sample uptake rate. Such interaction supports the presumption that the noise originating from sample introduction can affect the signal stability and interact with the acquistion parameters. If this is the case, it would be a good practice to optimize the acquisition parameters after changing sample uptake rate or other sample introduction parameters that are potential cause of non-random temporal noise.

Brennetot et al. included multiple plasma parameters and CRC parameters in their optimization of Gd analysis from spent nuclear fuel.[68] However, no prominent interaction effects were found in the optimization. Although some interactions might be expected, as the gas flows of the plasma can effect the kinetic energy of ions originating in the plasma. Although no interactions were found in the study, a possibility of such interactions should be kept in mind when designing optimization experiments.

7 Conclusions

Based on the current state of research, experimental design is a powerful tool for efficient optimization of ICP-MS methods. As the literature on the subject is scarce, however, little information is available on interactions that are likely to occur in optimization. In addition, there are no established conventions on how to use DOE particularly for ICP-MS optimization. The fact that the research on using DOE for ICP-MS method development is not matured, emphasizes the importance of the chemists understanding on the physics of ICP-MS analysis. Although some interactions, such as the interactions between the plasma gasses, plasma power and sampling depth should be expected, the existence of all possible interactions cannot be estimated based on the current research or the theory of ICP-MS. Therefore, it is necessary to include screening designs in optimizations, to estimate the importance of the main effects of the factors in addition to possible interactions and quadratic terms.

So far, the most used experimental design used for ICP-MS optimization is the central composite design. This design has the advance, that a 2^2 factorial design can be used in the screening and star points can be added to the design as needed for the evaluation of quadratic effects with a CCD. This often used strategy greatly reduces the number of experiments needed. Also the rotatability of the CCD design is a desirable quality in optimization. Most of the studies have succesfully used quadratic models with second degree interactions for optimization, while some used quadratic third order interaction models. Therefore, these models are propably sufficient to describe the response of an ICP-MS instrument for most purposes, although a possibility for a need to use more complex models cannot be excluded.

As most multivariate optimization studies have found interactions between the optimized parameters, it is likely that univariate studies would have failed to find equally good responses. This highlights the effectiveness of multivariate techniques for optimization, in addition to the obvious benefits of optimizing multiple parameters with less experiments and in less time, compared to more conventional OVAT optimization. As ICP-MS methods often have multiple analytes, interferences and other possible responses that all need to be taken into account, the possibility to use the desirability approach is a considerable advantage of DOE. In this respect it is likely that ICP-MS research can benefit from multivariate techniques, not only as a powerful tool for method optimization but as a way to gain more insight in the physicochemical processes behind the measurements. The fact, that the same techniques used in multivariate optimization can also be used for multivariate calibration[70], for grouping of analytes[60,61], for evaluation of the robustness of analytical methods[71] and for multivariate validation[72] further emphasizes the importance of having such chemometric techniques available in the chemist's toolbox.

Experimental: Elemental analysis of mid-fraction fuels with ICP-MS from organic matrix

An existing in-house method used for simultaneous determination of elements was further developed by adding new analytes, (resulting total of 28 analytes[†]) by optimizing sample dilution ratios and standard viscosities, improving the sample preparation protocol and by adjusting the integration times of analytes. Validation of the method was performed for five different fuel products: fossil jet and diesel fuels, renewable hydrotreated vegetable oil (HVO) jet and diesel fuels and for fatty acid methyl ester (FAME) biodiesel reference blank standard. The samples were prepared by simple dilution in xylene, without any additonal sample preparation and internal standard method was used for calibration.

In addition to the developement and validation of the in-house method using xylene, a new method using a kerosine based Asolv™(Agilent, Santa Clara, USA) as a solvent was developed and optimized by using experimental designs and response surface methology. The new method was then validated for jet fuel, diesel and gasoline matrices. Furthermore, the stability of the analytes and analysis conditions of the methods using different solvents were measured and compared.

The two new methods introduced in the current work are for the most part identical and only minor differences exists between the two. The methods were developed sequentally by first improving and validating the existing xylene method and using it as a starting point for the development of the Asolv method that was validated after the optimization. However, for the sake of clarity, the complete methods are described together in the following chapter, highlighting the differences between the two methods as necessary. Then, the development and optimization of the methods are discussed separately in the next two chapters, after which the validations of the methods are presented together in the following chapter. Finally the results of the study are discussed.

[†] Analytes included: Al, B, Na, Mg, Al, Si, P, K, Ca, Ti, V, Cr, Mn, Fe, Co, Ni, Cu, Zn, As, Sr, Mo, Pd, Cd, Sn, Ba, W, Pt and Pb.

8 Description of the new methods

8.1 Reagents, sample preparation and equipment

The same equipment and procedures were used throughout the study unless otherwise noted.

Reagents

Mixture of *o*- and *p*-xylene (AnalaR Normapur, VWR, Radnor, USA) or a kerosine based Asolv™(Agilent, Santa Clara, USA) were used as the solvents in the xylene and Asolv methods respectively. Conostan™stabilizer (SCP Science , Quebec, Canada) was added to the Asolv (0.4 g/l) to improve the stability of the analytes in solution.

Standards used in the study were prepared by using commercial 1000 mg/kg organometallic element standards acquired from Conostan, LGC (Middlesex, UK), and Agilent (Santa Clara, USA). The quality of the analysis was monitored by analyzing quality control (QC) samples in each run. Most elements were added from a standard mixture (Conostan S-21+K[‡] or an equivalent Agilent A21+K mixture), rest were added from single element standards. Different brands or batches were used to prepare standards and QC samples.

The viscosities of the element standards were 20 cSt while the viscosity of the standard mixtures were 75 cSt. As the viscocity can have a major impact on sample input flow, when using free aspiration to introduce the sample, as well as on atomization process, mineral oil (Conostan Blank oil, 75 cSt) was added to the calibration standards and QC samples to increase the viscosity, when xylene was used as a solvent.

Samples used in the method developement and validation

Two different kind of jet fuels (Jet fuel 1 and Jet fuel 2), and two diesel fuels (Diesel 1 and Diesel 2), with differing chemico-physical properties were obtained for the method developement and validation. The fuels included a fossil diesel and jet fuel in addition to HVO diesel an jet fuel. From each fuel type, two to three batches were used in the validation. In addition Agilent B100 FAME-type biodiesel reference blank was used in the validation. The laboratory samples were stored in glass bottles in darkness at room temperature during the study.

For the method development and validation of the analysis of gasoline, a synthetic gasoline mixture was prepared by mixing equal volumes of three batches of technical quality petroleum spirits obtained from VWR. The used commercial petroleum spirits had boiling ranges of 40-60°C, 60-95°C and 80-100°C. The mixture was stored in a refrigerator during the study.

[‡] Elements included in the S-21+K standard: Ag, Al, B, Ba, Ca, Cd, Cr, Cu, Fe,K, Mg, Mn, Mo, Na, Ni, P, Pb, Si, Sn, Ti, V, Zn.

General equipment

The solutions were prepared in volumetric borosilicate glass flasks capped with either plastic or PTFE stoppers. The glassware and teflon caps were cleaned with a dishwasher and by a subsequent treatment with traceCLEAN^{TM}(Milestones, Sorisole, Italy) acid steam cleaning system, that uses nitric acid to remove any remaining contaminants. Plastic caps were only washed using the dishwasher that uses aqueous acetic acid for rinsing.

For weighting, Mettler Toledo (Ohio, US) XPE-205 laboratory precision balance was used. The scale was equipped with a Mettler Toledo Universal AntiStatic Kit for discharging the samples to avoid any measuring errors caused by static electricity. The condition of the balance was each week, by measuring calibration weights of 1 g and 10 g.

For volumetric measurements, automatic pipettes were used in addition to volumetric flasks. The pipettes used were manufactured by Sartorius (Göttingen, Germany) and Biohit (Helsinki, Finland). Plastic pipette tips from Sartorius were used in all pipettes. All the measurements were done using the reverse pipetting technique to avoid errors caused by the vapor pressure and solutions sticking inside the pipette tip.

8.2 ICP-MS instrumentation

The ICP-MS analysis was performed by using Agilent 7700 series ICP-MS system equipped with an Agilent ASX-500 series autosampler, an octopole reaction cell and a quadrupole mass analyzer. No peristaltic pump was used for sample introduction and free aspiration was used instead to introduce the sample to a concentric nebulizer.

Argon was used as a nebulizer and plasma gas. As an auxiliary gas 40 % O_2-Ar mixture was used to improve sample oxidation and to reduce the accumulation of carbon deposit inside the instrument. In the reaction cell helium and hydrogen were used as the reaction/collision gasses.

In daily maintainance the plasma torch and the cones of the instrument were inspected and cleaned if necessary. The instrument was operated by using Agilent MassHunter for ICP-MS software. An overview of the instrumentation is given in Table 15.

Table 15 The ICP-MS instrument setup used in the study

Part	Type
ICP-MS instrument	Agilent 7700 ICP-MS
Autosampler	Agilent ASX-500
Nebulizer	Agilent MicroMist concentric nebulizer
Spray chamber	Double pass Scott design quartz spray chamber with thermoelectric cooling
Plasma torch	Fassel design with injector diameter of 1.5 mm
Plasma gasses	
Nebulizer gas	Argon
Plasma gas	Argon
Auxiliary gas	40 % O_2-Ar mixture
Interface cones	
Sampling cone	Platinum cone with orifice size of 0.3 mm
Skimmer cone	Platinum cone
Reaction cell	Octopole reaction cell
Reaction/collision gasses	He, H_2
Software	Agilent ICP-MS MassHunter 4.3

8.3 ICP-MS operating parameters

In the analysis four different *gasmodes* were used to remove any interferences. In *Nogas mode* no reaction gas was used, in *He mode* helium was used as a collision gas, in *High Energy Helium (HEHe)* gas mode, a higher helium flow was used compared to He-mode, and in *H_2 mode* hydrogen was use as a reaction gas. Each analyte was measured by using one or more gasmodes. The gas modes were changed sequentally and all m/Z-ratios were measured during a single autosampler visit by using appropriate gas mode(s) .

The two analysis methods presented used otherwise similar instrument parameters with the exception of carrier gas flow and sampling depth, that were set to different values in the xylene method and Asolv method. In addition to using different reaction/collision gasses, each gasmode had individual ion lense potentials, some of which were automatically optimized prior each analysis run by using an automatic tuning option of the instrument.

An overview of the instrument parameters common to all gas modes can be seen in Table 16. Gas mode spesific parameters, including representative lens voltages for different gasmodes are given in Table 17. For integration times, measured isotopes and gasmodes used for the analytes, see Table 19 on page 45.

Table 16 ICP-MS instrumental parameters common to every gas mode used. Both the xylene method and the Asolv method use the same parameters, with the exeption of carrier gas flow and sampling depth (shown in bold).

Parameter	Xylene method	Asolv method
Plasma parameters		
Radiofrequency power	1500 W	1500 W
Sampling depht	**8 mm**	**8.2 mm**
Carrier gas flow	**0.45 l/min**	**0.6 l/min**
Option gas flow	23.5 %	23.5 %
Makeup/dilution gas flow	0.10 l/min	0.10 l/min
Spray chamber temperature		
For Jet fuel analysis	**-5°C**	**5°C**
For Diesel analysis	5°C	5°C
For Gasoline analysis	-	**5°C**
Aquisition parameters		
Peak measurement pattern	1 point/peak	1 point/peak
Replicate measurements	3	3
Sweeps/replicate measurement	100	100
Total acquirement time/sample	2 min 54 s	2 min 54 s
Prerun		
Stabilization time before measurment	90 s	90 s
Rinse after sample measurement		
Rinse solvent	xylene	xylene
Rinse time in vial 1	60 s	60 s
Rinse time in vial 2	55 s	55 s

Table 17 Gas mode spesific ICP-MS instrument parameters used in both new methods. The same parameters were throughout the study.

Gas mode	Nogas	Helium (He)	High energy helium (HEHe)	Hydrogen (H2)
Reaction cell parameters				
He flow	-	5.5 ml/min	11.0 l/min	-
H_2 flow	-	-	-	6.0 l/min
Octopole bias	-8.0 V	-18 V	-100 V	-18 V
Octobole RF voltage*	120 V	200 V	200 V	190 V
Energy disrimination	5 V	3 V	7 V	3 V
Ion lense potentials				
Extract 1	-40 V	-34 V	-41 V	-40 V
Extract 2*	-200 V	-200 V	-200 V	-185 V
Omega bias*	-120 V	-120 V	-110 V	-110V
Omega lens*	10 V	10 V	5 V	-10 V
Cell entrance	-40 V	-40 V	145 V	-40 V
Cell exit	-60 V	-70 V	150 V	-68 V
Deflect*	16 V	1 V	-75 V	-4 V
Plate Bias	-50 V	-60 V	-150 V	-60

* The potentials were adjusted by automatic tuning prior each analysis run. The voltages values shown are given in representative purpose only to give an approximate magnitude of the used voltages.

8.4 Preparation of the solutions

The standard and test sample solutions were prepared by simple dilution in the solvent of choice (xylene or Asolv). As an internal standard, 100 μg/l of beryllium, scandium and yttirium was added to each standard and test sample to be analyzed. After the dilution, the solutions were mixed by shaking vigorously for 30 seconds. The samples were then analyzed within 36 hours after the preparation.

Standard solutions

As the detection limit and abundance of each analyte was different, the elements were divided to two groups with different calibration ranges. For the elements with higher limit of detection and elements that are often found in higher concentrations in the samples, the concentration range of 0 μg/l to 1000 μg/l was used in the calibration. For elements with few interferences and low background a concentration range of 0 μg/l to 100 μg/l was used instead.

Two blank samples and four to seven calibration standards with differing concentrations were prepared before each run. Each standard contained all the analytes so that the concentration of the elements of the smaller concentration range in each calibration

standard was 1/10 of the concentration of the elements of the higher concentration range. In addition to the calibration standards, four QC samples with varying analyte concentrations were prepared by using separate stock solutions, so possible contaminations in the standards could be noticed.

When xylene was used as the solvent, 40 g/l of mineral oil (75 cSt) was added to each standard, blank and QC sample to correct for differences in viscosity between the standards and the test samples.

Test samples

Depending on the sample matrix and the solvent used, different dilution ratios were used when preparing the test samples. Mineral oil was also added to lighter distillates to increase the viscosity. Optimized dilution ratios for the studied matrices are shown in Table 18.

Table 18 Dilution ratios used in the sample preparation as amount of laboratory sample and mineral oil (75 cSt) dissolved in 20 ml of solvent. The shown dilution ratios were used in validation of the methods.

	Xylene method		Asolv method	
Sample matrix	**Sample (g/20ml)**	**Mineral oil (g/20ml)**	**Sample (g/20ml)**	**Mineral oil (g/20ml)**
Jet fuel 1	5*	0.8	5.5*	4
Jet fuel 2	3*	-	10	-
Diesel 1	2.5*	-	9*	-
Diesel 2	2.5*	-	10	-
Agilent biodiesel	2.5*	-	5 to 9	-
Gasoline	-	-	2.7*	5.4

* Method validated for the matrix

Measurement

The voltages of the ion lenses were automatically optimized by an automated tuning of the instrument before each run. After the tuning the instrument was calibrated against daily prepared calibration standards.

Prior analysis the solutions were activated by shaking and approximately 7.5 ml of each solution was transferred to the autosampler in test tubes. Both blank samples were measured twice from separate test tubes. After every few sample, blank samples and QC samples were measured to monitor possible changes in sensitivity and to detect possible malfunctions or contaminations. Blank samples were also measured after any high concentration standard or sample with standard addition to reduce the background caused by memory effects.

Calibration

Internal standard method was used to correct variations in the instruments sensitivity, caused by matrix effects and sensitivity drift. Although Be and Sc were added to the samples, in practice only Y was used as an ISTD, so Be and Sc were mainly used as a mean to monitor the instrument response and as a backup ISTD in the case of a possible contamination. Yttrium signal measured with the same gas mode with the analyte in question was used in the calibration. A full list of analytes is shown in Table 19 along with the calibration ranges, the measured isotopes, gas modes used in the measurements and the corresponding integration times for each isotope-gasmode combination.

The calibration of each isotope-gasmode combination was automatically performed by using MassHunter software. The ratio of the signal intensity I [counts per second, CPS] of the measured m/Z-ratio to the intensity of the ISTD signal was calculated and expressed as a function of analyte concentration c for each calibration standard according to Eq. 1.

$$\frac{I_{\text{analyte}}}{I_{\text{ISTD}}} = ac_{\text{Analyte}} + b \tag{1}$$

The coefficient a of the equation was then obtained by linear regression of the measured data. The regression line was forced to go through the average $I_{analyte}/I_{ISTD}$ ratio measured from the blank samples, so that the coefficient b was obtained exclusively from the blank sample measurements. The equation was then used to calculate the analyte concentrations in the test samples. The instrumentsresponce during the calibration was highly linear (R$\approx$ 1) as an example, a calibration curve of Al measured with the xylene method is shown in Figure 2.

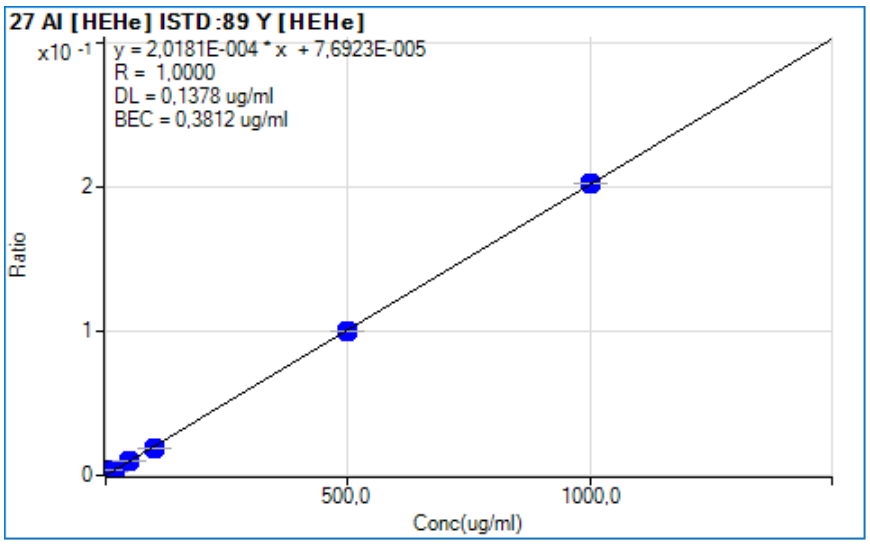

Figure 2 Calibration curve of Al measured with the xylene method. The highly linear calibration curve was typical for most elements.

Table 19 Analytes included in the methods with their respective calibration ranges along with isotopes, gas modes and integration times used for the measurements.

Measured isotope	Calibration range (ng/g)	Integration times on different gas modes (s)			
		Nogas	He	HEHe	H_2
^{7}Li	0-1000	0.1	-	-	-
^{9}Be	ISTD	0.1	0.1	0.2	0.1
^{10}B	0-1000	0.1	-	-	-
^{11}B	0-1000	0.1	0.1	-	0.1
^{23}Na	0-1000	0.1	0.1	0.4	-
^{24}Mg*	0-1000	-	-	-	0.5
^{27}Al*	0-1000	-	-	0.99	-
^{28}Si	0-1000	-	-	-	1.0
^{31}P	0-1000	0.1	-	0.99	-
^{39}K*	0-1000	-	-	2.0	0.5
^{40}Ca*	0-1000	-	-	-	0.2
^{45}Sc	ISTD	0.09	0.12	0.2	0.05
^{47}Ti	0-1000	-	-	-	0.1
^{51}V	0-1000	-	-	0.51	-
^{52}Cr	0-1000	-	-	0.99	-
^{55}Mn	0-1000	-	-	0.51	-
^{56}Fe*	0-1000	-	0.1	-	-
^{59}Co	0-1000	-	0.1	-	0.4
^{60}Ni	0-1000	-	-	0.51	-
^{63}Cu*	0-1000	-	-	0.51	-
^{66}Zn	0-1000	-	-	-	0.2
^{75}As	0-100	-	2.0	2.0	4.0
^{88}Sr	0-100	-	-	-	0.1
^{89}Y	ISTD	0.06	0.15	0.3	0.09
^{95}Mo	0-1000	-	-	0.51	-
^{105}Pd	0-100	-	0.1	-	-
^{114}Cd†	0-100	0.99	-	-	-
^{118}Sn	0-1000	0.51	-	0.7	-
^{137}Ba	0-1000	0.51	-	-	-
^{182}W	0-100	0.1	-	0.15	-
^{195}Pt	0-100	0.1	-	-	-
^{206}Pb*‡	0-1000	0.41	-	-	-
^{207}Pb*‡	0-1000	0.51	-	-	-
^{208}Pb*‡	0-1000	0.3	-	-	-

* Element included in the ASTM D8110 standard

† A mathematical correction equation was used in the calculation of cadmium concentration to correct an isobaric interference caused by ^{114}Sn. The concentration of Cd was obtained by substracting the ratio of natural abundances of ^{114}Sn and ^{118}Sn times the measured ^{118}Sn counts from the measured counts at m/Z 114: $I(^{114}\text{Cd}) = I(^{114}\text{Cd} + ^{114}\text{Sn}) - (0.65\%/24.23\%) \times I(^{114}\text{Sn})$

‡ The concentration of Pb was obtained by measuring all existing isotopes of lead and using the sum of the signals to calculate the concentration.

8.5 Changes made compared to the previous method

Addition of new analytes

Six new analytes (W, Pd, Pt, Ce, Sr and Sb), were added to the method. As tungsten had been used as an internal standard, it was repurposed as an analyte. Based on their atomic mass and theoretical interferences, the new analytes were expected to have relatively low detection limits. As they are also hardly found in a laboratory enviroment as possible contaminants, they were added to the group of elements with the smaller calibration concentration range. Antimony, however, can be found in some commercial wear metal standard mixtures, which made it practical to use the same higher calibration range fos Sb as for with other elements found in standard mixtures.

Selecting the gasmodes to be used in the method

After few trial and error measurements experimenting with different gas modes and isotopes, the best gas modes and isotopes were selected to be used in the analysis, based on the calibration curve fit, blank equivalent concentration (BEC), and RSD%-values. During these tests, no benefit was found in using indium over yttrium as an ISTD, so indium was omitted from the purpose, leaving Be, Sc and Y as internal standards.

Improvements on the procedure for preparing solutions

In addition to the changes discussed in this chapter minor changes were made to the integration times used in the measurements and the amount of mineral oil added to the standards was changed from 14 g/l or 100 g/l for more viscous samples to 40 g/l, which allowed better match between the viscosities of the standards and samples. It also made it possible to analyze wider range of different sample matrices using the same standards. These changes were done after optimization and are further discussed in the following sections.

To speed up the preparation of the standards and test samples, few modifications were made to the procedure used to prepare the solutions. As considerable amount of time was used to weight the mineral oil for each standard, a faster method for dispensing the BO was necessary. The 75 cSt mineral oil was too viscous to be accurately measured with a pipette, however, it was found that when dissolved to to xylene (40 g/ 100 ml), the following mixture can be pipetted by using the reverse pipetting technique. This lead to considerable reduction in the prepartion time of the solution.

In the original method, separate stock solutions were prepared for analytes with different concentration range in the calibration. This lead to unnecessary pipetting as for each standard it was necessary to pipette analytes from two different stock solutions. Changing the concentrations of analytes in the standards, allowed all analytes to be dispensed from a single stock solution, thus reducing preparation time. This also reduced the number of stock solutions needed.

When the calibration curve is forced through blank sample, any contaminations in blank sample can have major effect on the calculated concentrations at small concentrations. To make the method more robust, a second blank sample was added to the method.

Table 20 Comparison of the differences between the original in-house method and the new xylene method.

Procedure	**Old method**	**New xylene method**
Method of dispensing mineral oil to the standards	By weighting	By pipetting
Elements added as ISTD	Be, Sc, Y, In, W	Be, Sc, Y
Analytes	Li, B, Na, Mg, Al, Si, P, K, Ca, Ti, V, Cr, Mn, Fe, Co, Ni, Cu, Zn, As, Mo, Cd, Sn, Pb	Li, B, Na, Mg, Al, Si, P, K, Ca, Ti, V, Cr, Mn, Fe, Co, Ni, Cu, Zn, As, **Sr**, Mo, **Pd**, Cd, Sn, **Sb**, **Ce**, **W**, Pt, Pb
Number of blank samples	1	2
Mineral oil concentration in the standards	14 g/l	40 g/l

9 Optimization of the xylene method

9.1 Optimization of the integration times used for the measurement

The statistical prediction for the relative standard deviation of measurement, when N ions are detected, follows the equation Eq. 2.

$$\text{RSD\%} = \frac{\sqrt{N}}{N} \times 100\% \tag{2}$$

This means that the square root of the noise in the measurement is proportional to the measuring time. In other words, increasing the measurement time decreases the error of the measurement. However, this is only practical approach to certain extent, before the analysis time becomes unreasonable long. It is also unpropable that the system follows the statistical prediction without exceptions.

To reduce the variation of the measurements, while keeping the analysis time sufficiently short, integration times were optimized for each analyte. The same calibration standards were measured in seven consecutive runs with varying integration times. The integration times of the analytes in these seven runs were 0.25, 0.5, 1, 2, 4 and 8 times the integration times used in the original in-house method. For new analytes, arbitrary integration times of 0.025 s, 0.05 s, 0.1s 0.2 s, 0.4 s and 0.8 s were used instead. As the analysis took a long time to finish, the measurements were done in random order to reduce any time dependent effects. In each run, an RSD% error of six replicate measurements ,measured by single autosampler visit, was calculated for each isotope-gasmode combination measured from every calibration standard.

The calculated RSD% values were plotted against integration time used for the measurement. From the resulting graphs a good tradeoff between analysis time and precision was made by visually selecting suitable integration time for each analyte/gasmode. For the integration times, see Table 19 on page 45. For the graphs see Appendix A.

9.2 Optimizing the dilution factors and the viscosity of the standards

During the initial experimentation, it became evident, that the ISTD recovery (calculated as the ISTD signal intensity measured from a test sample divided by the average signal intensity of the calibration blanks) of diesel samples was systematically too low. This indicates a difference in the properties between the standards and test samples, leading to possible changes in the ionization conditions and therefore a likely deterioration of accuracy. As measured the samples had a low total dissolved solids (TDS) content and the matrix had the same magnitude effect on all the ISTD elements regardless of their mass, poor recovery was unlikely a result of a space-charge matrix suppression.

Higher viscosity of the samples compared to the calibration standards could lead to a reduced sample flow, when using free aspiration to introduce the sample into the nebulizer. It can also reduce the ionization by affecting the droplet formation in the nebulizer. As these so called sample transport effects could reduce the amount of sample delivered to

the plasma, it was reasonable to assume, that the poor ISTD recoveries might be a result of a viscosity difference between the samples and the calibration standards.

To test this hypothesis and to find optimal experimental conditions to achieve approximately 100% ISTD yields for every matrix studied, an experiment was designed to investigate the effect of changing the dilution ratio of the samples and the amount of mineral oil added to the calibration standards and the sample dilution factors.

Investigation of the effect of changing the dilution ratio of samples and the viscosity of the standards

Four sample dilution series were prepared from Diesel 1, Diesel 2, Jet fuel 1 and Jet fuel 2. Each series contained five samples with 1.2 g, 1.8 g, 2.4 g, 3 g, 3.6 g and 4.2 g of respective fuel dissolved in 20 ml of xylene. Four calibration standard series along with QC-samples and blank samples were prepared with increasing mineral oil (75 cSt) concentrations of 10g/l, 14g/l, 20g/l and 30g/l.

The samples were measured and the ISTD yields of the samples were calculated in respect to different blanks made with varying mineral oil concentrations of 10 g/l, 14 g/l and 20 g/l. The results were plotted to visualize the effect of changing the dilution ratio or added base oil concentration in the standards. The resulting plots can be seen in Figure 4 on page 66.

Optimizing the dilution factors used in the sample preparation

After the first experiment, it was clear that the optimal conditions were outside the experimental space, so a new experiment was conducted in the purpose of finding suitable dilution factors and the best possible calibration standard mineral oil concentration for kerosine matrices. Based on the first optimization experiment it was found that adding mineral oil to the standards leads to lower signal intensity and therefore an increase in the ISTD recoveries of the test samples.

To find experimental conditions suitable for all the studied matrices, a series of Jet fuel 2 test samples with varying dilution ratios was prepared and analyzed. As the Jet fuel 1 had higher ISTD recoveries compared to other matrices, four test sample series with varying dilution ratio and additional mineral oil concentrations were prepared to measure the effect of added mineral oil. In addition blank sample series with varying mineral oil concentration was prepared with two duplicate samples. An overview of the prepared samples can be seen in Table 21.

The samples were prepared to the volume of 10 ml by pipetting varying amounts of appropriate jet fuel diluted with xylene (15.00 g/25 ml), mineral oil-xylene mixture (20 g /l), internal standard mixture (10 mg/l, Be, Sc, Y in xylene) and xylene into test tubes. The test tubes were capped with plastic caps and shaked vigorously for 30 seconds. The caps were then removed, the tubes were transferred to the autosamplers and measured as usually. All the prepared samples were measured in the same run.

Two duplicate measurements were done from each prepared blank sample, so total of four measurements were obtained from each blank oil mineral oil concentration. The ISTD

Table 21 Jet fuel 1 and 2 sample series prepared for the optimization of sample dilution ratios and the mineral oil concentration of calibration standards for the xylene method.

Blank samples		**Jet fuel 1 samples**			**Jet fuel 2 samples**	
Number	Mineral oil conc. (g/20 ml)	Number	Dil. ratio (g/20 ml)	Mineral oil conc. (g/20 ml)	Number	Dil. ratio (g/20 ml)
1	0	1	1.2	-	1	1.2
2	0	2	2.4	-	2	2.4
3	1	3	3.6	-	3	3.6
4	1	4	4.8	-	4	4.8
5	2	5	6	-	5	6
6	2	6	8	-	6	9
7	3	7	1.2	1		
8	3	8	2.4	1		
9	4	9	3.6	1		
10	4	10	4.8	1		
11	5	11	6	1		
12	5	12	8	1		
13	6	13	1.2	2		
14	6	14	2.4	2		
15	8	15	3.6	2		
16	8	16	4.8	2		
		17	6	2		
		18	8	2		
		19	1.2	4		
		20	2.4	4		
		21	3.6	4		
		22	4.8	4		
		23	6	4		
		24	9	4		

recoveries of the jet fuel samples were then calculated for every gas mode with respect to the average signal intensities of the blank sample measurements of every blank sample mineral oil concentration studied. Also the average of yttrium recoveries measured from different gas modes was calculated.

The measured ISTD recoveries for Jet fuel 1 and Jet fuel 2 were plotted as a function of the dilution factor and the mineral oil concentration in blank or test samples to visualize how the experimental conditions affect the ISTD yield. The results can be seen in Figure 5 on page 67 and in Figure 6 on page 67 for Jet fuel 1 and for Jet fuel 2 respectively. From the resulting graphs, proper dilution factors and mineral oil concentrations were selected.

As high dilution leads to increased limit of detection it was important to find a point where 100 % ITSD recovery can be achieved with as little dilution as possible. Another criteria for the selected conditions was, that several sample types with different viscosities

could be measured simultaneously in the same run.

By visual analysis of the results, it was found that ≈100 % ISTD yields could be achived for both jet fuel matrices by adding 40 g/l of blank oil to calibration standards and to Jet fuel 1 samples prepared with a dilution ratio of 5 g/20ml. At the same time Jet fuel 2 samples could be analyzed with a dilution ratio of 3 g/20ml without any mineral oil added to the samples. Based on the previous experiments, it was also reasonable to assume that diesel fuel could be analyzed with a slightly smaller dilution ratio. Based on this assumption the dilution ratio of both studied diesel fuels was set to 2.5 g/20ml for the validation.

10 Development of a method using Agilent Asolv as the solvent

To examine if Agilent Asolv would have any benefit over xylene as the solvent in the analysis, a few measurements were run using the same instrumental parameters and procedures that were used in the xylene method.

A blank sample was prepared in Asolv was measured against calibration standards prepared in xylene with 40g/l of added mineral oil to how investigate the solvent behaves in the analysis. The measured ISTD recovery of the Asolv blank sample was just ≈30%, most propably because of the visibly higher viscosity of Asolv, that reduces the sample intake compared to the thinner xylene.

After it became evident, that there was no need to add any mineral oil to the Asolv, a trial run was then performed to match the viscosities of test and blank samples prepared in Asolv. Few samples were prepared and measured in a trial and error fashion, after which dilution ratios and added mineral oil concentrations giving close to 100% ISTD recoveries with highest possible dilution ratios were found for six different sample matrices (Jetfuel 1, Jetfuel 2, Diesel 1, Diesel 2, Agilent biodiesel blank and for a gasoline type refinery intermediate product). The dilution ratios were significantly higher compared to the ones used in the xylene method.

In another run few Diesel 1 and gasoline type samples with variable dilution ratios were measured along with the same Diesel 1 samples with standard additions of 600 ng/g (or 60 ng/g of the analytes of smaller calibration range) of all the analytes included in the methods. The analyte recoveries were found to be comparable or better to using xylene as a solvent. It was also found that gasoline could be analyzed by using Asolv as the solvent and that changing the dilution ratio had a major impact on the analyte recoveries.

10.1 Optimization of the carrier gas flow, sampling depth and Diesel 1 dilution ratio for the Asolv method

After initial experiments, it became evident that Asolv had a potential to enhance the analysis. To further improve the analysis, response surface methodology was used to optimize the analyte recoveries when carrier gas flow, the sampling depth and the dilution ratio of Diesel 1 were varied. In the optimization a three level full factorial experimental design was used along with a desirability approach to find the best overall recovery for the analytes.

As the Asolv is more viscous compared to xylene, less sample was sprayed to the plasma leading to a decrease in the signal intensity. A change in solvent might also affect the droplet formation in the nebulizer, so that instrument parameters optimized for xylene might not be optimal for using Asolv. To increase the signal intensity, reduce the background and to optimize the atomization process, carrier gas flow and dilution ratio were selected to the parameters to be optimized.

It was also reasonable to assume that using a different solvent, carrier gas flow and dilution ratio would change the ionization conditions in the plasma and move the ionization

regions of the analytes relative to the sampling cone. As the relative degrees of ionization have a direct impact on the analyte recoveries, sampling depth i.e. the distance between the plasma torch and the sampling cone was also included as a factor in the optimization. The analyte recoveries were choosed to be the responses to be optimized.

To optimize these parameters, a three level full factorial experiment was used to obtain the data for RSM. Based on real time monitoring of signal intensities of the analytes with different instrumental conditions and initial test runs with varying carrier gas flows and sampling depths, an intuitive understanding of suitable experimental space was obtained. The experimental space was set based on this understanding and the selected factor values are shown in Table 22.

Table 22 The experimental space used in the optimization of Asolv method.

Variable	**level**		
	-1	**0**	**+1**
x_1 = Carrier gas flow (l/min)	0.4	0.55	0.7
x_2 = Sampling depth (mm)	6	8	10
x_3 = Diesel 1 dilution ratio (mm)	3	6	9

The experiment was performed by preparing three Diesel 1 samples with differing dilution ratios and three Diesel 1 samples with the same dilution ratios spiked with every analyte included in the method. The concentration of standard additions was 600 ng/g or 60 ng/g per gram of laboratory sample for analytes in the larger and smaller calibration range respectively. The standard additions were done by addition of the same stock solutions as was used in the preparation of the calibration standards.

Nine runs were then performed with varying carrier gas flows and sampling depths levels according to the experimental design and the samples were measured once in every run so that the analyte recoveries could be calculated at the 27 different points corresponding to the experiments of the three level full factorial design. However, due to an error in operating the instrument, the analysis of the run with carrier gas flow of 0.55 l/min and sampling depth of 10 mm failed and thus the experimental design was missing three measurements.

In addition, two replicate runs were measured with the parameters corresponding to the center of the experimental design in order to calculate the error of the measurement. Two of the replicate runs were measured on different days and two as the first and last run of the day to include possible drifting effects and interday variation in the measurement error. See Table 23 for the design matrix.

The instrument was automatically tuned and calibrated before each run and the samples were measured once in every run. The experiments were performed during two consecutive days and fresh samples and calibration standards were prepared on both days before the measurements.

Table 23 Experimental matrix used in the optimization study. The factors and levels are shown with nominal notation, see Table 22 for the parameter values. Spiked and uspiked samples were measured to obtain analyte recoveries at every point of the matrix.

	Factor levels				Factor levels		
Experiment	x_1	x_2	x_3	**Experiment**	x_1	x_2	x_3
1	-1	1	1	19	-1	1	1
2	-1	1	0	20	-1	1	0
3	-1	1	-1	21	-1	1	-1
4	-1	0	1	22	-1	0	1
5	-1	0	0	23	-1	0	0
6	-1	0	-1	24	-1	0	-1
7	-1	-1	1	25	-1	-1	1
8	-1	-1	0	26	-1	-1	0
9	-1	-1	-1	27	-1	-1	-1
(10)*	0	1	1	28†	-1	1	-1
(11)*	0	1	0	29†	-1	1	-1
(12)*	0	1	-1	30†	-1	1	0
13	0	0	1	31†	-1	1	0
14	0	0	0	32†	-1	1	1
15	0	0	-1	33†	-1	1	1
16	0	-1	1				
17	0	-1	0				
18	0	-1	-1				

* The measurement failed, no results were obtained

† Replicate measurement

After the measurements, the analyte recoveries measured with all all isotope/gasmode combinations were calculated at every experimental point by substracting the analyte concentrations measured from the unspiked samples from the measured concentrations of the spiked samples having the same dilution factor. The analyte recoveries were the obtained by dividing with the spiked concentration of 600 ng/g (or 60 ng/g for the elements of the small calibration range).

Regression analysis was then used to fit a three factor second degree polynomial model (Eq. 3) to the recoveries of the analytes measured at the points of the design matrix. By solving the coefficients of the equation, response surfaces were obtained for different isotope/gasmode combinations. The response surfaces allow the computation of predicted recoveries $\hat{Y}_i$ of the analytes at any point of the design space.

$$\hat{Y}_i = b_0 + b_1x_1 + b_2x_2 + b_3x_3 + b_{11}x_1^2 + b_{22}x_2^2 + b_{33}x_3^2 + b_{12}x_1x_2 + b_{13}x_1x_3 + b_{23}x_2x_3 \qquad (3)$$

From the response surfaces the best overall desirability D was calculated by computing individual desirabilities $d_i(\hat{Y}_i)$ by using Derringer's desirability function (Eq. 4) and using the desirability approach.

$$d_i(\hat{Y}_i) = \begin{cases} 0 & \text{if} \quad \hat{Y}_i < L_i \\ \left(\dfrac{\hat{Y}_i(x) L_i}{T_i - L_i}\right)^s & \text{if} \quad L_i \leq \hat{Y}_i \leq T_i \\ \left(\dfrac{\hat{Y}_i(x) U_i}{T_i - U_i}\right)^t & \text{if} \quad T_i \leq \hat{Y}_i \leq U_i \\ 0 & \text{if} \quad \hat{Y}_i \geq U_i \end{cases} \tag{4}$$

First individual desirabilities d_i were numerically calculated for every analyte from their corresponding response surfaces. The lower and upper acceptable recoveries were set to $L_i = 0\%$ and $U_i = 200\%$ respectively and T_i was set to 100% recovery. Both, the r and the s parameter were set to 1.

With these parameters, the desirability function gives a number between 0 and 1, that for all practical purposes tells the distance from the desired 100% yield at any given point of the design space, so that the analyte recoveries between 0% and 100% correspond directly to the desirability functions value at the point in question. Recoveries between 100% and 200% correspond to desirability values between 1 and 0, while recovery values less than zero or over 200% are completely undesirable and correspond to zero desirability at a given point in the design space.

From the desirablities of the analytes measured by using varying gasmodes and isotopes, the overall desirability D was obtained as a geometric mean of the individual desirabilities (Eq. 5).

$$D = \Big(\prod_{i=0}^{n} d_i\Big)^{\frac{1}{n}} \tag{5}$$

The calculations were done numerically by using Python programming language. The maximum of the function was found with carrier gas flow of 0.6 ml/min, 8.4 mm sampling depth and dilution ratio of 9 g/20 ml. These values gave the overall desirability of 96.5%. The calculated response surfaces of individual analytes can be seen in Appendix B. For the visualized overall desirability and discussion of the results, see Section 12.3 on page 68.

Some isotopes/gasmodes were left out of the calculation of D, as corresponding analytes were regarded as less important compared to others and using mulltiple desirabilities calculated for a single analyte from measurements with different isotope/gasmodes would

have lead to excessive contributions on the global desirability. Therefore some measurements were omitted. Based on the response surface of Pt, the analyte was considered too sensitive to changes in the analysis conditions or very unstable in solutions so it was left out from the calculation to prevent the distortion of the results. The omitted measurements are shown in Table 24.

Table 24 Measurements omitted from the computation of the overall desirability in the optimization of the Asolv method

Isotope	Gasmode
^{10}B	Nogas
^{23}Na	Nogas
^{75}As	HEHe
^{118}Sn	Nogas
^{121}S	H_2
^{140}Ce	He
^{140}Ce	H_2
^{195}Pt	Nogas
^{182}W	Nogas

10.2 Optimization of the dilution ratios and added mineral oil concentrations of gasoline and Jetfuel 1 test samples analyzed with the Asolv method

After the the carrier gas flow and the sampling depth were optimized for the Diesel 1 matrix, the dilution ratio and mineral oil concentration added in the sample preparation step were optimized for gasoline and Jet fuel 1. The optimizations were done by using Doehlert designs with RSM and utilizing desirability approach to find the best overall analyte recoveries.

The weight to weight ratio of undiluted sample to mineral oil added to the test samples was used as a factor in the optimizations along the dilution ratio of the sample. The experimental space was set separately for both studied matrices based on the dilution ratios and mineral oil concentrations, that had yielded suitable ISTD recoveries in the previous experiments using Asolv as the solvent. The levels of the factors for gasoline and Jet fuel 1 are shown in Tables 25 and 26 respectively.

From both studied matrices, samples with standard addition of 600 ng/g (or 60 ng/g for the analytes of the smaller calibration range) of every analyte included in the method were prepared and measured according to the respective Doehlert designs in use. The standard additions were done by using the same stock solutions that were used in the preparation of the calibration standards. In addition two replicate samples were prepared and measured at the center point.

Table 25 The experimental space used in the optimization of Gasoline samples. The mineral oil concentration is in unit gram of mineral oil per gram of undiluted laboratory sample diuted to 20 ml. The experimental design is based on the Doehlert design.

Variable	level				
	-1	**-0.5**	**0**	**0.5**	**+1**
x_1 = Dilution ratio (g/20 ml)	1	2	3	4	5
x_2 = mineral oil conc. (g/g) of laboratory sample)	1.5	-	1	-	2

Table 26 The experimental space used in the optimization of Jet fuel 1 samples. The mineral oil concentration is in unit gram of mineral oil per gram of undiluted laboratory sample diluted to 20 ml. The experimental design is based on the Doehlert design.

Variable	level				
	-1	**-0.5**	**0**	**0.5**	**+1**
x_1 = Dilution ratio (g/20 ml)	1	3	5	7	9
x_2 = mineral oil conc. (g/g)	0.3	-	0.6	-	0.9

To reduce the amount of samples, the analyte recoveries for both matrices were obtained by measuring three unspiked samples at the center point of the designs only and using the average concentration of the measurements to calculate the sample recoveries. As the analyte concentrations in the uspiked samples were small compared to the spiked ones (with the exception of almost 2 μg/l of Si in Jet fuel 1b) the error caused by not measuring unspiked samples at every point of the design matrix was considered acceptable (see Appendix G for the measured elemental composition of the matrices). An overview of the measured samples of both matrices can be seen in Table 27. For the results of the optimization and for the response surfaces for overall desirabilities of the jet fuel and gasoline matrices see Section 12.3 (pp. 69). The response surfaces of the individual analytes/gasmodes as given in appendices C and D for gasoline and jet fuel respectively.

Table 27 The experimental Doehlert matrices used in the optimization of the dilution ratios and additional mineral oil concentrations for gasoline and Jet fuel 1 test samples.

Gasoline experiments			Jet fuel 1 experiments		
Experiment	**Dil. ratio** (g/20 ml)	**Mineral oil** (g/g)	**Experiment**	**Dil ratio** (g/20 ml)	**Mineral oil** (g/g)
1	1	1.5	1	1	0.6
2	2	1	2	3	0.3
3	2	2	3	3	0.9
4	3	1.5	4	5	0.6
5*	3	1.5	5*	5	0.6
6*	3	1.5	6*	5	0.6
7	4	1	7	6	0.3
8	4	2	8	6	0.9
9	5	1.5	9	7	0.6

* replicate measurement

11 Validation of the methods and stability of the analysis conditions

11.1 Validation experiments

After the optimization the both studied methods were validated for different fuel matrices. The xylene method was validated for Jet fuel 1, Jet fuel 2, Diesel 1, Diesel 2 and for Agilent biodiesel reference blank. The validation of diesel fuels and the jet fuels were done at different times and by using different spray chamber temperatures of -5°C for jet fuels and +5°C for dielsels. A less comprehensive validation of the Asolv method was performed for Diesel 1, gasoline and Jetfuel 1. All the validation experiments using asolv as the solvent were done with the spray chamber set to the temperature of +5°C.

Sample batches included in the validation

The xylene method was first validated for the jet fuels, by using three different batches of Jet fuel 1 (Jet fuel 1a, Jet fuel 1b and Jet fuel 1c) and two different batches of Jet fuel 2 (Jet fuel 2a and Jet fuel 2b). After the validation of the jet fuels was finished, the method was validated for the diesel fuels. Two laboratory sample batches of each kind of diesel were obtained (Diesel 1a, Diesel 1b, Diesel 2a and diesel 2b) with the expection of Agilent biodiesel reference blank from which only one batch was used. In the validation of the Asolv method only single batch of each fuel was used in the validation.

Preparation of the test samples

From each sample batch, fuel samples with and without standard additions were prepared and measured. For measuring the analyte recoveries, samples spiked with 50 ng/g, 100 ng/g or 600 ng/g per gram of laboratory sample of analytes in the large calibration range and 5ng/g, 10 ng/g or 60 ng/g of analytes of the smaller calibration range respectively. The standard additions were done by adding approptiate amounts of the same stock solutions that were used for making the calibration standards for the analysis run. The dilution ratios used in the preparation of samples for the validation of methods using both solvents can be seen in the description of the methods in the Table 18 on page 43.

For each validation run, four QC samples with analyte concentrations of 600&60 μg/l, 100&10 μg/l, 50&5 μg/l and 10&1 μg/l were prepared. For the determineation of the limit of detection and limit of quantification, additional blank samples were measured between the test samples in addition to the blank samples used for calibration and quality control.

Jet fuel samples were measured over a three week period and diesel samples were measured over a five week period. The samples were uniformly distributed over the validation runs. In the validation of the Asolv method the measurements were measured over a two week period and the measurements of every matrix were done in over three separate runs in different days, except for the validation of Jet fuel 1, that was performed in only two runs on separate days. An overview of all validation samples can be seen in Table. F.2 and Table F.3, for the xylene method and for the Asolv method respectively.

Measurement of the samples

The validation samples were measured in the order of increasing spike concentration and blank samples were measured after samples spiked with high concentratios of analytes to avoid errors caused by memory effects. The measurement order of samples was different in each run to exclude any time dependent effects on the results. The validation samples were measured in same runs with daily routine samples analyzed in the laboratory, including variable middle distillate refinery intermediates and products. The QC-samples were measured after every few samples, as they would be analyzed in normal use.

The quality of the analyses was followed by monitoring the recoveries of the internal standards. In the validation of the jet fuels, the ISTD recoveries for Y were for the most part within 90-110%. In the validation of the diesels, the ICP-MS instruments condition was less than optimal, and more variation was seen in the ISTD recoveries. The allowed ISTD-yield limits were set to 70-130 % and all the measurements exceeding these limits were excluded from the validation. If the ISTD-yield of any of the the calibration standards was outside this limit, the whole run was omitted.

During the validation of the jet fuels, a depleted arsenic standard was replaced with a defective standard having a concentration of about half of the declared one. The mistake went unnoticed for few measurements. The measured yields for arsenic were still used in the validation as it was reasonable to assume, that the accuracy of the measurement does not increase with decreased arsenic concentration. However, 23 to 25 measurement of the QC-sample of varying concentration obtained by using faulty As standard were discarded from the validation.

Data analysis

The data analysis of the validation was done by using Agilent MassHunter, Python (vrs. 3.6.3) programming language and Microsoft Excel. The calibration, curve fitting and calculation of concentrations were done in MassHunter. The results of each experiment were exported from MassHunter as a text file and a Python script was used to automatically filter and organize the data based on the sample name to create an an Excel file that contained all validation data in appropriate tables. Excel was the used to compute the statistical measures.

From the validation sample measurements, the accuracy of the measurements was evaluated by calculating the analyte recoveries from the spiked samples. The statistical measures for the evaluation of precision included standard deviation and repeatibility for each sample type. The following statistical measures were computed for the measurements of every analyte measured from different matrix with different isotope/gasmode combinations.

- Arithmetic mean $\bar{c}$ for n number of concentration measurements c_i:

$$\frac{1}{n}\sum_{i=1}^{n} c_i, \tag{6}$$

- Sample standard deviation s_r:

$$s_r = \sqrt{\frac{\sum(c_i - \bar{c})^2}{n-1}} \tag{7}$$

- Relative standard deviation as percents RSD%:

$$\text{RSD\%} = \frac{s_r}{\bar{c}} \times 100\% \tag{8}$$

- Repeatibility r:

$$r = \sqrt{2} s_r f(t), \tag{9}$$

  where $f(t)$ is the inverse cumulative distribution function for Student's two tailed T-distribution of the measurements with 95% confidence interval.

For standard addition samples and QC samples analyte recoveries were calculated for each spiked concentration of sample batch by substracting the measured concentration of the uspiked sample $\bar{c}_{Unspiked}$ from the one of spiked sample $\bar{c}_{Spiked}$ and dividing with the spiked concentration c_{Added}:

$$\text{Recovery\%} = \frac{\bar{c}_{Spiked} - \bar{c}_{Unspiked}}{c_{Added}} \times 100\% \tag{10}$$

From the measurements of validation blank samples, average concentration, repeatibility, sample standard deviation (STD) and RSD% were calculated for each measurement with different isotope and gasmode combination. In addition, limit of detection (LOD) for different analytes measured with varying gasmodes from test samples was calculated to be three times the STD of the measurement in question. The limit of quantification (LOQ) was calculated as ten times the sample standard deviation.

To correct for the effect of sample dilution, the LOD for undiluted laboratory samples was obtained by multiplying by the dilution factor of the sample. The dilution factor in this context is defined as the volume of the test sample, divided by the weight of the laboratory sample used in the sample preparation i.e. the inverse of the dilution ratio.

After the statistical measures were calculated for every analyte gas mode combination measured from different laboratory sample batches, aritmethic means of the statistical values were calculated for each matrix type examined from the results of the according sample batches. See Chapter 12.5 for the results of the validation.

11.2 Study of the stability of the analysis conditions

In ICP-MS analysis, drifting of the instrument's sensitivity can take place in long measurements. To study the stability of the analysis conditions over time, the same calibration standards and test samples used in the validation were measured multiple times during the same run. The experiment was repeated for both studied methods, the xylene and the Asolv method. The duration of the both measurements was around 35 hours and the instrument was only calibrated at the beginning of each measurement. The results of the measurements are given in Section 12.4 (pp. 76-79).

11.3 Study of the stability of standard stock solutions prepared in xylene

As significant time was consumed in daily preparation of stock solutions, two experiments were performed to investigate the shelf life of stock solutions prepared in xylene. Stock solutions, containing 10 ng/l or 1 ng/l of the analytes of the large and small calibration range respectively, were used in the preparation of calibration standards. Stock solutions prepared for analyses were collected over a three week period and stored at room temperature in darkness. The stock solutions were 8, 15, 19, 21, 22 and 23 days old at the time of the measurements. From the solutions, 500 (or 50) ng/g standards were prepared and measured against standards prepared from a fresh stock solution.

Two standards were prepared at the day of the measurement and one of which was measured twice in during the analysis run, so total of three measurements was done with fresh standards. An average was calculated from the measured concentration of the fresh standards and the concentrations of the standards were normalized with respect to 100% recovery measured from the fresh standard. For the results see Table 31 on page 91.

12 Results and discussion

12.1 Optimization of the xylene method

The effect of changing the integration times

As expected, increasing the integration time of the measurements reduced the relative standard deviation of the analyte concentrations. The RSD% of few analytes plotted against respective integration times are shown in Figure 3. For the rest of the analytes, see Appendix A.

It can be noticed, that with small integration times, the precision of most analytes increases rapidly as a function of integration time. As the integration time is further increased, the effect becomes less pronounced. This effect is more distinct when measuring standards with small analyte concentration. These effects are in an agreement with the Equation 2 as both, an increase in concentration or integration time, leads to an increment in the number of detected ions.

However, when standards with high concentration of analytes are measured, the increasing integration time seems to have no effect on the precision. This is not in agreement with the equation 2. Most propably the measurement error in this case is not random by nature, so the results do not follow gaussian distribution and the precision can not be further increased a after certain point. For some analytes the precision could be further enhanced by increasing the integration times, but the analysis time would become impractically long.

It is seen in the results, that some analytes seem to follow the statistical prediction quite accurately, while others do not. Six replicate measurements from a single sample is most propably not enough to calculate the RSD% values in a reproducible manner. Also, in such a long measurement the instability of the analytes and drifting of sensitivity can also be an issue, as the instrument was not tuned before each experiment.

Although the results give a quite rough approximation of the effects of changing the integration time, they nevertheless enabled selecting suitable integration times for all the analytes, offering the best possible tradeoff between analysis time and precision. After selecting the integration times, it was found that all the analytes already had appropriate integration times and only minor changes were made to the original integration times (not shown). The optimized integration times can be seen in Table 19 on page 19.

The instruments sensitivity during the experiment was less than usual, as the experiment was done after an exceptionally long time without detector maintenance. Hereby, it can be concluded, that by choosing proper integration times based on the experiment, the assigned integration times are more than good enough for a properly maintained instrument.

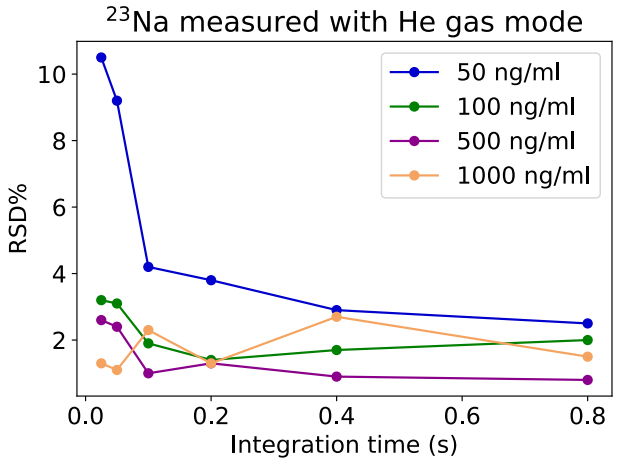

(a)

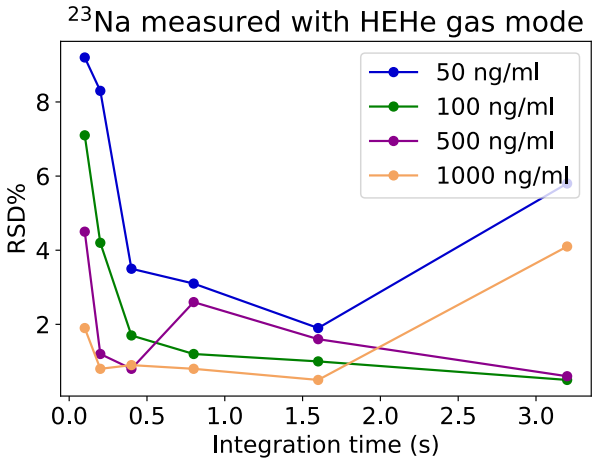

(b)

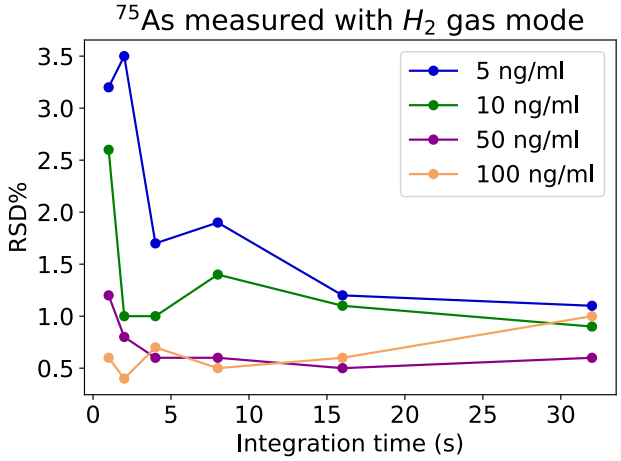

(c)

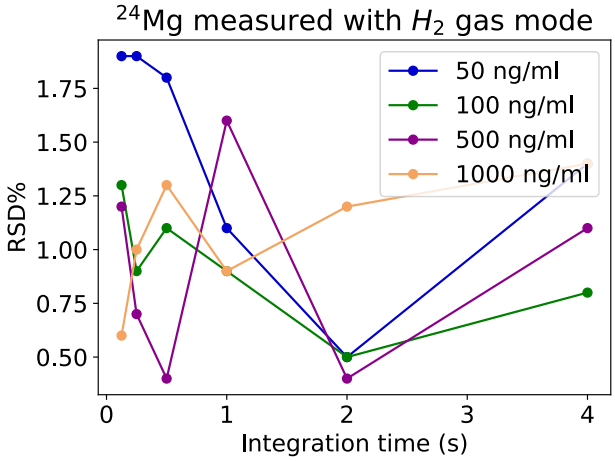

(d)

Figure 3 Relative standard deviation of measured analyte signal intensities as a function of integration time. The same calibration standards with varying analyte concentrations were measured multiple times with different integration times by using the xylene method. Six replicate measurements were obtained during single autosampler visit to to calculate the RSD%

12.2 The effects of changing the dilution ratio and the viscosity of samples

The results of the first optimization experiment

The results of the first experiment, designed to optimize the dilution ratios for ldiesels and jet fuels and to find an approptiate mineral oil concentration for the calibration standards, are shown in Figure 4. The figure shows the yttrium recoveries from test samples with varying dilution ratios, measured against calibration standards having differing mineral oil concentrations.

It can be seen, that there are significant differences in the ISTD recoveries between the studied matrices. These differences are presumably for the most part caused by viscosity differences between the test samples, as the both kind of jet fuels have higher ISTD recoveries compared to the heavier diesel fuels.

Based on the results, increasing the dilution ratio of the test samples leads to a decrease of the ISTD recoveries, most probably due to an increase in the viscosity of the test samples. For the same reason, increasing the mineral oil concentration of the calibration standards leads to an increase in ISTD recoveries from the test samples. As the viscosity of the standards are increased, less sample is atomized, leading to a decrease in the ISTD signal intensity from the standards. In other words, the relative ISTD signal intensity of the test samples to calibration standards is increased.

The results of the second experiment

The second study was designed to find a suitable mineral oil concentration along with an appropriate dilution ratios for both types of jet fuels. A plot of ISTD recoveries measured from Jet fuel 1 be seen in Figure 5. The plot shows the average of recoveries measured different gas modes. For recoveries measured with individual gasmodes, see Appendix E. The gasmode average recoveries for Jet fuel 2 are shown in Figure 6.

The results are in an agreement with the first optimization experiment and it can be seen, that increasing the viscosity of the test samples or calibration standards by addition of mineral oil leads to reduced signal intensity, as less sample is atomized and transferred to the plasma. As in the previous experiment, increasing the dilution ratio of test samples reduces the ISTD recoveries for both jet fuel types.

It can be seen in Figure 6, that the response of the instruments sensitivity to a change in the mineral oil concentration is close to linear. A linear response is also seen when the dilution ratio of Jet fuel is increased. Both effects are likely resulting from sample transport effects, primarly changes in the aspiration speed of samples.

Based on the results of the both experiments, an appropriate calibration standard mineral oil concentration was visually approximated to be 4 g/l. By using such standards, dilution ratios of 3 g/l 20 ml, 2.5 g/ 20 ml and 2.5 g/20 ml were found to produce close to 100% ISTD recoveries for Jet Fuel 2, Diesel 1 and Diesel 2 respectively. For the simultaneous analysis of Jetfuel 1 a dilution ratio of 5 g/20 ml was found appropriate when 2 g/20ml of mineral oil is added to the test samples. These results were confirmed in later measurements.

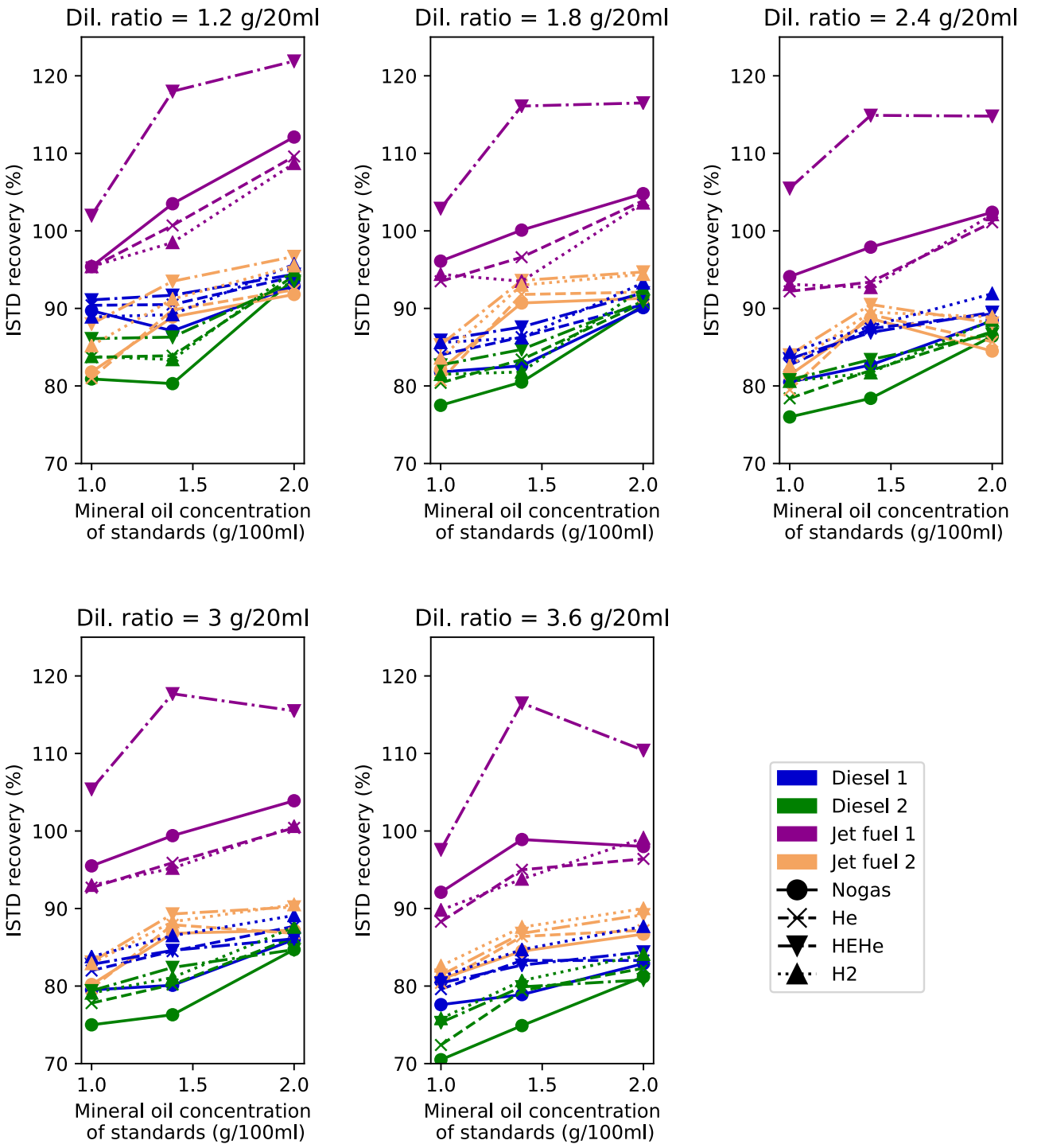

Figure 4 Measured yttrium recoveries as a function of mineral oil (75 cSt) concentration of blank samples. The colors represent the different sample matrices studied and the different linestyles representthe different gasmodes used for the measurement. Recoveries from the test samples having different dilution ratios are shown in different figures.

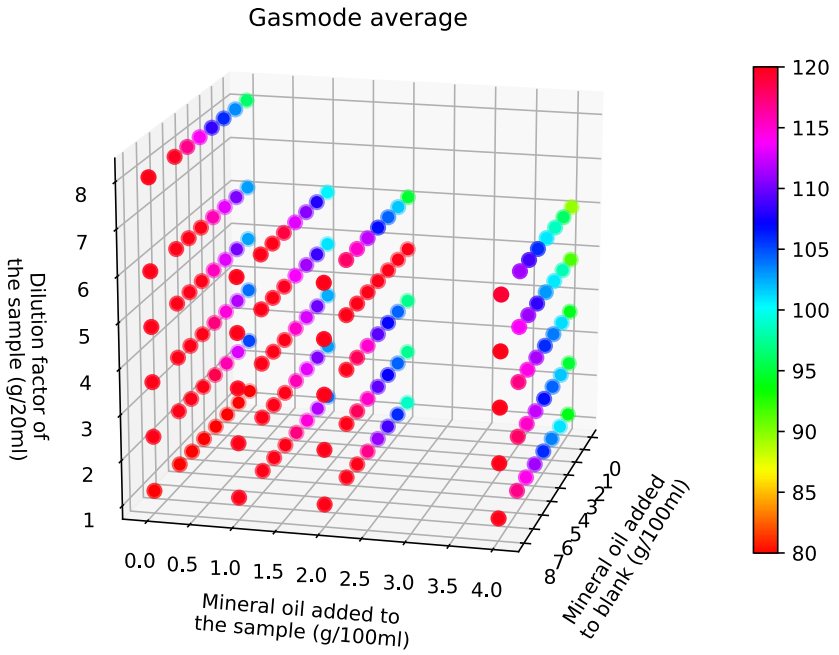

Figure 5 Gasmode average ISTD recoveries from Jet fuel 1. The color represents the recovery%.

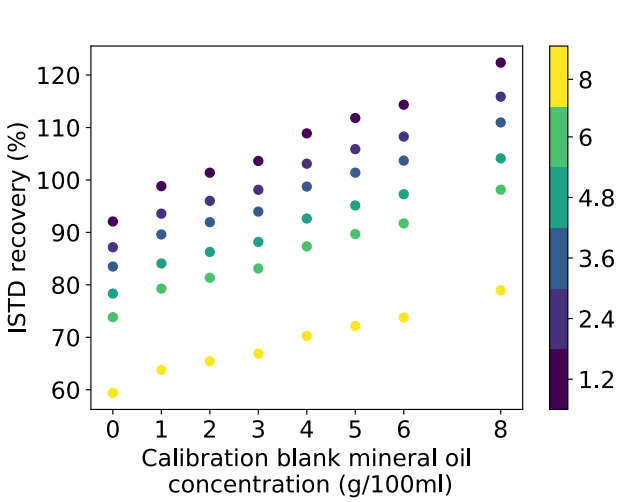

(a) ISTD recoveries as a function of calibration blank mineral oil concentration. The color represent the dilution ratio (g/20 ml of the sample).

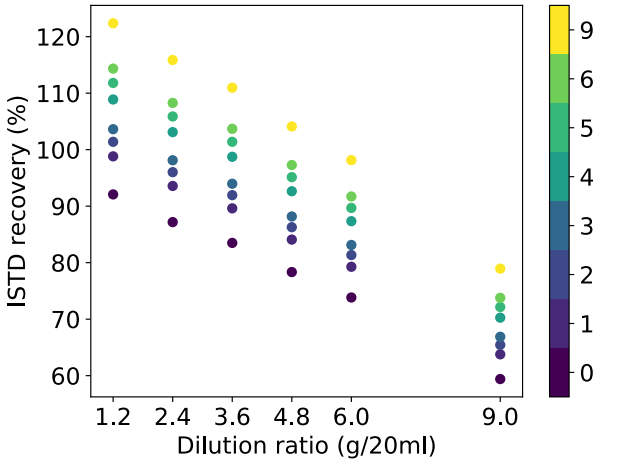

(b) ISTD recoveries as a function of the dilution factor. The color represents the mineral oil concentration in the calibration standards (g/100 ml).

Figure 6 Gas mode average ISTD yields for Jetfuel 2 samples measured with the xylene method. with varying sample dilution factors and blank sample mineral oil concentrations.

12.3 The optimization and developement of the Asolv method

Optimization of the carrier gas flow, sampling depth and dilution ratio for Diesel 1

A response surface showing the overall desirability of the analyte recoveries when carrier gas flow, sampling depth and dilution ratio of Diesel 1 are varied can be seen in Figure 7. The plotted response surfaces of the measurements with different isotopes/gas modes are given in Appendix B. The maximum overall desirability was found with following parameter values: carrier gas flow of 0.60 l/min, sampling depth of 8.40 mm and dilution ratio of 9.06 g/20 ml. To get a nice rounded number, dilution ratio of 9.0 was used in the validation. The optimal factor values were within the experimental space, so the selection of the experimental space therefore the optimization can be regarded succesful. Based on the plot, however, slightly higher carrier gas flow of 0.65 l/min would have lead to more robust conditions with a slight decrease in desirability.

The optimal carrier gas flow rate was higher compared to the one used in the xylene method (0.45 l/min). It can be seen, that the recoveries of many analytes decrease rapidly with smaller carrier gas flows, while no analyte has a notable increase in recovery. In addition some analytes sensitive to changes in carrier gas flow have too high recoveries when using higher flow rates. Assumably this happens, because the higher viscosity of Asolv compared to xylene reduces the aspiration rate of the sample solution. It is also possible that the atomization process is disturbed with low carrier gas flows, when a more viscous sample is analyzed. Both effects can have an influence on the degree of ionization of the analytes in the plasma as well as the kinetic energy distribution of the ions.

The extent of ionization of the analytes depends on the location of the plasma under consideration and the sample matrix, hence both the dilution ratio and the sampling depth can have an influence on the analyte recoveries as can be seen in the results. In most cases, however, the sampling depth had only a minor effect on the analyte recoveries with two prominent exceptions of ^{55}Co and ^{66}Zn measured with the H_2 mode. The magnitude of the impact of changing these factors seems to be highly dependent on the analyte and gasmode used for the measurement. The measurements of different analytes also seem to be sensitive to a change of one of these parameters independently of the other.

While the recovery of many analytes is highly dependent on one or many of the studied variables, other elements are barely influenced by a change in any of the factors and good analyte recoveries are obtained at almost every point of the experimental space. Few elements (Li, Na and K) have poor recoveries at every point, while the recovery of most of the studied elements can have a recovery of higher or lower than 100% depending on the factor values, therefore making it possible to find conditions leading to truly optimal accuracy for these analytes. However when multiple analytes are measured the result is always a compromise between the accuracy of different analytes.

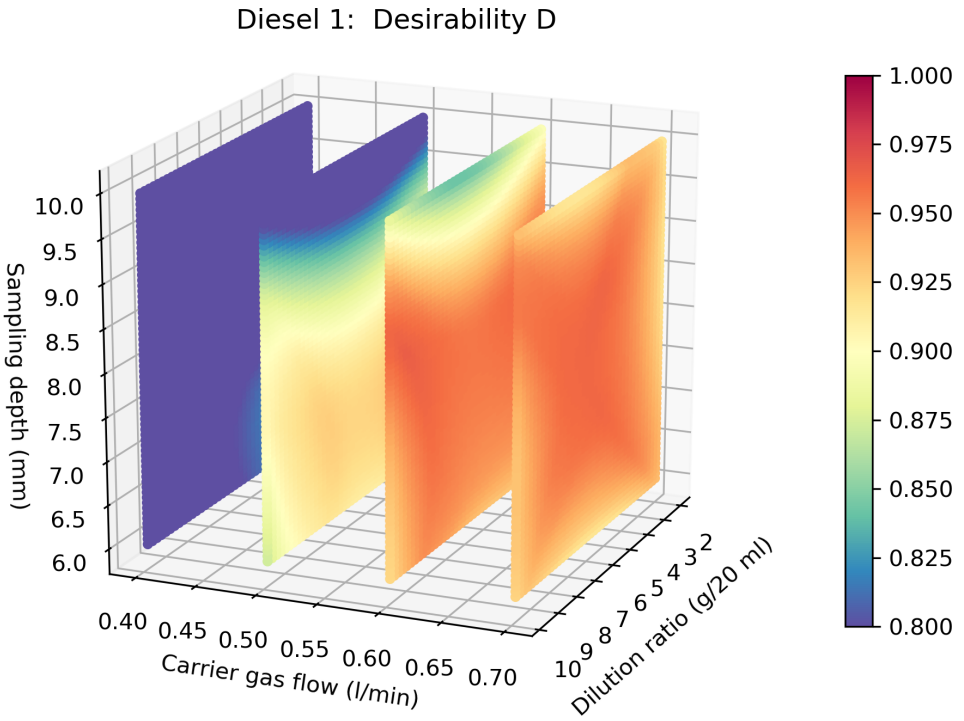

Figure 7 The response surface showing the overall desirability of the analyte recoveries from Diesel 1 measured with the Asolv method with varying sampling depth, carrier gas flow and sample dilution ratio. The color tells the overall desirability of analyte recoveries at any given point on the four slices taken from the response surface.

Optimization of the gasoline and Jet fuel 1 dilution ratio and mineral oil concentration added to the test samples

The plotted overall desirabilities from the optimizations of the gasoline and Jet fuel 1 test sample dilution ratios and mineral oil concentrations, can be seen in figures 8 and 9 respectively. For graphs of the response surfaces of measurements with different isotopes/gasmodes, see Appendix C and Appendix D. The best overall desirability of 0.92 for gasoline was found with the dilution ratio of 2.67 g/20 ml and with 2.0 g of mineral oil added per g of laboratory sample. The best overall desirability for Jet fuel 1 (0.95) was found by using the dilution ratio of 5.45 g /20 ml and adding 0.73 g of mineral oil per g of laboratory sample.

It can be concluded, that the optimization of the experimental conditions for Jet fuel 1 was succesful as the maximum of the global desirability is well within the experimental space, so the optimal conditions were found. The optimal desirability of the gasoline samples, however, is located at the edge of the experimental space. This indicates that the optimal conditions are outside the experimental space and the the analysis could be further improved by increasing the mineral oil concentration of samples.

The results of the optimization show, that the effect of changing the dilution ratio and

adding varying amounts of mineral oil to test samples does have a major impact on the analyte recoveries from both sample matrices. Based on the response surfaces, the overall desirability seems to be less sensitive to the changes in the test sample composition when analyzing Jet fuel 1 compared to analyzing gasoline. A likely explanation for this behavior is that there are less chemical and physical differences between Jet fuel 1 and Asolv, compared to gasoline and Asolv, as both are kerosene based products. Gasoline on the other hand is composed of lighter hydrocarbons and therefore has much higher vapor pressure and lower viscosity compared to Asolv. As it is known that high vapor pressure solvents can disrupt the plasma, it is no suprise that gasoline is a more difficult matrix to be analyzed.

There is, however, a high degree of similarity between the shape of the response surfaces of the overall desirabilities of both matrices, although the experimental space was different. It can be seen that for both matrices, adding more mineral oil to the samples with appropriate dilution ratios increases the overall desirability. As both studied matrices are less viscous compared to Asolv, increasing the mineral oil concentration evens the difference between the the volume of samples and standards introduced to the plasmat, until the viscosity of the sample will be higher compared to the viscosity of Asolv. It is also likely, that the reduction of the volume of sample introduced in the plasma, caused by the increasing the sample viscosity, reduces the disruption of the plasma induced by the difference in vapor pressures between the standards prepared in Asolv and test samples containing volatile components. This can explain, why the overall desirability keeps improving with increasing mineral oil concentration, even after the vicosity of the samples exceeds the viscosity of the standards.

The optimal analyte recoveries were obtained with conditions, that are significantly different from those yielding $\approx$100% ISTD recoveries (the center points of the experimental spaces). This effect was more pronounced when analyzing gasoline, as with the optimized conditions gasoline had an ISTD recovery significantly less than 100% and the response would have been even better with higher mineral oil concentration that would further decrease the ISTD recovery. Therefore the results suggest, that finding ISTD recoveries corresponding to recoveries from the calibration standards, is not a suitable way to optimize the test sample composition, as it does not take into account differences in vapor pressure or other factors affecting the relative ionization and the kinetic energy distribution of the analytes.

One could think that by using smaller the dilution ratios, the differences between the calibration standards and test samples would be reduced, therefore leading to higher desirability at low dilution ratios. Unexpectedly, this does not seem to be the case. Although this presumption holds, when analyzing gasoline samples with small mineral oil concentration, the interactions between the factors are more complex in the analysis of the both studied matrices.

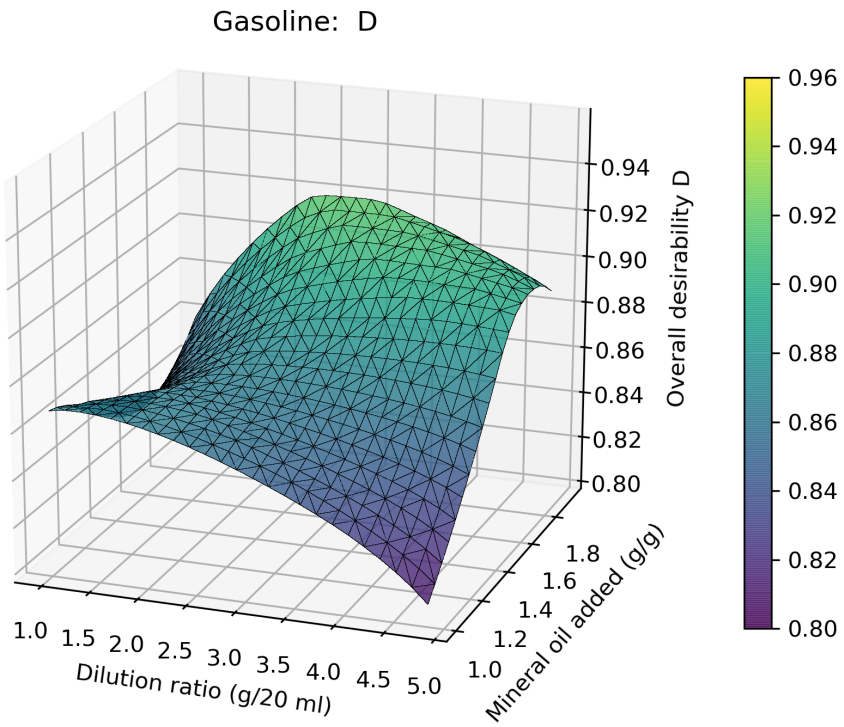

Figure 8 The overall desirability of gasoline test sample composition.

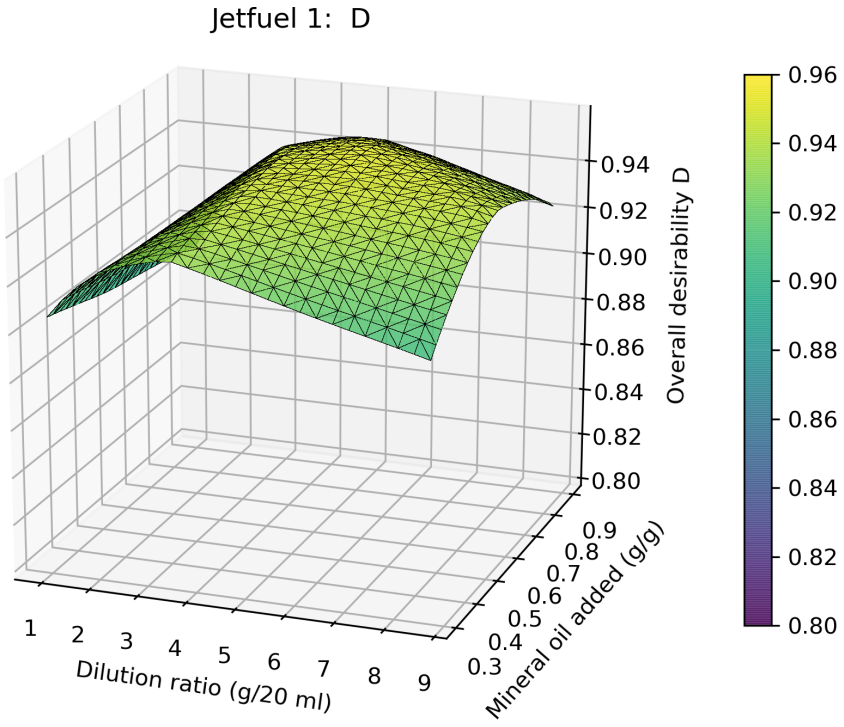

Figure 9 The overall desirability of Jet fuel 1 test sample composition.

The response of analytes measure from different matrices

There are many similarities in the overall desirabilities of the matrices, as well as in the response surfaces of individual analytes measured from different matrices, although the response surfaces come in various shapes. Regardless of the shape of the calculated response surfaces and differences in analyte recoveries between the studied matrices, the same analytes seems to be more sensitive or robust to the changes the experimental conditions independent of the studied matrix.

At the moment, there is no unambiguous explanation for this behavior. There does not seem to be clear correlation between the robustness of the analytes and the elemental features such as ionization energy and atom mass. One clear trend is, however, that the alkali metals are very sensitive to the changes in the composition of test samples prepared from any studied matrix. Meanwhile many transition metals give very good and robust recoveries with every studied matrix. Differences in the chemical stability of the analytes might explain some of the observations. The gasmode settings a used to measure the analytes most propably have a major effect on the recoveries of the analytes and the robustness of the analysis.

The effect of the gasmodes on the response surfaces

The results of the optimization of carrier gas flow, sampling depth and Diesel 1 dilution ratio show, that there are considerable differences between the response surfaces of same analyte measured with different gasmodes. For example when measuring ^{118}Sn, the recoveries obtained with nogas mode, are much more sensitive to the changes in experimental conditions compared to those measured with HEHe mode. Using the Nogas mode therefore leads to highly unpredictable results, that are very sensitive to changes in conditions. This also leads to difficulties when optimizing recoveries for multiple analytes and results in poor analyte recoveries. Therefore it is obvious, that HEHe mode should be preferred over Nogas mode.

Similarly the response of ^{55}Co, is very different using H_2 mode compared to He mode. When the response surfaces of ^{55}Co and ^{66}Zn measured are compared, the shape is very similar. This brings in a question, if the responses the two analytes would also be similar when using He mode, and if the robustness and recoveries of Zn could therefore be improved by changing the gas mode. Similarly cahngin the gasmode for other analytes with undesirable response could lead to more robust analysis and better yields.,

It does not come as a suprise that using a reaction/collision gas can make an ICP-MS analysis more robust, after all reaction/collision gasses are used to remove interferences. Suprisingly, differences between analyte recoveries measured with different gasmodes can be observed in the responses of B and W measured from Diesel 1 even though they should not have any spectral interferences based on their mass. Unexpectedly, it is seen, that the response of these elements is more robust when reaction/collision gasses are used.

Therefore the results suggest, that the observed differences between gasmodes are at least partially a result of differences in the gasmode spesific voltages of the ion optics, differences in the kinetic energy distribution of the analytes caused by variation in the

plasma conditions and collision induced reduction in the kinetic energy of the analytes in the reaction cell. These factors might change the quantity of analyte/ISTD ions excluded by the energy discrimination potential between the reaction cell and the detector, in a manner that depends on the relation between discrimination voltage and the energy distribution of the ions.

This interpretation suggests, that both, the robustness of the analysis and the analyte recoveries, could be enhanced by changing gas modes and optimizing the electric potentials of the ion optics. For analytes with no existing interferences, optimizing the voltages without using a reaction/collision gas would be better alternative to just using a more robust gas mode as using a reaction/collision gas leads to a decrease in signal intensity and therefore to a deterioration of precision. As adding new gasmodes would not significantly increase the analysis time, the gasmodes could be optimized for individual analytes or groups of analytes. RSM could be used in such optimization to gain knowledge on the robustness of the system.

Error of the optimization

As the measurements needed to optimize the carrier gas flow, sampling depth and the dilution ratio of Diesel 1 were relatively long, it is likely that the instability of analytes might have contributed to measurement error. In addition, the full factorial design was missing three experiments, which might have added to some uncertainty. As no quantitative error analysis was done for the optimization the uncertainty is not known.

In contrast, the measurements for optimizaton of gasoline and Jet fuel 1 samples were done single relatively short runs, so it is unlikely, that the deterioration of samples have contributed to the measurement error. Although the analytes are likely to have varying stability in different solutions and some reduction of concentration is likely happens, this should not be regarded as an error, but a property of a test sample composition to be optimized.

12.4 Estimation of error caused by the sample preparation and other error sources

Error limits of the commercial organometallic standards used in study

The deviation from the nominal concentration $u_{c,std}$ of the standards used was less than 1%.

Weighting error

When weighting the organometallic standards for stock solutions of the calibration standards, two different error sources exist. The scale it self has an unavoidable an error in every measurement. The precision of the balance was measured weekly using calibration standards and the measuring error was within $\pm$0.02 mg or $\pm$0.1 mg as measured by using 1 g and 10 g weights respectively. This gives a maximum measurement error of 0.002%.

In addition, there is an error caused by inability to dispense precisely the right amount

of standard, so that the real concentration in the standards would be the same as is used in the calculations of the calibration, as entering the accurate concentrations manually on a computer before each analysis would be a too laborious. This error can be estimated to be $\pm 0.5\%$ based on a record of the measurements. As the error of the scale is negligible compared to errors caused by other sources, it can be omitted so that the uncertainty of the mass u_m is therefore $u_m = \pm 0.5\%$. This uncertainty can be overcome after finding out the shelf life of stock solution, so bigger stock solution batches can be prepared to be used for several days/weeks. As larger amounts of standards are easier to dispense, this will improve the uncertainty.

The error of the pipettes

Pipettes used for the measurements were periodically tested and calibrated by Finas. However, as the calibration was most propably done by using water as the solvent, the precision of the 1 ml pipette was measured by pipetting 250 μl xylene and weighting the amount of xylene pipetted. From 30 consecutive measurements, the average mass $\bar{m}$ was 0.212 g and the sample standard deviation $s_{m,pipette}$ of the measurements was 0.389 mg. The precision of the pipette $u_V, pipette$ was then obtained by dividing the standard deviation with the average mass. For a two σ confidence interval the precision of the pipette is therefore:

$$u_{V,pipette} = 2\big(\frac{s_m}{\bar{m}} \times 100\%\big) = 2\big(\frac{0.389\text{mg}}{0.212\text{g}} \times 100\%\big) = \pm 0.368\% \tag{11}$$

According to the manufacturer, the density of the isomeric mixture of xylene was between 0.86 to 0.88 kg/l. A rough estimate of the accuracy can be obtained by calculating the pipetted volume V by dividing the average mass of xylene by the approximated density of xylene $\rho_{Xyl} = 0.87\text{g/ml}$:

$$V_{pipette} = \frac{\bar{m}}{\rho_{xyl}} = 0.242\text{ml} \tag{12}$$

Accuracy can then be calculated by substracting the measured value from the nominal value and by dividing with the nominal value:

$$\Delta V_{pipette} = \frac{V_{Nominal} - V_{Experimental}}{V_{Nominal}} \times 100\% = -2.73\% \tag{13}$$

It is unclear, if the error of the 5 ml pipette used in the preparation of standards and stock solutions has a similar error to the 1 ml pipette tested. In addition, pure xylene might behave differently from xylene-mineral oil solution or Asolv. A systematic error of 2.7% is nevertheless a major source of inaccuracy. The accuracy of pipettes should be therefore be carefully tested and calibrated with an appropriate solvent as needed to eliminate the the systematic error in pipetting.

Error of the volumetric flasks

Volumetric flasks of 20 ml, 25 ml and 50 ml were used in the analysis with measurement errors of $\pm$0.04 ml, $\pm$0.04 ml and $\pm$0.06 ml respectively. This means that the 20 ml flask has the biggest error of:

$$u_{V,flask} = \frac{0.04\,\mathrm{ml}}{20\,\mathrm{ml}} = \pm 0.2\% \tag{14}$$

Uncertainty of the analyte concentration in calibration standards

By using the law of propagation of uncertainty for multiplications (Eq. 15)

$$u = \sqrt{\sum_i u_i^2} \tag{15}$$

it is possible to estimate the uncertainty of concentration in calibration standards u_c from the uncertainties of mass, volume and concentration of commercial standards (Eq. 16) The error of the flask has to taken in to account only during the dilution of standard solutions, as using ISTD corrects the volumetric error when diluting the calibration standards.

$$u_c = \sqrt{u_{c,std}^2 + u_m^2 + RSD_{V,pipette}^2 + \Delta V_{pipette}^2 + 2u_{V,flask}^2} \tag{16}$$

$$\Rightarrow u_c = 2.99\% \tag{17}$$

However the result is only an approximation, as it assumes that every standard is prepared the same way, by weighting and dilution followed by a single pipetting step. In reality the preparation of the standards was more complex. Also, the reduction of RMS error caused by increasing sample size when several standards are prepared for calibration is omitted for simplicity.

It should also be noted, that u_c does not show up in the results of the validation as the spiked samples were prepared by using the same stock solutions as were used for calibration standards. Therefore, the relative concentration remains unchanged between different solutions regardless of the concentration in the stock solution used. The uncertainty of concentration is, however, a concern when real samples are analyzed.

Uncertainty in the concentration of the spiked samples

When measuring a sample the ISTD solution have to be pipetted twice, once during the preparation of the standards and a second time when preparing samples. As only the relative concentration of ISTD matters when calculating the concentrations, any systematic errors in pipetting does not add up to the error. The error caused by a difference in ISTD

concentration between calibration standards and in a test sample is therefore:

$$u_{ISTD} = \sqrt{2u^2_{V,pipette}} \tag{18}$$

$$\Rightarrow u_{ISTD} = 0.520\% \tag{19}$$

The error of standard additions is acquired from the uncertainty of the pipette when measuring the ISTD and when measuring the standard stock solution. Therefore the uncertainty of the standard addition is obtained with Eq. 20.

$$u_{c,spike} = \sqrt{u^2_{ISTD} + 2u^2_{V,pipette}} = 0.637\% \tag{20}$$

Unlike the uncertainty of the analyte concentration in calibration standards the uncertainty of the standard additions is included in the error seen in the validation results.

Error caused by instrument drifting

The results of the stability of the analysis conditions of the xylene and the Asolv methods can be seen in figure 11. The results show the normalized analyte concentrations of calibration standards and test samples with varying sample matrices during 35 and 45 hour long analysis runs.

It is unclear, how much of the drifting is caused by changes in the instruments sensitivity, that can be a result of accumulation of dirt and carbon deposit inside the instrument, and how much is related to changes in the chemical composition of the measured solutions. Nevertheless, it is likely that a major part of the drifting is a result of poor stability of the analytes in sample solutions. As some of the validation runs were up twelve hours long, it can be estimated, that the error caused by sensitivity drifting can be up to 10% depending on the analyte.

An important detail can be seen in the drifting plot of the calibration standard with the concentration of 500 or 50 ng/g of different analytes (Fig. 11a). In the plot, boron stands out showing a very rapid reduction of concentration. The same pattern is also seen in spiked Jet fuel 1 sample prepared in xylene, but is obsolete in measurements of the calibration standard or spiked Jet fuel 1 sample prepared in Asolv.

If the results of the drifting measurements are compared to the measurement errors of the validations, boron stands out in both results showing poor yields and precision in the validation and significant drifting in the stability measurements with the xylene method, with the Asolv method, the results are comparable to other analytes. Further, when comparing the boron calibration curves of the two methods there is a distinct difference. While the calibration curve measured with the Asolv method is highly linear, the calibration curve in xylene has a very distinct round shape (Figure 10), yet using a second order curve fit in the calibration failed to give reproducible boron recoveries. These results suggest that it is the unstability of boron in xylene solution, rather than non-linear instrument response, that renders the xylene method unsuitable for boron analysis.

Other noticable phenomena seen in the drifing measurements is the magnitude of the drifting depends on the sample matrix. It can be seen that the drifting is most prominent

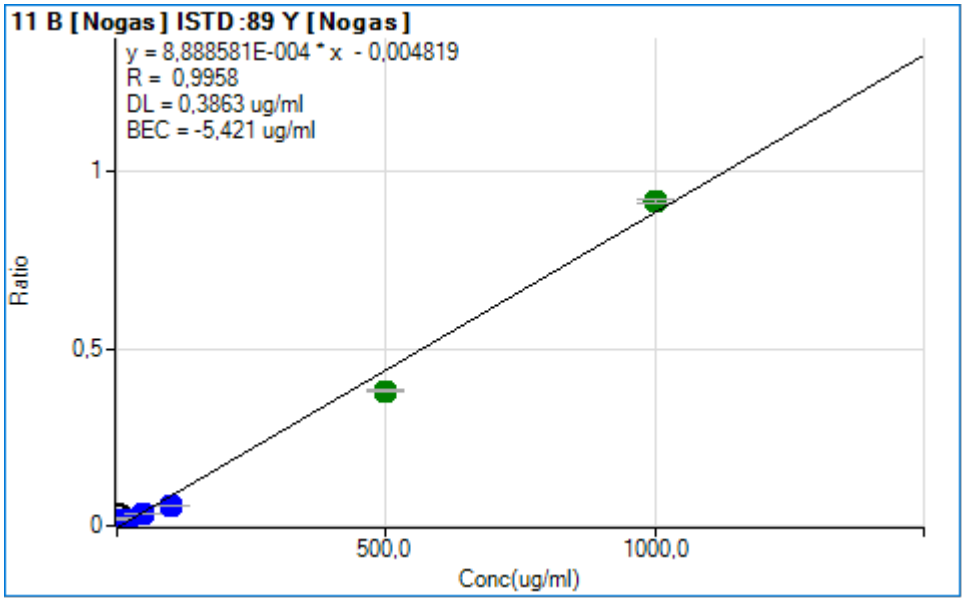

Figure 10 Typical boron calibration line used in the calibration of the xylene method. Same although less pronounced calibration curve shape was seen in the calibration of Li. In contrast the calibration curve of B when usin the Asolv method, the response was highly linear (R≈1.0000)

in the gasoline sample (Fig. 11f) measured with the Asolv method. Overall, less drifting is happening in the samples and standards prepared in xylene compared to those prepared in Asolv. Therefore the results suggests, that by overall, the analytes are more stable in xylene solution, compared to Asolv with the exeption of boron. At the moment it is unclear if the Conostan stabilizer added to the Asolv would also stabilize elements in xylene or if the stability of boron is unrelated to the stabilizer.

To address this issue, a further study should be designed to measure the chemical stability of the elements independently from the instruments sensitivity drifting to see if the stability of xylene could be improved with Conostan Stabilizer or other additives. In any case, it is best to avoid too long measurements and not to store samples or standards for prolonged times.

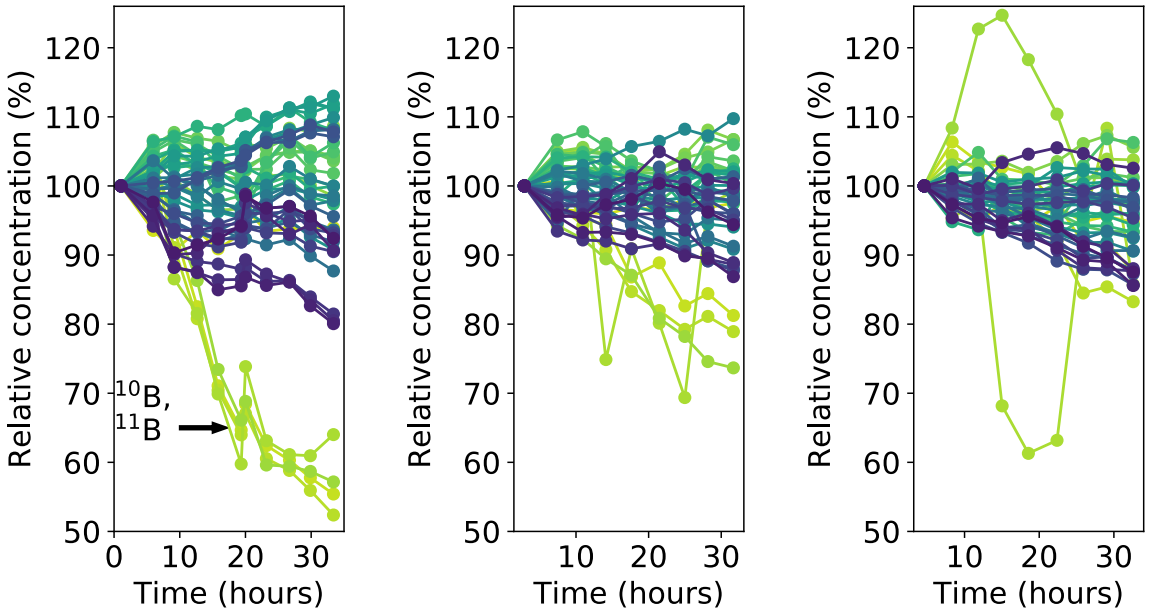

(a) Calibration standard (500&50 ng/g) measured with the **xylene** method.

(b) Spiked Jet fuel 1 (600&60 ng/g) measured with the **xylene** method

(c) Spiked Jet fuel 2 (600&60 ng/g) measured with the **xylene** method

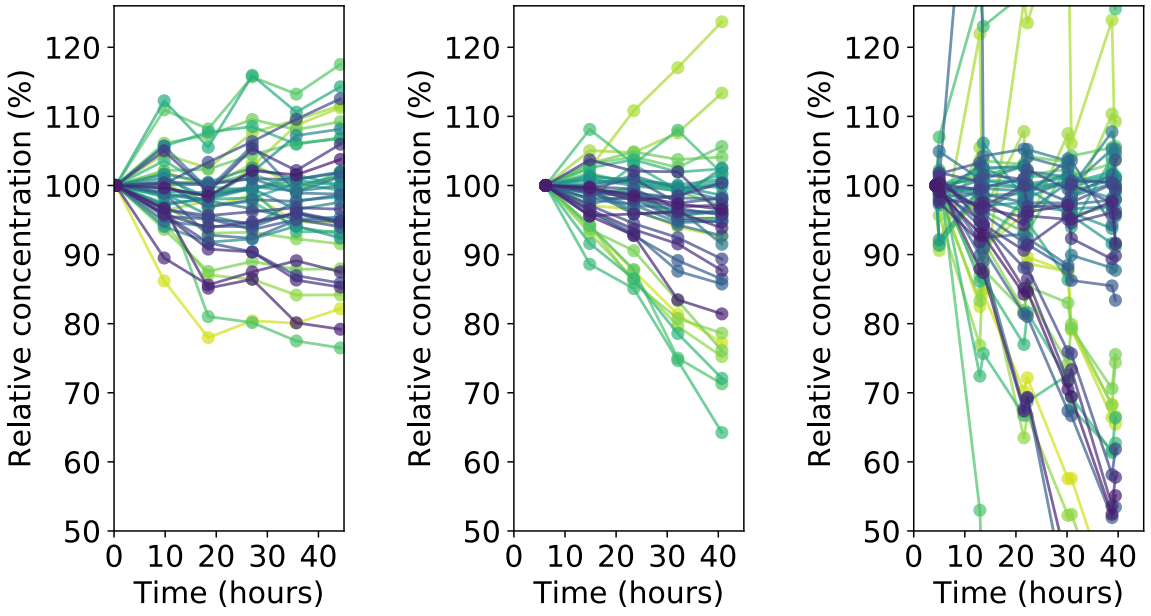

(d) Calibration standard (500&50 ng/g) measured with the **Asolv** method.

(e) Spiked Jet fuel 1 (600&60 ng/g) measured with the **Asolv** method

(f) Spiked gasoline (600&60 ng/g) measured with the **Asolv** method

Figure 11 Drifting of the analyte concentrations measured from varying matrices with the xyl method and the Asolv method. The colors indicate analytes with different m/Z ratio. The lightest elements are shown in light green and the heaviest elements are plot in dark blue.

Linearity of the instrument response

The response of the instument was highly linear for most analytes and the deviations from the linearity were most propably a result of poor stability of the analytes in the calibration standards. Therefore, it can be assumed that the calibration of the instrument did not result any significant error.

Memory effect

A major source of error influencing the analysis is the memory effect where after measuring a sample containing high concentration of analytes the analytes are visible in the next sample, although the following sample would not contain any analytes. This can lead to a major increase of the detection limits of the analytes, but the magnitude of the effects on the validation results are unclear.

The memory effect is caused by residual analytes released from the instrument and proper washing step between the analytes can be used to reduce this effect. However washing is the most time-consuming step in the measurement runs of both studied methods. As prolonged runs can lead to increased drifting effects and lead to problems with analyte stabilities, unnecessary washing should be avoided.

To reduce the analysis time as well as reduce the background caused by the memory effect, automated washing should be utilized. This functionality, that is supported by Agilent MassHunter software, measures the concentration of selected analytes during the washing step and the washing is continued until the measured concentrations are below a selected value. This ensures a sufficient washing time after a sample containing high concentration of analytes. On the other hand if the measured sample barely contains any analytes, unnecessary washing is avoided.

Possible contamination sources

As analytes can be measured at ppb levels by using ICP-MS, the sensitivity makes the analysis very prone to contaminations. Materials that were used in the sample and standard preparation and could have lead to possible contamination include volumetric glass flasks and test tubes, plastic pipettes, plastic pipette tips and plastic caps used to seal the flasks. Also dust coming from textiles, paper, human tissue and other sources in the laboratory might have caused contamination issues.

It is unlikely that the glass vessels used in the sample preparation would have caused any significant contamination, as the they were cleaned in vigourously acidic conditions before analysis and non-polar organic solvents used in the analysis are poor solvents for inorganic contaminants. However, the plastic caps used to seal the flasks could have potentially lead to cross contamination or leaking of contaminants into the samples. When it comes to contamination, using PTFE caps would be better alternative as they can be cleaned in an acid cleaner with the glass vessels.

The pipette tips used were a potential source of phosphorus contamination, so blank samples prepared by using freshly prepared mineral oil-xylene solution were measured in the same run with blank samples prepared using an old mineral oil-xylene solution. As

the mineral oil solution was dispensed using an automatic pipette and the solution was released back to the solution to stabilize vapor pressure, polential contaminants in the pipette tips would have been accumulated in the old solution. However, no significant difference was found in the elemental composition between the samples.

Plastic disposable pipettes were used to dispense organometallic standards when weighting them in the preparation of standard stock solutions. One of the used pipette batches was later found out to leak silicon in ppm range into test samples, when laboratory samples were dispensed using the pipettes. However, it is unclear if this caused any significant contaminations in the validation of the methods. That said, a possibility of contamination should be noted when interpreting the validation results.

It is unclear if dust present in the laboratory air is a source of contamination. This could be investigated by analyzing dust samples collected from the laboratory and comparing the elemental composition of dust to the BEC values obtained from the validation. The potential dust contamination could be resolved by using a laminar hood, keeping the laboratory tidy and avoiding unnecessary use of paper in the laboratory. Using a hairnet and a face mask would reduce contamination coming from the analyst.

12.5 Results of the validation and comparison of the studied methods

The detection limits and the background equivalent concentrations obtained from the validation of the both studied methods are given in Table 28 on page 83. The calculated analyte recoveries and the relative standard deviations of the test samples spiked with 600 ng/g and 60 ng/g of different analytes are shown in Table 29 on page 85. For comprehensive tables of results of the validation samples spiked with smaller concentration of analytes see Appendix H. For the measured concentrations of analytes present in the unspiked samples used in the validation, see Appendix G.

The effect of the spray chamber temperature on the LOD and BEC

As expected, a significant overall improvement of detection limits and BEC values of the analytes can be seen when the lower spray chamber temperature of -5°C is used instead of +5°C with the xylene method. The most likely explanation for this behavior is the reduced solvent load of the plasma when using the lower spray chamber temperature.

Comparison of the validation results measured with the xylene method and with the Asolv method

When the BEC values, measured with the spray chamber temperature of +5°C, are compared between the xylene method and the Asolv method, it is seen that while the BEC values of many analytes are comparable, there are major differences in the BEC of other analytes. While some of the analytes have much lower background with one method, some have better background with the other. A same kind of behavior can be seen in detection limits of test samples and there is a correlation between the BEC values and detection limits of the two methods as the analytes having lower BEC value on one method also have

lower LOD compared to the other method. The observed differences could be linked to the stability of the analytes in the calibration standards, as is likely with boron, or they can be related to possible interferences and background coming from the solvent.

When the detection limits of Diesel 1 fuels are compared between the xylene method and the Asolv method, it should be appreciated, that when the dilution of the samples is taken into account, the higher dilution ratio used in the Asolv method leads to a significant decrease of detection limits. This makes the detection limits of almost every analyte smaller on the Asolv method with the exceptions of Si, P, Zn and Sb, that are somewhat lower with the xylene method.

When the analyte recoveries from the Diesel 1a are compared, it is seen that the Asolv method has better analyte recoveries of almost every analyte. In addition the concentration RSD% of the spiked samples are lower with the Asolv method, with the only exception being Pt. Therefore it can be concluded that the Asolv method is superior to the xylene method when analyzing Diesel.

No obvious overall benefit is seen on one method over the other, when the xylene method with the spray chamber temperature of -5°C or the Asolv method with the spray chamber temperature of +5°C are used to analyze Jet fuel 1. However, the effect of the spray chamber temperature should be taken into account and it is highly propable that using the lower temperature with the Asolv method would lead to lower detection limits.

Possible contaminations and interferences

The BEC values of most analytes analytes were low. Few notable exeptions were ^{28}Si, ^{31}P (measured with Nogas mode), ^{39}K and ^{40}Ca. The high BEC values of these elements might be a result of possible contaminatios or spectral interferences and resolving these could decrease the detection imits of these analytes.

The BEC value of silicon is among the highest of analytes regardless of the method used for measurement. This can be a sign of a possible contamination. As contaminated pipettes were used in the standard preparation, care should be taken when interpreting the results. The high BEC value could also be a result of a $^{14}N_2^+$ or $^{12}C^{16}O^+$ interference on ^{28}Si. If this is the case, the gasmode parameters could be optimized to remove the interferences.

In the case of P, several polyatomic inteferences originating from air, solvent and plasma gasses are most likely causing significant interferences on ^{31}P when Nogas mode is used. This is seen as a high or highly negative BEC value regardless of the method. The fact that ^{31}P measured with H_2 mode has a BEC value comparable to other analytes rules out the possibility that the high BEC is caused by a contamination. Therefore it is essential to use a reaction gas when measuring ^{31}P and using Nogas mode cannot be recommended. HEHe mode on the other hand seems to be quite effective in removing interferences in both methods.

In the case of Na and K it is seen that the BEC values are very high or very negative when using the xylene method. In addition the recoveries of these analytes are among the poorest in both methods although the Asolv method has substantially better recoveries

and precision when measuring these elements. In addition these elements had poorly recoveries in the optimization of the Asolv method regardless of the analysis conditions. In addition Na ^{23}Na does not have spectral interferences based on its mass. Therefore it is likely that the difficulties in analyzing these elements are related to chemical unstability of the analytes in hydrocarbon solutions. On the other hand ^{39}K also seems to suffer from $^{38}Ar^{1}H^{+}$ interference the measurements with H_2 unambiguously have lower BEC and LOD compared to measurements with HEHe mode.

It is unclear why ^{40}Ca has a relatively high BEC on both studied methods, although excellent analyte recoveries are obtained with both methods. Neither, the possibility of a $^{40}Ar^{+}$ interference on ^{40}Ca, or a possible background contamination can not be excluded.

Furhermore, it is impossible to tell, if any of the studied analytes had caused spectral interferences on other analytes. As multiple analytes were added to the standards and to the spiked samples, signals caused by possible interferences would have increased in relation to increasing analyte concentrations and left unnoticed. To examine the possible interferences, it is therefore necessary to analyze samples spiked with only a few analytes at the time. Additionally commercial reference standards could be used for assurance.

12.6 The analyte recoveries and the standard deviations

When the RSM% values from the spiked validation samples are compared, it is obvious that the Asolv method offers higher precision for almost every analyte. In addition somewhat better overall analyte recoveries are obtained with the Asolv method. These differences might be related to more robust plasma conditions when using Asolv, as less volatile solvent is used with smaller sample aspiration rate. The differences can also be related to better optimization of the Asolv method leading to more robust analysis.

Table 28 Detection limits and background equivalent concentrations of different sample matrices measured using different methods and gasmodes

		Xylene method (+5°C)			Xylene method (-5°C)			
			LOD (μg/kg)			LOD (μg/kg)		
Isotope	**Gasmode**	**BEC**	Test smpl.	Diesel 1&2	**BEC**	Test smpl.	Jetfuel 1	Jet fuel 2
^{7}Li	Nogas	−0.0702	0.636	5.09	−0.0883	0.896	3.58	5.97
^{10}B	Nogas	51.9	156.0	1250.0	5.99	28.1	112.0	187.0
^{11}B	Nogas	55.1	164.0	1310.0	9.88	20.5	81.8	136.0
^{11}B	He	76.7	212.0	1700.0	8.90	30.7	123.0	204.0
^{11}B	H_2	48.5	140.0	1120.0	8.54	17.0	68.2	114.0
^{23}Na	Nogas	4.51	64.2	514.0	−1.62	15.7	62.9	105.0
^{23}Na	He	4.80	61.9	495.0	−2.16	15.4	61.7	103.0
^{23}Na	HEHe	4.65	63.8	510.0	−2.20	16.4	65.5	109.0
^{24}Mg	H_2	0.994	2.76	22.0	0.0386	0.99	3.96	6.60
^{27}Al	HEHe	0.401	1.22	9.75	−0.272	0.471	1.88	3.14
^{28}Si	H_2	1.57	7.39	59.1	2.99	30.3	121.0	202.0
^{31}P	Nogas	5.26	51.1	409.0	1.75	17.0	67.9	113.0
^{31}P	HEHe	0.295	2.83	22.6	−0.0855	4.01	16.0	26.7
^{39}K	HEHe	5.75	27.6	221.0	6.69	21.2	85.0	142.0
^{39}K	H_2	3.54	22.7	181.0	2.60	14.6	58.5	97.4
^{40}Ca	H_2	2.44	13.1	105.0	0.827	11.2	45.0	75.0
^{47}Ti	H_2	0.188	2.86	22.9	−0.18	1.05	4.20	7.00
^{51}V	HEHe	0.0419	0.165	1.32	0.005 32	0.113	0.452	0.754
^{52}Cr	HEHe	0.0902	0.455	3.64	−0.0368	0.244	0.977	1.63
^{55}Mn	HEHe	0.560	1.96	15.7	−0.0117	0.469	1.88	3.13
^{56}Fe	He	0.502	4.29	34.3	0.178	2.14	8.57	14.3
^{59}Co	He	−0.105	0.372	2.98	−0.247	0.229	0.918	1.53
^{59}Co	H_2	−0.072	0.257	2.06	−0.173	0.158	0.632	1.05
^{60}Ni	HEHe	0.652	2.39	19.1	0.001 02	0.568	2.27	3.79
^{63}Cu	HEHe	0.151	1.62	13.0	0.0294	0.483	1.93	3.22
^{66}Zn	H_2	0.653	2.38	19.0	0.27	2.71	10.8	18.1
^{75}As	He	0.006 66	0.0401	0.321	0.0187	0.0658	0.263	0.439
^{75}As	HEHe	0.005 23	0.0406	0.325	0.0179	0.0592	0.237	0.395
^{75}As	H_2	0.005 16	0.0395	0.316	0.0204	0.0596	0.238	0.397
^{88}Sr	H_2	0.066	0.216	1.72	0.009 13	0.0702	0.281	0.468
^{95}Mo	HEHe	0.0318	0.111	0.886	−0.007 93	0.0875	0.350	0.583
^{105}Pd	He	−0.006 22	0.0421	0.337	0.005 26	0.0270	0.108	0.180
^{114}Cd	Nogas	0.525	1.86	14.9	0.0448	0.612	2.45	4.08
^{118}Sn	Nogas	−0.009 17	0.278	2.22	−0.11	0.56	2.24	3.73
^{118}Sn	HEHe	−0.0172	0.319	2.56	−0.0539	0.341	1.36	2.27
^{121}Sb	HEHe	0.0169	0.0637	0.509	0.0190	0.0564	0.226	0.376
^{121}Sb	H_2	0.0168	0.0624	0.499	0.0174	0.0493	0.197	0.329
^{137}Ba	Nogas	0.192	1.01	8.08	0.002 73	0.406	1.62	2.71
^{140}Ce	He	0.0673	0.260	2.08	0.007 66	0.017	0.0679	0.113
^{140}Ce	HEHe	0.0584	0.229	1.83	0.007 34	0.0157	0.0629	0.105
^{140}Ce	H_2	0.0519	0.202	1.62	0.004 84	0.0134	0.0535	0.0892
^{182}W	Nogas	0.002 04	0.0198	0.158	0.002 48	0.0169	0.0677	0.113
^{182}W	HEHe	0.001 82	0.0148	0.118	0.003 27	0.0143	0.0571	0.0951
^{195}Pt	Nogas	0.003 91	0.0490	0.392	−0.0205	0.198	0.793	1.32
Pb*	Nogas	0.421	1.81	14.4	0.0317	0.634	2.54	4.23

* The concentration of Pb was obtained by using a sum of signals of ^{206}Pb, ^{207}Pb and ^{208}Pb.

Table 28 continued Detection limits and background equvalent concentrations of different sample matrices measured using different methods and gasmodes

		Asolv method (+5°C)				
			LOD (μg/kg)			
Isotope	**Gasmode**	**BEC**	Test sample	Diesel 1	Jetfuel 1	Gasoline
^{7}Li	Nogas	0.182	0.409	0.908	1.37	3.03
^{10}B	Nogas	−0.985	3.94	8.74	13.2	29.2
^{11}B	Nogas	−1.19	4.19	9.30	14.1	31.0
^{11}B	He	−3.51	13.8	30.6	46.3	102.0
^{11}B	H_2	−1.01	5.52	12.2	18.5	40.9
^{23}Na	Nogas	−0.162	11.6	25.8	39.0	85.9
^{23}Na	He	1.53	22.4	49.8	75.4	166.0
^{23}Na	HEHe	−0.580	18.8	41.7	63.1	139.0
^{24}Mg	H_2	0.127	0.478	1.06	1.60	3.54
^{27}Al	HEHe	0.850	5.97	13.2	20.1	44.2
^{28}Si	H_2	4.14	48.6	108.0	163.0	360.0
^{31}P	Nogas	−6.43	46.4	103.0	156.0	344.0
^{31}P	HEHe	0.547	17.3	38.4	58.1	128.0
^{39}K	HEHe	2.07	38.5	85.5	129.0	285.0
^{39}K	H_2	0.577	6.46	14.3	21.7	47.8
^{40}Ca	H_2	2.60	9.01	20.0	30.3	66.7
^{47}Ti	H_2	0.308	1.55	3.45	5.22	11.5
^{51}V	HEHe	−0.005 51	0.236	0.525	0.795	1.75
^{52}Cr	HEHe	0.044	0.223	0.496	0.751	1.66
^{55}Mn	HEHe	0.0678	0.203	0.452	0.684	1.51
^{56}Fe	He	−0.0603	0.554	1.23	1.86	4.11
^{59}Co	He	0.0711	1.09	2.43	3.68	8.11
^{59}Co	H_2	−0.0014	0.0858	0.190	0.288	0.635
^{60}Ni	HEHe	−0.027	0.216	0.480	0.727	1.60
^{63}Cu	HEHe	−0.737	6.02	13.4	20.2	44.6
^{66}Zn	H_2	−5.12	27.8	61.8	93.5	206.0
^{75}As	He	0.0110	0.0671	0.149	0.225	0.497
^{75}As	HEHe	0.002 03	0.0444	0.0986	0.149	0.329
^{75}As	H_2	0.008 15	0.0525	0.117	0.176	0.389
^{88}Sr	H_2	0.113	0.663	1.47	2.23	4.91
^{95}Mo	HEHe	0.0835	0.21	0.465	0.704	1.55
^{105}Pd	He	−0.0266	0.103	0.229	0.346	0.764
^{114}Cd	Nogas	0.0263	0.131	0.291	0.440	0.971
^{118}Sn	Nogas	0.576	2.10	4.66	7.05	15.5
^{118}Sn	HEHe	0.589	2.97	6.59	9.97	22.0
^{121}Sb	HEHe	0.179	0.831	1.84	2.79	6.15
^{121}Sb	H_2	0.0916	0.471	1.05	1.58	3.49
^{137}Ba	Nogas	0.0863	0.599	1.33	2.01	4.44
^{140}Ce	He	−0.003 85	0.0349	0.0774	0.117	0.258
^{140}Ce	HEHe	−0.002 08	0.0348	0.0772	0.117	0.257
^{140}Ce	H_2	0.002 07	0.0428	0.0950	0.144	0.317
^{182}W	Nogas	0.005 28	0.0358	0.0795	0.120	0.265
^{182}W	HEHe	0.0067	0.0276	0.0613	0.0928	0.205
^{195}Pt	Nogas	0.0057	0.0749	0.166	0.252	0.555
Pb*	Nogas	−0.154	0.761	1.69	2.56	5.64

* The concentration of Pb was obtained by using a sum of signals of ^{206}Pb, ^{207}Pb and ^{208}Pb.

Table 29 Measurement RSD% and analyte recoveries from validation samples spiked with 600 ng/g or 60 ng/g of analytes. The values for analytes spiked with 60 ng/g are marked with bold.

		Xylene method -5°C				**Xylene method +5°C**			
		Jet 1 avg.		**Jet 2 avg.**		**Diesel 1 avg.**		**Diesel 2 avg.**	
Isotope	**Gasmode**	RSD%	Recov.%	RSD%	Recov.%	RSD%	Recov.%	RSD%	Recov.%
^{7}Li	Nogas	**17.1**	**84.3**	**15.4**	**76.3**	**32.6**	**46.7**	**12.9**	**66.2**
^{10}B	Nogas	29.6	51.4	58.9	18.6	60.7	57.1	114.0	−1.47
^{11}B	Nogas	29.5	49.5	42.8	17.6	65.7	55.4	129.0	−5.23
^{11}B	He	31.7	46.3	42.1	12.3	75.1	11.2	129.0	−60.1
^{11}B	H_2	30.2	55.3	42.1	22.1	60.4	77.0	98.1	15.6
^{23}Na	Nogas	23.6	87.9	19.6	85.4	55.3	62.8	31.9	62.3
^{23}Na	He	23.8	90.4	19.5	85.6	57.9	61.7	32.2	63.3
^{23}Na	HEHe	22.8	87.4	19.0	87.1	60.2	61.8	30.0	66.7
^{24}Mg	H_2	4.53	95.6	3.87	88.8	15.6	90.1	14.0	85.6
^{27}Al	HEHe	4.35	98.2	4.32	90.9	10.2	93.4	9.07	85.7
^{28}Si	H_2	4.03	92.5	10.3	−17.1	12.6	98.7	9.60	97.0
^{31}P	Nogas	6.83	100.0	12.3	81.5	56.2	42.2	59.3	52.9
^{31}P	HEHe	4.46	102.0	6.21	98.5	23.1	99.9	23.6	98.7
^{39}K	HEHe	20.0	78.9	38.4	101.0	48.1	31.9	27.9	56.6
^{39}K	H_2	20.1	78.7	38.4	102.0	42.8	42.5	26.1	68.5
^{40}Ca	H_2	4.89	100.0	4.48	96.1	19.8	101.0	16.6	91.7
^{47}Ti	H_2	4.22	96.5	5.18	96.7	14.2	99.3	12.7	97.8
^{51}V	HEHe	4.12	99.0	6.85	88.4	10.0	95.8	6.20	85.1
^{52}Cr	HEHe	2.24	103.0	2.00	101.0	6.02	101.0	6.36	97.2
^{55}Mn	HEHe	2.45	100.0	2.55	96.0	5.65	94.9	6.57	89.1
^{56}Fe	He	2.65	100.0	5.34	94.7	8.50	93.3	9.55	89.7
^{59}Co	He	**3.23**	**97.2**	**3.00**	**89.8**	**9.21**	**90.4**	**8.86**	**84.2**
^{59}Co	H_2	**3.05**	**94.9**	**1.57**	**90.3**	**7.05**	**93.8**	**6.30**	**90.0**
^{60}Ni	HEHe	3.17	97.2	3.12	91.7	8.12	91.3	6.80	86.7
^{63}Cu	HEHe	1.79	104.0	2.13	98.7	5.24	94.8	4.90	94.7
^{66}Zn	H_2	3.07	95.6	3.32	94.0	8.85	93.4	8.80	94.8
^{75}As	He	**1.98**	**99.7**	**2.01**	**97.3**	**16.4**	**94.3**	**15.9**	**93.8**
^{75}As	HEHe	**2.25**	**99.2**	**2.80**	**97.9**	**16.9**	**95.8**	**16.0**	**96.5**
^{75}As	H_2	**3.93**	**93.9**	**3.58**	**98.4**	**19.6**	**101.0**	**17.6**	**104.0**
^{88}Sr	H_2	**3.03**	**94.6**	**5.86**	**92.4**	**13.0**	**89.7**	**10.8**	**88.6**
^{95}Mo	HEHe	2.52	97.7	5.67	92.5	9.97	90.8	3.71	88.8
^{105}Pd	He	**2.90**	**98.5**	**2.94**	**94.8**	**6.78**	**96.9**	**5.93**	**89.1**
^{114}Cd	Nogas	3.64	96.0	3.80	90.3	9.30	89.1	10.4	83.7
^{118}Sn	Nogas	3.04	95.7	5.37	93.7	8.31	91.7	6.94	88.4
^{118}Sn	HEHe	4.75	88.7	8.39	88.1	8.71	93.4	7.21	90.3
^{121}Sb	HEHe	2.08	97.2	4.76	96.1	9.15	96.1	7.17	95.0
^{121}Sb	H_2	1.87	99.9	5.16	96.2	9.31	92.7	5.94	92.2
^{137}Ba	Nogas	3.30	89.7	7.07	91.0	6.82	89.7	8.96	86.3
^{140}Ce	He	**3.34**	**91.7**	**5.85**	**90.4**	**6.08**	**94.6**	**9.24**	**86.5**
^{140}Ce	HEHe	**2.56**	**92.4**	**6.58**	**90.7**	**6.24**	**96.5**	**7.43**	**90.0**
^{140}Ce	H_2	**4.54**	**88.2**	**5.53**	**92.8**	**8.26**	**102.0**	**7.83**	**98.3**
^{182}W	Nogas	**5.41**	**89.0**	**8.11**	**92.1**	**10.9**	**90.7**	**8.43**	**88.2**
^{182}W	HEHe	**4.40**	**93.9**	**7.81**	**93.0**	**12.2**	**93.0**	**8.24**	**90.3**
^{195}Pt	Nogas	**3.89**	**89.9**	**3.87**	**93.4**	**7.80**	**97.4**	**7.77**	**93.0**
Pb*	Nogas	4.88	88.9	7.78	91.1	10.8	90.6	13.4	80.4

* The concentration of Pb was obtained by using a sum of signals from ^{206}Pb, ^{207}Pb and ^{208}Pb.

Table 29 continued Measurement RSD% and analyte recoveries from validation samples spiked with 600 ng/g or 60 ng/g of analytes. The values for analytes spiked with 60 ng/g are marked with bold.

		Xyl. method +5°C		**Asolv method +5°C**					
		FAME B100		**Diesel 1a**		**Jet 1b**		**Gasoline**	
Isotope	**Gasmode**	RSD%	Recov.%	RSD%	Recov.%	RSD%	Recov.%	RSD%	Recov.%
^{7}Li	Nogas	**18.7**	**43.6**	**16.0**	**89.8**	**4.57**	**87.6**	**20.2**	**79.9**
^{10}B	Nogas	117.0	644.0	10.8	104.0	1.35	100.0	7.78	88.2
^{11}B	Nogas	102.0	541.0	10.5	104.0	1.15	99.5	7.71	87.5
^{11}B	He	111.0	668.0	12.2	99.4	6.22	102.0	6.71	75.6
^{11}B	H_2	112.0	613.0	9.82	106.0	3.58	104.0	8.84	86.2
^{23}Na	Nogas	11.2	133.0	16.9	90.0	3.86	89.0	17.5	81.3
^{23}Na	He	14.5	135.0	16.6	90.0	3.42	93.6	18.1	81.0
^{23}Na	HEHe	12.4	138.0	16.7	90.1	4.20	91.7	16.3	80.7
^{24}Mg	H_2	21.0	86.9	2.52	102.0	1.57	106.0	3.67	103.0
^{27}Al	HEHe	14.5	84.6	0.71	99.4	0.839	101.0	1.54	100.0
^{28}Si	H_2	3.99	107.0	4.91	105.0	2.51	190.0	6.82	105.0
^{31}P	Nogas	48.5	130.0	11.0	99.8	1.56	96.3	22.2	33.7
^{31}P	HEHe	26.5	110.0	10.2	115.0	4.40	107.0	17.8	99.6
^{39}K	HEHe	40.4	44.8	6.65	85.8	6.16	87.4	17.2	63.3
^{39}K	H_2	42.9	43.4	15.0	82.5	5.14	88.7	12.0	86.7
^{40}Ca	H_2	16.5	93.5	2.18	100.0	1.15	103.0	2.85	106.0
^{47}Ti	H_2	17.8	98.6	4.99	101.0	3.14	104.0	5.50	108.0
^{51}V	HEHe	9.61	84.7	1.47	97.0	0.458	97.7	0.478	98.4
^{52}Cr	HEHe	5.16	100.0	1.39	97.0	0.583	97.8	1.09	98.6
^{55}Mn	HEHe	5.84	87.1	0.651	97.9	1.03	98.2	0.896	96.5
^{56}Fe	He	12.1	87.6	1.51	96.4	0.778	99.0	1.80	97.5
^{59}Co	He	**9.57**	**82.5**	**1.97**	**95.1**	**2.89**	**97.6**	**2.83**	**94.4**
^{59}Co	H_2	**3.97**	**95.4**	**1.19**	**100.0**	**0.974**	**102.0**	**3.24**	**103.0**
^{60}Ni	HEHe	4.65	90.8	2.68	97.9	0.803	96.2	1.71	96.2
^{63}Cu	HEHe	6.55	88.5	3.52	99.0	1.38	97.2	1.59	96.1
^{66}Zn	H_2	7.22	103.0	2.98	97.6	1.27	97.6	4.19	98.6
^{75}As	He	**21.6**	**93.0**	**7.92**	**104.0**	**1.21**	**104.0**	**3.83**	**97.5**
^{75}As	HEHe	**21.0**	**97.2**	**7.76**	**105.0**	**1.31**	**104.0**	**4.14**	**95.2**
^{75}As	H_2	**24.0**	**106.0**	**8.00**	**109.0**	**1.88**	**105.0**	**5.43**	**104.0**
^{88}Sr	H_2	**6.60**	**92.3**	**0.958**	**97.9**	**1.24**	**95.9**	**2.00**	**95.7**
^{95}Mo	HEHe	2.73	83.0	1.95	94.3	1.00	93.9	1.15	95.6
^{105}Pd	He	**4.41**	**93.0**	**3.95**	**95.8**	**1.71**	**97.4**	**2.29**	**93.1**
^{114}Cd	Nogas	10.9	78.8	2.23	98.4	0.791	96.7	3.29	96.7
^{118}Sn	Nogas	10.1	86.0	1.40	98.0	1.44	94.7	1.98	95.6
^{118}Sn	HEHe	10.2	92.5	1.59	94.9	0.912	92.4	1.64	93.2
^{121}Sb	HEHe	12.5	89.3	2.65	98.7	0.985	98.3	1.86	97.2
^{121}Sb	H_2	10.3	87.7	2.75	99.0	1.55	98.1	1.74	96.0
^{137}Ba	Nogas	8.49	88.3	0.824	98.2	0.554	95.2	1.33	98.3
^{140}Ce	He	**7.82**	**80.0**	**1.99**	**95.2**	**1.42**	**95.6**	**1.66**	**94.7**
^{140}Ce	HEHe	**6.43**	**85.9**	**1.36**	**96.7**	**0.959**	**94.8**	**1.12**	**97.2**
^{140}Ce	H_2	**7.31**	**95.2**	**4.64**	**104.0**	**2.30**	**99.6**	**5.41**	**111.0**
^{182}W	Nogas	**13.7**	**83.9**	**1.52**	**97.5**	**0.689**	**94.3**	**1.69**	**96.6**
^{182}W	HEHe	**11.7**	**86.7**	**3.78**	**92.9**	**1.33**	**88.7**	**2.80**	**92.0**
^{195}Pt	Nogas	**5.09**	**95.2**	**9.51**	**105.0**	**0.857**	**100.0**	**10.5**	**94.1**
Pb*	Nogas	13.5	79.8	0.828	97.6	0.682	94.4	0.512	95.9

* The concentration of Pb was obtained by using a sum of signals from ^{206}Pb, ^{207}Pb and ^{208}Pb.

Table 29 continued Measurement RSD% and analyte recoveries from validation samples spiked with 600 ng/g or 60 ng/g of analytes. The values for analytes spiked with 60 ng/g aremarked with bold.

		Xyl. method +5°C		Xyl. method -5°C	
		Diesel 1a		Jet 1b	
Isotope	**Gasmode**	RSD%	Recov.%	RSD%	Recov.%
^{7}Li	Nogas	**15.1**	**59.7**	**21.3**	**88.0**
^{10}B	Nogas	65.5	65.4	24.6	50.2
^{11}B	Nogas	73.4	63.5	21.4	49.2
^{11}B	He	62.7	41.0	31.2	45.8
^{11}B	H_2	69.2	89.3	25.5	55.8
^{23}Na	Nogas	42.3	80.9	27.8	96.0
^{23}Na	He	42.1	80.3	27.9	100.0
^{23}Na	HEHe	41.8	81.1	27.3	94.3
^{24}Mg	H_2	13.1	91.3	5.06	97.2
^{27}Al	HEHe	9.43	91.3	5.38	99.4
^{28}Si	H_2	7.77	99.0	3.63	90.8
^{31}P	Nogas	48.8	52.8	7.98	107.0
^{31}P	HEHe	22.0	98.2	3.58	103.0
^{39}K	HEHe	31.1	46.1	21.3	80.4
^{39}K	H_2	26.6	54.4	21.4	79.6
^{40}Ca	H_2	20.1	102.0	6.62	102.0
^{47}Ti	H_2	11.0	99.2	3.42	96.2
^{51}V	HEHe	5.75	96.2	4.51	100.0
^{52}Cr	HEHe	4.60	99.1	2.45	105.0
^{55}Mn	HEHe	4.32	94.5	2.86	101.0
^{56}Fe	He	7.48	92.6	3.23	102.0
^{59}Co	He	**7.41**	**90.5**	**4.12**	**98.5**
^{59}Co	H_2	**5.23**	**94.0**	**3.36**	**94.8**
^{60}Ni	HEHe	5.55	91.2	3.44	98.3
^{63}Cu	HEHe	3.54	95.4	2.02	105.0
^{66}Zn	H_2	6.99	96.9	3.13	94.9
^{75}As	He	**13.9**	**94.0**	**2.23**	**100.0**
^{75}As	HEHe	**13.9**	**96.1**	**2.25**	**99.6**
^{75}As	H_2	**16.2**	**102.0**	**4.48**	**92.6**
^{88}Sr	H_2	**8.93**	**89.6**	**3.40**	**93.8**
^{95}Mo	HEHe	5.68	88.4	2.71	97.7
^{105}Pd	He	**4.47**	**94.4**	**3.51**	**98.9**
^{114}Cd	Nogas	7.77	88.9	3.81	95.5
^{118}Sn	Nogas	7.29	90.5	2.45	94.9
^{118}Sn	HEHe	7.17	92.5	4.62	88.7
^{121}Sb	HEHe	4.62	95.9	2.36	96.7
^{121}Sb	H_2	3.91	92.7	1.59	99.6
^{137}Ba	Nogas	7.06	87.5	3.72	87.1
^{140}Ce	He	**5.29**	**93.6**	**2.80**	**90.8**
^{140}Ce	HEHe	**5.04**	**95.6**	**2.93**	**91.4**
^{140}Ce	H_2	**6.48**	**101.0**	**5.07**	**85.4**
^{182}W	Nogas	**9.33**	**89.8**	**4.09**	**86.2**
^{182}W	HEHe	**8.29**	**92.5**	**5.02**	**91.8**
^{195}Pt	Nogas	**6.21**	**94.4**	**3.58**	**87.2**
Pb*	Nogas	10.9	88.0	4.23	85.3

* The concentration of Pb was obtained by using a sum of signals from ^{206}Pb, ^{207}Pb and ^{208}Pb.

12.7 Confidence intervals of the measurements

The accuracy of the measurement Δc_{meas} is the same as the analyte recovery measured in the validation. The standard deviation of the unspiked validation samples were insignificant comprared to those measured from samples spiked with 600 and 60 ng/g of analytes, and are therefore omitted from the calculations. The uncertainty of a measurement with 95% confidence limit u_{meas} is therefore calculated as follows:

$$u_{meas} = 2 \times RSD\% \tag{21}$$

To acquire the total uncertainty of the analysis, the errors caused by imprecision and inaccuracy of the measurements have to be taken in to account along with the uncertainty of the concentration of the calibration standards. The total uncertainty u_{tot} is therefore calculated with the Equation 22.

$$u_{tot} = \sqrt{\Delta c_{meas}^2 + u_{meas}^2 + u_c^2} \tag{22}$$

The total uncertainties of different analytes measured with different sample matrices with the xylene method and with the Asolv method are given in Table 30. For comparison, the results of the xylene method are given for same diesel and jet fuel batches that were used in the validation of the Asolv method. The results show, that the uncertainty of the measurements varies considerably depending on the method, analyte and the matrix.

When the uncertainties of the Asolv method and the xylene method are compared, it is clear that the Asolv method has truly superior performance compared to the xylene method as it has lower uncertainties almost without exceptions. In addition the Asolv has by far lower detection limits compared to the xylene method. Therefore it is clear that the xylene method has no benefit over the Asolv method even when the smaller spray temperature of -5°C is used. Even the uncertainties from gasoline are better to comparable to those obtained with the xylene method, alhough gasoline can be considered a more difficult sample matrix.

It is seen that an uncertainty of only few percent is achieved for many analytes when using the Asolv method while the uncertainty of the concentration of calibration standards u_c is 3%. Therefore the standard and sample preparation steps are a major source of error for these analytes. This means that the precision of some of the analytes cannot be further improved by optimizing the instrument parameters, but the procedure for preparation of the samples should be enhanced instead.

Table 30 Total uncertainty of the measurements u_c with a 95% confidence expressed as a percentage measured from samples spiked with 600&60 ng/g of analytes.

		Xylene method		Asolv method		
Analyte	**Gasmode**	**Diesel 1a**	**Jet fuel 1b**	**Diesel 1a**	**Jet fuel 1b**	**Gasoline**
^{7}Li	Nogas	50.3	44.2	33.6	15.4	45.1
^{10}B	Nogas	135.5	70.0	22.0	2.7	19.5
^{11}B	Nogas	151.3	66.4	21.4	2.4	19.9
^{11}B	He	138.6	82.7	24.5	12.5	27.9
^{11}B	H_2	138.9	67.5	20.4	8.0	22.4
^{23}Na	Nogas	86.7	55.7	35.3	13.4	39.8
^{23}Na	He	86.4	55.9	34.7	9.4	40.9
^{23}Na	HEHe	85.8	54.8	34.8	11.8	37.9
^{24}Mg	H_2	27.7	10.5	5.4	6.8	8.0
^{27}Al	HEHe	20.8	10.8	1.6	2.2	3.1
^{28}Si	H_2	15.6	11.7	10.8	90.2†	14.5
^{31}P	Nogas	108.4	17.5	22.1	4.8	79.7
^{31}P	HEHe	44.0	7.8	25.3	11.0	35.6
^{39}K	HEHe	82.3	46.9	19.5	17.6	50.3
^{39}K	H_2	70.1	47.4	34.8	15.2	27.4
^{40}Ca	H_2	40.2	13.3	4.4	4.0	8.6
^{47}Ti	H_2	22.1	7.8	10.1	7.4	13.9
^{51}V	HEHe	12.1	9.0	4.2	2.5	1.9
^{52}Cr	HEHe	9.2	7.1	4.1	2.5	2.6
^{55}Mn	HEHe	10.3	5.8	2.5	2.7	3.9
^{56}Fe	He	16.7	6.6	4.7	1.9	4.4
^{59}Co	He	17.6	8.4	6.3	6.3	8.0
^{59}Co	H_2	12.1	8.5	2.4	2.6	7.0
^{60}Ni	HEHe	14.1	7.1	5.8	4.1	5.1
^{63}Cu	HEHe	8.5	6.4	7.1	3.9	5.0
^{66}Zn	H_2	14.3	8.1	6.4	3.5	8.5
^{75}As	He	28.3	4.5	16.3	4.5	8.0
^{75}As	HEHe	28.1	4.5	16.4	4.4	9.6
^{75}As	H_2	32.4	11.6	18.2	6.0	11.7
^{88}Sr	H_2	20.7	9.2	2.8	4.8	5.9
^{95}Mo	HEHe	16.2	5.9	6.9	6.4	5.0
^{105}Pd	He	10.5	7.1	8.9	4.3	8.3
^{114}Cd	Nogas	19.1	8.9	4.8	3.7	7.4
^{118}Sn	Nogas	17.4	7.1	3.5	6.1	5.9
^{118}Sn	HEHe	16.2	14.6	6.0	7.8	7.5
^{121}Sb	HEHe	10.1	5.7	5.5	2.6	4.6
^{121}Sb	H_2	10.7	3.2	5.6	3.6	5.3
^{137}Ba	Nogas	18.8	14.9	2.5	5.0	3.2
^{140}Ce	He	12.4	10.8	6.3	5.2	6.2
^{140}Ce	HEHe	11.0	10.4	4.3	5.6	3.6
^{140}Ce	H_2	13.0	17.8	10.0	4.6	15.4
^{182}W	Nogas	21.3	16.0	3.9	5.8	4.8
^{182}W	HEHe	18.2	12.9	10.3	11.6	9.8
^{195}Pt	Nogas	13.6	14.6	19.7	1.7	21.7
Pb*	Nogas	24.9	16.9	2.9	5.8	4.3

* The concentration of Pb was obtained by using a sum of signals from ^{206}Pb, ^{207}Pb and ^{208}Pb.

† A likely contamination

12.8 Shelf life of standard stock solutions

No significant deterioration of concentration was observed in the stock solutions containing 10 and 1 μg/ml of analytes of the large and small calibration range espectively. It should be noted, however, that significant instrument drifting occured during the analysis, that made the results mostly quantitative. As the samples were measured in the order of their age (exept fresh samples, from which multiple measurement fas obtained), the reduction of concentration caused by drifting and deterioration of the stock solutions is indistinguishable. Based on the measurements, the differences in concentration are small, however, and it is likely safe to give a one week shelf life for the stock solutions. It is possible that the solutions could be used longer, but more research is needed to determine the precise expiration date.

12.9 Comparison of different internal standards

The statistical measures obtained from the validation of jet fuels measured with the xylene method were calculated by using Be and Sc as the ISTD to see if the different ionization potentials and atomic masses of these elements would make them more suitable as internal standards for some elements (data not shown). It was found however, that there are no benefits in using these elements as ISTD and that by using yttrium, slightly better analyte recoveries and precisions are obtained.

Table 31 Deterioration of stock solutions prepared in xylene.

		Concentration (%) of the measured stock solution stored for (days)						
Analyte	**Gasmode**	**0 days**	**8 days**	**15 days**	**19 days**	**21 days**	**22 days**	**23 days**
^{7}Li	Nogas	100	100.7	100.0	100.6	101.7	99.8	98.6
^{10}B	Nogas	100	95.8	97.9	98.0	102.9	103.9	117.5
^{11}B	Nogas	100	95.9	98.9	98.3	102.3	103.6	110.8
^{11}B	He	100	91.2	96.0	97.1	93.8	98.6	95.7
^{11}B	H_2	100	91.0	96.4	95.0	100.9	103.3	107.5
^{23}Na	Nogas	100	100.9	99.0	99.6	98.3	96.7	97.2
^{23}Na	He	100	99.7	100.5	98.5	97.0	96.1	96.4
^{23}Na	HEHe	100	100.5	99.4	97.9	96.6	97.0	96.3
^{24}Mg	H_2	100	101.9	102.0	101.5	101.6	99.3	96.9
^{27}Al	HEHe	100	102.6	102.1	101.6	100.0	99.0	96.6
^{28}Si	H_2	100	105.0	103.2	101.7	101.2	98.5	96.8
^{31}P	Nogas	100	104.5	102.8	103.3	100.7	96.8	92.0
^{31}P	HEHe	100	101.6	101.5	101.1	99.1	96.1	92.6
^{39}K	HEHe	100	102.9	100.7	100.0	97.2	96.6	94.3
^{39}K	H_2	100	102.4	101.4	99.6	98.6	97.5	95.6
^{40}Ca	H_2	100	103.5	102.9	103.2	103.1	100.5	97.1
^{47}Ti	H_2	100	101.7	101.3	100.4	100.5	98.2	95.1
^{51}V	HEHe	100	102.6	102.6	102.5	101.0	99.6	96.8
^{52}Cr	HEHe	100	102.3	101.2	102.3	100.8	100.0	96.6
^{55}Mn	HEHe	100	103.8	101.8	102.1	101.0	100.1	98.0
^{56}Fe	He	100	103.0	102.5	102.5	101.1	98.9	96.8
^{59}Co	He	100	103.5	101.9	101.9	101.1	99.9	97.3
^{59}Co	H_2	100	102.3	101.2	100.6	101.6	99.2	97.9
^{60}Ni	HEHe	100	103.3	101.1	102.0	101.0	99.6	98.0
^{63}Cu	HEHe	100	101.4	101.3	102.3	100.1	99.1	97.7
^{66}Zn	H_2	100	102.2	101.4	99.9	102.0	99.3	97.2
^{75}As	He	100	*	*	103.2	103.9	101.4	99.6
^{75}As	HEHe	100	*	*	103.6	103.2	101.0	99.1
^{75}As	H_2	100	*	*	102.8	104.6	101.2	100.0
^{88}Sr	H_2	100	106.1	103.6	104.0	104.3	102.6	103.0
^{95}Mo	HEHe	100	102.5	101.6	102.4	101.8	100.8	99.0
^{105}Pd	He	100	106.7	108.1	107.3	106.5	104.3	102.3
^{114}Cd	Nogas	100	102.6	101.0	102.8	101.8	99.9	95.9
^{118}Sn	Nogas	100	103.5	103.0	104.0	102.6	100.6	98.2
^{118}Sn	HEHe	100	102.2	101.7	101.6	102.3	101.5	99.1
^{121}Sb	HEHe	100	104.1	101.7	103.1	102.5	101.1	99.2
^{121}Sb	H_2	100	101.9	101.5	101.1	102.8	101.2	98.9
^{137}Ba	Nogas	100	103.4	101.2	103.0	102.2	100.6	97.7
^{140}Ce	He	100	102.7	102.1	102.6	102.4	100.5	99.6
^{140}Ce	HEHe	100	101.8	98.5	105.3	104.7	104.2	102.8
^{140}Ce	H_2	100	103.0	101.5	101.6	103.0	100.9	100.2
^{182}W	Nogas	100	102.5	100.7	102.7	102.5	100.8	99.0
^{182}W	HEHe	100	101.6	101.2	101.8	101.2	101.8	100.3
^{195}Pt	Nogas	100	103.5	104.5	103.4	104.1	100.4	98.9
$^{206-208}$Pb	Nogas	100	101.9	101.5	103.7	102.8	101.7	99.8

* A defective As standard used, no results obtained.

12.10 Further developements

Upgrading the xylene method

Based on the results of the validation, it is clear that the Asolv method has many benefits over the xylene method in the elemental analysis of middle distillates. Nevertheless, it is unclear how many of these benefits are related to the solvent properties and how many are related to better optimization of the Asolv method.

Most likely many of the benefits of the Asolv method could be gained also by using xylene, if a proper optimization for a method is performed. As an aromatic solvent, xylene has preferable solvation properties and can solvate wide range of various matrices. Therefore it is the solvent of choice for less soluble matrices and it can not be completely replaced by Asolv. On the other hand Asolv has a lower toxicity and flammability and therefore it can be regarded as a greener alternative.

The most distinct differences between the solvents are the higher viscosity and lower vapor pressure of Asolv. Based on the results of the optimization of the Asolv method, it is likely that increasing the viscosity of samples reduces the disruption of the plasma caused by the solvent load and the differences in the sample matrices, as less solvent is introduced to the plasma. The higher viscosity of standards and test samples therefore allows the analysis of highly volatile matrices like gasoline in addition to enabling higher dilution ratios, therefore reducing the detection limits. The lower vapor pressure can also be seen as an advance when using Asolv when analyzing matrices with low vapor pressure, such as diesel. On the other hand the more volatile xylene could be advantageous in the analysis of gasoline, it the viscosity of the sample solutions is increased enough and the method is optimized.

Adding more mineral oil to the calibration standards could increase the accuracy and precision of the analysis by reducing solvent load of the plasma in addition to allowing higher dilution ratios and therefore reduced detection limits. As the amount of sample introduced into the plasma is reduced, the sensitivity of the instrument decreases. However, this can be compensated by increasing the dilution ratios.

It is likely, that at some point the decrease of the sensitivity will start to have a negative effect on the precision. Nevertheless, based on the optimization of the integration times of the xylene method, the viscosity of xylene solutions could be further increased without significant deterioration in precision. If needed the integration times can be increased with only a small effect on the analysis time.

That said, further developements should be focused on optimizing the analyte recoveries of the xylene method by optimizing the viscosity of xylene solutions along with dilution ratios plasma conditions. Response surface methodology and desibility approach could be utilized as effective tools for a such multivariate optimization. Based on the results of the Asolv optimization, carrier gas flow is a promising factor to compensate for the change in viscosity as both factors control the amount of sample entering the plasma.

However, when the carrier gas flow is optimized without changing the flowrate of auxiliary gas, the interaction between the gasflows might result non-optimal plasma conditions. Furthermore, when organic matrices are analyzed, it is important to ensure sufficient oxi-

dation of the sample matrix to prevent carbon from accumulating on the instruments surfaces. A faster carbon deposit formation was observed after the Asolv method for analyzing gasoline was put into routine use. A too high carrier gas to auxiliary gas flow ratio might be responsible for the formation of the carbon deposit. Therefore, the ratio of the two gas flows should be optimized to ensure that the auxiliary gas is sufficiently high to provide enough oxygen for complete oxidation of the sample matrix. The carrier gas to auxiliary gas ratio could then be fixed and be used as a factor in further optimization without a need to worry about carbon accumulation.

Optimization of the gas modes

Based on the optimization of the Asolv method, RSM is powerful too for selecting of the most robust gas modes for each analyte. By using the same technique it is possible to optimize the gas mode parameters and ion optics potentials to achieve a more robust analysis. By measuring each analyte with with several gas modes, suitable gas modes could be selected for best possible overall recovery of the analytes.

Stability of analytes

The stability of analytes in calibration standards prepared with different solvents should be further studied and the effect of adding Conostan stabilizer or other analyte stabilizing additives should be evaluated. Measurements should be made as short as possible to prevent the degration of the solutions during analysis. Automated washing of the ICP-MS instrument should be preferred to reduce the analysis time.

Validation of a multivariate model

In the validation of new methods, an experimental space could be designed to include different matrices with known variability in viscosity, vapor pressure and density. RSM could then be used to derive response surfaces for analyte recoveries and standard deviations of the analytes when the physical properties of the samples are varied. By properly validating the resulting RSM model, the quality of analysis could be confirmed even for a completely new kind of sample matrix as long as the physical properties fit inside the experimental space. The RSM model could also be used to predict the best possible test sample dilution ratio an viscosity for new sample matrices.

13 Conclusions

Two new ICP-MS methods for the simultaneous analysis of 28 elements from middle distillate products were developed based on a previously used method. One of the methods uses xylene as a solvent while the other one uses kerosene based Asolv as a solvent. A validation for multiple matrices was performed for both methods. Based on the validation, Asolv method can be used to measure all analytes at sub ppb or at ppb levels, from diesel and jet fuel matrices. The xylene method was found to be suitable for the determination of most studied analytes, although, poor precision and accuracy were obtained for B, Na and K making the method unsuitable for quantification of these elements in the studied concentration range. Even though smaller uncertainties were achieved when measuring these elements from jet fuel compared to diesel, the concentrations measured with the xylene method should be regarded as rough estimations with uncertainties of more than 45%, reducing the method for qualitative work in the concentration range of $\leq$600 ppb. The Asolv method was found to be superior for the analysis of every analyte from any matrix. It is however unclear, if this is a result of solvent properties or an outcome of a better optimization of the Asolv method.

The effect of changing integration times of the xylene method on the precision of the analysis was studied. The relative standard deviations were found to follow statistical prediction up to a certain point precision. The effect of changing the viscosity and dilution ratios of the samples was found to have a linear correlation to the instruments sensitivity, when xylene was used as a solvent. It is unclear, however, if the response is linear with higher viscosities.

Response surface methodology and desirability approach were used in the optimization of the Asolv method. These techniques allowed a simultaneous optimization of the carrier gas flow, sampling depth and dilution ratio for diesel samples. In addition RSM and desirability approach were utilized in the optimization of gasoline and jet fuel sample dilution ratios and mineral oil concentrations for the Asolv method. Best overall analyte recoveries were found by using Derringer's desirability function and computing the overall desirability of the analyte recoveries as a geometric mean of the desirability functions of individual analytes.

The RSM was found to be a useful tool for a multivariate optimization of an ICP-MS analysis. In addition to reducing the optimization time and giving the true optimum, by using RSM it is possible to gain a real insight on how the system under research behaves. Also the desirability approach proved to be a useful tool along with RSM in the multivariate optimization of ICP-MS method having multiple responses to be optimized.

Significant drifting in the measurements was found by measuring the same samples multiple times during two same extended runs using different methods. Based on the results it is likely that chemical instability of the analytes in diluted solutions results in considerable measurement error seen as a decrease in analyte recoveries and as an increase in background equivalent concentrations. In many cases, however, it is impossible to say, whether an uncertainty or high signal background seen in validation measurements is originating from spectral interferences, instability of the analyte, from a contamination or from

matrix interferences.

To address this issue, the stability of the analytes should be thoroughly investigated. Additionally, possible contamination sources should be examined and automated washing should be included in the methods in use to reduce the background. The viscosity of the samples/standards, analyzed with the xylene method, should be optimized to maximize analyte recoveries, to decrease matrix interferences by acquiring more robust plasma conditions, and to reduce analyte background by allowing the usage of higher dilution ratios. The carrier gas flow should be optimized at the same time as there are significant interactions between the two parameters. The reaction gasses and the reaction cell parameters, including the energy discrimination voltages, could then be optimized for the new method to increase the robustness of the method and to decrease polyatomic interferences. RSM should be used in the optimization, as there are multiple variables to be optimized and considerable interactions between the variables can be expected.

Bibliography

[1] S. C. Wilschefski and M. R. Baxter, *Clin. Biochem. Rev.*, 2019, **40**, 115–133.

[2] D. Pröfrock and A. Prange, *Appl. Spectrosc.*, 2012, **66**, 843–868.

[3] W. Yang, Y. Gao and J. F. Casey, *Solut. Chem. Adv. Res. Appl.*, 2018, 159–205.

[4] M. d. G. Andrade Korn, E. S. da Boa Morte, D. C. M. Batista dos Santos, J. T. Castro, J. T. P. Barbosa, A. P. Teixeira, A. P. Fernandes, B. Welz, W. P. C. dos Santos, E. B. G. Nunes dos Santos and M. Korn, *Appl. Spectrosc. Rev.*, 2008, **43**, 67–92.

[5] R. Thomas, *Practical guide to ICP-MS*, Marcel Dekker, New York, 1st edn, 2004, ch. 1, pp. 1–6.

[6] R. Thomas, *Practical guide to ICP-MS*, Marcel Dekker, New York, 2004, ch. 3, pp. 13–22.

[7] R. Thomas, *Practical guide to ICP-MS*, Marcel Dekker, New York, 1st edn, 2004, ch. 4, pp. 23–29.

[8] R. Thomas, *Practical guide to ICP-MS*, Marcel Dekker, New York, 1st edn, 2004, ch. 7, pp. 49–59.

[9] T. Robert, *Practical guide to ICP-MS*, Marcel Dekker, New York, 1st edn, 2004, ch. 8, pp. 61–69.

[10] T. Robert, *Practical guide to ICP-MS*, Marcel Dekker, New York, 1st edn, 2004, ch. 9, pp. 71–79.

[11] N. Jakubowski, L. Moens and F. Vanhaecke, *Spectrochim. Acta Part B At. Spectrosc.*, 1998, **53**, 1739–1763.

[12] R. Thomas, *Practical guide to ICP-MS*, Marcel Dekker, New York, 1st edn, 2004, ch. 11, pp. 91–100.

[13] R. Thomas, *Practical guide to ICP-MS*, Marcel Dekker, New York, 1st edn, 2004, ch. 14.

[14] T. W. May and R. H. Wiedmeyer, *At. Spectrosc.*, 1998, **19**, 150–155.

[15] R. Thomas, *Practical guide to ICP-MS*, Marcel Dekker, New York, 1st edn, 2004, ch. 5, pp. 23–38.

[16] D. Wollenweber, S. Straßburg and G. Wünsch, *Fresenius. J. Anal. Chem.*, 1999, **364**, 433–437.

[17] R. Thomas, *Practical guide to ICP-MS*, Marcel Dekker, New York, 1st edn, 2004, ch. 10, pp. 81–90.

[18] S. D. Tanner, V. I. Baranov and D. R. Bandura, *Spectrochim. Acta - Part B At. Spectrosc.*, 2002, **57**, 1361–1452.

[19] S. D. Tanner, V. I. Baranov and U. Vollkopf, *J. Anal. At. Spectrom.*, 2000, **15**, 1261–1269.

[20] L. Balcaen, E. Bolea-Fernandez, M. Resano and F. Vanhaecke, *Anal. Chim. Acta*, 2015, **894**, 7–19.

[21] N. N. Sesi and G. M. Hieftje, *Spectrochim. Acta Part B At. Spectrosc.*, 1996, **51**, 1601–1628.

[22] Y. Morishige and A. Kimura, *SEI Tech. Rev.*, 2008, 106–111.

[23] C. Agatemor and D. Beauchemin, *Anal. Chim. Acta*, 2011, **706**, 66–83.

[24] R. Thomas, *Practical guide to ICP-MS*, Marcel Dekker, New York, 2004, ch. 13, pp. 149–164.

[25] A. Leclercq, A. Nonell, J. L. Todolí Torró, C. Bresson, L. Vio, T. Vercouter and F. Chartier, *Anal. Chim. Acta*, 2015, **885**, 57–91.

[26] G. D. Woods and F. I. Fryer, *Anal. Bioanal. Chem.*, 2007, **389**, 753–761.

[27] T. A. Maryutina, O. N. Katasonova, E. Y. Savonina and B. Y. Spivakov, *J. Anal. Chem.*, 2017, **72**, 490–509.

[28] A. W. Boorn and R. F. Browner, *Anal. Chem.*, 1982, **54**, 1402–1410.

[29] M. C. Brennan, *A Practical Approach to Quantitative Metal Analysis of Organic Matrices*, John Wiley & Sons, Ltd, Chichester, UK, 2008, pp. 133–160.

[30] *ASTM D8110-17, Standard Test Method for Elemental Analysis of Distillate Products by Inductively Coupled Plasma Mass Spectrometry (ICP-MS)*, ASTM International, West Conshohocken, PA, 2017.

[31] *NIST/SEMATECH e-Handbook of Statistical Methods, 5.3.3.3. Full factorial designs*, `https://www.itl.nist.gov/div898/handbook/pri/section3/pri333.htm`.

[32] T. Lundstedt, E. Seifert, L. Abramo, B. Thelin, Å. Nyström, J. Pettersen and R. Bergman, *Chemom. Intell. Lab. Syst.*, 1998, **42**, 3–40.

[33] D. Drain and D. Drain, *Handb. Exp. Methods Process Improv.*, 1997, 1–16.

[34] *NIST/SEMATECH e-Handbook of Statistical Methods, 5.3.3.5. Plackett-Burman designs*, https://www.itl.nist.gov/div898/handbook/pri/section3/pri335.htm.

[35] *NIST/SEMATECH e-Handbook of Statistical Methods, 5.3.3.9. Three-level full factorial designs*, https://www.itl.nist.gov/div898/handbook/pri/section3/pri339.htm.

[36] *NIST/SEMATECH e-Handbook of Statistical Methods, 5.3.3.6.1. Central Composite Designs (CCD)*, https://www.itl.nist.gov/div898/handbook/pri/section3/pri3361.htm.

[37] *NIST/SEMATECH e-Handbook of Statistical Methods, 5.3.3.6.2. Box-Behnken designs*, https://www.itl.nist.gov/div898/handbook/pri/section3/pri3362.htm.

[38] S. L. Ferreira, R. E. Bruns, H. S. Ferreira, G. D. Matos, J. M. David, G. C. Brandão, E. G. da Silva, L. A. Portugal, P. S. dos Reis, A. S. Souza and W. N. dos Santos, *Box-Behnken design: An alternative for the optimization of analytical methods*, 2007.

[39] S. L. Ferreira, W. N. dos Santos, C. M. Quintella, B. B. Neto and J. M. Bosque-Sendra, *Talanta*, 2004, **63**, 1061–1067.

[40] C. G. Novaes, M. A. Bezerra, E. G. P. da Silva, A. M. P. dos Santos, I. L. d. S. Romão and J. H. Santos Neto, *Microchem. J.*, 2016, **128**, 331–346.

[41] M. A. Bezerra, S. L. C. Ferreira, C. G. Novaes, A. M. P. dos Santos, G. S. Valasques, U. M. F. da Mata Cerqueira and J. P. dos Santos Alves, *Talanta*, 2019, **194**, 941–959.

[42] S. L. C. Ferreira, R. E. Bruns, E. G. P. da Silva, W. N. L. dos Santos, C. M. Quintella, J. M. David, J. B. de Andrade, M. C. Breitkreitz, I. C. S. F. Jardim and B. B. Neto, *J. Chromatogr. A*, 2007, **1158**, 2–14.

[43] D. B. Hibbert, *J. Chromatogr. B*, 2012, **910**, 2–13.

[44] S. L. C. Ferreira, M. d. G. A. Korn, H. S. Ferreira, E. G. P. da Silva, R. G. O. Araújo, A. S. Souza, S. M. Macedo, D. d. C. Lima, R. M. de Jesus, F. A. C. Amorim and J. M. Bosque-Sendra, *Appl. Spectrosc. Rev.*, 2007, **42**, 475–491.

[45] F. Bianchi and M. Careri, *Curr. Anal. Chem.*, 2008, **4**, 142–151.

[46] E. S. Hecht, A. L. Oberg and D. C. Muddiman, *J. Am. Soc. Mass Spectrom.*, 2016, **27**, 767–785.

[47] S. L. Ferreira, M. M. Silva Junior, C. S. Felix, D. L. da Silva, A. S. Santos, J. H. Santos Neto, C. T. de Souza, R. A. Cruz Junior and A. S. Souza, *Food Chem.*, 2019, **273**, 3–8.

[48] J. Andrade-Garda, *Basic Chemometric Techniques in Atomic Spectroscopy*, Royal Society of Chemistry, Cambridge, 1st edn, 2013.

[49] R. P. Niedz and T. J. Evens, *Vitr. Cell. Dev. Biol. - Plant*, 2016, **52**, 547–562.

[50] V. Dufailly, L. Noël, J.-M. Frémy, D. Beauchemin and T. Guérin, *J. Anal. At. Spectrom.*, 2007, **22**, 1168.

[51] M. Mulugeta, G. Wibetoe, C. J. Engelsen and A. Asfaw, *Anal. Bioanal. Chem.*, 2009, **393**, 1015–1024.

[52] J. Avivar, L. Ferrer, M. Casas and V. Cerdà, *J. Anal. At. Spectrom.*, 2012, **27**, 327.

[53] A. Kötschau, G. Büchel, J. Einax, C. Fischer, W. von Tümpling and D. Merten, *Microchem. J.*, 2013, **110**, 783–789.

[54] Y. Gao, R. E. Sturgeon, Z. Mester, X. Hou and L. Yang, *Anal. Chim. Acta*, 2015, **901**, 34–40.

[55] T. Dagnac, A. Padró, R. Rubio and G. Rauret, *Anal. Chim. Acta*, 1998, **364**, 19–30.

[56] P. N. Nomngongo and J. C. Ngila, *Spectrochim. Acta Part B At. Spectrosc.*, 2014, **98**, 54–59.

[57] F. Bianchi, M. Careri, M. Maffini, A. Mangia and C. Mucchino, *Rapid Commun. Mass Spectrom.*, 2003, **17**, 251–256.

[58] H. Pyhtilä, P. Perämäki, J. Piispanen, M. Niemelä, T. Suoranta, M. Starr, T. Nieminen, M. Kantola and L. Ukonmaanaho, *Microchem. J.*, 2012, **103**, 165–169.

[59] D. Ciavardelli, P. Sacchetta, G. Federici, C. Di Ilio and A. Urbani, *Talanta*, 2010, **80**, 1513–1525.

[60] K. Kahen, A. Strubinger, J. R. Chirinos and A. Montaser, *Spectrochim. Acta Part B At. Spectrosc.*, 2003, **58**, 397–413.

[61] A. Tangen and W. Lund, *Spectrochim. Acta Part B At. Spectrosc.*, 1999, **54**, 1831–1838.

[62] J. R. de Souza, C. B. Duyck, T. C. O. Fonseca and T. D. Saint'Pierre, *J. Anal. At. Spectrom.*, 2012, **27**, 1280.

[63] Á. Woller, H. Garraud, J. Boisson, A. M. Dorthe, P. Fodor and O. F. Donard, *J. Anal. At. Spectrom.*, 1998, **13**, 141–149.

[64] A. Kadar, L. Noël, R. Chekri, C. Vastel, S. Millour and T. Guérin, *Talanta*, 2011, **85**, 2605–2613.

[65] M. Colon, M. Iglesias and M. Hidalgo, *Spectrochim. Acta Part B At. Spectrosc.*, 2007, **62**, 470–475.

[66] R. Brennetot, L. Pierry, T. Atamyan, G. Favre and D. Vailhen, *J. Anal. At. Spectrom.*, 2008, **23**, 1350.

[67] C. R. Quétel, B. Thomas, O. F. Donard and F. E. Grousset, *Spectrochim. Acta Part B At. Spectrosc.*, 1997, **52**, 177–187.

[68] R. Brennetot, A.-L. Becquet, H. Isnard, C. Caussignac, D. Vailhen and F. Chartier, *J. Anal. At. Spectrom.*, 2005, **20**, 500.

[69] S. Stürup, H. Dahlgaard and S. Chen Nielsen, *J. Anal. At. Spectrom.*, 1998, **13**, 1321–1326.

[70] J. M. Andrade, M. J. Cal-Prieto, M. P. Gómez-Carracedo, A. Carlosena and D. Prada, *J. Anal. At. Spectrom.*, 2008, **23**, 15–28.

[71] S. L. Ferreira, A. O. Caires, T. d. S. Borges, A. M. Lima, L. O. Silva and W. N. dos Santos, *Microchem. J.*, 2017, **131**, 163–169.

[72] T. A. Little, *BioPharm Int.*, 2014, **27**, 56–60.

Appendices

Appendix A

Concentration RSD as a function of integration time of analytes

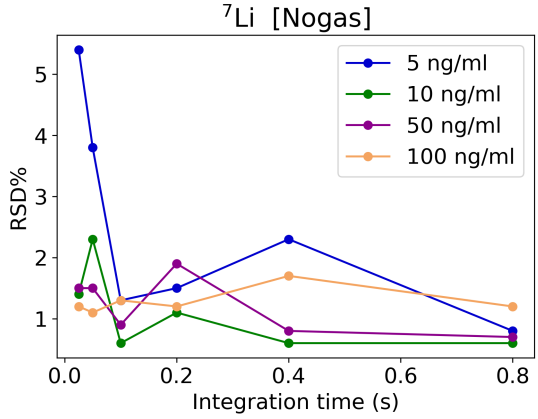
^{7}Li [Nogas]
5 ng/ml
10 ng/ml
50 ng/ml
100 ng/ml
RSD%
Integration time (s)

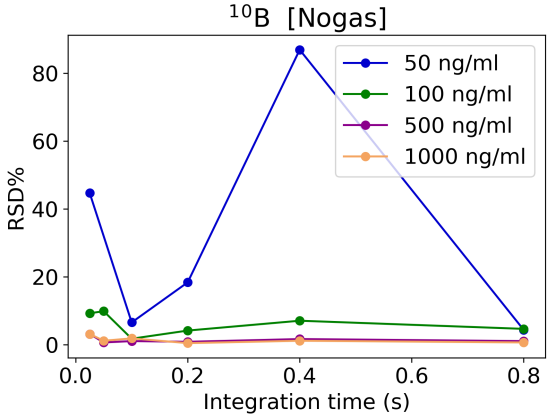
^{10}B [Nogas]
50 ng/ml
100 ng/ml
500 ng/ml
1000 ng/ml
RSD%
Integration time (s)

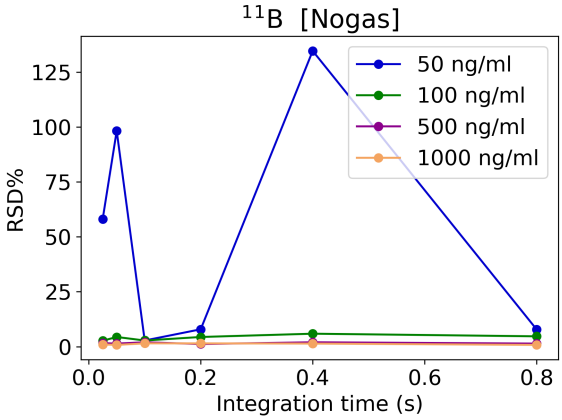
^{11}B [Nogas]
50 ng/ml
100 ng/ml
500 ng/ml
1000 ng/ml
RSD%
Integration time (s)

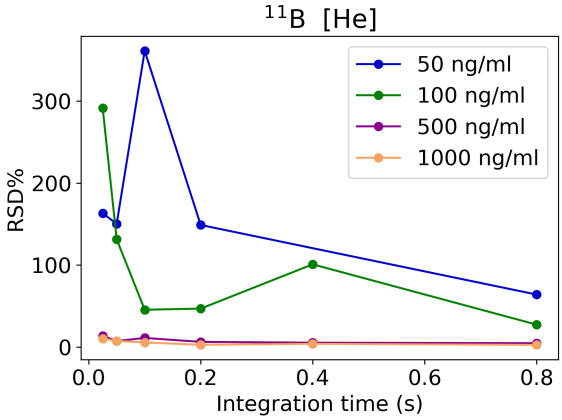
^{11}B [He]
50 ng/ml
100 ng/ml
500 ng/ml
1000 ng/ml
RSD%
Integration time (s)

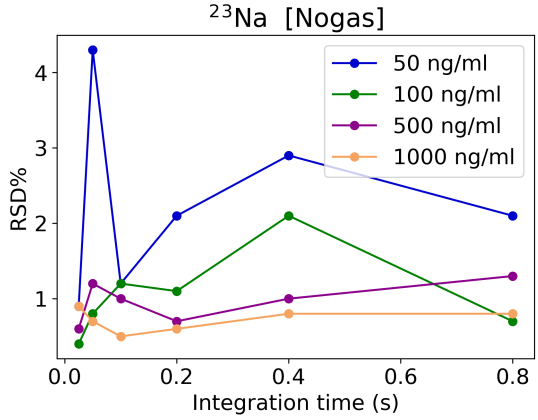
^{23}Na [Nogas]
50 ng/ml
100 ng/ml
500 ng/ml
1000 ng/ml
RSD%
Integration time (s)

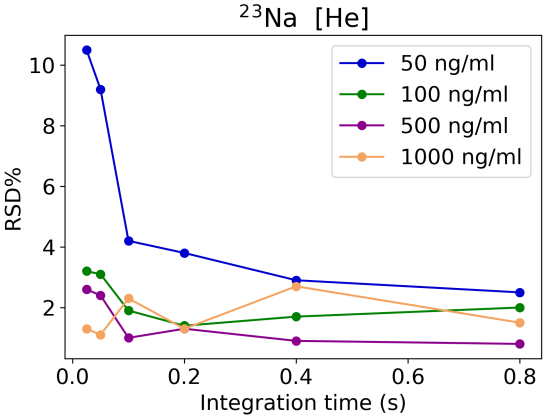
^{23}Na [He]
50 ng/ml
100 ng/ml
500 ng/ml
1000 ng/ml
RSD%
Integration time (s)

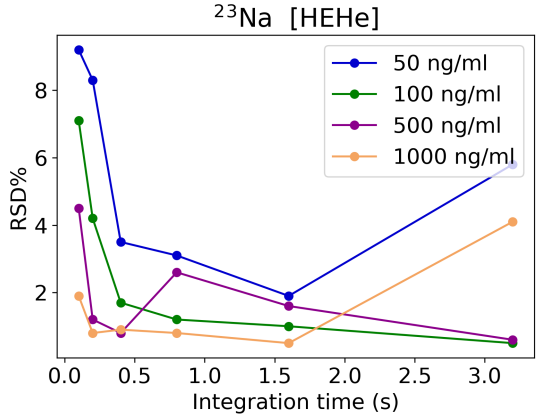
^{23}Na [HEHe]
50 ng/ml
100 ng/ml
500 ng/ml
1000 ng/ml
RSD%
Integration time (s)

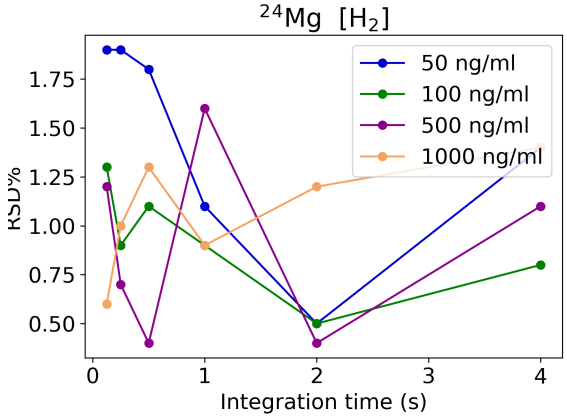
^{24}Mg [H_2]
50 ng/ml
100 ng/ml
500 ng/ml
1000 ng/ml
RSD%
Integration time (s)

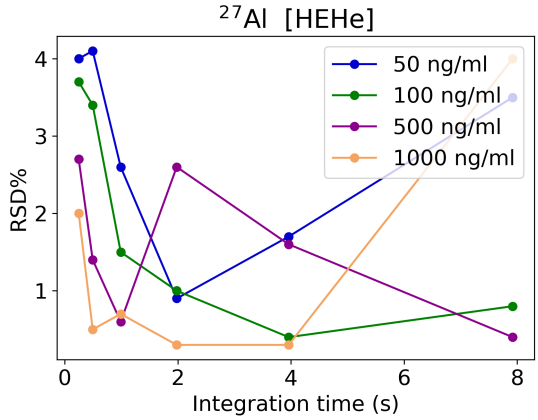
^{27}Al [HEHe]
50 ng/ml
100 ng/ml
500 ng/ml
1000 ng/ml
RSD%
Integration time (s)

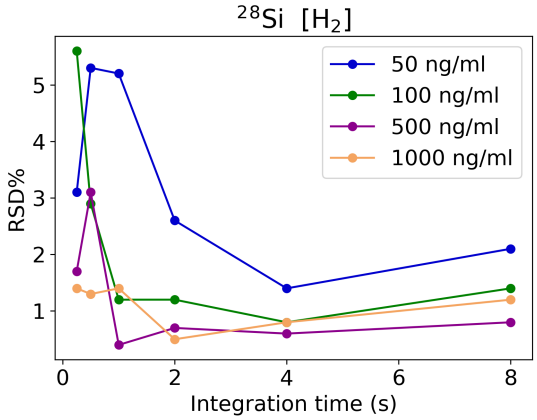
^{28}Si [H_2]
50 ng/ml
100 ng/ml
500 ng/ml
1000 ng/ml
RSD%
Integration time (s)

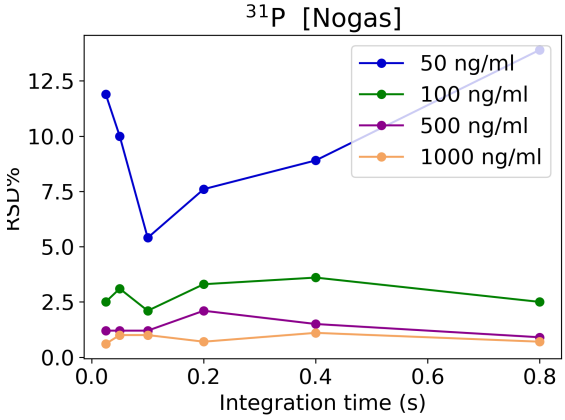
^{31}P [Nogas]
50 ng/ml
100 ng/ml
500 ng/ml
1000 ng/ml
RSD%
Integration time (s)

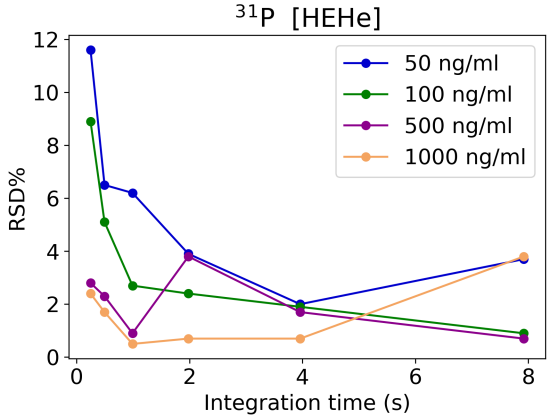
^{31}P [HEHe]
50 ng/ml
100 ng/ml
500 ng/ml
1000 ng/ml
RSD%
Integration time (s)

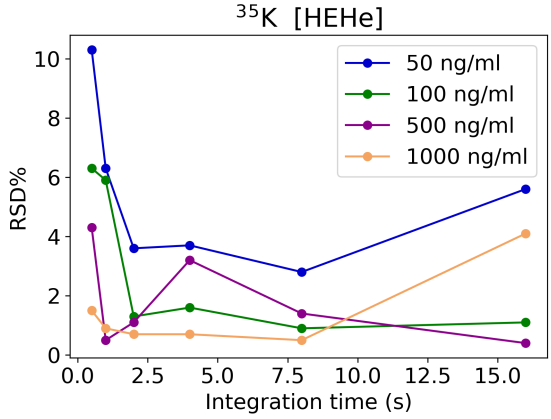
^{35}K [HEHe]
RSD%
Integration time (s)
50 ng/ml
100 ng/ml
500 ng/ml
1000 ng/ml

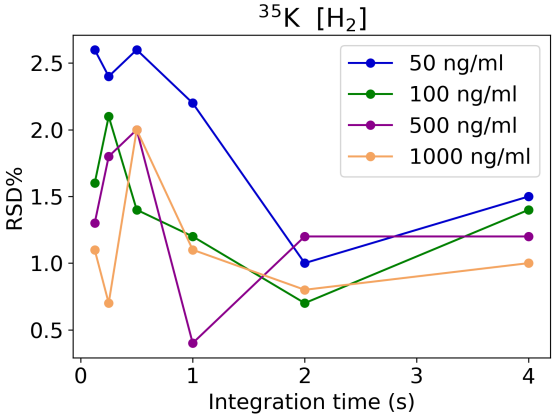
^{35}K [H_2]
RSD%
Integration time (s)
50 ng/ml
100 ng/ml
500 ng/ml
1000 ng/ml

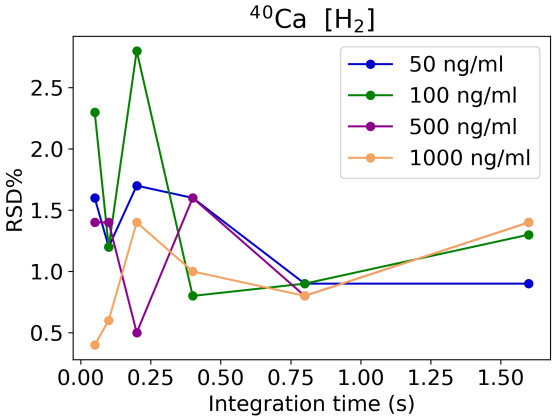
^{40}Ca [H_2]
RSD%
Integration time (s)
50 ng/ml
100 ng/ml
500 ng/ml
1000 ng/ml

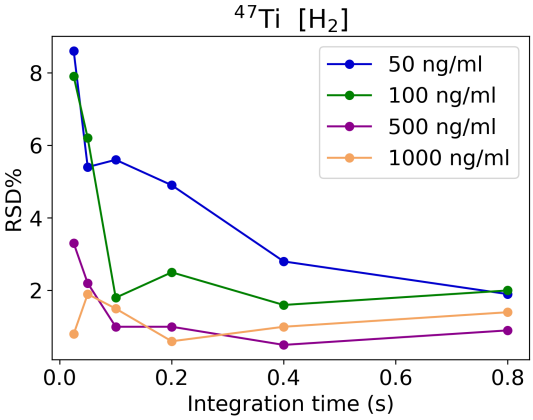
^{47}Ti [H_2]
RSD%
Integration time (s)
50 ng/ml
100 ng/ml
500 ng/ml
1000 ng/ml

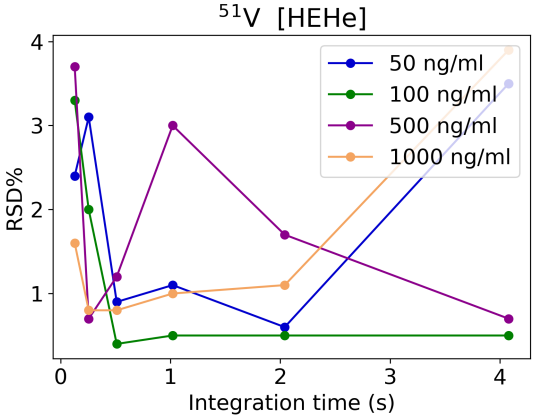
^{51}V [HEHe]
RSD%
Integration time (s)
50 ng/ml
100 ng/ml
500 ng/ml
1000 ng/ml

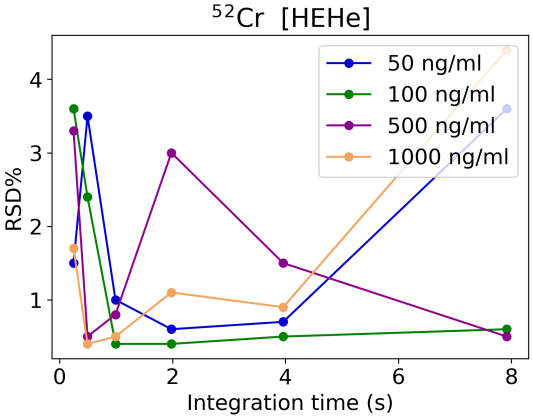
^{52}Cr [HEHe]
RSD%
Integration time (s)
50 ng/ml
100 ng/ml
500 ng/ml
1000 ng/ml

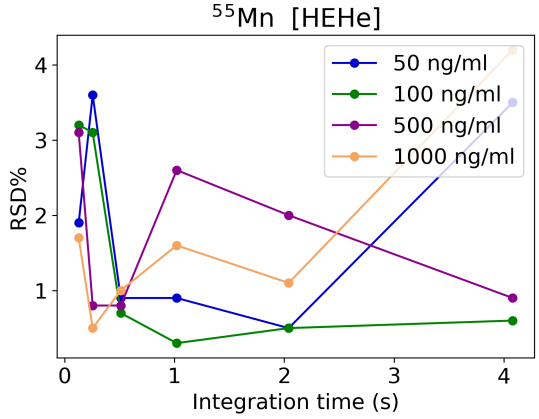
^{55}Mn [HEHe]
50 ng/ml
100 ng/ml
500 ng/ml
1000 ng/ml
RSD%
Integration time (s)

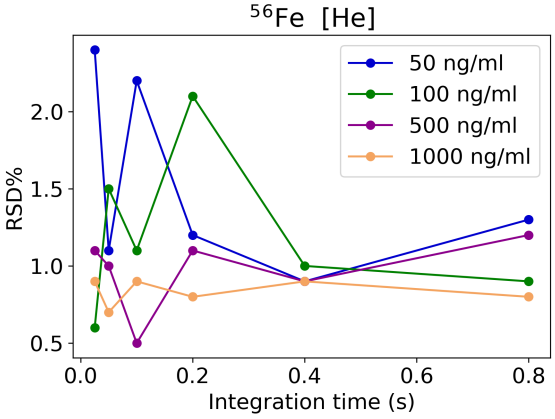
^{56}Fe [He]
50 ng/ml
100 ng/ml
500 ng/ml
1000 ng/ml
RSD%
Integration time (s)

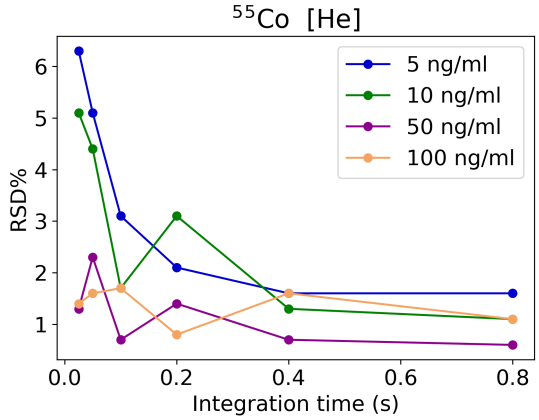
^{55}Co [He]
5 ng/ml
10 ng/ml
50 ng/ml
100 ng/ml
RSD%
Integration time (s)

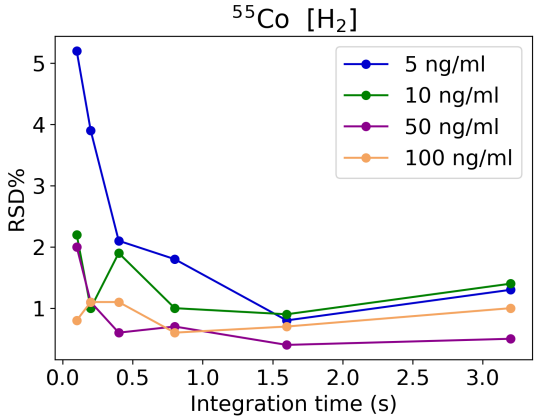
^{55}Co [H_2]
5 ng/ml
10 ng/ml
50 ng/ml
100 ng/ml
RSD%
Integration time (s)

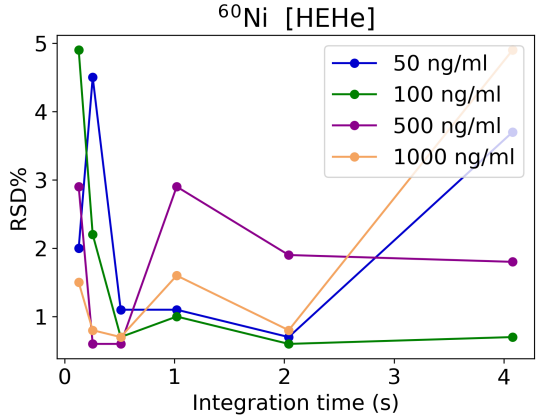
^{60}Ni [HEHe]
50 ng/ml
100 ng/ml
500 ng/ml
1000 ng/ml
RSD%
Integration time (s)

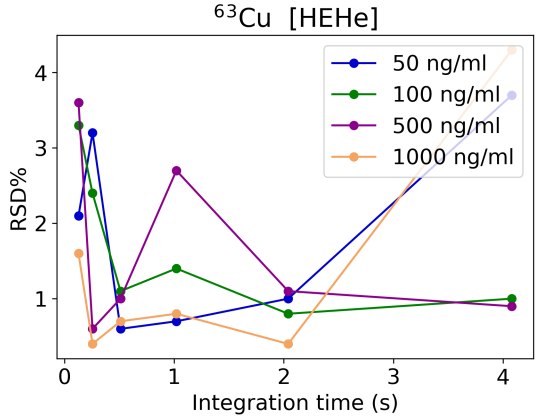
^{63}Cu [HEHe]
50 ng/ml
100 ng/ml
500 ng/ml
1000 ng/ml
RSD%
Integration time (s)

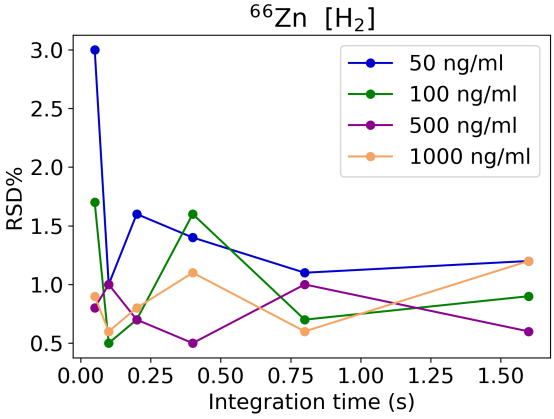
^{66}Zn [H_2]
50 ng/ml
100 ng/ml
500 ng/ml
1000 ng/ml
RSD%
Integration time (s)

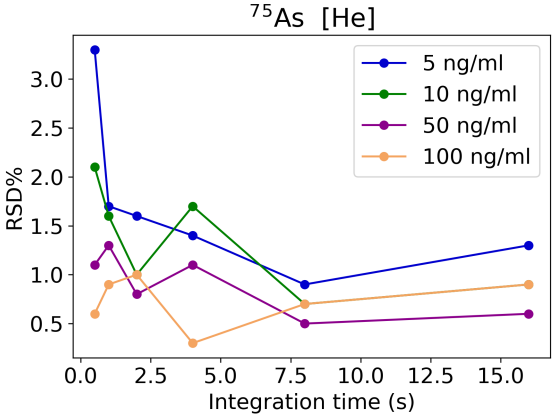
^{75}As [He]
5 ng/ml
10 ng/ml
50 ng/ml
100 ng/ml
RSD%
Integration time (s)

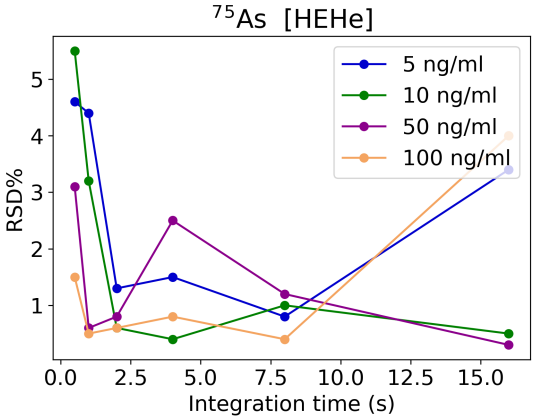
^{75}As [HEHe]
5 ng/ml
10 ng/ml
50 ng/ml
100 ng/ml
RSD%
Integration time (s)

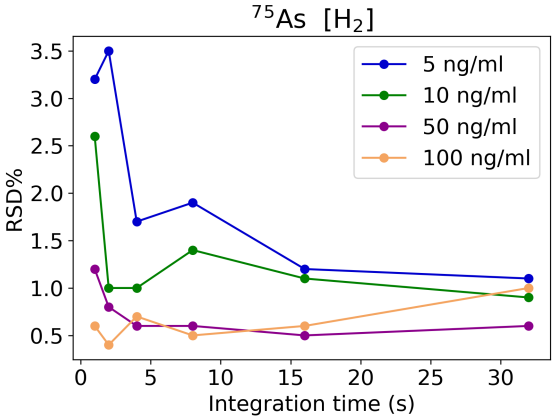
^{75}As [H_2]
5 ng/ml
10 ng/ml
50 ng/ml
100 ng/ml
RSD%
Integration time (s)

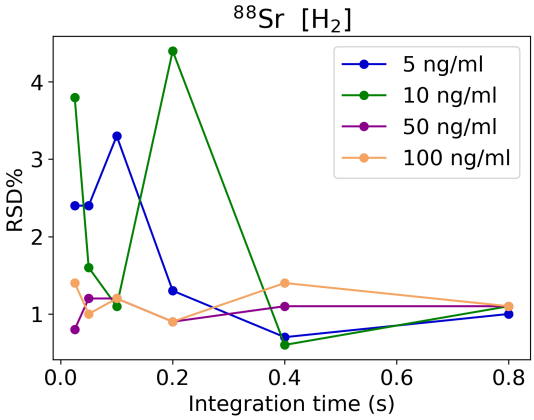
^{88}Sr [H_2]
5 ng/ml
10 ng/ml
50 ng/ml
100 ng/ml
RSD%
Integration time (s)

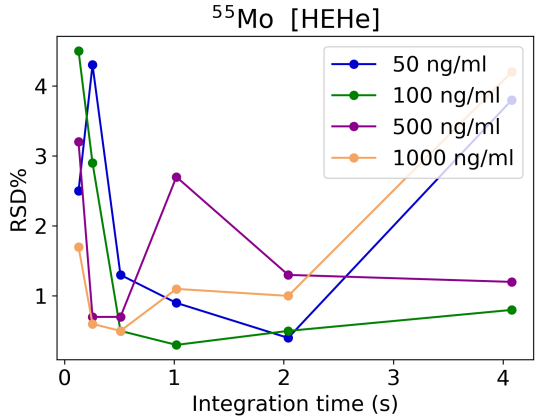
^{55}Mo [HEHe]
50 ng/ml
100 ng/ml
500 ng/ml
1000 ng/ml
RSD%
Integration time (s)

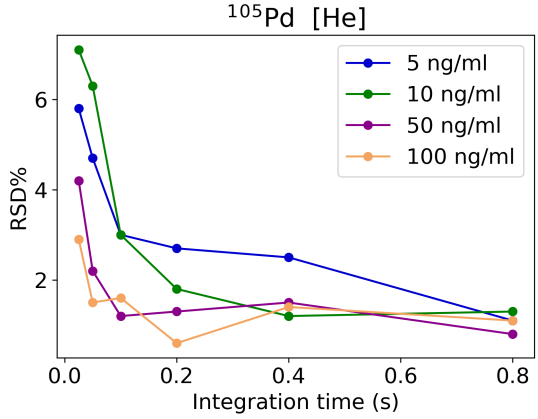
^{105}Pd [He]
5 ng/ml
10 ng/ml
50 ng/ml
100 ng/ml
RSD%
Integration time (s)

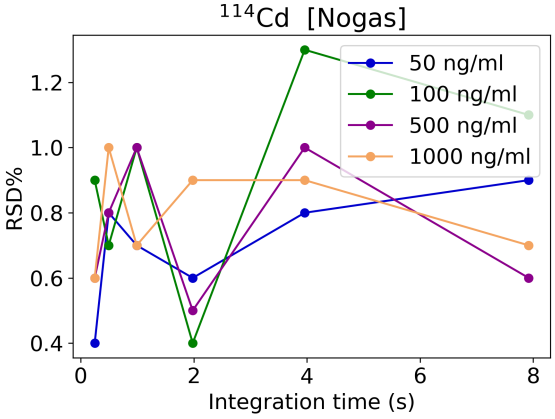
^{114}Cd [Nogas]
50 ng/ml
100 ng/ml
500 ng/ml
1000 ng/ml
RSD%
Integration time (s)

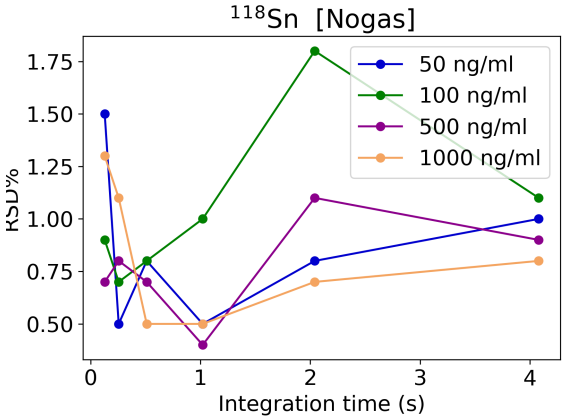
^{118}Sn [Nogas]
50 ng/ml
100 ng/ml
500 ng/ml
1000 ng/ml
RSD%
Integration time (s)

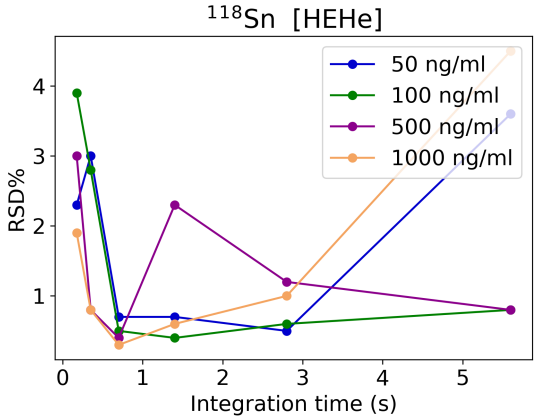
^{118}Sn [HEHe]
50 ng/ml
100 ng/ml
500 ng/ml
1000 ng/ml
RSD%
Integration time (s)

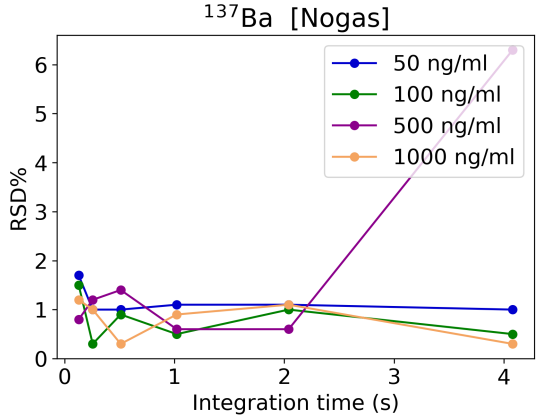
^{137}Ba [Nogas]
50 ng/ml
100 ng/ml
500 ng/ml
1000 ng/ml
RSD%
Integration time (s)

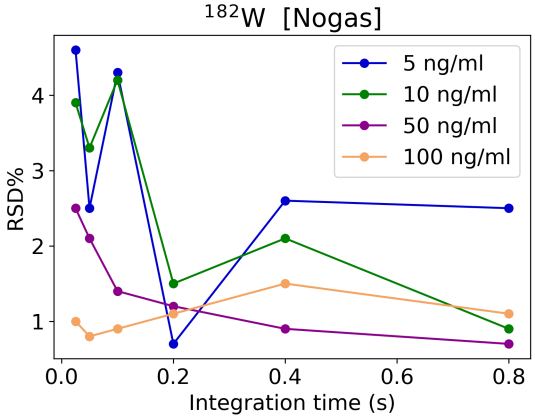
^{182}W [Nogas]
5 ng/ml
10 ng/ml
50 ng/ml
100 ng/ml
RSD%
Integration time (s)

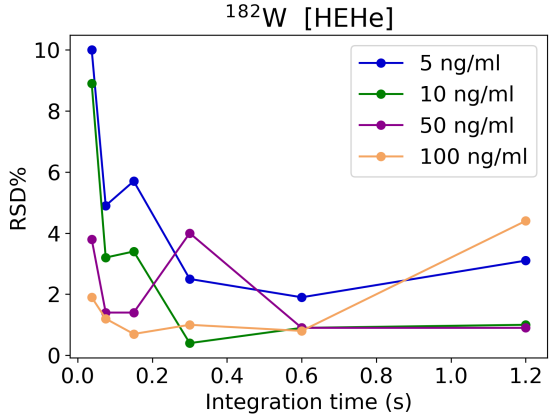
^{182}W [HEHe]
5 ng/ml
10 ng/ml
50 ng/ml
100 ng/ml
RSD%
Integration time (s)

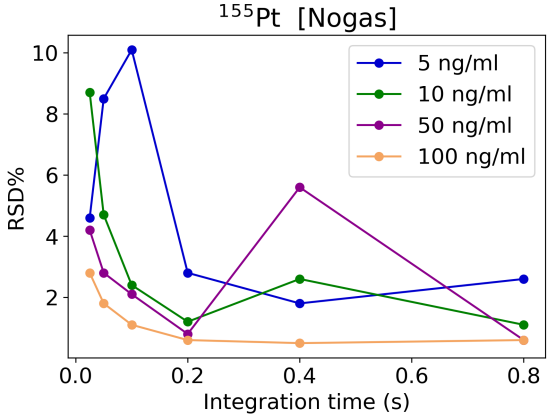
^{155}Pt [Nogas]
5 ng/ml
10 ng/ml
50 ng/ml
100 ng/ml
RSD%
Integration time (s)

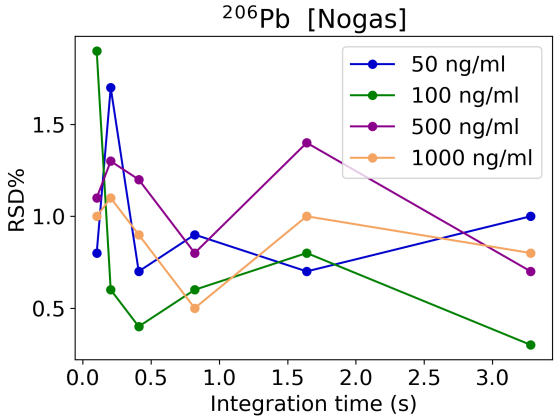
^{206}Pb [Nogas]
50 ng/ml
100 ng/ml
500 ng/ml
1000 ng/ml
RSD%
Integration time (s)

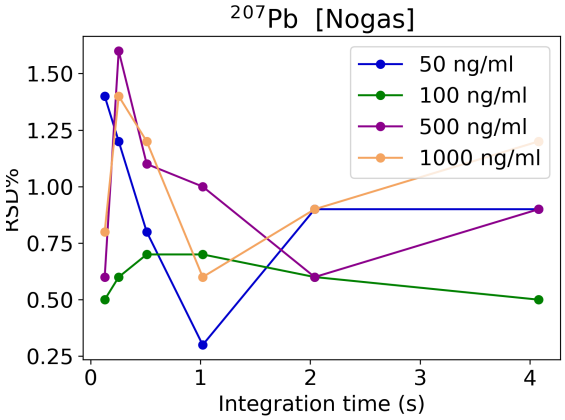
^{207}Pb [Nogas]
50 ng/ml
100 ng/ml
500 ng/ml
1000 ng/ml
RSD%
Integration time (s)

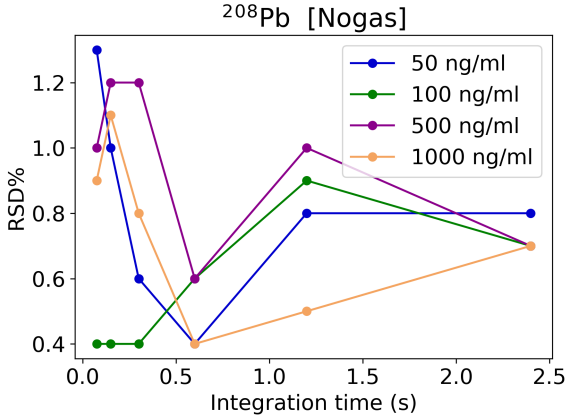
^{208}Pb [Nogas]
50 ng/ml
100 ng/ml
500 ng/ml
1000 ng/ml
RSD%
Integration time (s)

Appendix B

Diesel 1 response surfaces

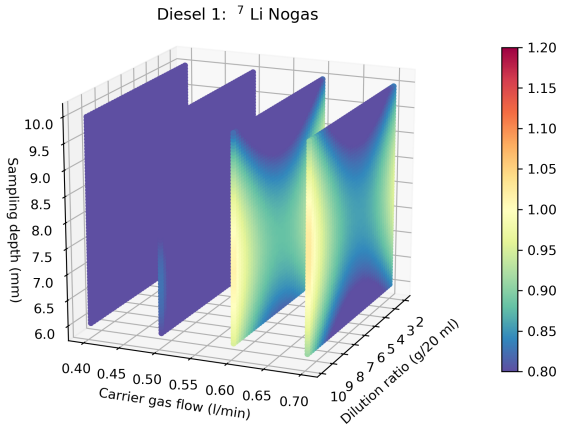
Diesel 1: ^{7} Li Nogas
Sampling depth (mm)
Carrier gas flow (l/min)
Dilution ratio (g/20 ml)

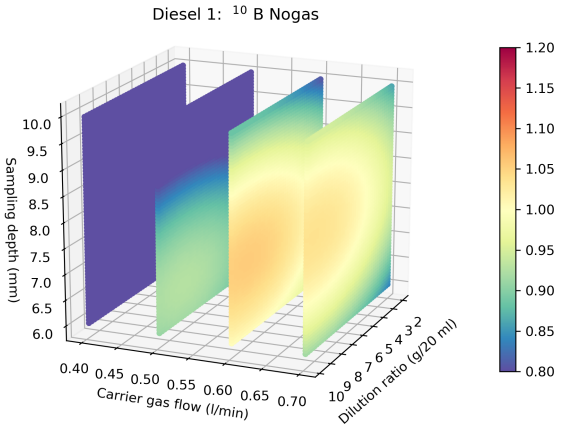
Diesel 1: ^{10} B Nogas
Sampling depth (mm)
Carrier gas flow (l/min)
Dilution ratio (g/20 ml)

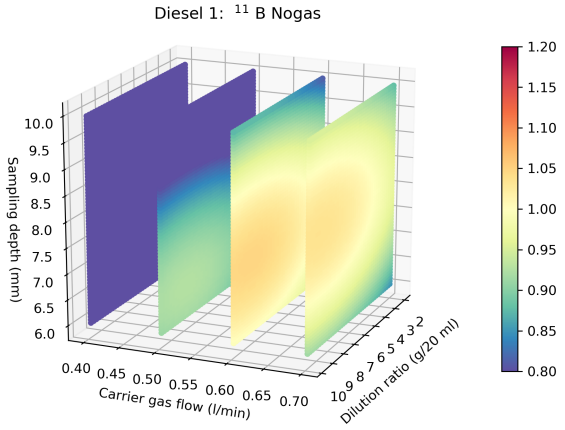
Diesel 1: ^{11} B Nogas
Sampling depth (mm)
Carrier gas flow (l/min)
Dilution ratio (g/20 ml)

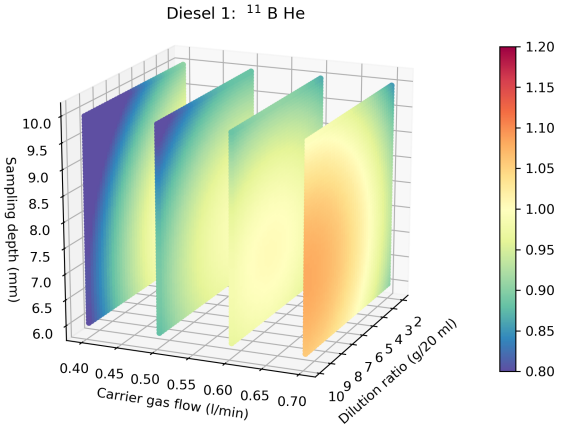
Diesel 1: ^{11} B He
Sampling depth (mm)
Carrier gas flow (l/min)
Dilution ratio (g/20 ml)

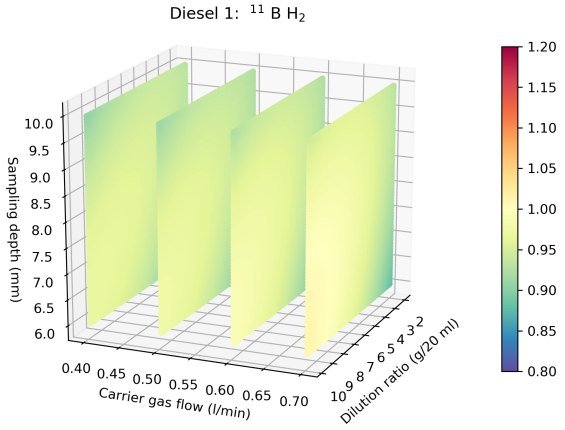
Diesel 1: ^{11} B H_2
Sampling depth (mm)
Carrier gas flow (l/min)
Dilution ratio (g/20 ml)

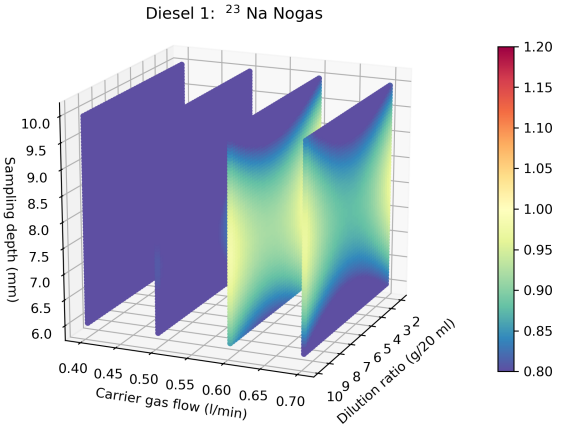
Diesel 1: ^{23} Na Nogas
Sampling depth (mm)
Carrier gas flow (l/min)
Dilution ratio (g/20 ml)

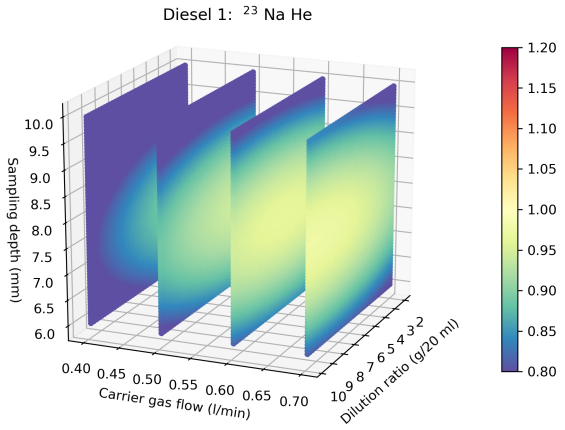
Diesel 1: ^{23} Na He
Sampling depth (mm)
Carrier gas flow (l/min)
Dilution ratio (g/20 ml)

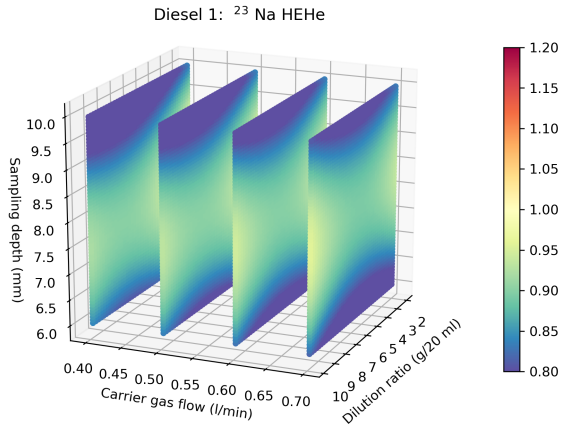
Diesel 1: ^{23} Na HEHe
Sampling depth (mm)
Carrier gas flow (l/min)
Dilution ratio (g/20 ml)

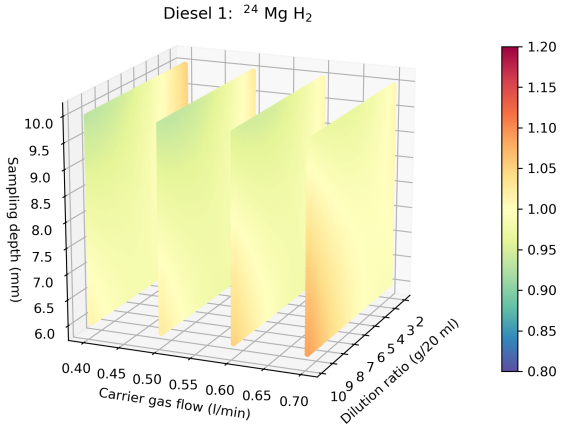
Diesel 1: ^{24} Mg H_2
Sampling depth (mm)
Carrier gas flow (l/min)
Dilution ratio (g/20 ml)

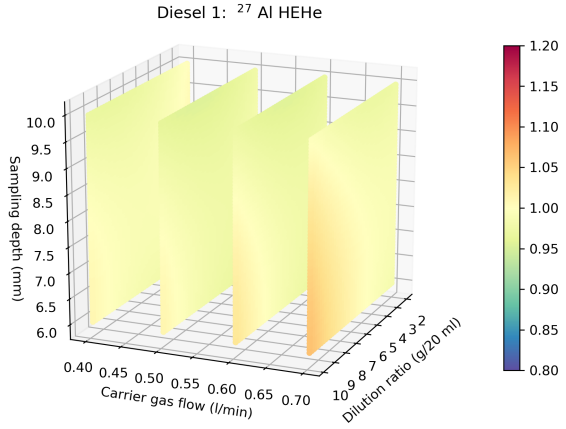
Diesel 1: ^{27} Al HEHe
Sampling depth (mm)
Carrier gas flow (l/min)
Dilution ratio (g/20 ml)

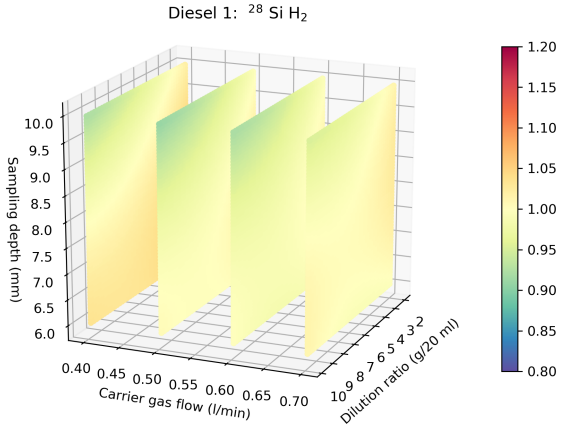
Diesel 1: ^{28} Si H_2
Sampling depth (mm)
Carrier gas flow (l/min)
Dilution ratio (g/20 ml)

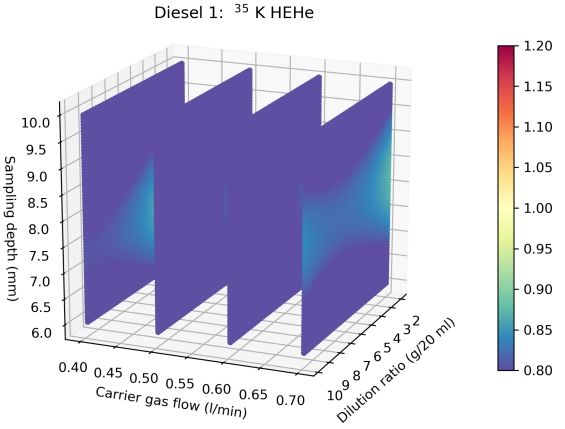
Diesel 1: ^{35} K HEHe
Sampling depth (mm)
Carrier gas flow (l/min)
Dilution ratio (g/20 ml)

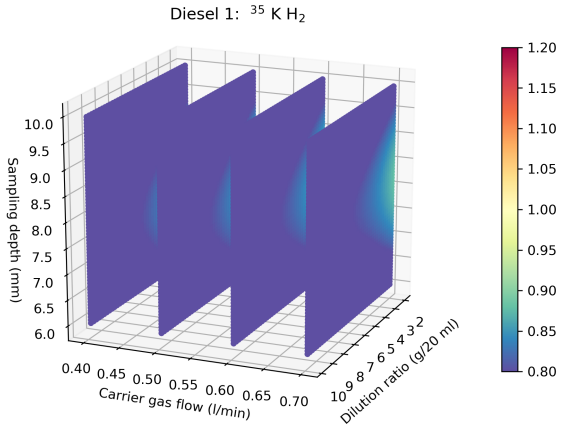
Diesel 1: ^{35}K H_2
Sampling depth (mm)
Carrier gas flow (l/min)
Dilution ratio (g/20 ml)

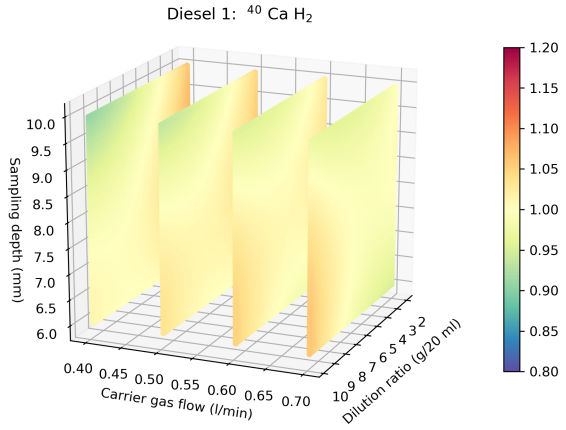
Diesel 1: ^{40}Ca H_2
Sampling depth (mm)
Carrier gas flow (l/min)
Dilution ratio (g/20 ml)

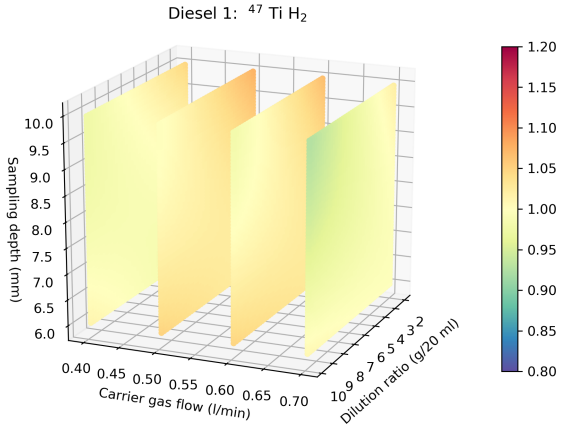
Diesel 1: ^{47}Ti H_2
Sampling depth (mm)
Carrier gas flow (l/min)
Dilution ratio (g/20 ml)

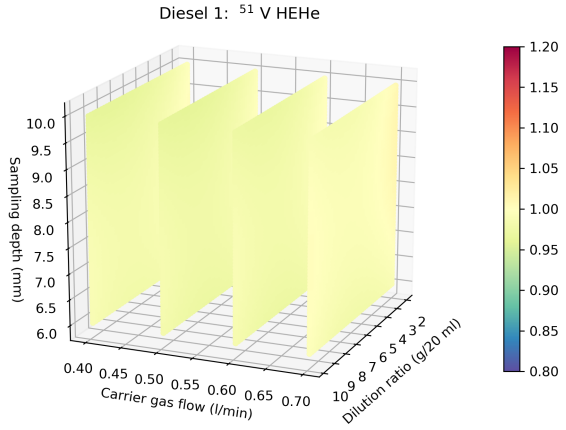
Diesel 1: ^{51}V HEHe
Sampling depth (mm)
Carrier gas flow (l/min)
Dilution ratio (g/20 ml)

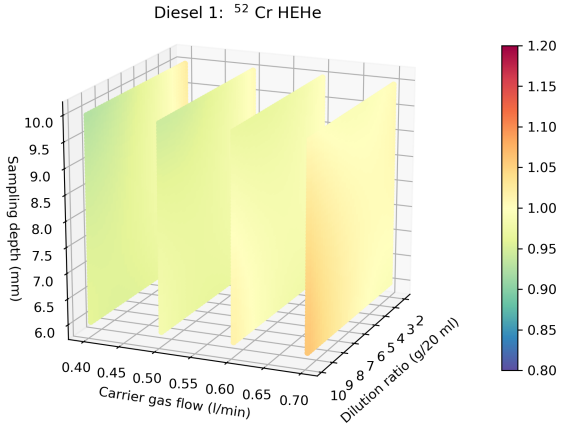
Diesel 1: ^{52}Cr HEHe
Sampling depth (mm)
Carrier gas flow (l/min)
Dilution ratio (g/20 ml)

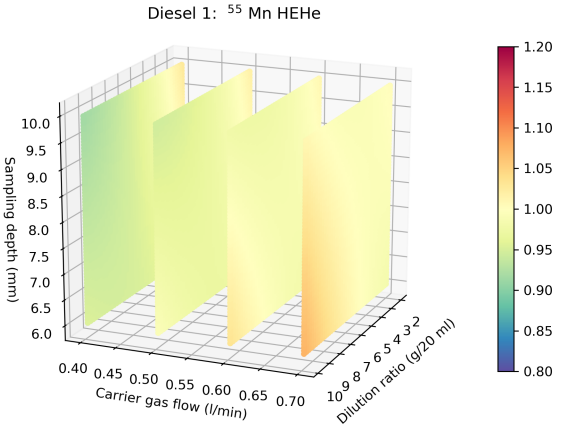
Diesel 1: ^{55}Mn HEHe
Sampling depth (mm)
Carrier gas flow (l/min)
Dilution ratio (g/20 ml)

Diesel 1: ^{56} Fe He

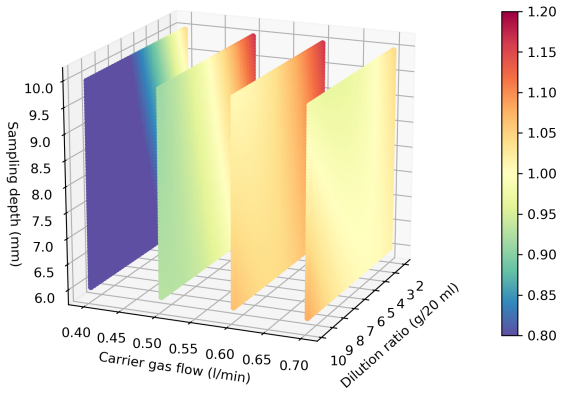

Diesel 1: ^{55} Co He

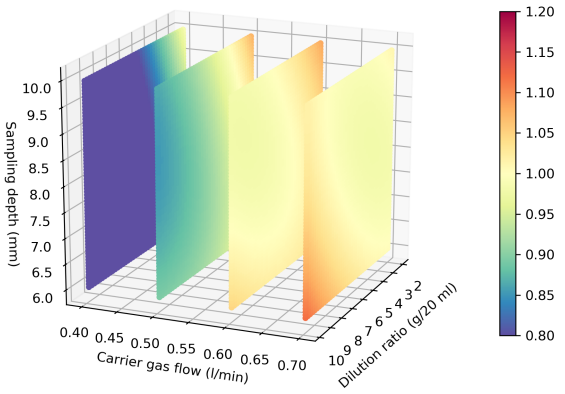

Diesel 1: ^{55} Co H_2

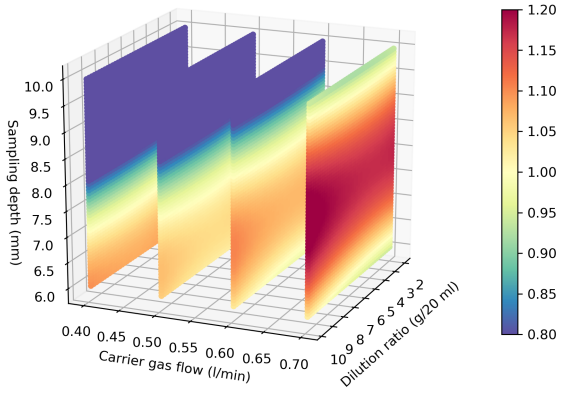

Diesel 1: ^{60} Ni HEHe

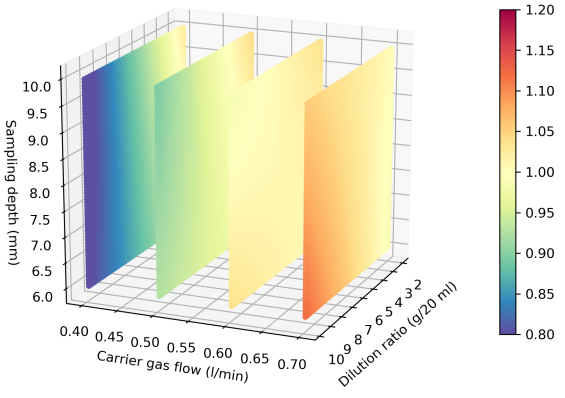

Diesel 1: ^{63} Cu HEHe

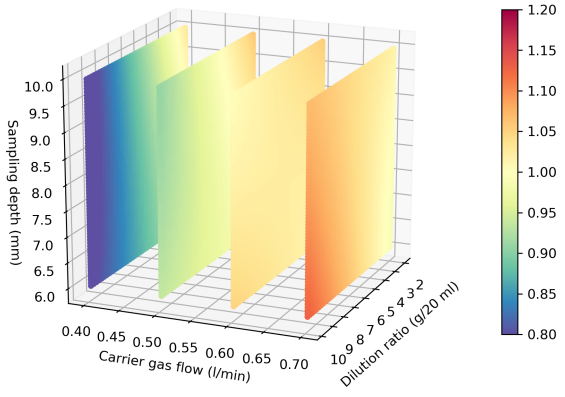

Diesel 1: ^{66} Zn H_2

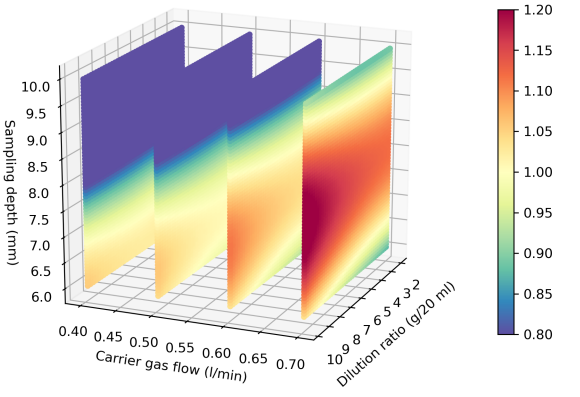

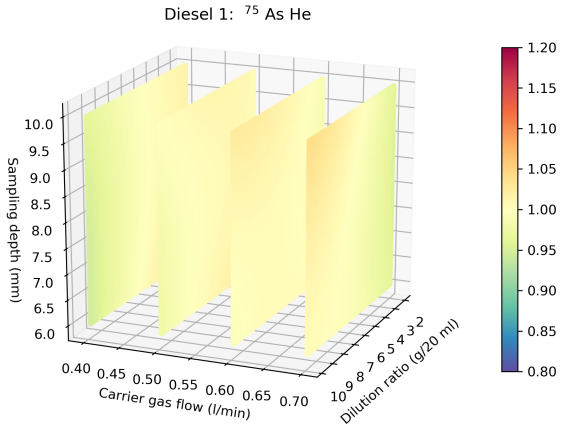
Diesel 1: ^{75} As He
Sampling depth (mm)
Carrier gas flow (l/min)
Dilution ratio (g/20 ml)

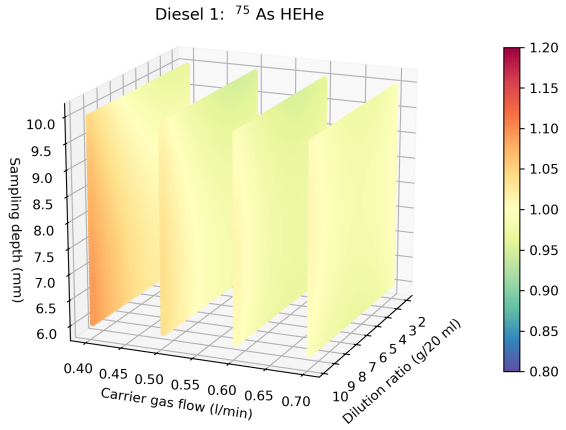
Diesel 1: ^{75} As HEHe
Sampling depth (mm)
Carrier gas flow (l/min)
Dilution ratio (g/20 ml)

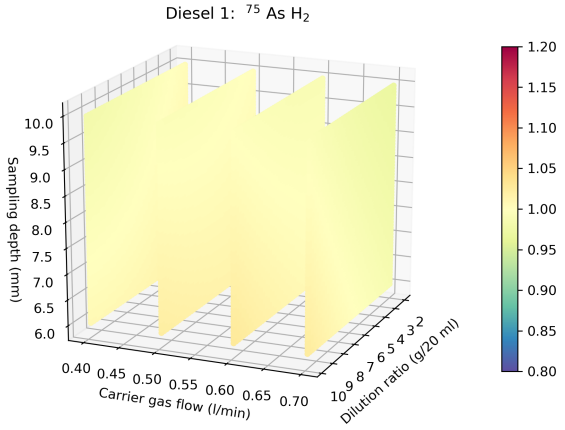
Diesel 1: ^{75} As H_2
Sampling depth (mm)
Carrier gas flow (l/min)
Dilution ratio (g/20 ml)

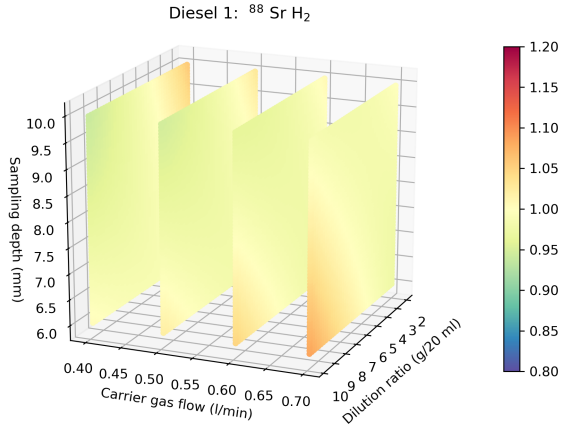
Diesel 1: ^{88} Sr H_2
Sampling depth (mm)
Carrier gas flow (l/min)
Dilution ratio (g/20 ml)

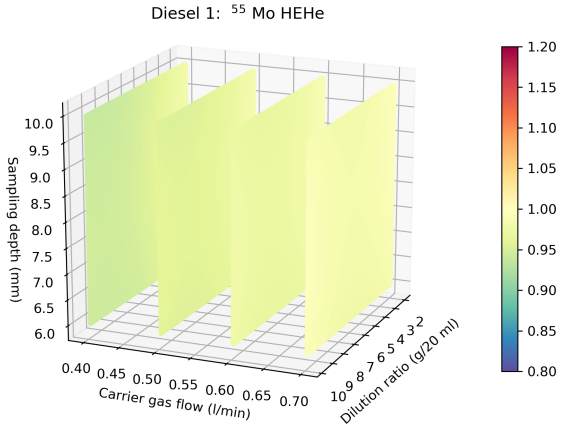
Diesel 1: ^{55} Mo HEHe
Sampling depth (mm)
Carrier gas flow (l/min)
Dilution ratio (g/20 ml)

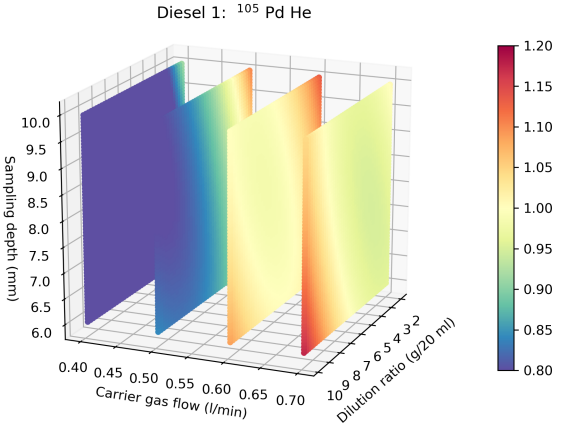
Diesel 1: ^{105} Pd He
Sampling depth (mm)
Carrier gas flow (l/min)
Dilution ratio (g/20 ml)

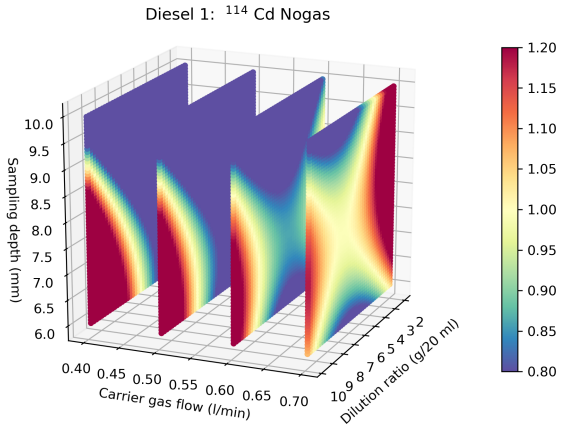
Diesel 1: ^{114} Cd Nogas
Sampling depth (mm)
Carrier gas flow (l/min)
Dilution ratio (g/20 ml)

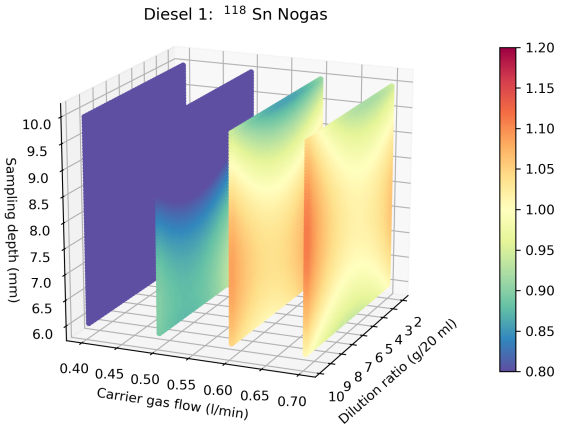
Diesel 1: ^{118} Sn Nogas
Sampling depth (mm)
Carrier gas flow (l/min)
Dilution ratio (g/20 ml)

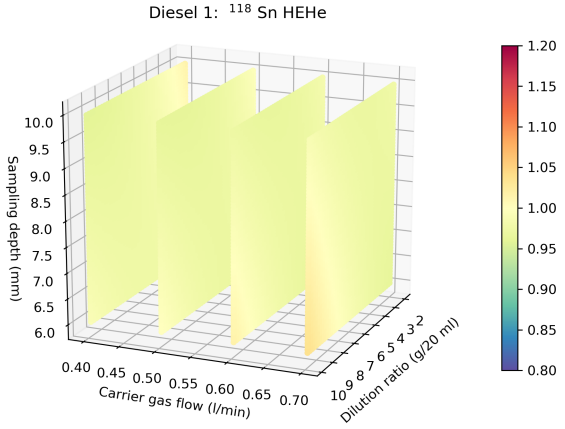
Diesel 1: ^{118} Sn HEHe
Sampling depth (mm)
Carrier gas flow (l/min)
Dilution ratio (g/20 ml)

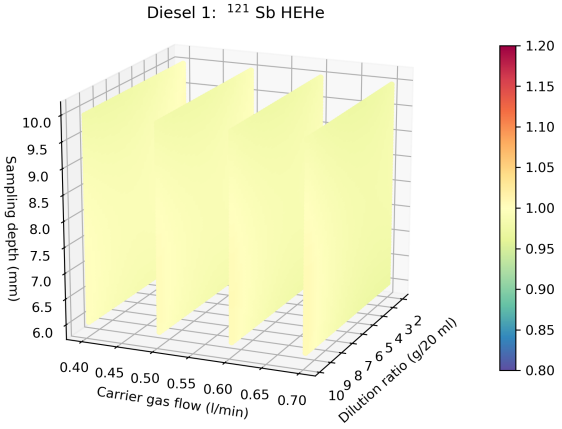
Diesel 1: ^{121} Sb HEHe
Sampling depth (mm)
Carrier gas flow (l/min)
Dilution ratio (g/20 ml)

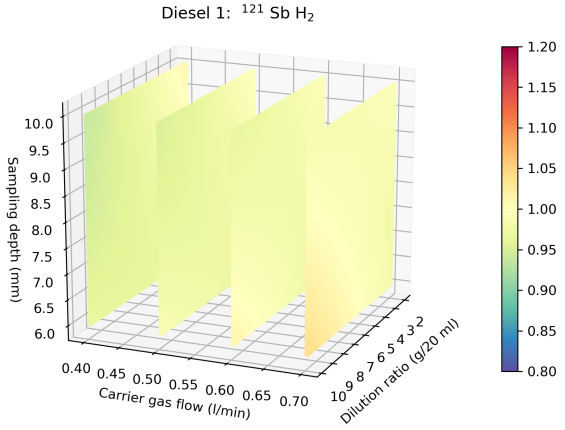
Diesel 1: ^{121} Sb H_2
Sampling depth (mm)
Carrier gas flow (l/min)
Dilution ratio (g/20 ml)

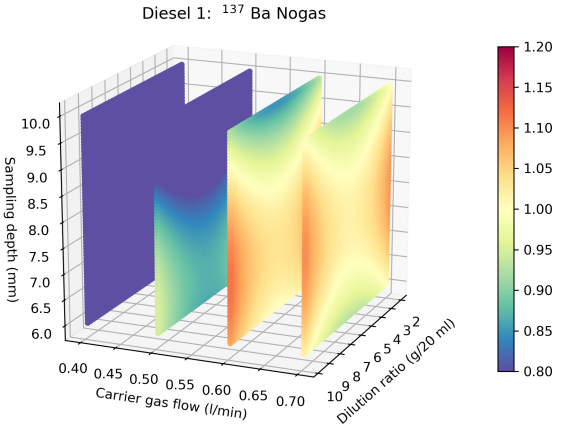
Diesel 1: ^{137} Ba Nogas
Sampling depth (mm)
Carrier gas flow (l/min)
Dilution ratio (g/20 ml)

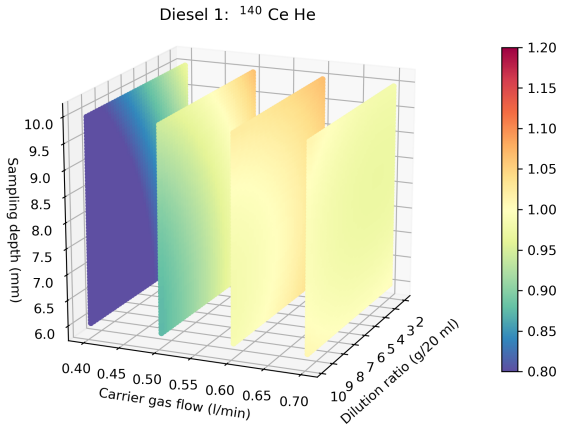
Diesel 1: ^{140} Ce He
Sampling depth (mm)
Carrier gas flow (l/min)
Dilution ratio (g/20 ml)

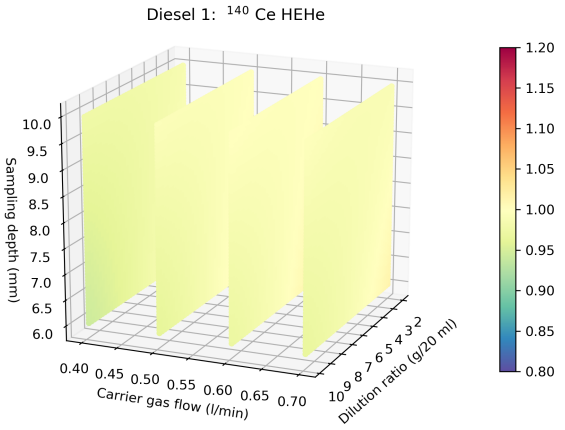
Diesel 1: ^{140} Ce HEHe
Sampling depth (mm)
Carrier gas flow (l/min)
Dilution ratio (g/20 ml)

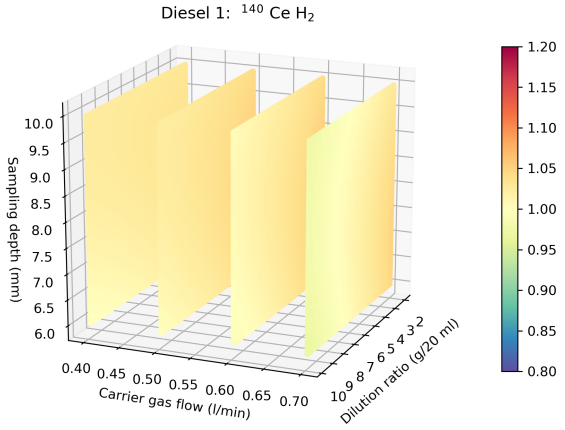
Diesel 1: ^{140} Ce H_2
Sampling depth (mm)
Carrier gas flow (l/min)
Dilution ratio (g/20 ml)

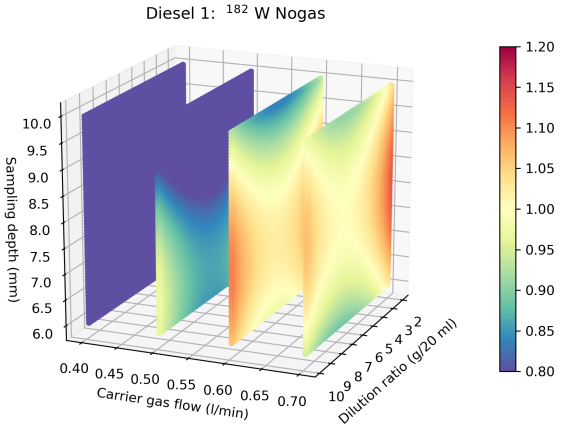
Diesel 1: ^{182} W Nogas
Sampling depth (mm)
Carrier gas flow (l/min)
Dilution ratio (g/20 ml)

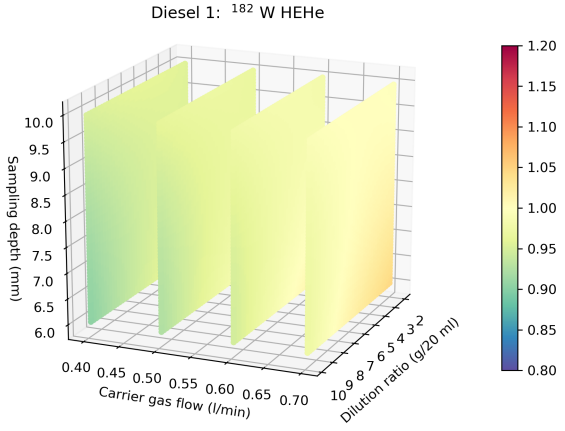
Diesel 1: ^{182} W HEHe
Sampling depth (mm)
Carrier gas flow (l/min)
Dilution ratio (g/20 ml)

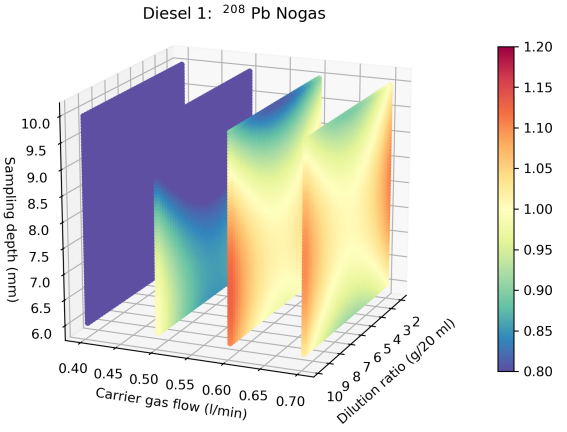
Diesel 1: ^{208} Pb Nogas
Sampling depth (mm)
Carrier gas flow (l/min)
Dilution ratio (g/20 ml)

Appendix C

Gasoline response surfaces

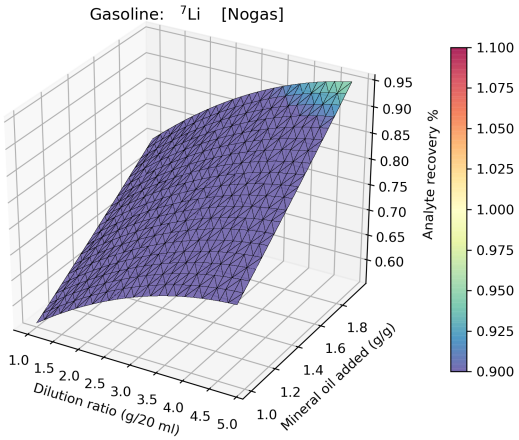
Gasoline: ^{7}Li [Nogas]
Analyte recovery %
Dilution ratio (g/20 ml)
Mineral oil added (g/g)

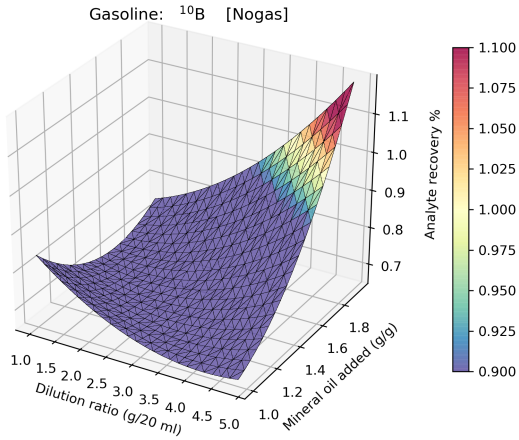
Gasoline: ^{10}B [Nogas]
Analyte recovery %
Dilution ratio (g/20 ml)
Mineral oil added (g/g)

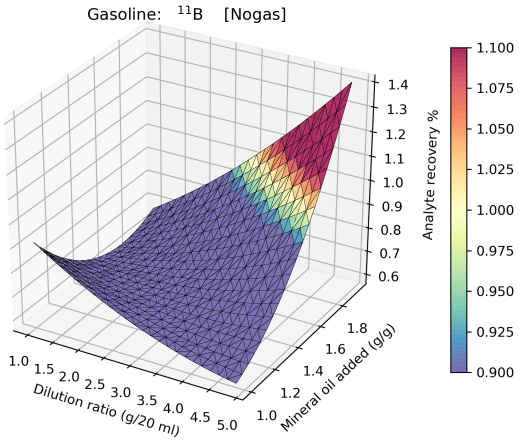
Gasoline: ^{11}B [Nogas]
Analyte recovery %
Dilution ratio (g/20 ml)
Mineral oil added (g/g)

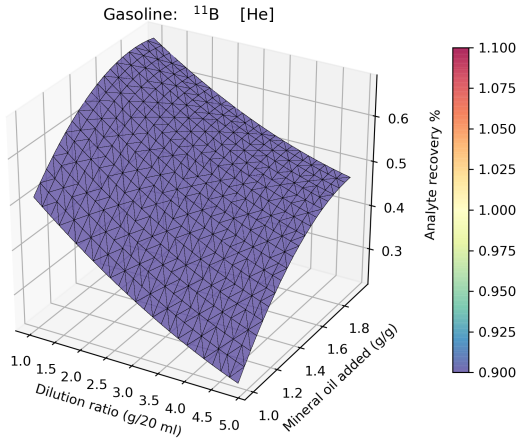
Gasoline: ^{11}B [He]
Analyte recovery %
Dilution ratio (g/20 ml)
Mineral oil added (g/g)

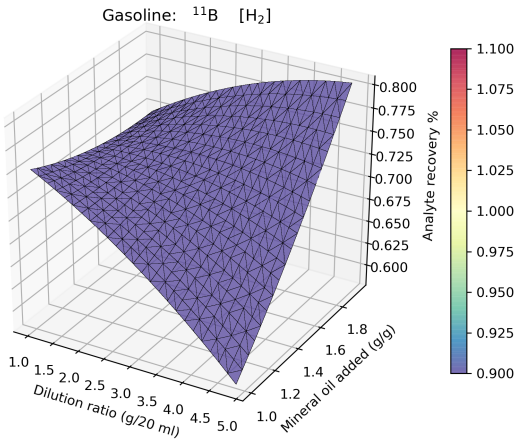
Gasoline: ^{11}B [H_2]
Analyte recovery %
Dilution ratio (g/20 ml)
Mineral oil added (g/g)

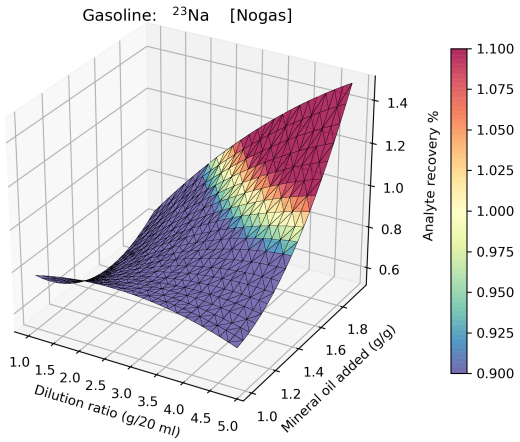
Gasoline: ^{23}Na [Nogas]
Analyte recovery %
Dilution ratio (g/20 ml)
Mineral oil added (g/g)

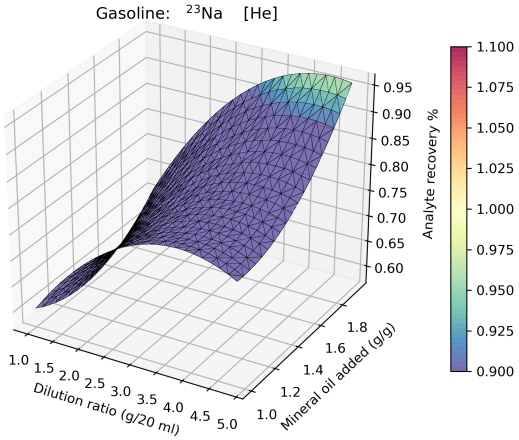
Gasoline: ^{23}Na [He]
Dilution ratio (g/20 ml)
Mineral oil added (g/g)
Analyte recovery %

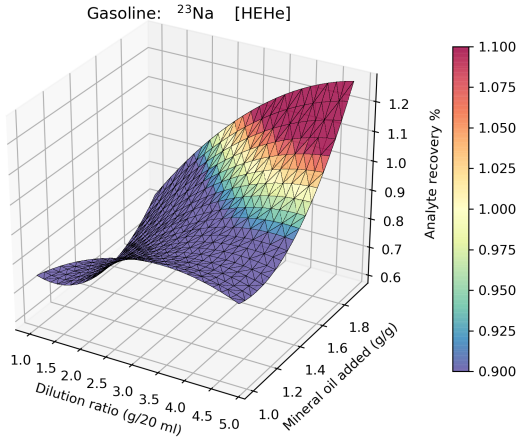
Gasoline: ^{23}Na [HEHe]
Dilution ratio (g/20 ml)
Mineral oil added (g/g)
Analyte recovery %

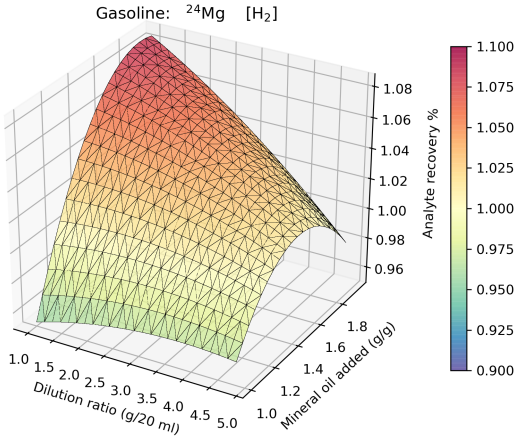
Gasoline: ^{24}Mg [H_2]
Dilution ratio (g/20 ml)
Mineral oil added (g/g)
Analyte recovery %

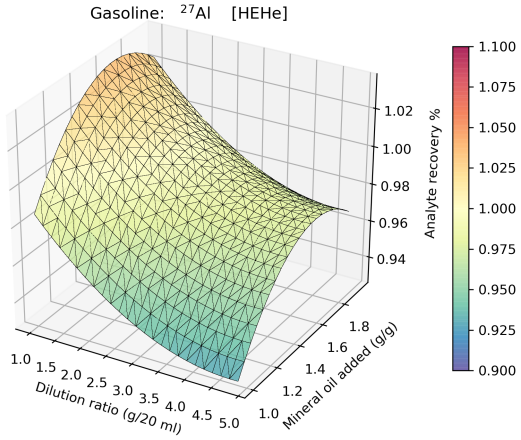
Gasoline: ^{27}Al [HEHe]
Dilution ratio (g/20 ml)
Mineral oil added (g/g)
Analyte recovery %

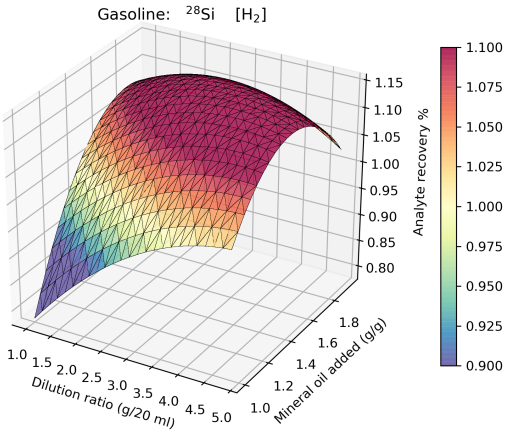
Gasoline: ^{28}Si [H_2]
Dilution ratio (g/20 ml)
Mineral oil added (g/g)
Analyte recovery %

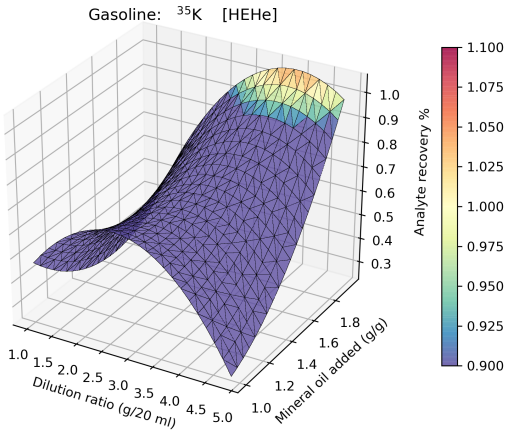
Gasoline: ^{35}K [HEHe]
Dilution ratio (g/20 ml)
Mineral oil added (g/g)
Analyte recovery %

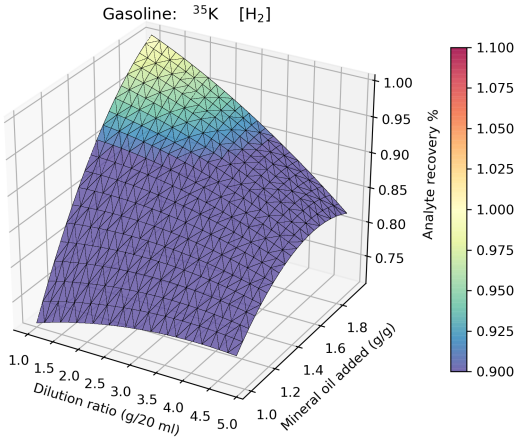
Gasoline: ^{35}K [H_2]
Analyte recovery %
Dilution ratio (g/20 ml)
Mineral oil added (g/g)

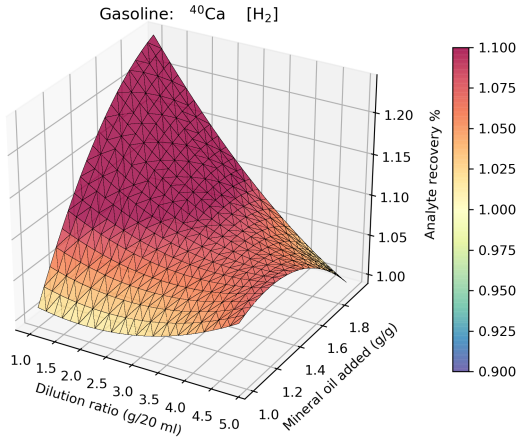
Gasoline: ^{40}Ca [H_2]
Analyte recovery %
Dilution ratio (g/20 ml)
Mineral oil added (g/g)

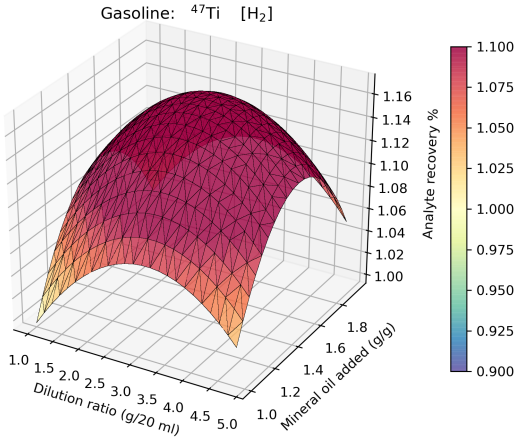
Gasoline: ^{47}Ti [H_2]
Analyte recovery %
Dilution ratio (g/20 ml)
Mineral oil added (g/g)

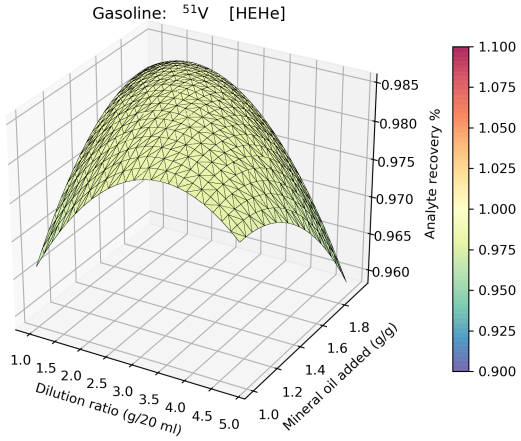
Gasoline: ^{51}V [HEHe]
Analyte recovery %
Dilution ratio (g/20 ml)
Mineral oil added (g/g)

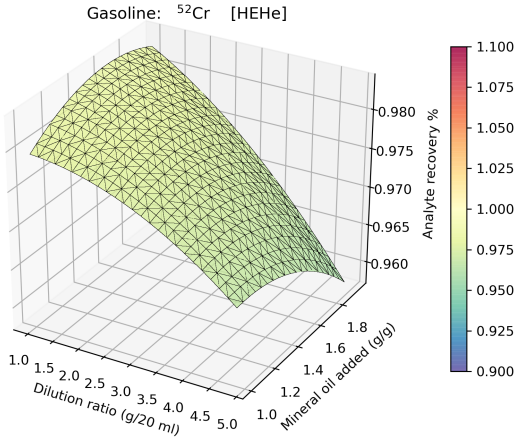
Gasoline: ^{52}Cr [HEHe]
Analyte recovery %
Dilution ratio (g/20 ml)
Mineral oil added (g/g)

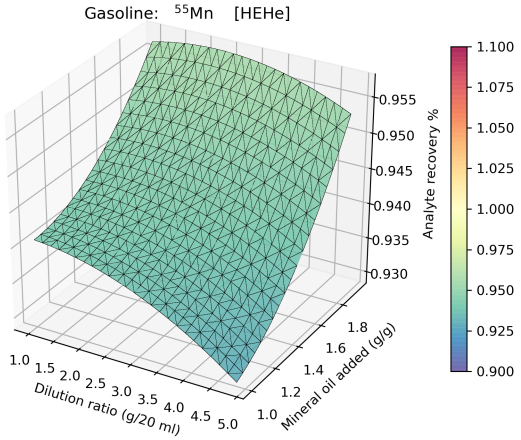
Gasoline: ^{55}Mn [HEHe]
Analyte recovery %
Dilution ratio (g/20 ml)
Mineral oil added (g/g)

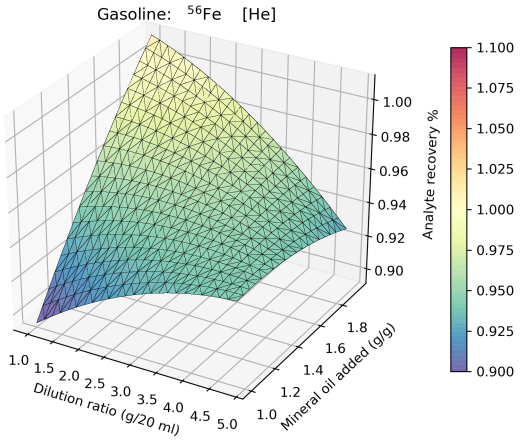
Gasoline: ^{56}Fe [He]
Dilution ratio (g/20 ml)
Mineral oil added (g/g)
Analyte recovery %

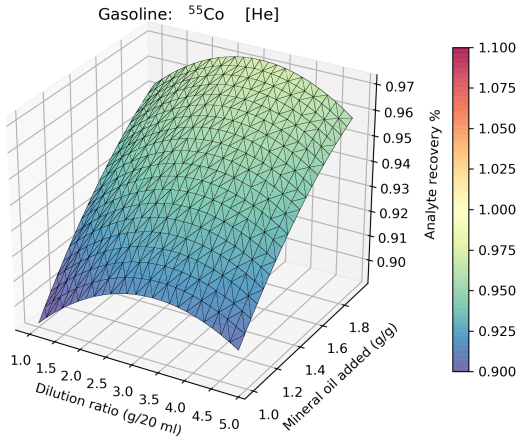
Gasoline: ^{55}Co [He]
Dilution ratio (g/20 ml)
Mineral oil added (g/g)
Analyte recovery %

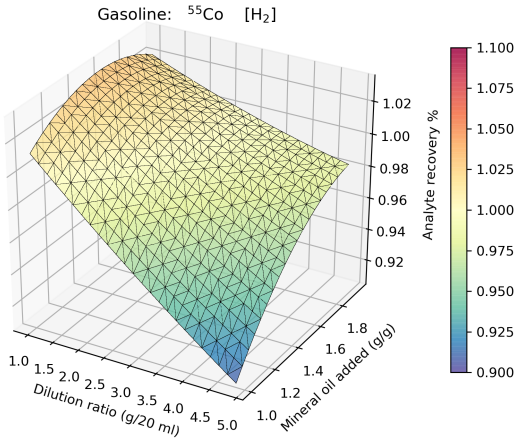
Gasoline: ^{55}Co [H_2]
Dilution ratio (g/20 ml)
Mineral oil added (g/g)
Analyte recovery %

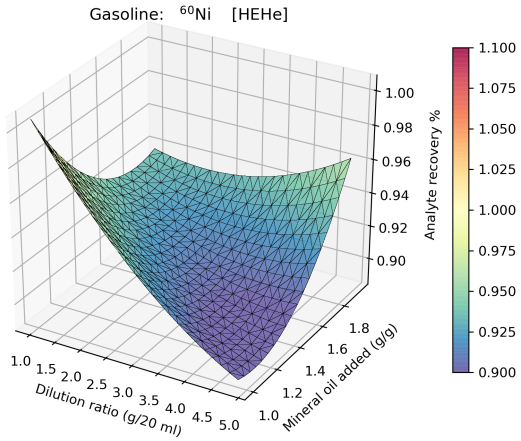
Gasoline: ^{60}Ni [HEHe]
Dilution ratio (g/20 ml)
Mineral oil added (g/g)
Analyte recovery %

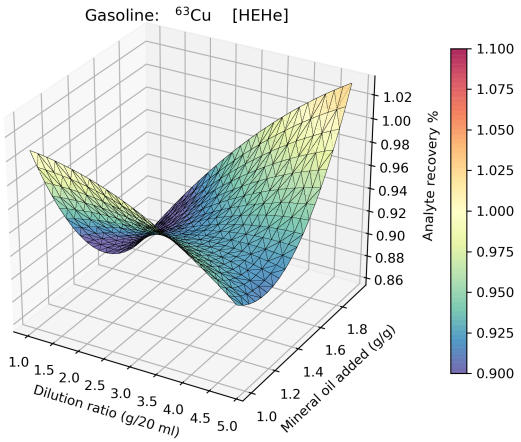
Gasoline: ^{63}Cu [HEHe]
Dilution ratio (g/20 ml)
Mineral oil added (g/g)
Analyte recovery %

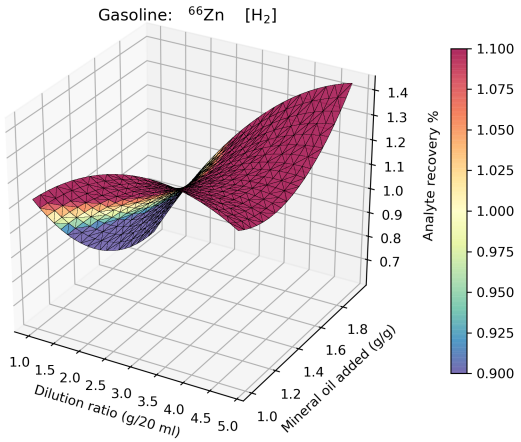
Gasoline: ^{66}Zn [H_2]
Dilution ratio (g/20 ml)
Mineral oil added (g/g)
Analyte recovery %

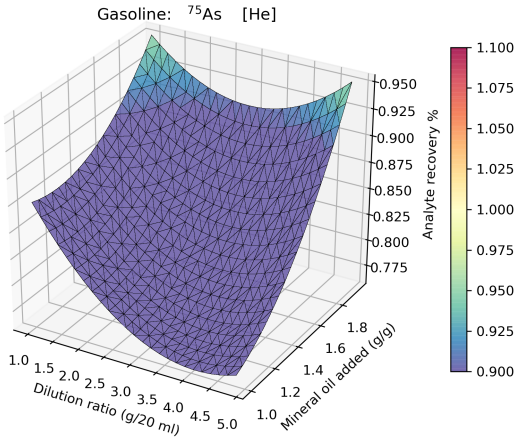
Gasoline: ^{75}As [He]
Analyte recovery %
Dilution ratio (g/20 ml)
Mineral oil added (g/g)

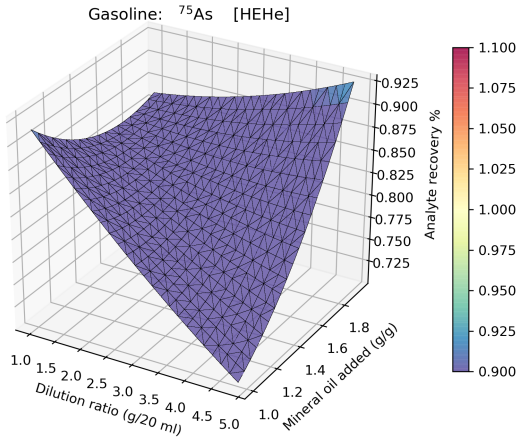
Gasoline: ^{75}As [HEHe]
Analyte recovery %
Dilution ratio (g/20 ml)
Mineral oil added (g/g)

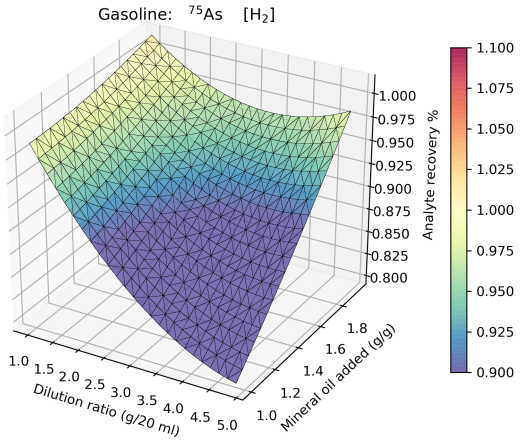
Gasoline: ^{75}As [H_2]
Analyte recovery %
Dilution ratio (g/20 ml)
Mineral oil added (g/g)

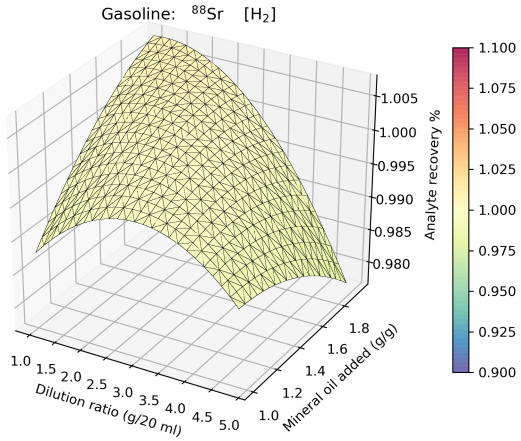
Gasoline: ^{88}Sr [H_2]
Analyte recovery %
Dilution ratio (g/20 ml)
Mineral oil added (g/g)

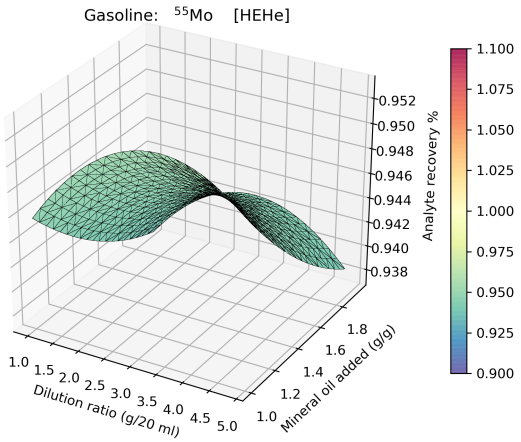
Gasoline: ^{55}Mo [HEHe]
Analyte recovery %
Dilution ratio (g/20 ml)
Mineral oil added (g/g)

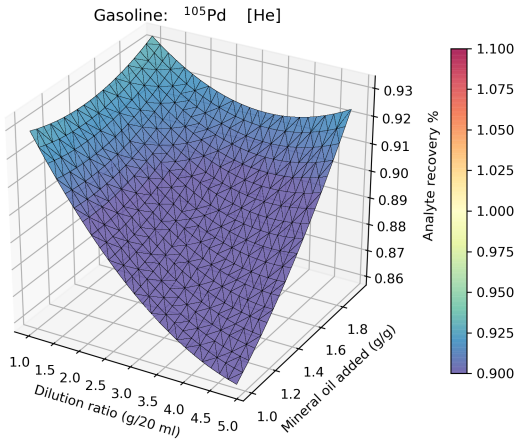
Gasoline: ^{105}Pd [He]
Analyte recovery %
Dilution ratio (g/20 ml)
Mineral oil added (g/g)

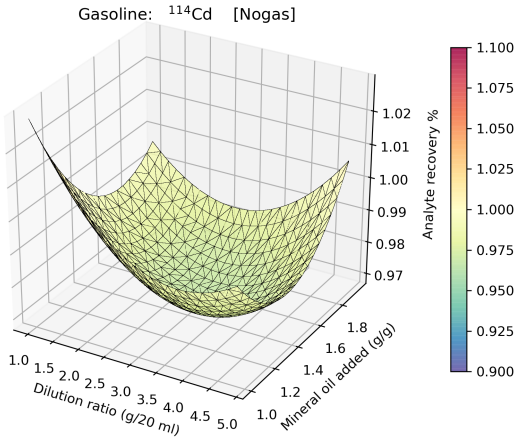
Gasoline: ^{114}Cd [Nogas]
Analyte recovery %
Dilution ratio (g/20 ml)
Mineral oil added (g/g)

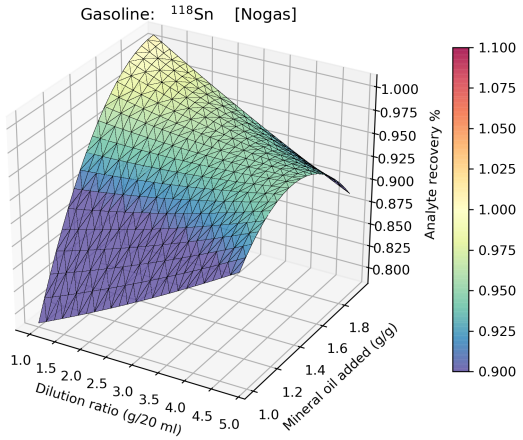
Gasoline: ^{118}Sn [Nogas]
Analyte recovery %
Dilution ratio (g/20 ml)
Mineral oil added (g/g)

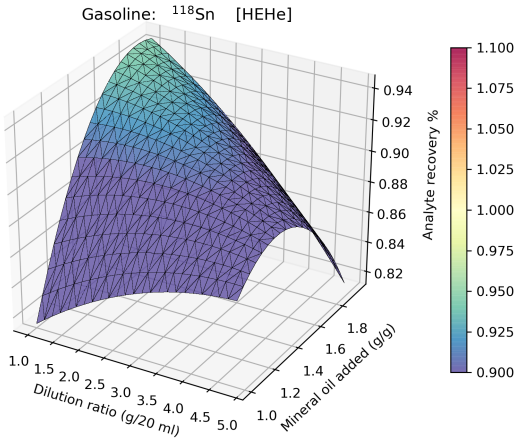
Gasoline: ^{118}Sn [HEHe]
Analyte recovery %
Dilution ratio (g/20 ml)
Mineral oil added (g/g)

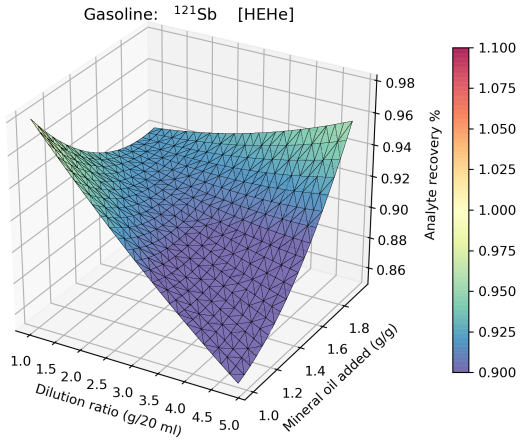
Gasoline: ^{121}Sb [HEHe]
Analyte recovery %
Dilution ratio (g/20 ml)
Mineral oil added (g/g)

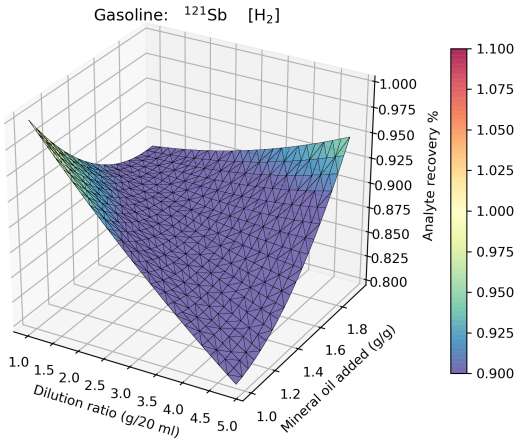
Gasoline: ^{121}Sb [H_2]
Analyte recovery %
Dilution ratio (g/20 ml)
Mineral oil added (g/g)

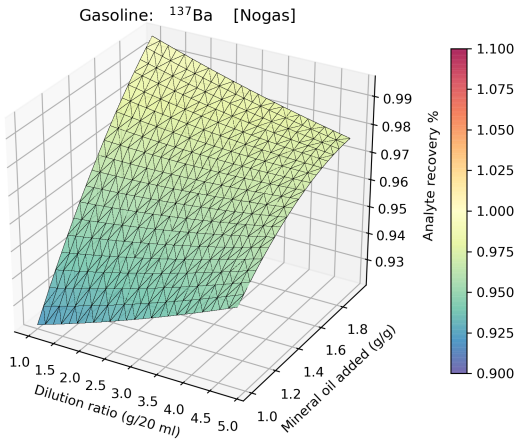
Gasoline: ^{137}Ba [Nogas]
Analyte recovery %
Dilution ratio (g/20 ml)
Mineral oil added (g/g)

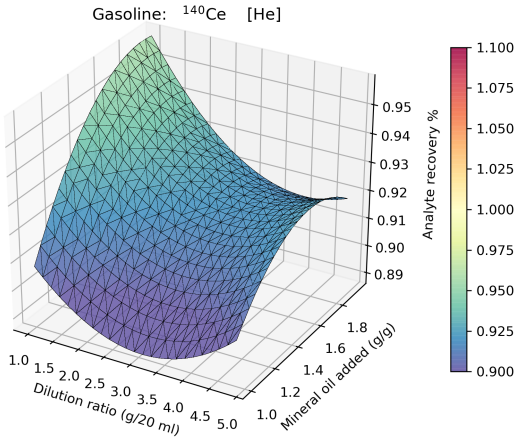
Gasoline: ^{140}Ce [He]
Analyte recovery %
Dilution ratio (g/20 ml)
Mineral oil added (g/g)

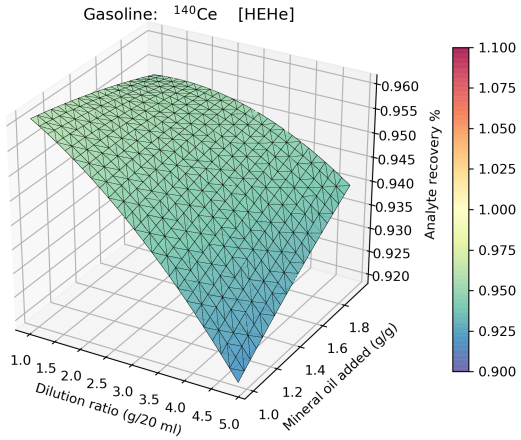
Gasoline: ^{140}Ce [HEHe]
Analyte recovery %
Dilution ratio (g/20 ml)
Mineral oil added (g/g)

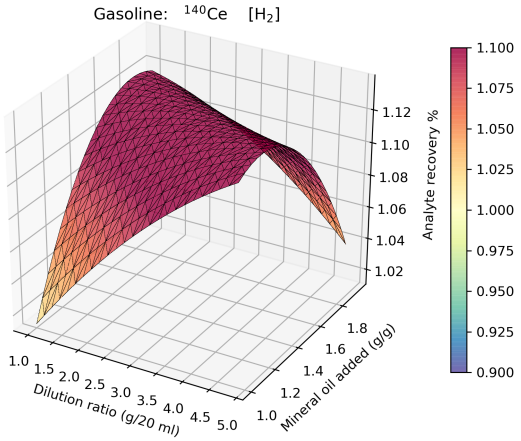
Gasoline: ^{140}Ce [H_2]
Analyte recovery %
Dilution ratio (g/20 ml)
Mineral oil added (g/g)

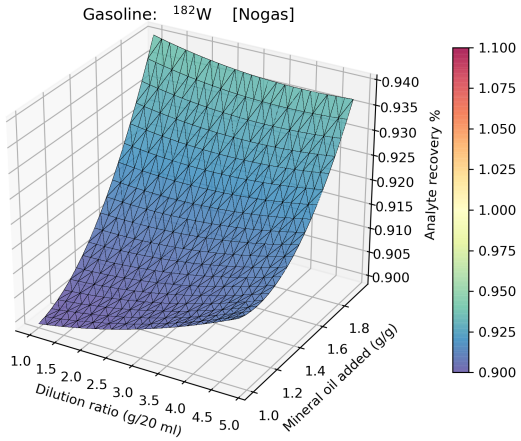
Gasoline: ^{182}W [Nogas]
Analyte recovery %
Dilution ratio (g/20 ml)
Mineral oil added (g/g)

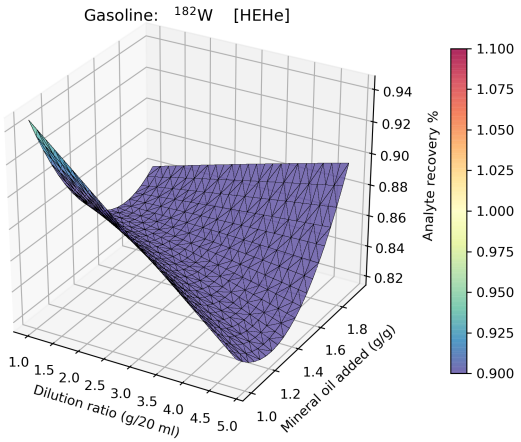
Gasoline: ^{182}W [HEHe]
Analyte recovery %
Dilution ratio (g/20 ml)
Mineral oil added (g/g)

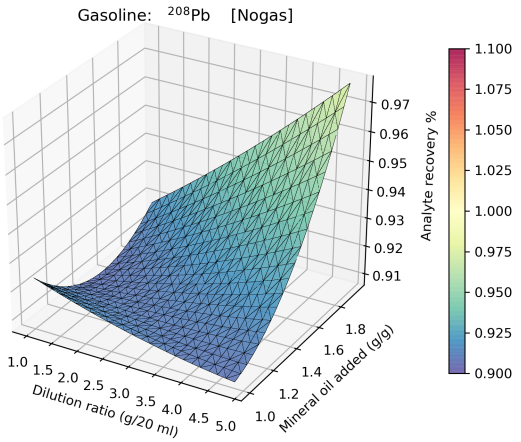
Gasoline: ^{208}Pb [Nogas]
Analyte recovery %
Dilution ratio (g/20 ml)
Mineral oil added (g/g)

Appendix D

Jet fuel 1 response surfaces

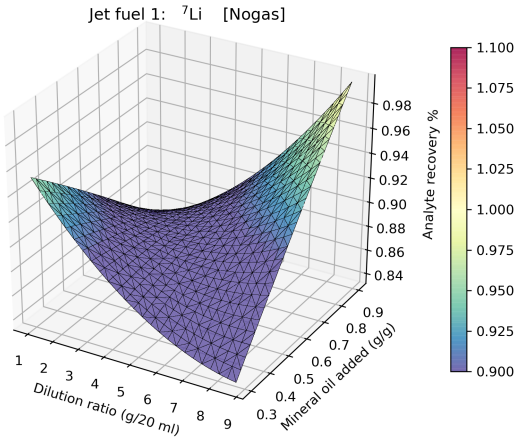
Jet fuel 1: ^{7}Li [Nogas]
Dilution ratio (g/20 ml)
Mineral oil added (g/g)
Analyte recovery %

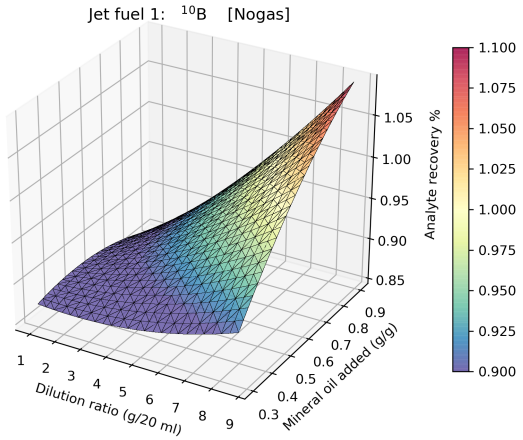
Jet fuel 1: ^{10}B [Nogas]
Dilution ratio (g/20 ml)
Mineral oil added (g/g)
Analyte recovery %

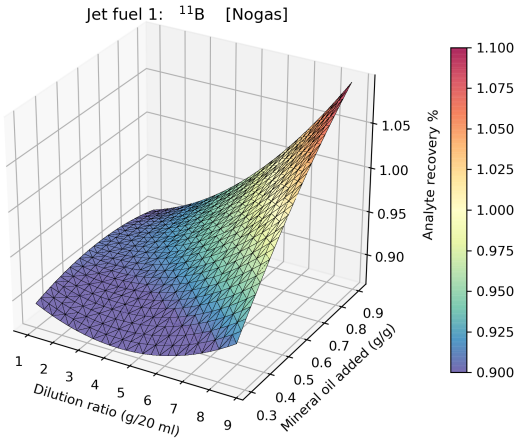
Jet fuel 1: ^{11}B [Nogas]
Dilution ratio (g/20 ml)
Mineral oil added (g/g)
Analyte recovery %

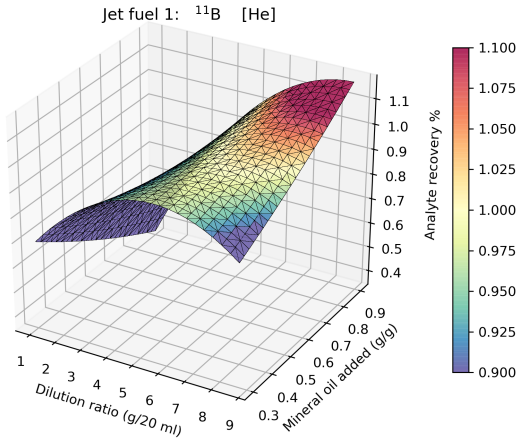
Jet fuel 1: ^{11}B [He]
Dilution ratio (g/20 ml)
Mineral oil added (g/g)
Analyte recovery %

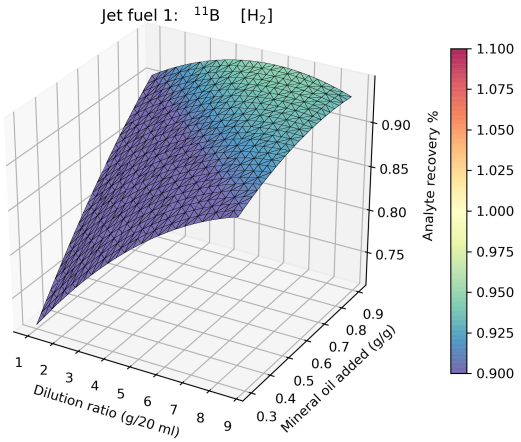
Jet fuel 1: ^{11}B [H_2]
Dilution ratio (g/20 ml)
Mineral oil added (g/g)
Analyte recovery %

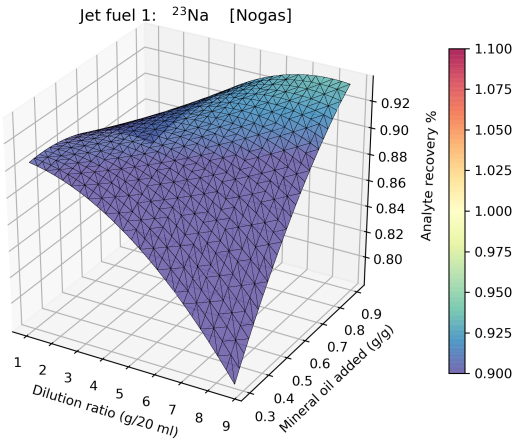
Jet fuel 1: ^{23}Na [Nogas]
Dilution ratio (g/20 ml)
Mineral oil added (g/g)
Analyte recovery %

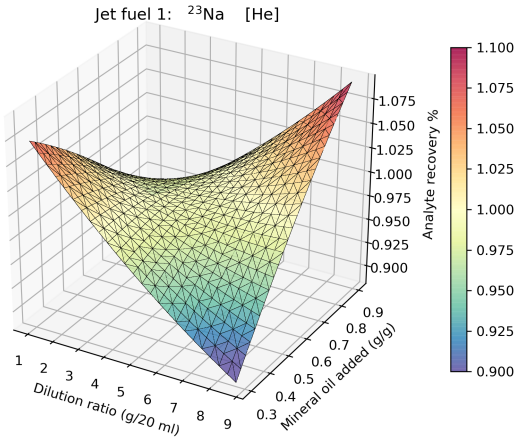
Jet fuel 1: ^{23}Na [He]
Analyte recovery %
Dilution ratio (g/20 ml)
Mineral oil added (g/g)

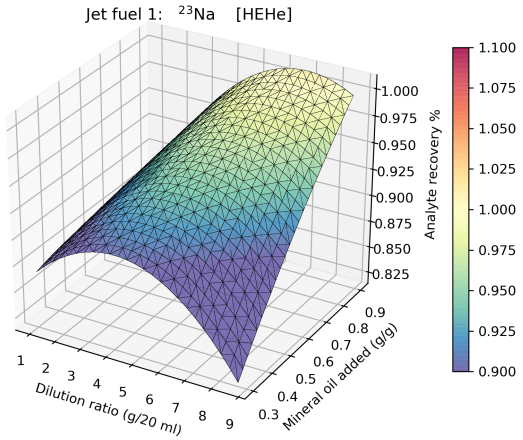
Jet fuel 1: ^{23}Na [HEHe]
Analyte recovery %
Dilution ratio (g/20 ml)
Mineral oil added (g/g)

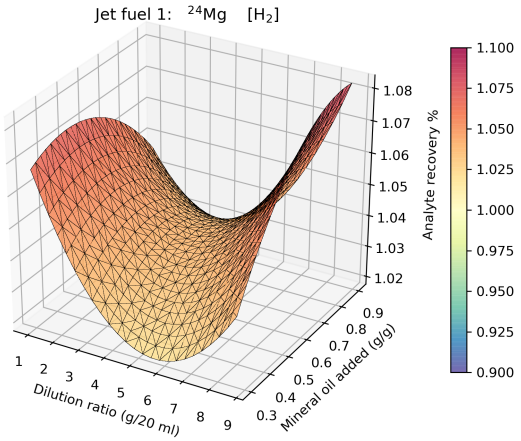
Jet fuel 1: ^{24}Mg [H_2]
Analyte recovery %
Dilution ratio (g/20 ml)
Mineral oil added (g/g)

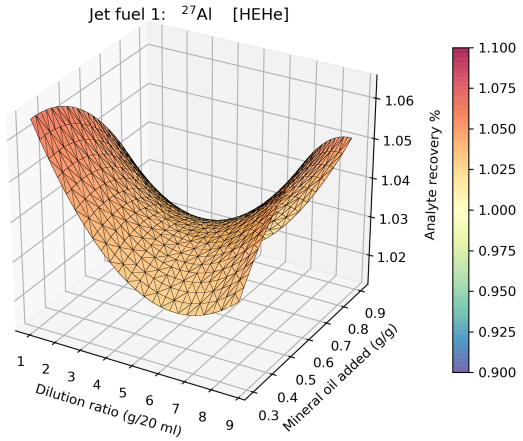
Jet fuel 1: ^{27}Al [HEHe]
Analyte recovery %
Dilution ratio (g/20 ml)
Mineral oil added (g/g)

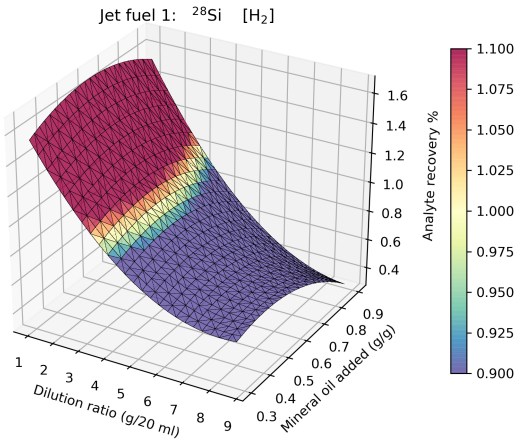
Jet fuel 1: ^{28}Si [H_2]
Analyte recovery %
Dilution ratio (g/20 ml)
Mineral oil added (g/g)

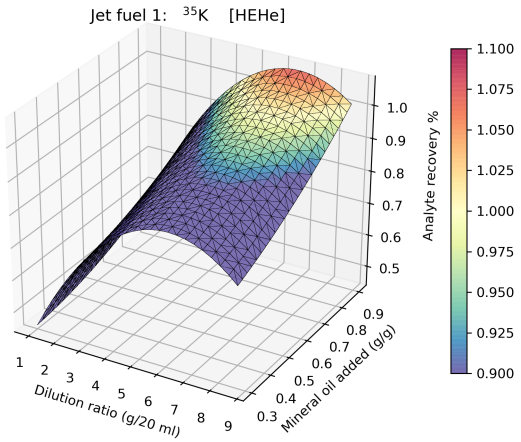
Jet fuel 1: ^{35}K [HEHe]
Analyte recovery %
Dilution ratio (g/20 ml)
Mineral oil added (g/g)

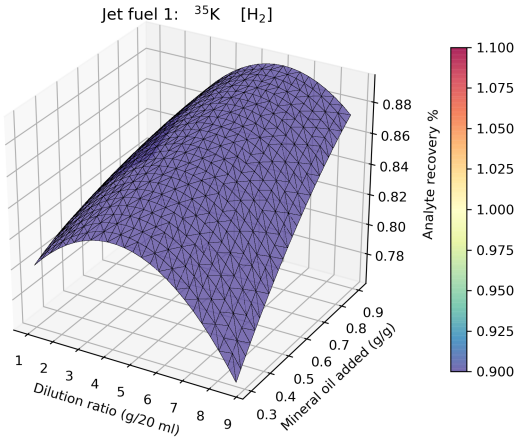
Jet fuel 1: ^{35}K [H_2]
Dilution ratio (g/20 ml)
Mineral oil added (g/g)
Analyte recovery %

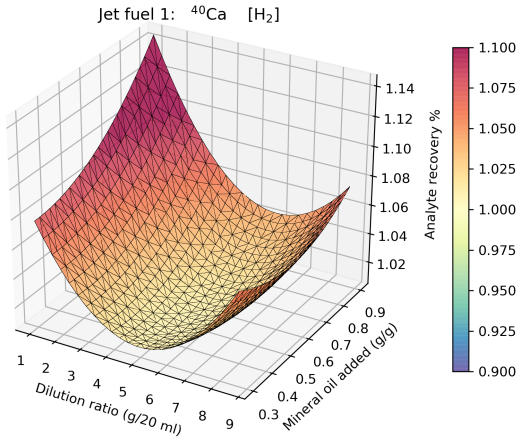
Jet fuel 1: ^{40}Ca [H_2]
Dilution ratio (g/20 ml)
Mineral oil added (g/g)
Analyte recovery %

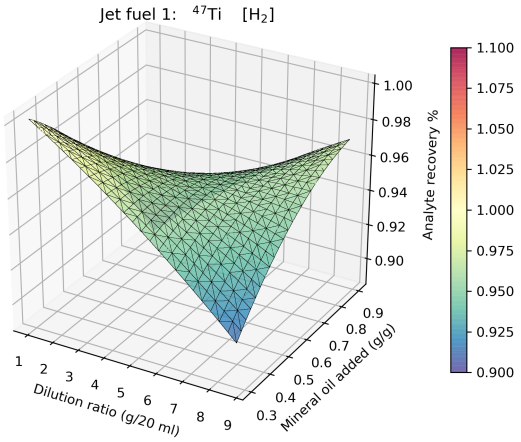
Jet fuel 1: ^{47}Ti [H_2]
Dilution ratio (g/20 ml)
Mineral oil added (g/g)
Analyte recovery %

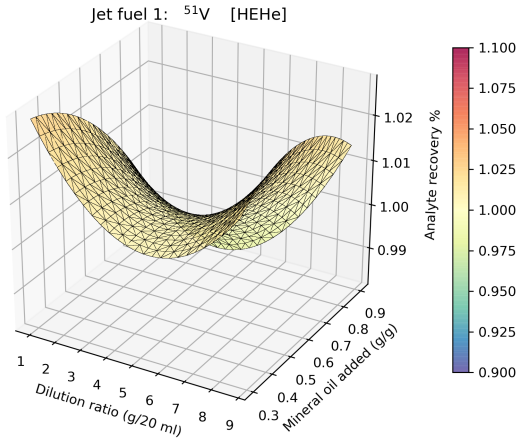
Jet fuel 1: ^{51}V [HEHe]
Dilution ratio (g/20 ml)
Mineral oil added (g/g)
Analyte recovery %

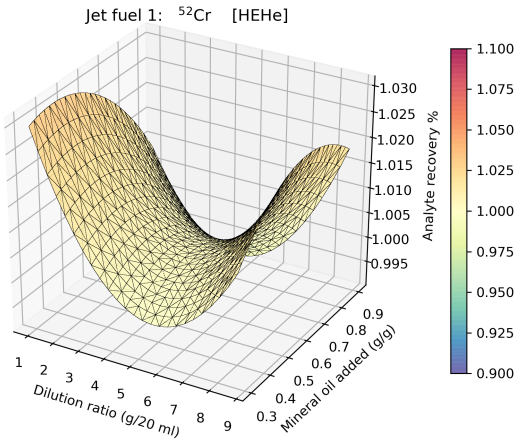
Jet fuel 1: ^{52}Cr [HEHe]
Dilution ratio (g/20 ml)
Mineral oil added (g/g)
Analyte recovery %

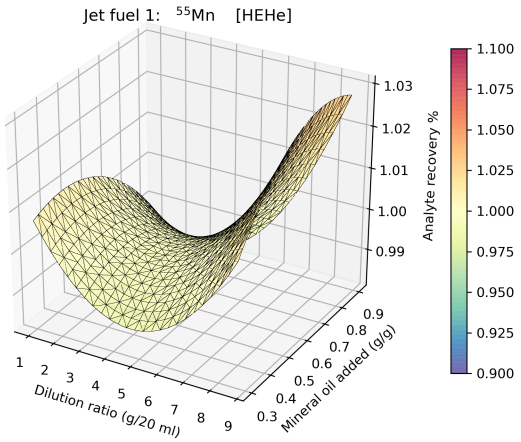
Jet fuel 1: ^{55}Mn [HEHe]
Dilution ratio (g/20 ml)
Mineral oil added (g/g)
Analyte recovery %

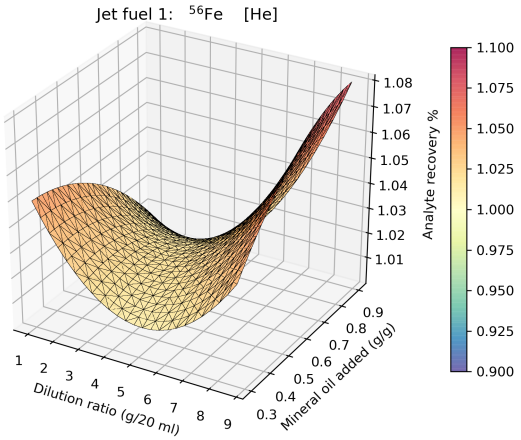
Jet fuel 1: ^{56}Fe [He]
Dilution ratio (g/20 ml)
Mineral oil added (g/g)
Analyte recovery %

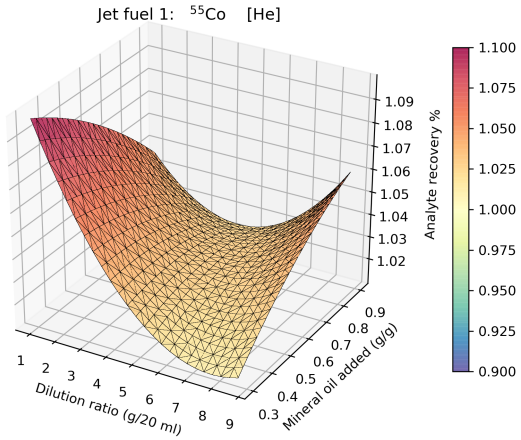
Jet fuel 1: ^{55}Co [He]
Dilution ratio (g/20 ml)
Mineral oil added (g/g)
Analyte recovery %

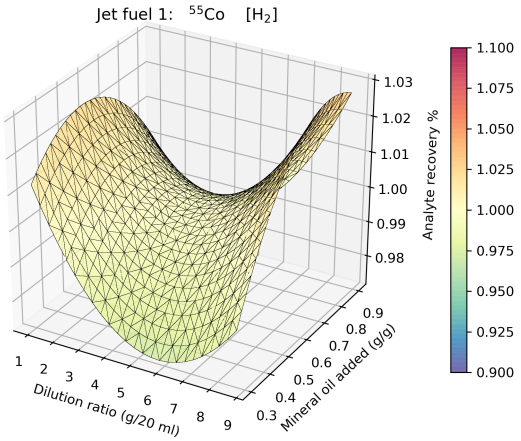
Jet fuel 1: ^{55}Co [H_2]
Dilution ratio (g/20 ml)
Mineral oil added (g/g)
Analyte recovery %

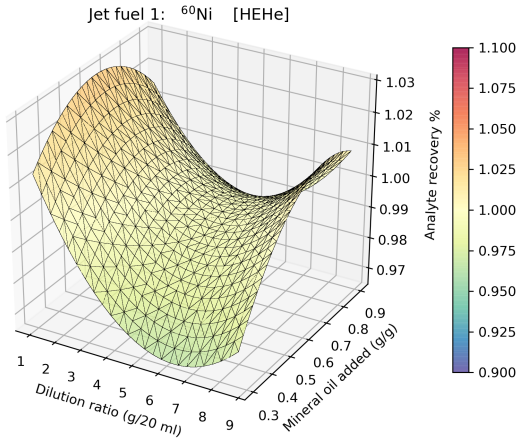
Jet fuel 1: ^{60}Ni [HEHe]
Dilution ratio (g/20 ml)
Mineral oil added (g/g)
Analyte recovery %

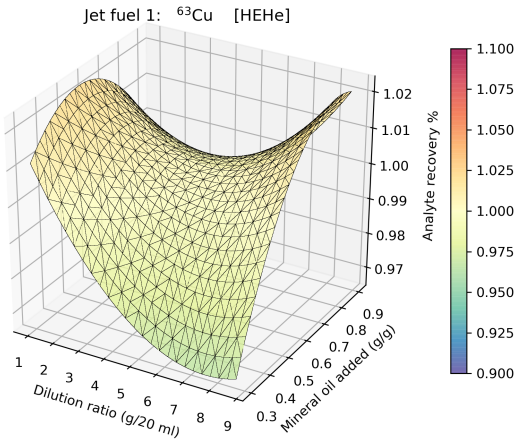
Jet fuel 1: ^{63}Cu [HEHe]
Dilution ratio (g/20 ml)
Mineral oil added (g/g)
Analyte recovery %

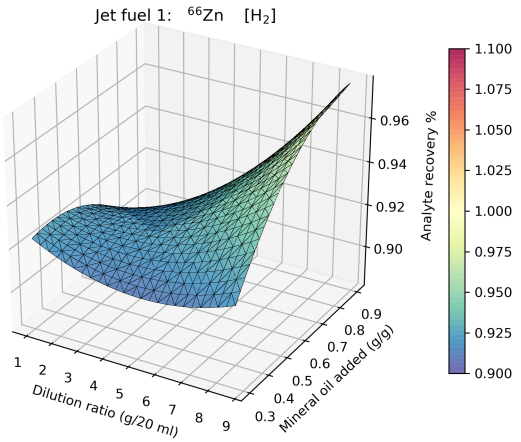
Jet fuel 1: ^{66}Zn [H_2]
Dilution ratio (g/20 ml)
Mineral oil added (g/g)
Analyte recovery %

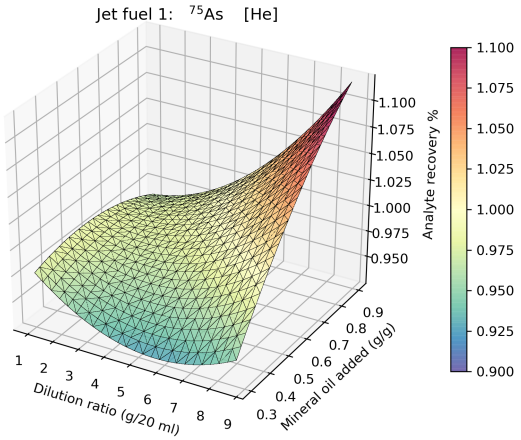
Jet fuel 1: ^{75}As [He]
Dilution ratio (g/20 ml)
Mineral oil added (g/g)
Analyte recovery %

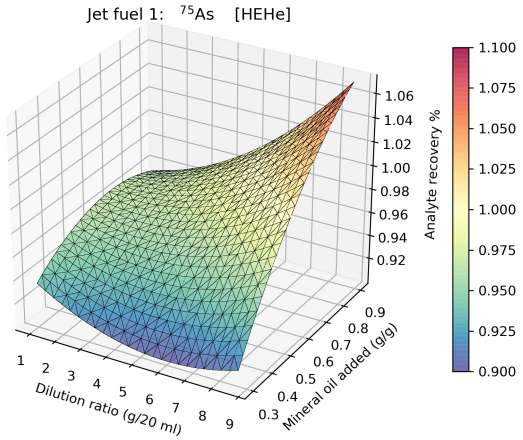
Jet fuel 1: ^{75}As [HEHe]
Dilution ratio (g/20 ml)
Mineral oil added (g/g)
Analyte recovery %

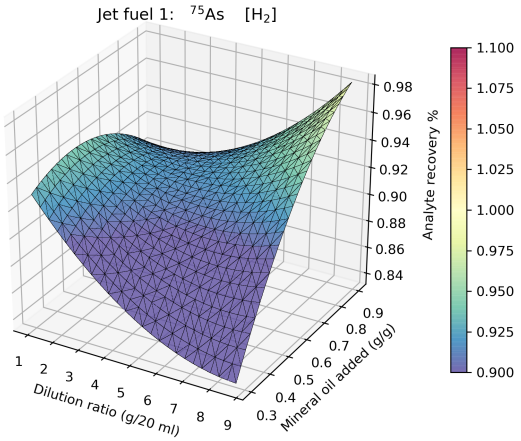
Jet fuel 1: ^{75}As [H_2]
Dilution ratio (g/20 ml)
Mineral oil added (g/g)
Analyte recovery %

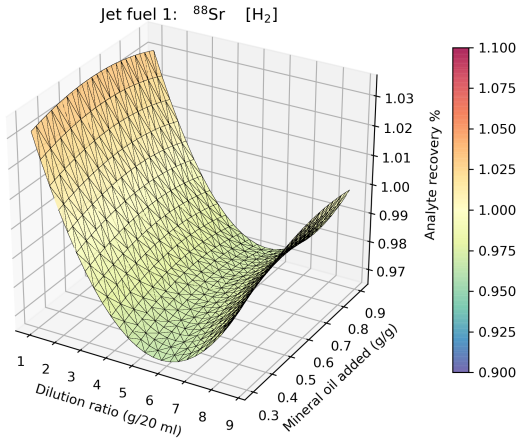
Jet fuel 1: ^{88}Sr [H_2]
Dilution ratio (g/20 ml)
Mineral oil added (g/g)
Analyte recovery %

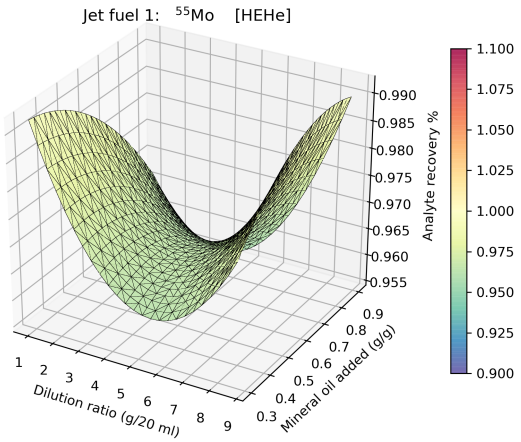
Jet fuel 1: ^{55}Mo [HEHe]
Dilution ratio (g/20 ml)
Mineral oil added (g/g)
Analyte recovery %

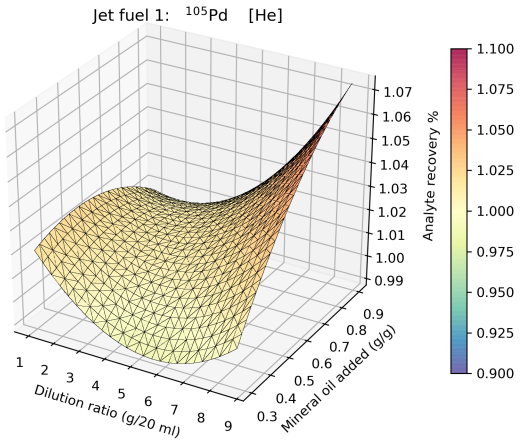
Jet fuel 1: ^{105}Pd [He]
Dilution ratio (g/20 ml)
Mineral oil added (g/g)
Analyte recovery %

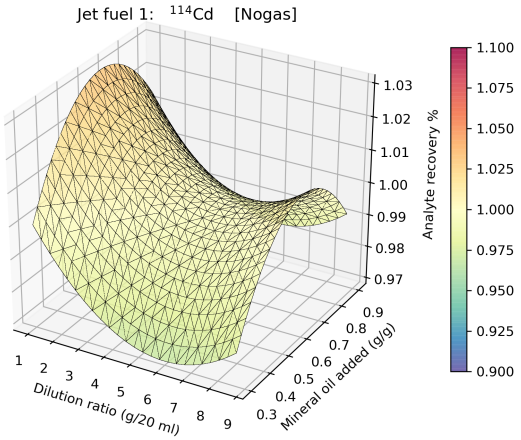
Jet fuel 1: ^{114}Cd [Nogas]
Analyte recovery %
Dilution ratio (g/20 ml)
Mineral oil added (g/g)

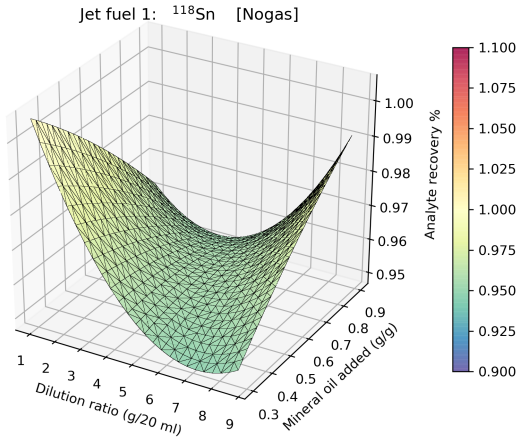
Jet fuel 1: ^{118}Sn [Nogas]
Analyte recovery %
Dilution ratio (g/20 ml)
Mineral oil added (g/g)

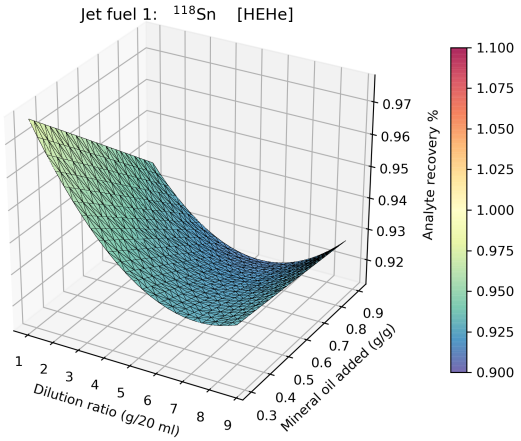
Jet fuel 1: ^{118}Sn [HEHe]
Analyte recovery %
Dilution ratio (g/20 ml)
Mineral oil added (g/g)

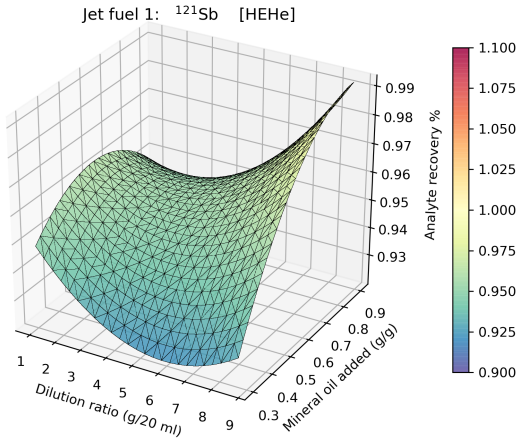
Jet fuel 1: ^{121}Sb [HEHe]
Analyte recovery %
Dilution ratio (g/20 ml)
Mineral oil added (g/g)

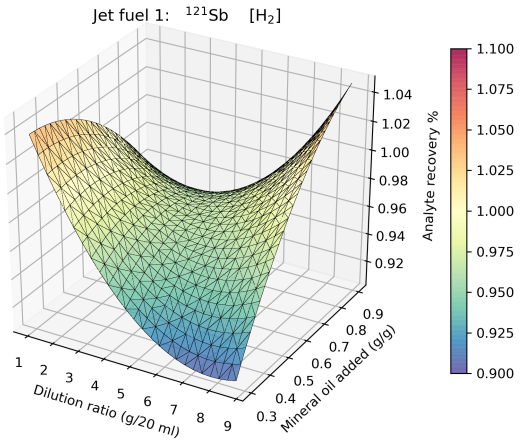
Jet fuel 1: ^{121}Sb [H_2]
Analyte recovery %
Dilution ratio (g/20 ml)
Mineral oil added (g/g)

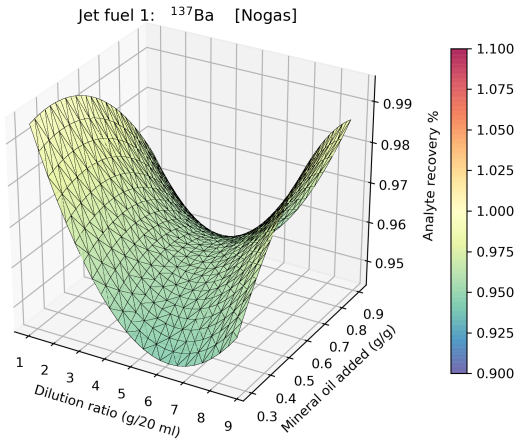
Jet fuel 1: ^{137}Ba [Nogas]
Analyte recovery %
Dilution ratio (g/20 ml)
Mineral oil added (g/g)

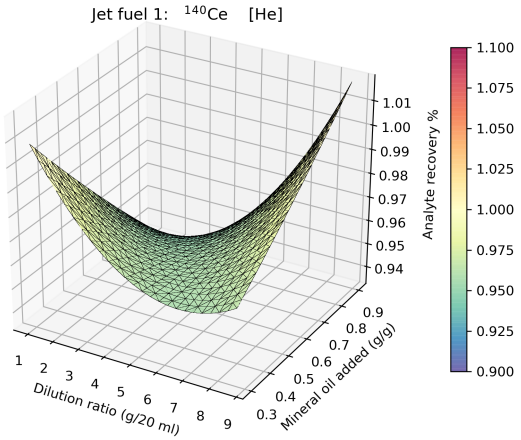
Jet fuel 1: ^{140}Ce [He]
Analyte recovery %
Dilution ratio (g/20 ml)
Mineral oil added (g/g)

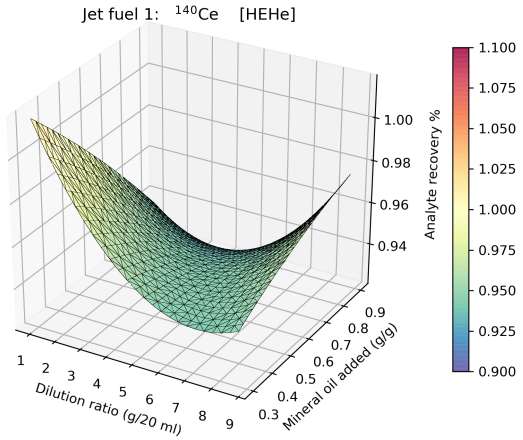
Jet fuel 1: ^{140}Ce [HEHe]
Analyte recovery %
Dilution ratio (g/20 ml)
Mineral oil added (g/g)

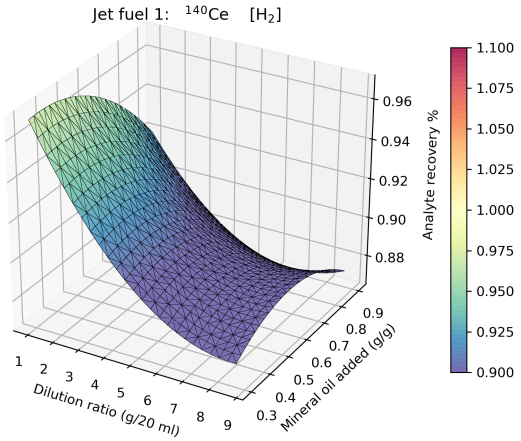
Jet fuel 1: ^{140}Ce [H_2]
Analyte recovery %
Dilution ratio (g/20 ml)
Mineral oil added (g/g)

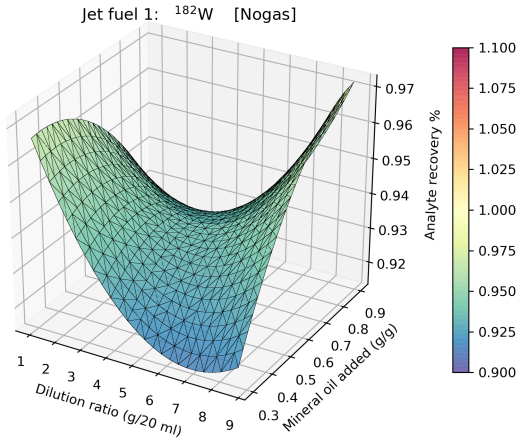
Jet fuel 1: ^{182}W [Nogas]
Analyte recovery %
Dilution ratio (g/20 ml)
Mineral oil added (g/g)

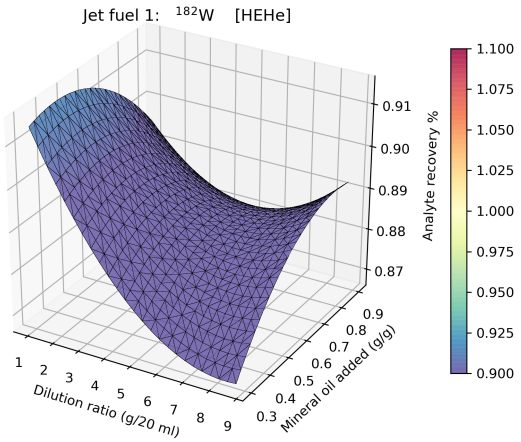
Jet fuel 1: ^{182}W [HEHe]
Analyte recovery %
Dilution ratio (g/20 ml)
Mineral oil added (g/g)

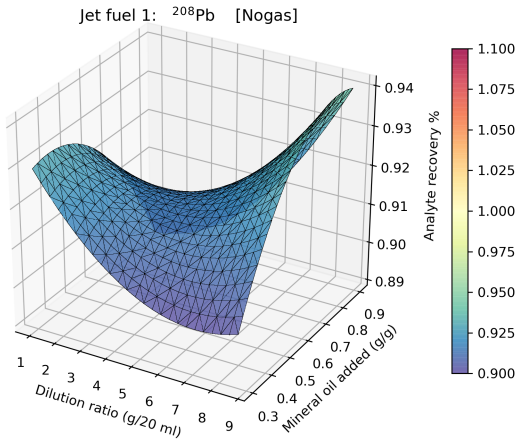
Jet fuel 1: ^{208}Pb [Nogas]
Analyte recovery %
Dilution ratio (g/20 ml)
Mineral oil added (g/g)

Appendix E

Jet fuel 1 ISTD recovery plotted agains calibration standard mineral oil composition, dilution ratio and additional mineral oil in test sample

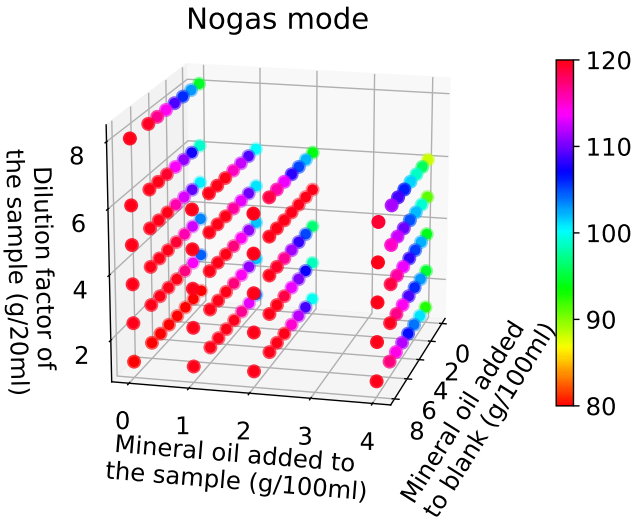

(a) ISTD recoveries with Nogas mode

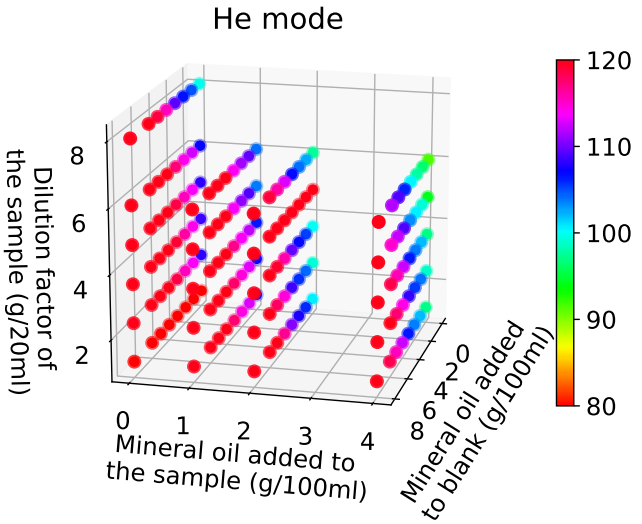

(b) ISTD recoveries with H_2 mode

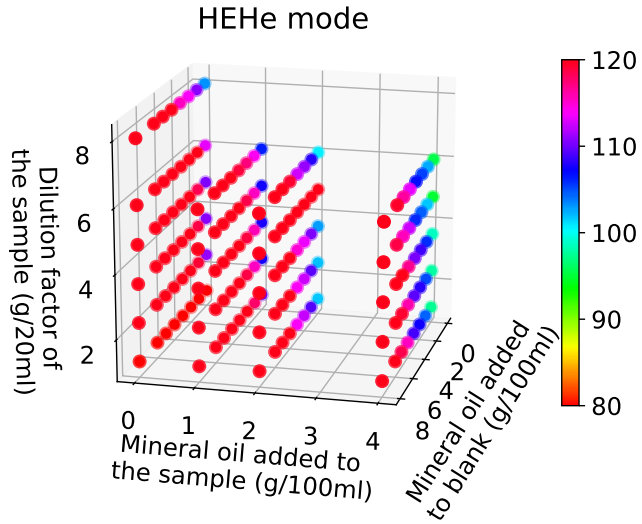

(c) ISTD recoveries for HEHe mode

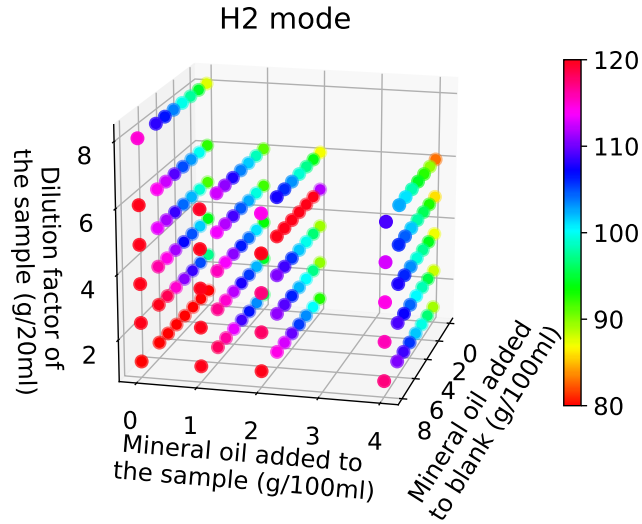

(d) ISTD recoveries fo H_2 mode

Figure E.1 ISTD recoveries from Jet fuel 1 as a fuction of sample dilution factor, calibration standard mineral oil concentration and test sample mineral concentration. Each figure represents a different gasmode used for the measurements and the color tells the ISTD recovery as percents.

Appendix F

Lists of measured samples

Table F.1 Overview of performed measurements in the validation of the xylene method for diesel fuels with the spray chamber temperature set to +5 °C

Sample type	Concentration of standard addition[a]		Number of measurements
	Elements of the large calibration range[b]	Elements of the small calibration range[c]	
Validation of diesel fuels at +5 °C			
Validation blank samples	-	-	25
Quality control samples			
QC 10 & 1	10 ng/ml	1 ng/ml	38
QC 50 & 5	50 ng/ml	5 ng/ml	37
QC 100 & 10	100 ng/ml	10 ng/ml	35
QC 600 & 60	600 ng/m	60 ng/ml	40
Diesel 1 (2.5 g/20 ml)			
Diesel 1a	-	-	10
Diesel 1a + 50 & 5 ng/g	50 ng/g	ng/g	10
Diesel 1a + 100 & 10 ng/g	100 ng/g	ng/g	9
Diesel 1a + 600 & 60 ng/g	600 ng/g	ng/g	10
Diesel 1b	-	-	9
Diesel 1b + 50 & 5 ng/g	50 ng/g	ng/g	9
Diesel 1b + 100 & 10 ng/g	100 ng/g	ng/g	9
Diesel 1b + 600 & 60 ng/g	600 ng/g	ng/g	9
Diesel 2 (2.5 g/20 ml)			
Diesel 2a	-	-	13
Diesel 2a + 50 & 5 ng/g	50 ng/g	ng/g	8
Diesel 2a + 100 & 10 ng/g	100 ng/g	ng/g	9
Diesel 2a + 600 & 60 ng/g	600 ng/g	ng/g	9
Diesel 2b	-	-	12
Diesel 2b + 50 & 5 ng/g	50 ng/g	ng/g	9
Diesel 2b + 100 & 10 ng/g	100 ng/g	ng/g	9
Diesel 2b + 600 & 60 ng/g	600 ng/g	ng/g	9

[a] Concentration of QC samples is given as ng per volume. Concentration of standard additions to samples is given as ng per gram of undiluted fuel.

[b] Elements of the large calibration range (0-100 ng/g): Li, Co, As, Sr, Mo, Pd, Ce, W and Pt.

[c] Elements of the small calibration range (0-1000 ng/g): B, Na, Mg, Al, Si, P, K, Ca Ti, V, Cr, Mn, Fe, Ni, Cu, Zn, Cd, Sn, Sb, Ba and Pb.

Table F.1 continuted. Overview of performed measurements in the validation of diesel fuels with the spray chamber temperature set to +5 °C

Sample type	Concentration of standard addition[a]		Number of measurements
	Elements of the large calibration range[b]	Elements of the small calibration range[c]	
Validation of diesel fuels at +5 °C			
Validation blank samples	-	-	25
Quality control samples			
QC 10 & 1	10 ng/ml	1 ng/ml	38
QC 50 & 5	50 ng/ml	5 ng/ml	37
QC 100 & 10	100 ng/ml	10 ng/ml	35
QC 600 & 60	600 ng/m	60 ng/ml	40
Agient biodiesel samples			
Biodiesel	-	-	10
Biodiesel + 50 & 5 ng/g	50 ng/g	5 ng/g	5
Biodiesel + 100 & 10 ng/g	100 ng/g	10 ng/g	5
Biodiesel + 600 & 60 ng/g	600 ng/g	60 ng/g	5

[a] Concentration of QC samples is given as ng per volume. Concentration of standard additions to samples is given as ng per gram of undiluted fuel.

[b] Elements of the large calibration range (0-100 ng/g): Li, Co, As, Sr, Mo, Pd, Ce, W and Pt.

[c] Elements of the small calibration range (0-1000 ng/g): B, Na, Mg, Al, Si, P, K, Ca Ti, V, Cr, Mn, Fe, Ni, Cu, Zn, Cd, Sn, Sb, Ba and Pb.

Table F.2 Overview of performed measurements in the validation of the xylene method for jet fuels, with the spray chamber temperature set to -5 °C

Sample type	Concentration of standard addition[a]		Number of measurements
	Elements of the large calibration range[b]	Elements of the small calibration range[c]	
Validation blank samples	-	-	24
Quality control samples			
QC 10 & 1	10 ng/ml	1 ng/ml	42
QC 50 & 5	50 ng/ml	5 ng/ml	42
QC 100 & 10	100 ng/ml	10 ng/ml	42
QC 600 & 60	600 ng/m	60 ng/ml	40
Jetfuel 1 samples:			
Jetfuel 1a	-	-	8
Jetfuel 1a + 50 & 5 ng/g	50 ng/g	5 ng/g	8
Jetfuel 1a + 100 & 10 ng/g	100 ng/g	10 ng/g	8
Jetfuel 1a + 600 & 60 ng/g	600 ng/g	60 ng/g	8
Jetfuel 1b	-	-	7
Jetfuel 1b + 50 & 5 ng/g	50 ng/g	5 ng/g	8
Jetfuel 1b + 100 & 10 ng/g	100 ng/g	10 ng/g	7
Jetfuel 1b + 600 & 60 ng/g	600 ng/g	60 ng/g	8
Jetfuel 1c	-	-	7
Jetfuel 1c + 50 & 5 ng/g	50 ng/g	5 ng/g	8
Jetfuel 1c + 100 & 10 ng/g	100 ng/g	10 ng/g	8
Jetfuel 1c + 600 & 60 ng/g	600 ng/g	60 ng/g	7
Jetfuel 2 samples			
Jetfuel 2a	-	-	7
Jetfuel 2a + 50 & 5 ng/g	50 ng/g	5 ng/g	7
Jetfuel 2a + 100 & 10 ng/g	100 ng/g	10 ng/g	7
Jetfuel 2a + 600 & 60 ng/g	600 ng/g	60 ng/g	7
Jetfuel 2b	-	-	8
Jetfuel 2b + 50 & 5 ng/g	50 ng/g	5 ng/g	8
Jetfuel 2b + 100 & 10 ng/g	100 ng/g	10 ng/g	8
Jetfuel 2b + 600 & 60 ng/g	600 ng/g	60 ng/g	8

[a]Concentration of QC samples is given as ng per volume. Concentration of standard additions to samples is given as ng per gram of undiluted fuel.
[b]Elements of the large calibration range (0-100 ng/g): Li, Co, As, Sr, Mo, Pd, Ce, W and Pt.
[c]Elements of the small calibration range (0-1000 ng/g): B, Na, Mg, Al, Si, P, K, Ca Ti, V, Cr, Mn, Fe, Ni, Cu, Zn, Cd, Sn, Sb, Ba and Pb.

Table F.3 Overview of performed measurements in the validation of Asolv method with the spray chamber temperature set to +5 °C

Sample type	Concentration of standard addition[a]		Number of measurements
	Elements of the large calibration range[b]	Elements of the small calibration range[c]	
Validation blank samples			12
Quality control samples			
QC 10 & 1	10 ng/ml	1 ng/ml	23
QC 50 & 5	50 ng/ml	5 ng/ml	25
QC 100 & 10	100 ng/ml	10 ng/ml	25
QC 600 & 60	600 ng/m	60 ng/ml	25
Gasoline samples Gasoline	-	-	4
Gasoline + 50 & 5 ng/g	50 ng/g	5 ng/g	5
Gasoline + 100 & 10 ng/g	100 ng/g	10 ng/g	4
Gasoline + 600 & 60 ng/g	600 ng/g	60 ng/g	6
Jet fuel 1 samples Jet fuel 1b	-	-	
Jet fuel 1b + 50 & 5 ng/g	50 ng/g	5 ng/g	
Jet fuel 1b + 100 & 10 ng/g	100 ng/g	10 ng/g	
Jet fule 1b + 600 & 60 ng/g	600 ng/g	60 ng/g	

[a] Concentration of QC samples is given as ng per volume. Concentration of standard additions to samples is given as ng per gram of undiluted fuel.

[b] Elements of the large calibration range (0-100 ng/g): Li, Co, As, Sr, Mo, Pd, Ce, W and Pt.

[c] Elements of the small calibration range (0-1000 ng/g): B, Na, Mg, Al, Si, P, K, Ca Ti, V, Cr, Mn, Fe, Ni, Cu, Zn, Cd, Sn, Sb, Ba and Pb.

Appendix G

Elemental composition of the sample matrices

Table G.1 Measured elemental composition of unspiked Diesel 1 samples used in the validation

Isotope	Gasmode	Diesel fuel 1a (N=10)				Diesel fuel 1b (N=9)			
		$\bar{c}$ (ng /g)	Std	RSD%	r	$\bar{c}$ (ng/g)	Std	RSD%	r
^{7}Li	Nogas	−1.3	1.9	−145.1	6.0	−1.4	1.8	−129.1	6.0
^{10}B	Nogas	495.2	467.5	94.4	1495.6	625.8	448.2	71.6	1461.5
^{11}B	Nogas	529.7	479.3	90.5	1533.4	679.0	470.9	69.4	1535.8
^{11}B	He	796.4	731.3	91.8	2339.5	1110.0	883.4	79.6	2881.0
^{11}B	H_2	348.6	349.1	100.1	1116.7	482.6	363.1	75.2	1184.1
^{23}Na	Nogas	−72.8	112.4	−154.4	359.6	−114.2	105.7	−92.5	344.6
^{23}Na	He	−56.7	110.7	−195.2	354.3	−96.6	103.3	−107.0	337.0
^{23}Na	HEHe	−51.1	107.6	−210.5	344.4	−86.9	97.1	−111.6	316.5
^{24}Mg	H_2	8.9	6.6	74.3	21.1	6.0	7.8	128.4	25.3
^{27}Al	HEHe	−2.0	2.6	−127.7	8.2	−3.0	2.5	−82.7	8.2
^{28}Si	H_2	28.2	39.1	138.5	125.2	43.4	36.9	85.0	120.3
^{31}P	Nogas	405.0	230.1	56.8	736.2	520.0	253.7	48.8	827.5
^{31}P	HEHe	27.8	7.3	26.1	23.2	11.9	7.4	62.1	24.1
^{39}K	HEHe	13.8	55.5	402.4	177.6	63.3	73.4	116.0	239.3
^{39}K	H_2	−23.5	43.9	−186.9	140.5	−5.2	59.8	−1143.5	194.9
^{40}Ca	H_2	61.4	58.5	95.2	187.1	16.1	60.3	375.7	196.8
^{47}Ti	H_2	3.3	7.4	220.8	23.6	3.1	8.4	268.3	27.4
^{51}V	HEHe	−0.2	0.6	−360.3	1.8	−0.3	0.5	−151.0	1.6
^{52}Cr	HEHe	0.9	1.6	166.6	5.0	1.3	1.8	133.6	5.7
^{55}Mn	HEHe	1.3	2.8	215.4	8.8	−2.8	2.2	−77.7	7.2
^{56}Fe	He	15.2	7.3	47.6	23.2	15.8	8.8	55.7	28.6
^{59}Co	He	−2.7	2.4	−90.9	7.8	−3.0	2.6	−87.4	8.5
^{59}Co	H_2	−1.9	1.7	−91.5	5.6	−2.2	1.9	−84.6	6.2
^{60}Ni	HEHe	−0.5	3.0	−600.2	9.6	−3.9	2.7	−69.6	8.8
^{63}Cu	HEHe	6.1	4.6	75.1	14.7	−2.7	4.3	−160.0	13.9
^{66}Zn	H_2	12.7	2.9	22.7	9.2	−1.6	3.2	−201.2	10.4
^{75}As	He	0.2	0.3	161.1	0.9	0.1	0.1	145.8	0.4
^{75}As	HEHe	0.1	0.2	168.2	0.7	0.1	0.1	133.7	0.4
^{75}As	H_2	0.1	0.2	168.7	0.7	0.1	0.1	187.1	0.4
^{88}Sr	H_2	0.3	0.2	90.5	0.8	−0.2	0.4	−148.5	1.2
^{95}Mo	HEHe	1.2	0.8	66.6	2.6	1.6	1.2	72.2	3.8
^{105}Pd	He	0.0	0.1	385.4	0.3	−0.0	0.1	−1402.9	0.4
^{114}Cd	Nogas	1.2	1.8	157.5	5.9	−2.9	2.2	−75.9	7.2
^{118}Sn	Nogas	0.4	1.4	308.9	4.3	0.7	1.5	223.0	4.8
^{118}Sn	HEHe	0.1	1.1	1128.1	3.5	0.3	1.3	459.6	4.2
^{121}Sb	HEHe	0.0	0.1	599.9	0.3	−0.0	0.1	−245.3	0.4
^{121}Sb	H_2	−0.0	0.1	−6776.2	0.3	−0.0	0.1	−186.1	0.3
^{137}Ba	Nogas	1.2	1.2	97.3	3.7	−1.0	1.0	−103.8	3.3
^{140}Ce	He	0.1	0.3	248.8	0.9	−0.2	0.2	−117.4	0.6
^{140}Ce	HEHe	0.1	0.3	248.5	0.8	−0.1	0.2	−104.4	0.5
^{140}Ce	H_2	0.0	0.2	471.4	0.7	−0.2	0.2	−110.9	0.6
^{182}W	Nogas	0.0	0.0	105.8	0.1	0.1	0.1	123.2	0.3
^{182}W	HEHe	0.0	0.0	253.1	0.1	0.0	0.1	274.4	0.2
^{195}Pt	Nogas	0.0	0.1	257.0	0.4	0.1	0.2	233.3	0.7
$^{206-208}$Pb	Nogas	2.7	4.5	165.5	14.5	−0.5	4.2	−915.7	13.7

Table G.2 Measured elemental composition of unspiked Diesel 2 samples used in the validation

Isotope	Gasmode	Diesel fuel 2a (N=9)				Diesel fuel 1b (N=9)			
		$\bar{c}$ (ng /g)	Std	RSD%	r	$\bar{c}$ (ng/g)	Std	RSD%	r
^{7}Li	Nogas	0.9	2.4	276.4	7.4	0.2	2.5	1026.5	7.9
^{10}B	Nogas	309.1	380.5	123.1	1172.5	332.9	319.5	96.0	994.5
^{11}B	Nogas	341.9	448.8	131.3	1382.8	361.6	368.9	102.0	1148.2
^{11}B	He	825.9	649.1	78.6	2000.1	640.0	458.1	71.6	1425.8
^{11}B	H_2	223.9	358.7	160.2	1105.4	297.1	341.8	115.0	1063.9
^{23}Na	Nogas	88.6	153.7	173.4	473.5	137.1	152.1	111.0	473.6
^{23}Na	He	88.0	145.9	165.8	449.6	142.6	141.7	99.4	441.1
^{23}Na	HEHe	84.5	150.0	177.5	462.3	144.4	151.9	105.1	472.8
^{24}Mg	H_2	15.9	14.5	91.0	44.6	13.6	11.6	85.1	36.1
^{27}Al	HEHe	3.1	4.5	146.6	13.9	3.5	5.0	142.7	15.5
^{28}Si	H_2	29.8	35.7	119.7	110.0	23.3	38.5	165.4	119.8
^{31}P	Nogas	392.5	225.4	57.4	694.5	306.1	201.0	65.7	625.6
^{31}P	HEHe	16.1	10.4	64.7	32.0	6.4	7.7	120.5	23.9
^{39}K	HEHe	122.8	135.0	110.0	416.1	135.8	139.5	102.8	434.3
^{39}K	H_2	69.2	120.3	174.0	370.8	97.2	141.6	145.7	440.9
^{40}Ca	H_2	26.8	42.0	156.7	129.3	52.8	41.1	77.9	128.1
^{47}Ti	H_2	2.7	10.5	382.7	32.3	2.9	7.6	258.8	23.7
^{51}V	HEHe	0.6	2.1	355.6	6.4	0.2	0.7	302.6	2.3
^{52}Cr	HEHe	1.5	2.0	131.0	6.2	1.0	1.7	176.5	5.2
^{55}Mn	HEHe	6.1	9.0	148.1	27.7	6.4	9.0	139.2	27.9
^{56}Fe	He	2.6	4.8	184.8	14.8	4.1	6.3	155.1	19.7
^{59}Co	He	−1.4	2.6	−182.4	8.1	−1.3	3.0	−225.2	9.3
^{59}Co	H_2	−1.1	1.9	−162.3	5.8	−1.0	2.1	−209.7	6.5
^{60}Ni	HEHe	5.2	7.4	142.3	22.9	6.2	8.9	142.8	27.7
^{63}Cu	HEHe	2.6	8.1	317.2	25.1	4.3	9.7	229.1	30.3
^{66}Zn	H_2	6.0	4.9	81.4	15.0	7.1	6.1	86.6	19.1
^{75}As	He	0.2	0.3	136.7	0.8	0.1	0.2	165.9	0.5
^{75}As	HEHe	0.2	0.3	137.4	0.8	0.1	0.1	159.2	0.4
^{75}As	H_2	0.1	0.2	142.9	0.6	0.1	0.1	198.6	0.4
^{88}Sr	H_2	0.4	0.6	149.1	1.8	0.5	0.6	117.3	1.8
^{95}Mo	HEHe	0.6	1.7	282.5	5.3	0.2	0.4	197.8	1.2
^{105}Pd	He	−0.0	0.1	−284.4	0.3	−0.1	0.1	−184.8	0.3
^{114}Cd	Nogas	6.6	8.6	129.5	26.5	7.2	9.3	129.6	29.0
^{118}Sn	Nogas	1.0	2.6	261.0	7.9	0.2	0.8	392.3	2.4
^{118}Sn	HEHe	0.5	2.1	425.9	6.6	−0.1	0.8	−1393.8	2.5
^{121}Sb	HEHe	0.4	0.9	220.3	2.9	0.2	0.2	135.0	0.7
^{121}Sb	H_2	0.3	0.7	200.7	2.0	0.1	0.2	165.4	0.6
^{137}Ba	Nogas	2.0	2.5	124.9	7.7	1.6	2.4	149.6	7.6
^{140}Ce	He	0.5	0.9	173.2	2.7	0.7	0.9	130.2	2.7
^{140}Ce	HEHe	0.4	0.8	190.0	2.5	0.6	0.8	134.4	2.4
^{140}Ce	H_2	0.4	0.7	193.9	2.2	0.5	0.7	136.0	2.2
^{182}W	Nogas	0.2	0.3	140.4	0.8	0.1	0.1	218.7	0.5
^{182}W	HEHe	0.1	0.2	161.4	0.7	0.0	0.1	239.3	0.3
^{195}Pt	Nogas	0.1	0.1	82.0	0.3	0.0	0.1	194.2	0.2
$^{206-208}$Pb	Nogas	6.2	6.3	100.9	19.4	4.7	6.9	146.9	21.6

Table G.3 Measured elemental composition of unspiked Jetfuel 1 samples used in the validation

Isotope	Gasmode	Jet fuel 1a (N=?)				Jet fuel 1b (N=?)			
		$\bar{c}$ (ng /g)	Std	RSD%	r	$\bar{c}$ (ng/g)	Std	RSD%	r
^{7}Li	Nogas	0.6	0.9	160.5	3.2	0.4	1.2	313.5	4.2
^{10}B	Nogas	55.3	42.8	77.3	143.0	72.8	26.5	36.4	91.8
^{11}B	Nogas	64.9	34.8	53.6	116.4	71.4	27.3	38.3	94.5
^{11}B	He	126.4	67.8	53.6	226.6	104.4	75.8	72.6	262.2
^{11}B	H_2	48.8	21.2	43.6	71.1	63.9	19.2	30.1	66.6
^{23}Na	Nogas	−5.3	22.5	−424.4	75.1	76.9	48.4	62.9	167.5
^{23}Na	He	−0.9	19.5	−2160.3	65.4	85.4	45.4	53.1	156.9
^{23}Na	HEHe	−3.3	22.9	−683.9	76.5	82.3	44.2	53.7	152.9
^{24}Mg	H_2	4.4	1.8	40.2	5.9	6.4	2.2	34.6	7.7
^{27}Al	HEHe	0.2	1.1	437.3	3.6	0.1	1.4	1455.0	5.0
^{28}Si	H_2	38.3	48.9	127.5	163.4	1850.7	59.5	3.2	205.8
^{31}P	Nogas	127.5	37.5	29.4	125.4	138.7	39.4	28.4	136.3
^{31}P	HEHe	3.8	5.2	134.1	17.3	37.0	2.7	7.4	9.5
^{39}K	HEHe	42.7	25.1	58.8	83.9	79.0	41.6	52.6	143.9
^{39}K	H_2	25.3	27.1	107.1	90.5	57.8	45.2	78.2	156.3
^{40}Ca	H_2	3.7	18.4	495.2	61.5	10.1	11.3	111.5	39.1
^{47}Ti	H_2	1.4	3.0	216.3	9.9	2.8	4.6	166.8	15.9
^{51}V	HEHe	0.1	0.2	180.5	0.6	0.2	0.3	166.7	0.9
^{52}Cr	HEHe	0.4	0.5	142.2	1.7	0.6	0.5	95.9	1.9
^{55}Mn	HEHe	1.0	0.6	63.2	2.1	1.8	2.0	111.4	6.9
^{56}Fe	He	3.9	7.7	197.3	25.9	3.0	5.2	174.5	17.9
^{59}Co	He	−0.4	0.5	−121.0	1.6	−0.2	0.6	−290.2	2.2
^{59}Co	H_2	−0.3	0.3	−117.3	1.1	−0.1	0.4	−477.5	1.5
^{60}Ni	HEHe	0.8	0.6	76.0	2.2	0.7	1.2	165.1	4.2
^{63}Cu	HEHe	1.3	0.8	62.9	2.8	1.6	1.7	107.5	6.0
^{66}Zn	H_2	1.8	1.2	70.0	4.1	1.8	1.6	87.2	5.4
^{75}As	He	0.3	0.3	83.9	0.9	2.1	0.6	30.9	2.2
^{75}As	HEHe	0.3	0.2	74.6	0.7	2.0	0.6	31.0	2.2
^{75}As	H_2	0.3	0.2	69.9	0.7	2.0	0.7	32.9	2.3
^{88}Sr	H_2	0.1	0.1	74.5	0.3	0.2	0.2	74.9	0.5
^{95}Mo	HEHe	0.1	0.1	149.4	0.4	0.2	0.2	96.0	0.7
^{105}Pd	He	0.0	0.1	313.2	0.3	0.1	0.1	75.4	0.3
^{114}Cd	Nogas	1.3	0.7	56.7	2.4	1.9	2.3	116.5	7.8
^{118}Sn	Nogas	−0.5	1.6	−304.2	5.2	−0.4	2.1	−523.5	7.4
^{118}Sn	HEHe	−0.4	1.2	−290.2	4.0	−0.4	1.4	−340.1	4.8
^{121}Sb	HEHe	0.1	0.0	57.8	0.1	0.2	0.3	164.0	0.9
^{121}Sb	H_2	0.1	0.0	72.7	0.1	0.0	0.0	77.3	0.1
^{137}Ba	Nogas	0.8	0.7	95.1	2.4	1.5	1.8	117.5	6.1
^{140}Ce	He	0.1	0.1	88.2	0.3	0.1	0.1	87.0	0.4
^{140}Ce	HEHe	0.1	0.1	90.9	0.2	0.1	0.1	86.3	0.4
^{140}Ce	H_2	0.1	0.0	71.6	0.1	0.1	0.1	99.9	0.3
^{182}W	Nogas	0.1	0.1	101.8	0.4	0.2	0.2	102.3	0.7
^{182}W	HEHe	0.1	0.1	73.0	0.2	0.1	0.1	108.8	0.4
^{195}Pt	Nogas	0.0	0.2	2712.7	0.7	0.1	0.3	340.9	1.0
$^{206-208}$Pb	Nogas	2.6	2.7	104.6	9.0	5.8	4.7	80.5	16.1

Table G.3 Continued...

Isotope	Gasmode	Jet fuel 1c (N=?)			
		$\bar{c}$ (ng /g)	Std	RSD%	r
^{7}Li	Nogas	0.5	1.1	240.8	3.9
^{10}B	Nogas	75.5	23.5	31.2	81.4
^{11}B	Nogas	82.5	11.7	14.2	40.5
^{11}B	He	120.8	52.3	43.3	181.0
^{11}B	H_2	78.5	15.1	19.3	52.3
^{23}Na	Nogas	19.1	22.9	119.7	79.3
^{23}Na	He	26.4	24.9	94.2	86.2
^{23}Na	HEHe	24.8	21.2	85.2	73.3
^{24}Mg	H_2	6.9	1.7	24.4	5.8
^{27}Al	HEHe	−0.5	1.3	−249.4	4.4
^{28}Si	H_2	987.8	37.5	3.8	129.9
^{31}P	Nogas	123.4	40.2	32.6	139.2
^{31}P	HEHe	5.3	3.2	61.2	11.1
^{39}K	HEHe	45.6	45.8	100.6	158.7
^{39}K	H_2	27.3	48.0	175.6	166.1
^{40}Ca	H_2	33.9	28.0	82.8	97.0
^{47}Ti	H_2	2.2	4.2	192.4	14.5
^{51}V	HEHe	0.2	0.2	88.5	0.7
^{52}Cr	HEHe	0.4	0.7	175.0	2.4
^{55}Mn	HEHe	1.6	0.8	47.1	2.6
^{56}Fe	He	2.6	5.2	198.9	17.8
^{59}Co	He	−0.2	0.5	−212.7	1.6
^{59}Co	H_2	−0.1	0.3	−434.5	1.2
^{60}Ni	HEHe	0.5	0.5	98.2	1.7
^{63}Cu	HEHe	1.4	0.5	37.4	1.8
^{66}Zn	H_2	20.1	3.0	14.9	10.4
^{75}As	He	0.8	0.2	27.0	0.8
^{75}As	HEHe	0.8	0.2	24.8	0.7
^{75}As	H_2	0.8	0.2	22.7	0.7
^{88}Sr	H_2	0.1	0.1	87.4	0.4
^{95}Mo	HEHe	0.2	0.2	95.1	0.7
^{105}Pd	He	0.1	0.1	58.9	0.2
^{114}Cd	Nogas	1.3	0.9	70.4	3.2
^{118}Sn	Nogas	−0.3	0.8	−232.7	2.7
^{118}Sn	HEHe	−0.5	1.1	−232.4	3.8
^{121}Sb	HEHe	0.2	0.2	133.5	0.8
^{121}Sb	H_2	0.1	0.0	82.3	0.2
^{137}Ba	Nogas	1.4	1.6	116.0	5.5
^{140}Ce	He	0.1	0.1	57.0	0.2
^{140}Ce	HEHe	0.1	0.1	63.2	0.2
^{140}Ce	H_2	0.1	0.0	64.3	0.2
^{182}W	Nogas	0.1	0.2	120.9	0.5
^{182}W	HEHe	0.0	0.0	74.2	0.1
^{195}Pt	Nogas	0.0	0.2	8369.2	0.7
$^{206-208}$Pb	Nogas	6.7	4.1	61.9	14.3

Table G.4 Measured elemental composition of unspiked Jetfuel 1 samples used in the validation

Isotope	Gasmode	Jet fuel 2a (N=?)				Jet fuel 2b (N=?)			
		$\bar{c}$ (ng /g)	Std	RSD%	r	$\bar{c}$ (ng/g)	Std	RSD%	r
^{7}Li	Nogas	0.8	1.7	227.3	6.0	0.8	1.7	217.7	5.6
^{10}B	Nogas	72.0	70.6	98.1	244.3	84.8	83.1	98.0	278.1
^{11}B	Nogas	95.8	43.5	45.4	150.7	103.3	63.0	60.9	210.5
^{11}B	He	176.4	91.3	51.8	316.0	202.5	138.3	68.3	462.5
^{11}B	H_2	80.4	56.4	70.2	195.1	85.5	64.6	75.5	216.0
^{23}Na	Nogas	−7.1	44.2	−625.5	152.8	34.1	80.3	235.4	268.6
^{23}Na	He	−1.9	49.5	−2642.1	171.3	37.5	84.7	226.0	283.1
^{23}Na	HEHe	−8.6	43.7	−509.1	151.4	32.5	76.0	233.7	254.2
^{24}Mg	H_2	8.7	7.0	79.9	24.2	9.7	5.6	57.8	18.7
^{27}Al	HEHe	0.5	3.7	695.8	12.9	0.3	2.4	958.0	8.1
^{28}Si	H_2	1297.6	189.0	14.6	653.9	55.6	70.5	126.9	235.7
^{31}P	Nogas	228.6	78.7	34.4	272.3	209.0	79.8	38.2	266.9
^{31}P	HEHe	3.8	8.9	235.2	30.9	7.6	9.0	118.6	30.2
^{39}K	HEHe	81.6	58.4	71.6	202.0	97.3	69.1	71.0	231.1
^{39}K	H_2	50.3	61.1	121.3	211.3	68.6	58.7	85.5	196.3
^{40}Ca	H_2	12.7	59.1	464.8	204.4	7.7	11.5	150.2	38.6
^{47}Ti	H_2	3.0	5.7	188.5	19.8	0.9	4.8	512.1	16.2
^{51}V	HEHe	0.5	1.2	230.0	4.2	0.2	0.4	209.7	1.4
^{52}Cr	HEHe	0.5	0.7	141.6	2.5	0.6	1.3	226.4	4.3
^{55}Mn	HEHe	1.5	2.7	172.3	9.2	1.1	2.5	228.8	8.4
^{56}Fe	He	1.4	3.0	210.9	10.4	0.8	1.7	213.8	5.8
^{59}Co	He	−0.5	1.4	−289.3	4.9	−0.7	1.0	−145.7	3.3
^{59}Co	H_2	−0.3	1.1	−404.0	3.8	−0.5	0.7	−146.7	2.4
^{60}Ni	HEHe	2.2	3.6	159.4	12.3	1.0	2.6	244.1	8.5
^{63}Cu	HEHe	2.4	3.0	121.7	10.2	1.3	1.5	114.9	5.1
^{66}Zn	H_2	2.6	5.5	210.0	19.0	4.7	2.5	53.4	8.4
^{75}As	He	0.4	0.4	111.3	1.5	0.2	0.3	115.7	0.9
^{75}As	HEHe	0.4	0.4	104.5	1.3	0.2	0.2	101.2	0.8
^{75}As	H_2	0.4	0.4	114.7	1.5	0.2	0.2	77.5	0.6
^{88}Sr	H_2	0.1	0.2	186.4	0.8	0.2	0.2	95.0	0.6
^{95}Mo	HEHe	0.0	0.2	454.7	0.7	0.1	0.2	436.6	0.8
^{105}Pd	He	0.1	0.1	149.3	0.3	0.0	0.1	305.1	0.3
^{114}Cd	Nogas	2.3	3.7	164.7	12.9	2.2	3.7	168.0	12.4
^{118}Sn	Nogas	0.6	2.1	334.2	7.3	0.0	1.5	3652.3	4.9
^{118}Sn	HEHe	−0.3	1.0	−350.2	3.4	0.3	1.3	490.4	4.4
^{121}Sb	HEHe	0.2	0.1	75.7	0.4	0.1	0.1	99.5	0.3
^{121}Sb	H_2	0.1	0.1	72.4	0.4	0.1	0.1	97.5	0.2
^{137}Ba	Nogas	0.8	1.3	153.3	4.5	1.2	1.3	108.3	4.3
^{140}Ce	He	0.2	0.2	116.4	0.8	0.1	0.1	101.5	0.4
^{140}Ce	HEHe	0.2	0.2	112.1	0.6	0.1	0.1	96.1	0.3
^{140}Ce	H_2	0.1	0.1	113.2	0.5	0.1	0.1	113.1	0.3
^{182}W	Nogas	0.3	0.3	106.8	1.0	0.3	0.4	161.3	1.4
^{182}W	HEHe	0.1	0.1	98.4	0.5	0.2	0.3	159.0	1.0
^{195}Pt	Nogas	−0.0	0.4	−1272.5	1.2	0.1	0.4	709.8	1.4
$^{206-208}$Pb	Nogas	6.4	9.3	146.3	32.2	3.0	3.8	124.4	12.6

Appendix H

Statistical measures of spiked samples

Table H.1 Jet fuel 1 batch average validation results, measured with the xylene method

		Conc. RSD%			Spike recovery%		
		Spike conc. ($\mu g/l$)			Spike conc. ($\mu g/l$)		
Isotope	**Gas mode**	50&**5**	100&**10**	600&**60**	50&**5**	100&**10**	600&**60**
^{7}Li	Nogas	**39.8**	**22.9**	**17.1**	**63.3**	**68.6**	**84.3**
^{10}B	Nogas	60.9	44.2	29.6	20.2	25.7	51.4
^{11}B	Nogas	41.1	35.3	29.5	24.6	23.4	49.5
^{11}B	He	73.6	71.6	31.7	−52.5	−2.22	46.3
^{11}B	H_2	44.4	38.3	30.2	30.0	29.5	55.3
^{23}Na	Nogas	70.2	37.3	23.6	67.1	79.5	87.9
^{23}Na	He	66.3	37.4	23.8	68.0	78.3	90.4
^{23}Na	HEHe	69.0	34.9	22.8	58.4	73.9	87.4
^{24}Mg	H_2	5.97	5.71	4.53	82.1	86.7	95.6
^{27}Al	HEHe	11.3	7.13	4.35	87.0	91.1	98.2
^{28}Si	H_2	19.3	10.3	4.03	41.2	85.3	92.5
^{31}P	Nogas	26.8	23.1	6.83	81.0	91.7	100.0
^{31}P	HEHe	9.63	4.97	4.46	105.0	105.0	102.0
^{39}K	HEHe	67.5	39.7	20.0	60.8	77.7	78.9
^{39}K	H_2	76.4	51.5	20.1	78.9	78.7	78.7
^{40}Ca	H_2	46.6	17.4	4.89	101.0	94.4	100.0
^{47}Ti	H_2	11.2	6.46	4.22	95.4	98.8	96.5
^{51}V	HEHe	9.32	5.56	4.12	84.7	91.4	99.0
^{52}Cr	HEHe	2.82	2.10	2.24	107.0	107.0	103.0
^{55}Mn	HEHe	3.83	2.24	2.45	94.8	98.3	100.0
^{56}Fe	He	3.91	3.80	2.65	96.0	101.0	100.0
^{59}Co	He	**19.6**	**7.64**	**3.23**	**81.7**	**90.2**	**97.2**
^{59}Co	H_2	**12.9**	**5.80**	**3.05**	**83.2**	**89.0**	**94.9**
^{60}Ni	HEHe	6.09	3.46	3.17	82.7	89.9	97.2
^{63}Cu	HEHe	4.05	4.39	1.79	96.5	100.0	104.0
^{66}Zn	H_2	3.58	2.61	3.07	86.0	92.5	95.6
^{75}As	He	**5.46**	**3.84**	**1.98**	**99.8**	**101.0**	**99.7**
^{75}As	HEHe	**5.46**	**3.10**	**2.25**	**100.0**	**101.0**	**99.2**
^{75}As	H_2	**6.43**	**4.32**	**3.93**	**94.4**	**95.5**	**93.9**
^{88}Sr	H_2	**5.38**	**4.19**	**3.03**	**93.5**	**93.7**	**94.6**
^{95}Mo	HEHe	11.0	5.19	2.52	81.7	91.0	97.7
^{105}Pd	He	**5.45**	**5.21**	**2.90**	**99.7**	**100.0**	**98.5**
^{114}Cd	Nogas	10.1	4.17	3.64	80.5	87.4	96.0
^{118}Sn	Nogas	6.58	3.71	3.04	89.5	92.8	95.7
^{118}Sn	HEHe	6.66	5.06	4.75	84.5	87.5	88.7
^{121}Sb	HEHe	3.35	2.46	2.08	96.1	98.6	97.2
^{121}Sb	H_2	6.19	4.70	1.87	95.8	96.7	99.9
^{137}Ba	Nogas	5.39	4.42	3.30	89.4	91.2	89.7
^{140}Ce	He	**4.83**	**4.34**	**3.34**	**93.3**	**93.6**	**91.7**
^{140}Ce	HEHe	**4.22**	**2.83**	**2.56**	**93.2**	**93.8**	**92.4**
^{140}Ce	H_2	**5.16**	**5.93**	**4.54**	**91.5**	**92.0**	**88.2**
^{182}W	Nogas	**9.30**	**8.60**	**5.41**	**88.8**	**90.2**	**89.0**
^{182}W	HEHe	**6.05**	**4.47**	**4.40**	**91.6**	**94.0**	**93.9**
^{195}Pt	Nogas	**9.08**	**5.58**	**3.89**	**93.1**	**93.0**	**89.9**
Pb*	Nogas	13.2	11.6	4.88	79.6	84.6	88.9

* The concentration of Pb was obtained by using sum of signals from ^{206}Pb, ^{207}Pb and ^{208}Pb.

Table H.2 Jet fuel 2 batch average validation results measured with the xylene method

		Conc. RSD%			Spike recovery%		
		Spike conc. ($\mu g/l$)			Spike conc. ($\mu g/l$)		
Isotope	**Gas mode**	50&**5**	100&**10**	600&**60**	50&**5**	100&**10**	600&**60**
^{7}Li	Nogas	**43.7**	**25.7**	**15.4**	**70.3**	**70.7**	**76.3**
^{10}B	Nogas	93.8	102.0	58.9	−4.48	13.5	18.6
^{11}B	Nogas	49.8	61.8	42.8	−11.0	5.81	17.6
^{11}B	He	86.9	71.5	42.1	−89.9	−6.06	12.3
^{11}B	H_2	58.9	76.5	42.1	−6.66	12.2	22.1
^{23}Na	Nogas	107.0	71.4	19.6	90.8	99.9	85.4
^{23}Na	He	110.0	72.9	19.5	86.7	96.5	85.6
^{23}Na	HEHe	115.0	76.0	19.0	88.7	102.0	87.1
^{24}Mg	H_2	14.2	6.20	3.87	74.3	76.9	88.8
^{27}Al	HEHe	14.0	7.13	4.32	84.7	85.9	90.9
^{28}Si	H_2	48.8	25.6	10.3	89.6	−573.0	−17.1
^{31}P	Nogas	39.5	31.1	12.3	7.13	30.7	81.5
^{31}P	HEHe	24.4	9.06	6.21	98.8	104.0	98.5
^{39}K	HEHe	57.9	55.6	38.4	167.0	154.0	101.0
^{39}K	H_2	67.9	61.3	38.4	175.0	157.0	102.0
^{40}Ca	H_2	61.6	32.6	4.48	92.2	111.0	96.1
^{47}Ti	H_2	22.8	10.1	5.18	96.8	98.8	96.7
^{51}V	HEHe	38.1	26.3	6.85	64.3	67.9	88.4
^{52}Cr	HEHe	8.66	3.23	2.00	110.0	106.0	101.0
^{55}Mn	HEHe	9.52	3.15	2.55	92.6	93.1	96.0
^{56}Fe	He	29.2	9.43	5.34	113.0	98.8	94.7
^{59}Co	He	**48.7**	**14.5**	**3.00**	**81.7**	**77.9**	**89.8**
^{59}Co	H_2	**30.1**	**10.4**	**1.57**	**79.4**	**78.8**	**90.3**
^{60}Ni	HEHe	12.5	4.87	3.12	78.0	80.1	91.7
^{63}Cu	HEHe	11.6	2.74	2.13	104.0	100.0	98.7
^{66}Zn	H_2	13.6	4.25	3.32	90.4	90.5	94.0
^{75}As	He	**12.7**	**5.66**	**2.01**	**100.0**	**97.6**	**97.3**
^{75}As	HEHe	**12.9**	**6.95**	**2.80**	**101.0**	**99.1**	**97.9**
^{75}As	H_2	**12.0**	**5.58**	**3.58**	**99.9**	**98.7**	**98.4**
^{88}Sr	H_2	**17.4**	**8.65**	**5.86**	**88.6**	**92.2**	**92.4**
^{95}Mo	HEHe	31.1	17.0	5.67	61.6	72.3	92.5
^{105}Pd	He	**9.76**	**1.82**	**2.94**	**101.0**	**98.4**	**94.8**
^{114}Cd	Nogas	18.2	2.59	3.80	88.7	88.1	90.3
^{118}Sn	Nogas	26.4	7.46	5.37	95.4	91.2	93.7
^{118}Sn	HEHe	14.9	8.86	8.39	85.2	86.7	88.1
^{121}Sb	HEHe	13.6	6.06	4.76	93.8	95.9	96.1
^{121}Sb	H_2	13.8	8.04	5.16	92.3	94.8	96.2
^{137}Ba	Nogas	19.2	12.3	7.07	85.2	88.5	91.0
^{140}Ce	He	**10.8**	**4.07**	**5.85**	**96.9**	**93.0**	**90.4**
^{140}Ce	HEHe	**11.3**	**4.13**	**6.58**	**95.0**	**94.3**	**90.7**
^{140}Ce	H_2	**12.6**	**3.24**	**5.53**	**97.5**	**95.8**	**92.8**
^{182}W	Nogas	**21.5**	**12.2**	**8.11**	**91.9**	**91.1**	**92.1**
^{182}W	HEHe	**14.9**	**11.2**	**7.81**	**88.7**	**92.3**	**93.0**
^{195}Pt	Nogas	**13.2**	**5.13**	**3.87**	**101.0**	**97.3**	**93.4**
Pb*	Nogas	17.9	11.6	7.78	82.7	86.8	91.1

* The concentration of Pb was obtained by using a sum of signals of ^{206}Pb, ^{207}Pb and ^{208}Pb.

Table H.3 Diesel 1 batch average validation results measured with the xylene method

		Conc. RSD%			Spike recovery%		
		Spike conc. ($\mu g/l$)			Spike conc. ($\mu g/l$)		
Isotope	**Gas mode**	50&**5**	100&**10**	600&**60**	50&**5**	100&**10**	600&**60**
^{7}Li	Nogas	**399.0**	**−407.0**	**32.6**	**21.4**	**24.6**	**46.7**
^{10}B	Nogas	172.0	146.0	60.7	−448.0	−133.0	57.1
^{11}B	Nogas	194.0	165.0	65.7	−546.0	−174.0	55.4
^{11}B	He	128.0	117.0	75.1	−754.0	−374.0	11.2
^{11}B	H_2	208.0	157.0	60.4	−327.0	−43.6	77.0
^{23}Na	Nogas	−145.0	472.0	55.3	25.3	49.4	62.8
^{23}Na	He	−184.0	255.0	57.9	19.2	42.9	61.7
^{23}Na	HEHe	−196.0	180.0	60.2	14.0	38.8	61.8
^{24}Mg	H_2	16.4	15.1	15.6	68.6	76.1	90.1
^{27}Al	HEHe	19.6	18.5	10.2	92.7	91.6	93.4
^{28}Si	H_2	29.5	23.7	12.6	110.0	98.4	98.7
^{31}P	Nogas	72.4	81.0	56.2	−348.0	−169.0	42.2
^{31}P	HEHe	21.7	20.5	23.1	102.0	99.9	99.9
^{39}K	HEHe	303.0	264.0	48.1	−28.3	−4.57	31.9
^{39}K	H_2	1340.0	302.0	42.8	45.9	35.2	42.5
^{40}Ca	H_2	51.0	34.8	19.8	78.2	91.3	101.0
^{47}Ti	H_2	38.9	25.3	14.2	88.6	95.5	99.3
^{51}V	HEHe	10.6	11.9	10.0	96.6	94.7	95.8
^{52}Cr	HEHe	6.30	4.88	6.02	109.0	108.0	101.0
^{55}Mn	HEHe	12.2	5.21	5.65	80.1	90.9	94.9
^{56}Fe	He	14.7	15.5	8.50	93.4	97.9	93.3
^{59}Co	He	**59.9**	**19.2**	**9.21**	**95.9**	**91.8**	**90.4**
^{59}Co	H_2	**33.5**	**13.2**	**7.05**	**93.9**	**91.7**	**93.8**
^{60}Ni	HEHe	10.6	8.88	8.12	81.9	87.1	91.3
^{63}Cu	HEHe	9.61	9.20	5.24	99.4	100.0	94.8
^{66}Zn	H_2	22.8	13.5	8.85	70.2	79.9	93.4
^{75}As	He	**27.0**	**21.5**	**16.4**	**89.0**	**93.1**	**94.3**
^{75}As	HEHe	**25.9**	**22.1**	**16.9**	**91.9**	**93.8**	**95.8**
^{75}As	H_2	**30.5**	**25.3**	**19.6**	**96.7**	**100.0**	**101.0**
^{88}Sr	H_2	**33.1**	**20.3**	**13.0**	**77.9**	**86.3**	**89.7**
^{95}Mo	HEHe	26.3	19.9	9.97	68.0	77.4	90.8
^{105}Pd	He	**6.94**	**4.08**	**6.78**	**104.0**	**102.0**	**96.9**
^{114}Cd	Nogas	18.9	10.2	9.30	66.4	80.5	89.1
^{118}Sn	Nogas	28.4	17.3	8.31	78.3	86.2	91.7
^{118}Sn	HEHe	29.6	19.3	8.71	79.1	86.3	93.4
^{121}Sb	HEHe	31.9	20.6	9.15	81.3	88.0	96.1
^{121}Sb	H_2	29.5	18.6	9.31	78.4	85.1	92.7
^{137}Ba	Nogas	35.4	19.8	6.82	73.7	83.6	89.7
^{140}Ce	He	**14.7**	**11.6**	**6.08**	**96.2**	**96.2**	**94.6**
^{140}Ce	HEHe	**14.8**	**13.5**	**6.24**	**97.1**	**97.7**	**96.5**
^{140}Ce	H_2	**14.4**	**13.0**	**8.26**	**103.0**	**105.0**	**102.0**
^{182}W	Nogas	**30.8**	**20.2**	**10.9**	**75.6**	**84.5**	**90.7**
^{182}W	HEHe	**26.2**	**19.2**	**12.2**	**77.9**	**86.5**	**93.0**
^{195}Pt	Nogas	**7.19**	**5.72**	**7.80**	**107.0**	**105.0**	**97.4**
Pb*	Nogas	33.2	18.1	10.8	66.8	80.8	90.6

* The concentration of Pb was obtained by using sum of signals from ^{206}Pb, ^{207}Pb and ^{208}Pb.

Table H.4 Diesel 2 batch average validation results measured with the xylene method

		Conc. RSD%			Spike recovery%		
		Spike conc. ($\mu g/l$)			Spike conc. ($\mu g/l$)		
Isotope	**Gas mode**	50&**5**	100&**10**	600&**60**	50&**5**	100&**10**	600&**60**
^{7}Li	Nogas	**65.5**	**37.4**	**12.9**	**40.2**	**52.8**	**66.2**
^{10}B	Nogas	163.0	164.0	114.0	−168.0	−133.0	−1.47
^{11}B	Nogas	198.0	224.0	129.0	−232.0	−175.0	−5.23
^{11}B	He	99.9	46.4	129.0	−462.0	−259.0	−60.1
^{11}B	H_2	215.0	232.0	98.1	−157.0	−116.0	15.6
^{23}Na	Nogas	138.0	75.4	31.9	68.9	32.7	62.3
^{23}Na	He	138.0	72.4	32.2	56.1	30.7	63.3
^{23}Na	HEHe	149.0	74.3	30.0	56.4	29.8	66.7
^{24}Mg	H_2	12.1	11.1	14.0	61.3	67.5	85.6
^{27}Al	HEHe	13.1	10.1	9.07	71.4	75.9	85.7
^{28}Si	H_2	36.8	24.5	9.60	103.0	102.0	97.0
^{31}P	Nogas	52.6	76.4	59.3	−152.0	−42.1	52.9
^{31}P	HEHe	18.2	24.8	23.6	100.0	104.0	98.7
^{39}K	HEHe	121.0	76.7	27.9	83.6	43.6	56.6
^{39}K	H_2	141.0	81.4	26.1	139.0	64.7	68.5
^{40}Ca	H_2	75.0	41.8	16.6	83.7	81.7	91.7
^{47}Ti	H_2	34.7	29.0	12.7	78.5	87.2	97.8
^{51}V	HEHe	33.4	17.5	6.20	45.8	53.5	85.1
^{52}Cr	HEHe	6.14	5.23	6.36	111.0	108.0	97.2
^{55}Mn	HEHe	7.62	5.56	6.57	74.9	82.0	89.1
^{56}Fe	He	10.1	7.42	9.55	93.4	95.0	89.7
^{59}Co	He	**38.6**	**14.6**	**8.86**	**78.5**	**78.4**	**84.2**
^{59}Co	H_2	**24.7**	**10.6**	**6.30**	**83.4**	**82.2**	**90.0**
^{60}Ni	HEHe	9.97	4.50	6.80	64.9	72.2	86.7
^{63}Cu	HEHe	10.2	6.47	4.90	101.0	101.0	94.7
^{66}Zn	H_2	7.33	8.33	8.80	74.9	84.8	94.8
^{75}As	He	**19.8**	**22.0**	**15.9**	**93.0**	**93.7**	**93.8**
^{75}As	HEHe	**19.3**	**22.0**	**16.0**	**93.6**	**96.0**	**96.5**
^{75}As	H_2	**21.3**	**25.4**	**17.6**	**98.9**	**101.0**	**104.0**
^{88}Sr	H_2	**23.6**	**21.5**	**10.8**	**74.5**	**78.7**	**88.6**
^{95}Mo	HEHe	17.1	11.6	3.71	45.6	59.4	88.8
^{105}Pd	He	**5.74**	**3.58**	**5.93**	**100.0**	**98.4**	**89.1**
^{114}Cd	Nogas	10.6	6.79	10.4	62.0	76.8	83.7
^{118}Sn	Nogas	22.6	15.4	6.94	78.8	84.3	88.4
^{118}Sn	HEHe	24.5	18.0	7.21	79.3	84.2	90.3
^{121}Sb	HEHe	25.0	17.8	7.17	78.8	85.8	95.0
^{121}Sb	H_2	24.6	20.6	5.94	75.5	80.2	92.2
^{137}Ba	Nogas	26.1	21.1	8.96	73.2	77.9	86.3
^{140}Ce	He	**12.0**	**13.1**	**9.24**	**80.7**	**83.8**	**86.5**
^{140}Ce	HEHe	**11.5**	**14.8**	**7.43**	**84.5**	**85.7**	**90.0**
^{140}Ce	H_2	**12.1**	**14.9**	**7.83**	**91.9**	**93.0**	**98.3**
^{182}W	Nogas	**23.3**	**20.2**	**8.43**	**75.9**	**79.4**	**88.2**
^{182}W	HEHe	**23.4**	**19.4**	**8.24**	**74.1**	**79.0**	**90.3**
^{195}Pt	Nogas	**20.4**	**4.91**	**7.77**	**117.0**	**105.0**	**93.0**
Pb*	Nogas	21.5	20.9	13.4	60.8	68.5	80.4

* The concentration of Pb was obtained by using sum of signals from ^{206}Pb, ^{207}Pb and ^{208}Pb.

Table H.5 Agilent biodiesel validation results measured with the xylene method

		Conc. RSD%			Spike recovery%		
		Spike conc. ($\mu g/l$)			Spike conc. ($\mu g/l$)		
Isotope	**Gas mode**	50&**5**	100&**10**	600&**60**	50&**5**	100&**10**	600&**60**
^{7}Li	Nogas	**−1520.0**	**141.0**	**18.7**	**0.867**	**23.9**	**43.6**
^{10}B	Nogas	95.3	59.0	117.0	340.0	16.9	644.0
^{11}B	Nogas	95.9	64.0	102.0	398.0	69.7	541.0
^{11}B	He	88.6	57.4	111.0	1130.0	367.0	668.0
^{11}B	H_2	93.8	52.3	112.0	325.0	−115.0	613.0
^{23}Na	Nogas	102.0	38.7	11.2	127.0	247.0	133.0
^{23}Na	He	56.3	26.4	14.5	273.0	246.0	135.0
^{23}Na	HEHe	49.8	25.3	12.4	278.0	241.0	138.0
^{24}Mg	H_2	32.5	25.7	21.0	76.6	76.3	86.9
^{27}Al	HEHe	29.7	25.5	14.5	65.7	73.2	84.6
^{28}Si	H_2	30.0	5.86	3.99	156.0	113.0	107.0
^{31}P	Nogas	74.1	58.9	48.5	396.0	347.0	130.0
^{31}P	HEHe	24.8	29.9	26.5	122.0	125.0	110.0
^{39}K	HEHe	93.3	72.2	40.4	157.0	95.9	44.8
^{39}K	H_2	210.0	111.0	42.9	98.7	62.4	43.4
^{40}Ca	H_2	52.0	22.0	16.5	125.0	77.0	93.5
^{47}Ti	H_2	48.5	45.6	17.8	96.1	87.8	98.6
^{51}V	HEHe	27.9	25.4	9.61	62.9	71.2	84.7
^{52}Cr	HEHe	11.5	6.89	5.16	99.5	104.0	100.0
^{55}Mn	HEHe	23.5	12.4	5.84	48.4	68.7	87.1
^{56}Fe	He	30.8	16.0	12.1	76.2	84.3	87.6
^{59}Co	He	**52.0**	**13.6**	**9.57**	**50.8**	**61.3**	**82.5**
^{59}Co	H_2	**24.4**	**9.16**	**3.97**	**71.9**	**80.2**	**95.4**
^{60}Ni	HEHe	34.6	8.90	4.65	41.7	65.1	90.8
^{63}Cu	HEHe	21.6	11.2	6.55	80.4	85.0	88.5
^{66}Zn	H_2	12.7	9.26	7.22	97.4	99.8	103.0
^{75}As	He	**43.0**	**34.5**	**21.6**	**64.5**	**77.9**	**93.0**
^{75}As	HEHe	**45.5**	**38.3**	**21.0**	**70.2**	**80.7**	**97.2**
^{75}As	H_2	**45.6**	**38.4**	**24.0**	**80.9**	**91.1**	**106.0**
^{88}Sr	H_2	**13.9**	**9.56**	**6.60**	**64.2**	**73.8**	**92.3**
^{95}Mo	HEHe	15.5	11.9	2.73	46.9	56.2	83.0
^{105}Pd	He	**5.26**	**3.59**	**4.41**	**89.9**	**95.0**	**93.0**
^{114}Cd	Nogas	40.4	11.8	10.9	37.2	65.1	78.8
^{118}Sn	Nogas	36.3	25.2	10.1	63.7	75.6	86.0
^{118}Sn	HEHe	37.5	25.6	10.2	69.5	80.0	92.5
^{121}Sb	HEHe	41.2	38.4	12.5	66.4	76.0	89.3
^{121}Sb	H_2	44.5	33.7	10.3	70.3	72.7	87.7
^{137}Ba	Nogas	37.1	26.5	8.49	67.9	78.8	88.3
^{140}Ce	He	**9.93**	**14.1**	**7.82**	**−10.6**	**34.7**	**80.0**
^{140}Ce	HEHe	**10.4**	**10.7**	**6.43**	**9.14**	**46.6**	**85.9**
^{140}Ce	H_2	**8.64**	**11.7**	**7.31**	**32.8**	**62.2**	**95.2**
^{182}W	Nogas	**38.2**	**26.0**	**13.7**	**62.1**	**73.9**	**83.9**
^{182}W	HEHe	**37.8**	**27.5**	**11.7**	**61.8**	**73.5**	**86.7**
^{195}Pt	Nogas	**6.03**	**7.43**	**5.09**	**99.0**	**107.0**	**95.2**
Pb*	Nogas	37.8	29.6	13.5	59.1	71.9	79.8

* The concentration of Pb was obtained by using a sum of signals of ^{206}Pb, ^{207}Pb and ^{208}Pb.

Table H.6 Diesel 1a validation results measured with the Asolv method

		Conc. RSD%			Spike recovery%		
		Spike conc. ($\mu g/l$)			Spike conc. ($\mu g/l$)		
Isotope	**Gas mode**	50&**5**	100&**10**	600&**60**	50&**5**	100&**10**	600&**60**
^{7}Li	Nogas	**57.4**	**28.0**	**16.0**	**67.9**	**82.0**	**89.8**
^{10}B	Nogas	66.2	13.9	10.8	138.0	104.0	104.0
^{11}B	Nogas	66.6	13.6	10.5	138.0	105.0	104.0
^{11}B	He	81.4	19.8	12.2	110.0	101.0	99.4
^{11}B	H_2	73.7	19.3	9.82	147.0	107.0	106.0
^{23}Na	Nogas	18.8	9.99	16.9	70.5	95.0	90.0
^{23}Na	He	22.5	11.7	16.6	79.0	97.3	90.0
^{23}Na	HEHe	20.9	11.0	16.7	79.9	98.9	90.1
^{24}Mg	H_2	4.71	3.38	2.52	107.0	102.0	102.0
^{27}Al	HEHe	9.46	1.61	0.71	104.0	103.0	99.4
^{28}Si	H_2	27.8	7.06	4.91	104.0	104.0	105.0
^{31}P	Nogas	22.9	15.6	11.0	−23.3	38.4	99.8
^{31}P	HEHe	17.7	6.61	10.2	116.0	113.0	115.0
^{39}K	HEHe	20.2	23.7	6.65	72.6	70.1	85.8
^{39}K	H_2	14.1	11.1	15.0	68.1	72.6	82.5
^{40}Ca	H_2	8.81	4.61	2.18	93.9	95.9	100.0
^{47}Ti	H_2	12.3	4.81	4.99	111.0	103.0	101.0
^{51}V	HEHe	8.06	1.49	1.47	99.2	97.9	97.0
^{52}Cr	HEHe	10.6	1.56	1.39	104.0	99.4	97.0
^{55}Mn	HEHe	8.93	1.66	0.651	100.0	97.6	97.9
^{56}Fe	He	10.3	2.54	1.51	104.0	99.1	96.4
^{59}Co	He	**15.7**	**4.68**	**1.97**	**100.0**	**100.0**	**95.1**
^{59}Co	H_2	**12.4**	**1.93**	**1.19**	**106.0**	**103.0**	**100.0**
^{60}Ni	HEHe	8.58	2.60	2.68	105.0	100.0	97.9
^{63}Cu	HEHe	10.1	2.96	3.52	107.0	102.0	99.0
^{66}Zn	H_2	5.13	4.14	2.98	97.5	96.9	97.6
^{75}As	He	**12.7**	**3.23**	**7.92**	**112.0**	**108.0**	**104.0**
^{75}As	HEHe	**11.8**	**2.07**	**7.76**	**114.0**	**108.0**	**105.0**
^{75}As	H_2	**9.86**	**3.89**	**8.00**	**116.0**	**112.0**	**109.0**
^{88}Sr	H_2	**12.7**	**1.34**	**0.958**	**104.0**	**99.8**	**97.9**
^{95}Mo	HEHe	10.8	2.51	1.95	97.4	95.3	94.3
^{105}Pd	He	**6.96**	**5.27**	**3.95**	**99.4**	**95.2**	**95.8**
^{114}Cd	Nogas	10.0	2.00	2.23	106.0	102.0	98.4
^{118}Sn	Nogas	29.8	9.60	1.40	100.0	100.0	98.0
^{118}Sn	HEHe	23.4	8.06	1.59	98.2	96.9	94.9
^{121}Sb	HEHe	11.5	2.89	2.65	107.0	101.0	98.7
^{121}Sb	H_2	8.80	2.05	2.75	107.0	101.0	99.0
^{137}Ba	Nogas	16.0	4.18	0.824	102.0	101.0	98.2
^{140}Ce	He	**14.0**	**2.75**	**1.99**	**102.0**	**98.3**	**95.2**
^{140}Ce	HEHe	**13.1**	**2.84**	**1.36**	**102.0**	**99.4**	**96.7**
^{140}Ce	H_2	**11.7**	**3.58**	**4.64**	**109.0**	**105.0**	**104.0**
^{182}W	Nogas	**16.6**	**4.88**	**1.52**	**101.0**	**99.8**	**97.5**
^{182}W	HEHe	**13.0**	**3.92**	**3.78**	**100.0**	**94.4**	**92.9**
^{195}Pt	Nogas	**13.7**	**7.33**	**9.51**	**125.0**	**111.0**	**105.0**
Pb*	Nogas	13.1	2.83	0.828	96.4	97.2	97.6

* The concentration of Pb was obtained by using a sum of signals of ^{206}Pb, ^{207}Pb and ^{208}Pb.

Table H.7 Jet fuel 1b validation results measured with the Asolv method

		Conc. RSD%			Spike recovery%		
		Spike conc. ($\mu g/l$)			Spike conc. ($\mu g/l$)		
Isotope	**Gas mode**	50&**5**	100&**10**	600&**60**	50&**5**	100&**10**	600&**60**
^{7}Li	Nogas	**5.98**	**5.14**	**4.57**	**66.3**	**88.8**	**87.6**
^{10}B	Nogas	16.6	7.91	1.35	93.1	101.0	100.0
^{11}B	Nogas	15.8	7.26	1.15	92.2	99.5	99.5
^{11}B	He	44.2	6.82	6.22	81.0	119.0	102.0
^{11}B	H_2	22.2	9.01	3.58	98.2	104.0	104.0
^{23}Na	Nogas	5.00	1.76	3.86	57.6	96.5	89.0
^{23}Na	He	8.20	5.37	3.42	63.2	95.2	93.6
^{23}Na	HEHe	2.40	3.33	4.20	83.7	86.2	91.7
^{24}Mg	H_2	3.25	1.14	1.57	105.0	102.0	106.0
^{27}Al	HEHe	5.40	2.54	0.839	102.0	101.0	101.0
^{28}Si	H_2	4.54	2.46	2.51	786.0	548.0	190.0
^{31}P	Nogas	13.5	1.54	1.56	3.94	69.4	96.3
^{31}P	HEHe	9.75	8.70	4.40	115.0	109.0	107.0
^{39}K	HEHe	22.0	23.9	6.16	57.8	45.3	87.4
^{39}K	H_2	8.28	9.56	5.14	65.7	85.0	88.7
^{40}Ca	H_2	109.0	5.73	1.15	343.0	102.0	103.0
^{47}Ti	H_2	9.56	4.09	3.14	110.0	96.6	104.0
^{51}V	HEHe	2.81	0.320	0.458	98.8	99.3	97.7
^{52}Cr	HEHe	1.81	0.383	0.583	101.0	99.5	97.8
^{55}Mn	HEHe	2.55	0.329	1.03	96.6	99.1	98.2
^{56}Fe	He	4.29	1.50	0.778	100.0	101.0	99.0
^{59}Co	He	**3.63**	**5.22**	**2.89**	**103.0**	**99.9**	**97.6**
^{59}Co	H_2	**0.471**	**1.76**	**0.974**	**105.0**	**105.0**	**102.0**
^{60}Ni	HEHe	1.93	1.35	0.803	98.5	99.0	96.2
^{63}Cu	HEHe	1.83	2.03	1.38	98.1	99.8	97.2
^{66}Zn	H_2	5.77	1.74	1.27	94.2	93.0	97.6
^{75}As	He	**2.17**	**2.63**	**1.21**	**103.0**	**108.0**	**104.0**
^{75}As	HEHe	**3.70**	**3.51**	**1.31**	**109.0**	**104.0**	**104.0**
^{75}As	H_2	**6.18**	**2.49**	**1.88**	**110.0**	**103.0**	**105.0**
^{88}Sr	H_2	**8.49**	**1.84**	**1.24**	**106.0**	**99.1**	**95.9**
^{95}Mo	HEHe	2.09	1.03	1.00	94.9	96.1	93.9
^{105}Pd	He	**4.66**	**2.27**	**1.71**	**98.2**	**102.0**	**97.4**
^{114}Cd	Nogas	0.465	0.540	0.791	98.4	99.8	96.7
^{118}Sn	Nogas	0.861	0.489	1.44	96.1	98.0	94.7
^{118}Sn	HEHe	2.22	0.762	0.912	93.0	94.4	92.4
^{121}Sb	HEHe	1.41	2.02	0.985	99.1	99.2	98.3
^{121}Sb	H_2	1.07	0.283	1.55	101.0	98.3	98.1
^{137}Ba	Nogas	1.27	0.294	0.554	96.0	98.0	95.2
^{140}Ce	He	**4.87**	**3.64**	**1.42**	**96.7**	**98.7**	**95.6**
^{140}Ce	HEHe	**2.70**	**2.21**	**0.959**	**100.0**	**98.0**	**94.8**
^{140}Ce	H_2	**2.78**	**0.95**	**2.30**	**103.0**	**101.0**	**99.6**
^{182}W	Nogas	**2.71**	**0.829**	**0.689**	**96.2**	**96.0**	**94.3**
^{182}W	HEHe	**2.08**	**1.53**	**1.33**	**92.0**	**91.5**	**88.7**
^{195}Pt	Nogas	**1.37**	**1.40**	**0.857**	**104.0**	**103.0**	**100.0**
Pb*	Nogas	1.54	0.348	0.682	90.1	93.6	94.4

* The concentration of Pb was obtained by using a sum of signals of ^{206}Pb, ^{207}Pb and ^{208}Pb.

Table H.8 Gasoline validation results measured with the Asolv method

		Conc. RSD%			Spike recovery%		
		Spike conc. ($\mu g/l$)			Spike conc. ($\mu g/l$)		
Isotope	**Gas mode**	50&**5**	100&**10**	600&**60**	50&**5**	100&**10**	600&**60**
^{7}Li	Nogas	**21.8**	**12.3**	**20.2**	**69.6**	**81.0**	**79.9**
^{10}B	Nogas	67.0	22.4	7.78	87.6	78.4	88.2
^{11}B	Nogas	75.5	19.5	7.71	86.0	76.1	87.5
^{11}B	He	101.0	51.3	6.71	−8.51	57.9	75.6
^{11}B	H_2	110.0	22.0	8.84	85.7	72.5	86.2
^{23}Na	Nogas	27.8	10.6	17.5	44.8	82.1	81.3
^{23}Na	He	19.4	9.77	18.1	52.6	82.0	81.0
^{23}Na	HEHe	21.6	16.5	16.3	7.64	79.8	80.7
^{24}Mg	H_2	5.69	6.27	3.67	105.0	107.0	103.0
^{27}Al	HEHe	4.15	4.35	1.54	99.6	106.0	100.0
^{28}Si	H_2	128.0	19.1	6.82	196.0	105.0	105.0
^{31}P	Nogas	46.6	75.3	22.2	−184.0	−56.4	33.7
^{31}P	HEHe	17.7	4.85	17.8	90.1	66.1	99.6
^{39}K	HEHe	18.9	42.3	17.2	−47.2	63.2	63.3
^{39}K	H_2	11.2	13.8	12.0	61.1	84.8	86.7
^{40}Ca	H_2	18.5	24.5	2.85	112.0	121.0	106.0
^{47}Ti	H_2	17.9	15.1	5.50	110.0	123.0	108.0
^{51}V	HEHe	2.53	1.96	0.478	98.0	100.0	98.4
^{52}Cr	HEHe	2.11	2.07	1.09	101.0	101.0	98.6
^{55}Mn	HEHe	4.90	2.05	0.896	92.6	96.9	96.5
^{56}Fe	He	8.04	3.13	1.80	94.5	96.1	97.5
^{59}Co	He	**17.9**	**4.56**	**2.83**	**92.5**	**96.0**	**94.4**
^{59}Co	H_2	**8.68**	**2.57**	**3.24**	**106.0**	**106.0**	**103.0**
^{60}Ni	HEHe	2.76	1.98	1.71	98.5	97.4	96.2
^{63}Cu	HEHe	2.58	1.16	1.59	96.2	95.9	96.1
^{66}Zn	H_2	35.1	6.76	4.19	87.1	97.2	98.6
^{75}As	He	**3.96**	**3.64**	**3.83**	**91.6**	**97.6**	**97.5**
^{75}As	HEHe	**5.89**	**2.20**	**4.14**	**92.1**	**100.0**	**95.2**
^{75}As	H_2	**7.88**	**7.45**	**5.43**	**104.0**	**108.0**	**104.0**
^{88}Sr	H_2	**9.85**	**2.80**	**2.00**	**101.0**	**96.6**	**95.7**
^{95}Mo	HEHe	2.00	1.69	1.15	97.2	97.6	95.6
^{105}Pd	He	**11.5**	**3.02**	**2.29**	**91.8**	**97.0**	**93.1**
^{114}Cd	Nogas	3.37	2.40	3.29	99.6	98.9	96.7
^{118}Sn	Nogas	3.35	2.43	1.98	98.1	98.6	95.6
^{118}Sn	HEHe	3.01	1.40	1.64	96.8	95.4	93.2
^{121}Sb	HEHe	10.2	5.44	1.86	102.0	99.6	97.2
^{121}Sb	H_2	2.59	1.77	1.74	94.4	94.6	96.0
^{137}Ba	Nogas	2.16	1.82	1.33	100.0	100.0	98.3
^{140}Ce	He	**4.09**	**1.51**	**1.66**	**94.9**	**98.2**	**94.7**
^{140}Ce	HEHe	**4.09**	**2.98**	**1.12**	**99.6**	**98.3**	**97.2**
^{140}Ce	H_2	**6.30**	**6.16**	**5.41**	**112.0**	**120.0**	**111.0**
^{182}W	Nogas	**9.85**	**1.40**	**1.69**	**104.0**	**97.6**	**96.6**
^{182}W	HEHe	**5.75**	**2.48**	**2.80**	**91.5**	**89.0**	**92.0**
^{195}Pt	Nogas	**35.5**	**4.72**	**10.5**	**103.0**	**91.9**	**94.1**
Pb*	Nogas	5.79	1.97	0.512	88.9	95.4	95.9

* The concentration of Pb was obtained by using a sum of signals of ^{206}Pb, ^{207}Pb and ^{208}Pb.